Micro-mechanical Properties of Niger Delta Sandstone Rock using Advanced Experiments and Multi-scale Modelling

Adeola Grace Olugbenga

Submitted in accordance with the requirements for the degree of
Doctor of Philosophy

The University of Leeds

School of Chemical and Process Engineering

February 2016

The candidate confirms that the work submitted is her own, except where work which has formed part of jointly authored publications has been included. The contribution of the candidate and the other authors to this work has been explicitly indicated below. The candidate confirms that appropriate credit has been given within the thesis where reference has been made to the work of others.

The work in Chapters 5, 6, 7 and 8 of the thesis has appeared in publication as follows:

A.G. Olugbenga, S. J. Antony and N. Ozerkan (2014) 'Measuring stress transmissions in opaque cementitious particulate materials', PSA2014, Particulate Systems Analysis, Manchester, UK (under the supervision of SJA, NO contributed to the analysis of this poster presentation)

S. J. Antony, A. Olugbenga, N. Ozerkan, O. Marumoame and G. Okeke (2016) 'Sensing temperature and stress distributions on rock samples under mechanical loading', ASCE Earth and Space Conference, No. 1570207489, Florida, USA (under the guidance of SJA, NO, OM and OG contributed temperature measurements data for the experimental programme)

S.J. Antony, A. Olugbenga, Z. Jahanger, N. Ozerkan, K.N. Sheeba, J. Sujatha and B. Manoj (2015) 'Micro-mechanical behaviour of Geo-materials: Advanced multi-scale experimental characterisations and modelling', International workshop on Geo-mechanics: From Micro to Macro (GM3), International Society of Soil Mechanics and Geotechnical Engineering, Nottingham, UK (under the guidance of SJA, ZJ, NO, KNS, JS and BM contributed other experimental methodologies to this joint publication)

The work in the above publications was carried out by the candidate (Olugbenga, Adeola Grace) supervised by Dr. S.J.Antony. The contribution of the other authors was in the field sampling of materials used.

Acknowledgements

I acknowledge that inspirations and intellectual abilities come from God, the omniscience. I would like to express my sincere gratitude to my supervisor, Dr S. J. Antony for his excellent supervision and guidance throughout the period of this research. I thank Petroleum technology development fund, for supporting my tuition fees during my PhD programme. My appreciation is also extended to Mr. Kirk Handley who supported me on conducting the ISRM - tri-axial test. I thank Dr. Ali Hassanpour and Dr. Colin Hare who gave support on DEM. Thanks to Mr Harry and Mr Stewart who gave support to SEM-EDS rock characterization. Mr. Simon Lloyds assisted in performing the semi-quantitative analysis with XRF. I would also like to thank members of my research group, Dr. George Okeke, Babatunde Arowosola, Saleh Alzahrani and Saeed Albaraki for their support. I am also thankful to my GP (Dr. P Antony), my husband (Engr. Olugbenga, Olumide), my Parents (Mr. and Mrs. Jadesola and Joseph Ajadi), my siblings (Mrs. Elizabeth Igbokwe, Engr. Benjamin Ajadi, Mrs Eunice Ibitoye, Engr. Israel Ajadi and Mr. John Oladapo Ajadi) and Mrs. Osasuyi Durisu supported me to overcome heath challenges during the period of this research programme.

Abstract

The focus of this investigation is to understand the micromechanical characteristics of the oil-bearing Niger Delta sandstone at different length scales. Initially, the sandstone samples are experimentally characterised to understand their morphological, physical, chemical and mechanical properties at grain scale and bulk scale where applicable. In spite of a significant level of scientific advancements made so far, sensing stress distribution characteristics of opaque and anisotropic materials such as sandstone rock remains as a stiff challenge in a wide range of science and engineering fields including geotechnical, geophysics, petroleum, mining, minerals, advanced materials and particulate science and engineering. Here we present an original framework for simulating and quantifying the strength characteristics of real sandstone samples using combined measurements and modelling strategy. Using photo-stress analysis methodology, first we sense elastic shear stress (or strain) distribution and its components along orthogonal directions on the surface of a V-notch sandstone sample under mechanical loading. Using this and applying a classical grain-scale model, the stiffness ratio of the sandstone is evaluated. This measure is also compared with using ultrasound sensors and a good level of agreement is obtained. Thereafter, the grain-scale stiffness ratio which characterises the signature of material anisotropy is fed as an input in to the discrete element modelling (DEM) of cylindrical sandstone rock samples subjected to uni-axial and tri-axial compression loading. Physical experiments are also conducted to evaluate their load-displacement characteristics and bulk fracture strength of sandstone sample under these loading conditions. A good level of agreement is obtained between the results of simulations and experiments. Taking advantage of the validated DEM simulations, an extensive level of parametric studies are conducted to evaluate the influences of different grain-scale properties on the bulk strength and fracture characteristics of sandstone. Thus the current multi-scale framework can be applied in future to quantify the strength characteristics of such complex and anisotropic materials in a reliable manner.

Table of Contents

List of Tables

List of Figures

Nomenclatures

Latin character

h	Sample thickness
G	Shear modulus
K	Bulk modulus
N	Fringe order
f	Fringe constant
t	Thickness of photo-elastic coating (bi-fringe materials)
A	Surface area
P	Stress applied to the sandstone granular assembly
k_n	Normal stiffness
k_s	Shear stiffness
V_p	P-wave velocity
V_s	S- Wave velocity
r	Grain radius
E	Young’s dynamic modulus of elasticity
P	Bulk density
v	Poisson’s dynamic ratio
k^s	Normal stiffness
k^n	Tangential stiffness
E_c	Contact Young's modulus
χ	Modulus-damage index
$\bar{E}$	Young's modulus of parallel bond
E	Macroscopic modulus
F	Force on the grain assembly
A	Average area of a single grain
C	Coordination number
k	Optic constant
I_{max}	Maximum light intensity
I_{min}	Minimum light intensity

r	radius of grains
P^n	Normal force
C	Cohesion of bond material

Greek characters

σ_n	Compressive strength of bond
ϕ	Porosity of sandstone
θ	Angle of incidence
θ_{pk}	Incidence maximum peak value for ¼ fringes
θ	Angle of incidence
ʎ	Wavelength
σ	Stress
ζ	Ratio of micro-modulus
ξ	Normal contact stiffness
$\sigma_1 - \sigma_2$	Principal stress differences
$\frac{\sigma_1 - \sigma_2}{2}$	Maximum shear stress
ε	Strain
$\boldsymbol{\lambda}$	Wavelength
k^{ξ}	Contact stiffness
k_A^{ζ}	Contact particle A
k_B^{ζ}	Contact particle B
ξ	Normal, Shear
δ	Retardation
$\Delta\theta$	Rotation angle of grains
f_σ	material fringe constant
μ	Internal frictional coefficient

Acronyms

DEM	Discrete Element Model

PSAT	Photo stress Analysis Tomography
XRF	X-Ray Fluorescence
XRD	X-Ray Diffraction
SEM	Scanning Electron Microscope
EDS	Electron Dispersive Spectrometry
AE	Acoustic Energy
UCS	Uniaxial Compressive Strength
PFC	Particle Flow Code
BPM	Bonded-Particle Model
FJM	Flat-Joint Model
UDEM	Universal Distinct Element Code
SJM	Smooth-Joint Model
2D	2-Dimension
3D	3-Dimension
DFN	Discrete Fracture Networks
FDM	Finite Difference Methods
FEM	Finite Element Methods
BEM	Boundary Element Methods
FVM	Finite Volume Methods
DDA	Discontinuous Deformation Analysis
RBM	Restricted Boltzmann Machines
BPM	Bonded Particle Model
CPM	Clumped Particle Model
ORC	Overlapping Rigid Clusters
ISRM	International Society for Rock Mechanics
PSTT	Photo Stress Tomography Technique
ASTM	American Society of Testing and Materials
FPZ	Fracture Process Zone
ANOVA	Analysis of Variance
SOCPI	Slightly Overlapped Circular Particle Interaction

NDE	Non-Destructive Evaluation
CI	Crack initiation
PFC2D	Particle Flow Code in Two Dimensions
PFC3D	Particle Flow Code in Three Dimensions
SIF	Stress Intensity Factor

Chapter 1

Introduction to project

1 INTRODUCTION

1.1 Background of research

Rock mechanics deals with the behaviour of rock and its response to the stress field around it. Rocks can either be stable or unstable when subjected to stress. Thus material failure must be prevented during mechanical handling by ensuring that operational stress of rock masses are below failure strength. Unconsolidated sandstone formation that bears crude oil fractures easily during mechanical handling. A major challenge in oil well drilling has to do with preventing well fractures because when accidental fractures occur, the well becomes unstable.

1.1.1 Rock mechanics and challenges in oil industry:

New technologies are being developed to help prevent problems such as undue well fractures in the oil industry. For example the Blowout preventer (Yenulis and Folsom, 1993) takes effect after the well has fractured and kick has occurred. These technologies prevent loss of life but the wells and subsurface equipment are lost. Thus, one consequences of wellbore instability is the financial loss of a well. Such occurrence can increase drilling cost to as high as 30% (Santarelli et al., 1992). This is a challenge to the oil industry.

Radial change in the stress field occurs during a drilling operation (Rendler and Vigness, 1966). The exposure of the wellbore to drilling fluids alters the physical environment of the rock formation. This leads to instability in the wellbore with enlarged hole, caused by potential subcritical crack growth. The consequence of this event is lost circulation, casing problem, poor cementing, sidewall core recovery difficulty, stuck pipe, side-tracks, logging and interpretation difficulties and even loss of the entire well.

Breakage of the rock has frequently lead to complications such as hole squeezing and server openings which are difficult to control (Resende et al., 2010). When targetted wells are drilled and the fractures are not avoided, the hole problems become more complicated resulting in a deformed hole. This causes poor cementation and undefined formation evaluation. Hole perforation becomes very

difficult and the cost of drilling soar by several dollars. Also, unwanted fractures in oil well can lead to a loss circulation or uncontrollable fluid flow at extreme pressures resulting into a potential loss of life and machinery.

1.1.2 The Friable nature of Niger delta sandstone to be addressed in this research

The sandstone in Ughelli depobelt, located in the Niger delta basin (Figure 1.1) is a source rock from which crude oil is produced (Adedapo et al., 2014). This is one of the source rocks in the Agbada formation where crude oil is produced (Evamy et al., 1978; Mouchet and Mitchell, 1989). Besides the syn-sedimentary deformation that causes increasing instability in the formation (Evamy et al., 1978), some layers of the sandstone are unconsolidated which usually fracture due to mud weight exceeding the pore pressure in the layer. In the event that the sandstone is unconsolidated, well instability occurs as a result of accidental fracture in the rock. While drilling with an excessive mud weight, pore pressure may be predicted wrongly as reported for reservoirs in the Niger Delta Basin by (Fertl et al., 1994; Nwozor and Onuorah, 2014)

Figure 1.1 Map showing oil field in Niger-delta Nigeria (https://www.google.co.uk/search?lnms&tbm=isch&sa=X&ved=0CAgQ_AUoA2oVChMI6c6VhoeYyQIVx0IUCh2vNQI3#tbm=isch&q)

During oil drilling, the Niger delta sandstone easily crumbles because of the friable nature of the sandstone (Lambert-Aikhionbare and Shaw, 1982). Sandstone layers occur in some strata down the well. Therefore, as the well is drilled at some several thousand meters of depth downward, sandstone layer is encountered (Lambert-Aikhionbare and Shaw, 1982). However, not all the layers are sandstone. The others are shale and sand. The sandstone rock contains the oil and is stressed due to pressure load of drilling string. The rock which is made of grains of size distribution that ranges from fine to coarse crushes and the clay grades are dislodged into the reservoir. Consequently, the clay particles mix up with the crude oil. Because the sandstone is predominantly composed of detrital quartz content, the clay content is low (Lambert-Aikhionbare and Shaw, 1982). These properties are expected to be observed in the Ughelli sandstone considered in this work. The problem of crumbling of the sandstone layer is increasingly jeopardising the current drilling activities in the Niger delta which constitute a major challenge to the oil industry. Therefore it is important to identify the effect of petrology on the strength of the oil-bearing rock in this area. Hence, the high strength sandstone from Niger-delta is used in this research for the strength analysis of formation rock of Niger-delta region.

1.1.3 Pressure in micro-mechanical investigations:

Operational safety as well as effective and efficient services are important in drilling sandstone formation. This requires more effort to be put into research for preventing well fractures (York et al., 2009). Such research has led to identifying the processes that leads to these accidents. Thus the mechanism of rock deformation has become a tool to predict fractures (Eberhardt, et al.,1998). Fractures encountered in situ begin when compressive stresses are applied. The strain response of rock to stresses significantly contributes to the gradual loss of strength. The eventual failure of the rock occurs and the well becomes unstable to manage. Theoretical and analytical methods have been applied to solve the problem of wellbore instability due to rock failure. Linear elastic problems are complex if they are to be solved based on analytical solutions which may be difficult to obtain because the assumptions defining the applied load are restricted. Numerical solution has also been applied in the last decade where, finite element modelling and other modelling tools have applied three dimensional approaches to the problem defining stress field in rocks (Jing, 2003). These approach is only adequate for initial design because they can merely handle complex geometry during well design. If the applied load on numerical sample is

placed on estimated numerical sample, the solution cannot be a true component behaviour. They are therefore better accepted if they agree with experimental results. But discrepancies are still emerging in most reports that estimate rock properties with failure progression. The most recent advance in discrete models have provided a way of identifying the stages of rock deformation at the least scale based on micro/grain models (Cundall and Strack, 1979a).

1.1.4 Knowledge in micro-mechanical damage:

Micro-mechanical damage has been studied with amplitude frequency distribution of acoustic emission stresses. The stress applications induce micro strain on rock. Statistically, the detection of micro-strain focuses on the evolution of the amplitude due to strain (Holcomb et al., 1990; Locknet and Byerlee, 1995; Meredith et al., 1990; Main et al., 1989) this amplitude frequency has also been passed through synthetic sandstone using discrete model and seismic reflection to replicate the response of the rock. Among these several works is the research on intensity and velocity of stress application on discrete models where fractures were represented by contact model (Zhao and Cai, 2001). In addition, Discrete Element Modelling (DEM) has been adopted to study stress wave interaction with fractured location. Muhlhaus and Oka (1996) simulated wave propagation through discrete model while, Cai (2001) showed the plane wave normal incident on fractures. His work employed a linear elastic stiffness, (at micro-scale), so that frequency was a function of transmitting wave and reflection ratio. The micro-mechanical properties were shear and normal stiffness parameter of the constituent grains that make up the rock.

Kim et al. (2006) studied the effect of joint direction under dynamic applications to obtain fracture, fragmentation and its propagation caused by high dynamic stresses. It is very rare that surrounding stresses are studied and identified. With extensive survey, it was evident that; the elastic stress surrounding the region of fracture should be considered. The only attempt till date is the extensive work of Hazzard and Young (2004). DEM was employed, to indicate anisotropy near damage zone by tri-axial deviator loading. In their work, the properties of propagating stress wave were provided. Apart from their work, in general, researchers did not indicate stress wave surrounding the location of fractures. Hence, attempt made to simulate rock deformability is still a stiff challenge. Although seismic reflection has produced indications of defective points in rock, the output has not been utilized to represent

the exact physical response of the rock to stress. This reveals the gap in knowledge between simulations and experiment where the actual microstructure of a physical material is still difficult to model. Therefore it is better to obtain rock parameters and incorporate them to simulate realistic rock behaviour. In the present work, rock parameters at single grain scale would be employed to replicate the actual response of the physical rock. The current research is the result of a representation of real rock under mechanical loading. Thus an improvement on the simulation of rock deformability is targeted.

The thrust of this further research is to enhance rock simulation. Although, the fact remains that; it might not be possible to fully verify and validate numerical model of natural process (Oreskes et al., 1994). Notwithstanding, this work have employed the technique of determining the realistic rock parameters to obtain elastic rock properties. This provides the link between experiment and simulation where hypotheses are corroborated, decision of modelling route was carried out, and sensitivity analysis was performed to obtain additional data. Further research, based on these future improvements, have been recommended.

1.1.5 Motivation

Hoek and Martin (2014) stated that the process of rock deformation governs both in-situ condition in its infinite mass and the small rock sample studied in the laboratory. The well-known brittle fracture theory (Griffith, 1921) was based on assumption that rock contains a randomly distributed uniform micro crack and that the original properties of the rock are constant throughout the crack initiation, propagation and deformation. It is motivating to investigate the mechanism of rock failure based on the hypothesis that; randomly distributed cracks were found within the grain assembly. Each of these bonded discrete grains (idealising a rock sample) has boundaries and the grains contact each other at their boundaries. To improve this hypothesis, assumptions were made during experimentation of rock behaviour. Mc Clintock and Walsh, (1962) and Hoek, (1966) modified the Griffith's theory using compressive stress to predict rock fracture by the propagation of fracture from crack tip. Brace (1963) worked with hard rock and discovered that cracks are initiated at grain boundaries (Hoek and Martin, 2014). Simplified Griffith assumption provided the insight for the techniques of crack closures detections. This work was validated by Hoek and Martin, (2014). The gap to be filled in understanding fractures exist

because of the complexities in the behaviour of rock which are due to the complex mineral constituent. These constituent are inherent by nature perhaps their digenesis during formation. And much more complications are due to the fact that inherent natures are unique to every rock. This work seeks to factor in this complex behaviour which is not possible in analytical procedure. In actual fact, chemical composition and physical definitions of rock materials are not cumulative. This has hindered the total understanding of deformation of natural process. Therefore an investigation on the strength characteristic is essential to provide clues to resolve the complexities posed by the mineralogical contributions. This is because analysis by experiments is more effective. The authenticity of experiments carried out in this work under static/dynamic conditions has addressed problems of complex composition which are not catered for in previous research because the grain scale elastic properties were obtained from the natural rock (containing all its constituent mineral). The rock parameters obtained are based on the interactions of the mineral components. The results resolve analytical difficulties even in solutions requiring three-dimensional geometry. Therefore, a complex mineral of discrete assemblies of grains under load with undefined elastic behaviour were found to be malleable in experimental investigation. Figure 1.2 is a schematic of the search context.

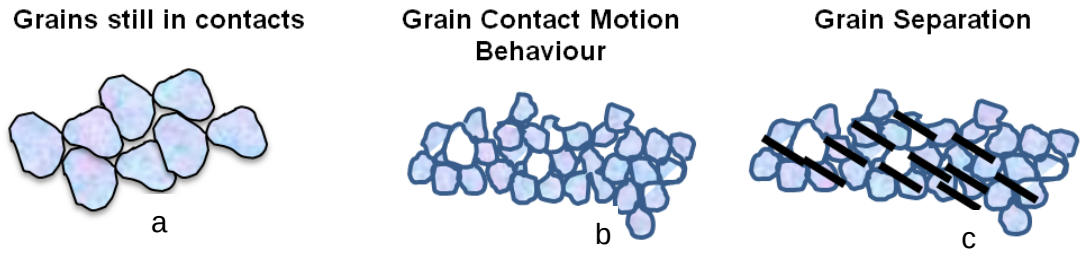

Figure 1.2 Schematics for the context of this research (a) intact bonded grain (b) grain contact gain momentum and (c) grain separation**.**

1.2 Aim of the research

To utilize experimentally characterized grain scale parameters of rock to simulate its macro deformability using discrete element modelling and to predict its bulk fracture strength.

1.2.1 Research objectives

In order to achieve the stated research aim, investigations were carried out to identify micro-mechanical analysis of bonded grains deformation. Below are the steps providing routes to achieving the aim of this project?

- Experimental characterization of the Niger-delta sandstone rock samples to define the mineralogical composition and the grain shape properties to reveal grain boundary, grain contact distribution, and grain shape and grain size.

- Development of a novel technique for sensing distribution on sandstone under mechanical loading using Photo-stress Analysis Tomography (PSAT) (Antony et al, 2015). Data collected were analysed to obtain stiffness parameters at a single grain level which serve as a building brick for bonded grains simulations using DEM. From this a model for representing the behaviour of grains in sandstone was developed. Next, behaviour of bonded grains was simulated to study the mechanical strength characteristics.

- Integrate the image data obtained from the Photo Stress Analysis Technique (PSAT) so as to interpret and analyse damage parameters.. This way, the procedure of obtaining point data is established as data acquisition. Interpretation can be made easy for engineers with limited knowledge of photo-elasticity.

- Analysis of micromechanical response of bonded grains under external loading using DEM, which involved inputs data from experiments.

- Validation of the grain-scale stiffness data to be done independently using ultrasound technique and bulk strength properties using tri-axial compression experiments. A number of micro parameters have been evaluated comprehensively which formed an input to DEM simulations of sandstone.

1.3 Project management

The urgent need to predict subtle fractures from the onset is critical for safe operations and economics of drilling rock, hence addressing the problem of sandstone fractures of the Niger Delta region of Nigeria. Over the years, well instability has challenged the drilling of oil wells because of the presence of

unconsolidated sandstones which deforms by crumbling. This results into a distorted hole. The current project is funded by Nigerian Petroleum Technology Development Fund (PTDF, Nigeria). The sponsor requires that this work explores the use of Nigerian sandstone to predict accidental fractures which are not desirable during rock drilling for petroleum extraction. In order to obtain detailed minerology and complex composition of the rock, experts were involved for the detailed characterization of the rock materials. Hence, the X-Ray fluorescence (XRF), the X-Ray Diffraction (XRD) and the scanning electron microscope–electron dispersive spectrometry (SEM-EDS) were carried out by support of technicians who are experts in these fields.

1.4 Framework of the thesis

This thesis is structured into 9 chapters. The steps taken is presented in this section as illustrated in Figure 1.3. This work provides a concrete understanding of the behaviour of granular rocks under mechanical loading. Each Chapter relays all experimental stage in details with a survey of relevant literature.

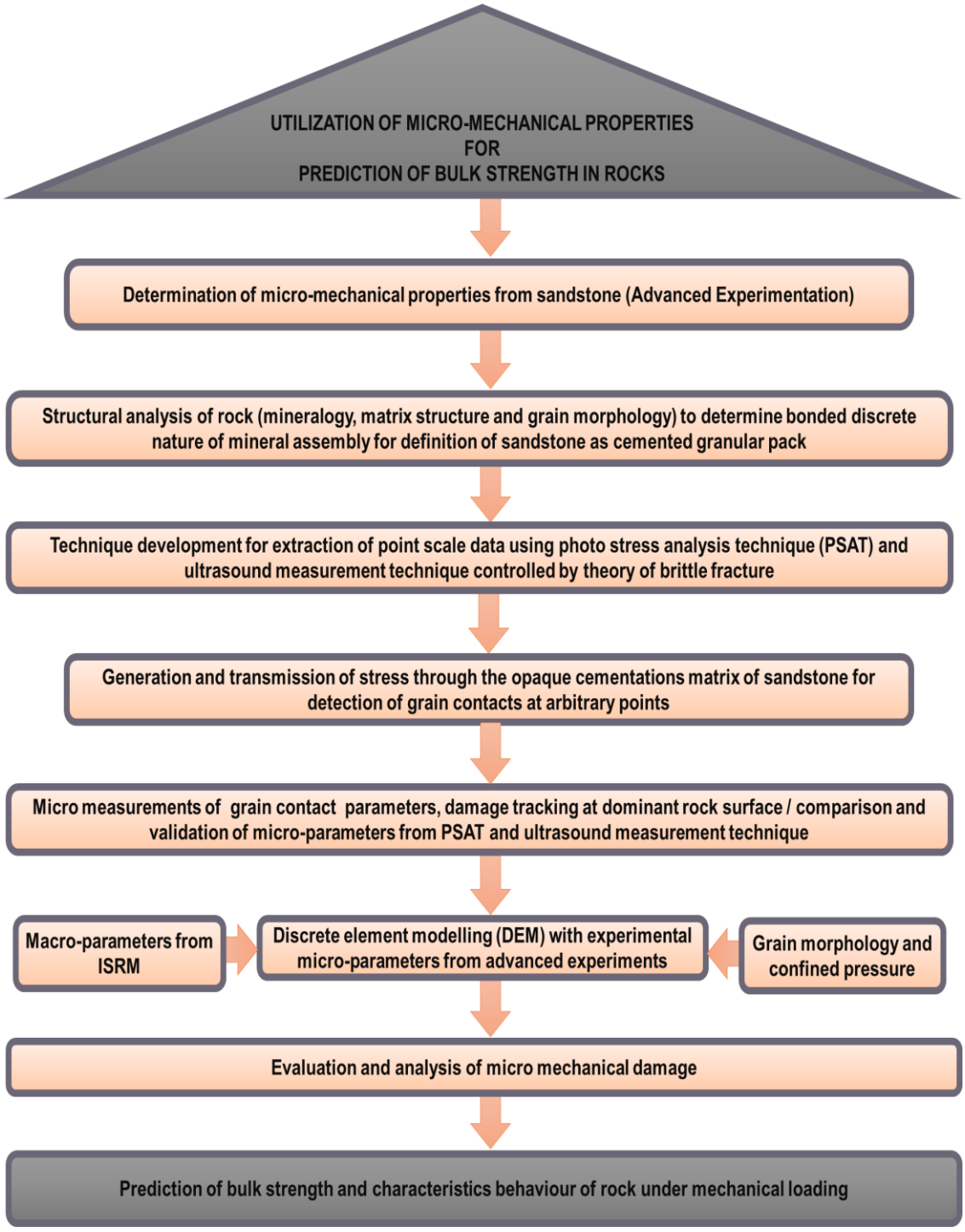

Figure 1.3 Framework of research

1.4.1 Overview of chapters

This work is based on the premise that by measuring stress and strain from an arbitrary point in a rock material, grain scale parameters can be estimated, and even more accurately with a synergetic input of elastic properties of the rock medium into the measurement route. These elastic properties are usually captured during grain contact resistance to stress in standard tri-axial test.
The thesis has been structured into 9 Chapters.

Chapter 1: this first chapter highlights the steps taken to achieve the set aim of the research. The aim of this present research is to investigate the strength characteristics of sandstone media.

Chapter 2: The literature survey on theoretical principle that leads to research hypothesis has been compiled in Chapter two. The survey identifies the broad composition of rocks as cemented-granular assembly of mineral grain and particles. The challenges of the experimental work are highlighted and the contribution to improving experimental work is presented. Next a review of discrete element modelling (DEM) with reference to their limitations and formulations to the simulation of rocks is presented. Then, a brief history of experimental determination of grain scale micro-parameters from rock is discussed. The applications of these micro-parameters to the physical modelling of rock deformability are presented to address the research gap. An understanding of the behaviour of cemented-granular rocks is provided. The experimental and simulation methodologies were supported by a survey of relevant literature in Chapter two.

Chapter 3: Specific emphasis has been made on the methodology employed to obtain micro parameters at grain contact, composition of rocks and the micro-mechanics of deformations. Finally the research methodology was outlined. The deductive spiral approach was explained in principles of brittle fractures provided by Griffith theory and stress concentrations around fracture tips

Chapter 4: Chapter 4 presents the different experimental characterization methodologies involved in the characterization of Niger delta sandstone. The results are presented in the same chapter. This chapter also included information on using such experimentally measured micro parameters as input into DEM simulations.

Chapter 5 and 6: Detailed investigation for determining stiffness parameters of sandstone using ultrasound measurement technics was presented in Chapter 4. The results and statistical descriptions of the stiffness parameter are discussed in Chapter 5. Stiffness was also estimated in Chapter 6 as contact model, using Photo Stress Analysis Tomography (PSAT) and its validation using ultrasound methodology is presented. Furthermore, the bond strength parameters were determined in Chapter 6.

Chapter 7: Implementation of the experimental-DEM hybrid was done. The experimentally measured grain-parameters are inputs for DEM to achieve modelling of the strength characteristics of sandstone.

Chapter 8: The influence of grain shape on the micro-mechanical damage modelling of Niger-delta sandstone is presented in this Chapter. The results are compared with the frequently and comprehensively studied Berea sandstone.

Chapter 9: The major conclusions of this entire study are highlighted and recommendation for future work has been provided.

Chapter 2

Literature Review

2 LITERATURE REVIEW

2.1 Introduction

The strength characteristics and deformability of natural granular rocks is complex to understand (Aydin et al., 2006). It has not yet been fully understood because of the lack of information on the interplay between the grains and inter-granular cement properties (Howarth and Rowlands, 1987). Sedimentary rock has mineral composition, physical and mechanical properties which vary largely because of the geological origin or history behind its deposition (Terzaghi et al., 1996). To this end, discrete analysis of the grains and the cementing matrix are complex (Camborde et al., 2000); In fact it is not possible to study all the inherent heterogeneities and complex phenomenological properties exhaustively without bringing the study to a manageable level of linking the micro and macroscopic strength. The first section of the literature review discusses the sedimentary rocks, and associated challenges encountered during the determination of the rock's mechanical response to stress in laboratory and field applications. Further, numerical methods and experimental modelling have shown to be a promising technique to understanding deformability. Test for natural rock at in-situ during mechanical application (in oil industry) are analysed for the purpose of understanding and investigating the strength characteristics of cracks in granular rocks. Discrete Element Medelling (DEM) capable of handling each discrete grain and simulates the behaviour of the rocks was discussed. Limitations encountered in modelling rock as cemented granular medium are presented. The novelty of following geometric figures to develop a physical contact model is presented to assist in understanding the deformation mechanics of natural rock. Knowledge gaps in this field are reviewed and summarized. The framework of the literature review is presented in Figure 2.1. Review of the importance and applicability of Acoustic Emission (AE) in indicating the crack number of rocks is also provided.

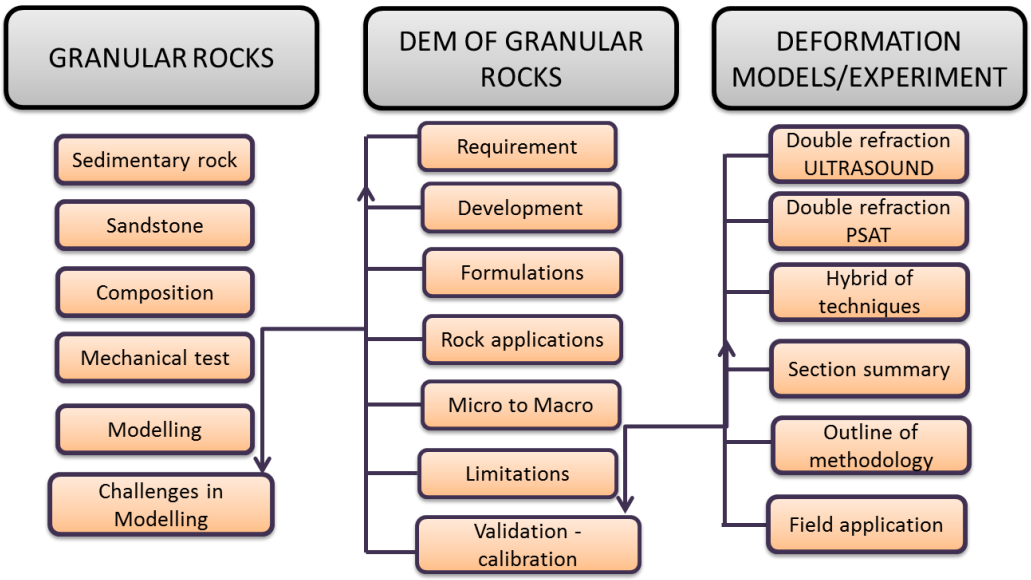

Figure 2.1 Structure and flow of the literature sections discussed in Chapter 2

2.2 Granular rocks

Generally, rock is a naturally-formed aggregate of mineral matter, constituting an essential and appreciable part of the earth's crust (Ramamurthy, 2004). Rocks are mainly divided into three main classes; igneous, sedimentary and metamorphic rocks depending on their mode of formation (Blatt et al., 2006). The texture of a rock is the major parameter that affects the mechanical behaviour and characteristics in a specific mode of deformation (Ramamurthy, 2004). Rocks are classified as either granular or non-granular rocks (Cross, 1902). Non-granular rocks refer to a rock class that have a glassy texture or consisting of very fine grains that is less than silt size, while granular rocks consist of crystals or grains joined together with some cementing materials. Irrespective of the geological origin and mineral composition, both granular and non-granular rocks belong to one of three basic types of rock (Huang, 1962). For instance, granular rocks can be sedimentary rocks such as sandstones, conglomerates etc., metamorphic rocks such as slates, phyllites quartzite etc. and igneous rocks such as granite, diorite etc. Similarly, non-granular rocks can be sedimentary rocks such as mudstones, limestone, shale, chert etc., metamorphic rock such as schists, marble etc. and igneous rock such as obsidian; basalts etc. (Huang, 1962). Non-granular rocks are treated as a single phase material consisting of homogeneous micro structure in laboratory testing, while granular rocks are normally considered as composite or two phase materials consisting of

Table 2.1 Classification of Sedimentary Rocks based on Grain Size and Mineral Composition (Standard, 1993)

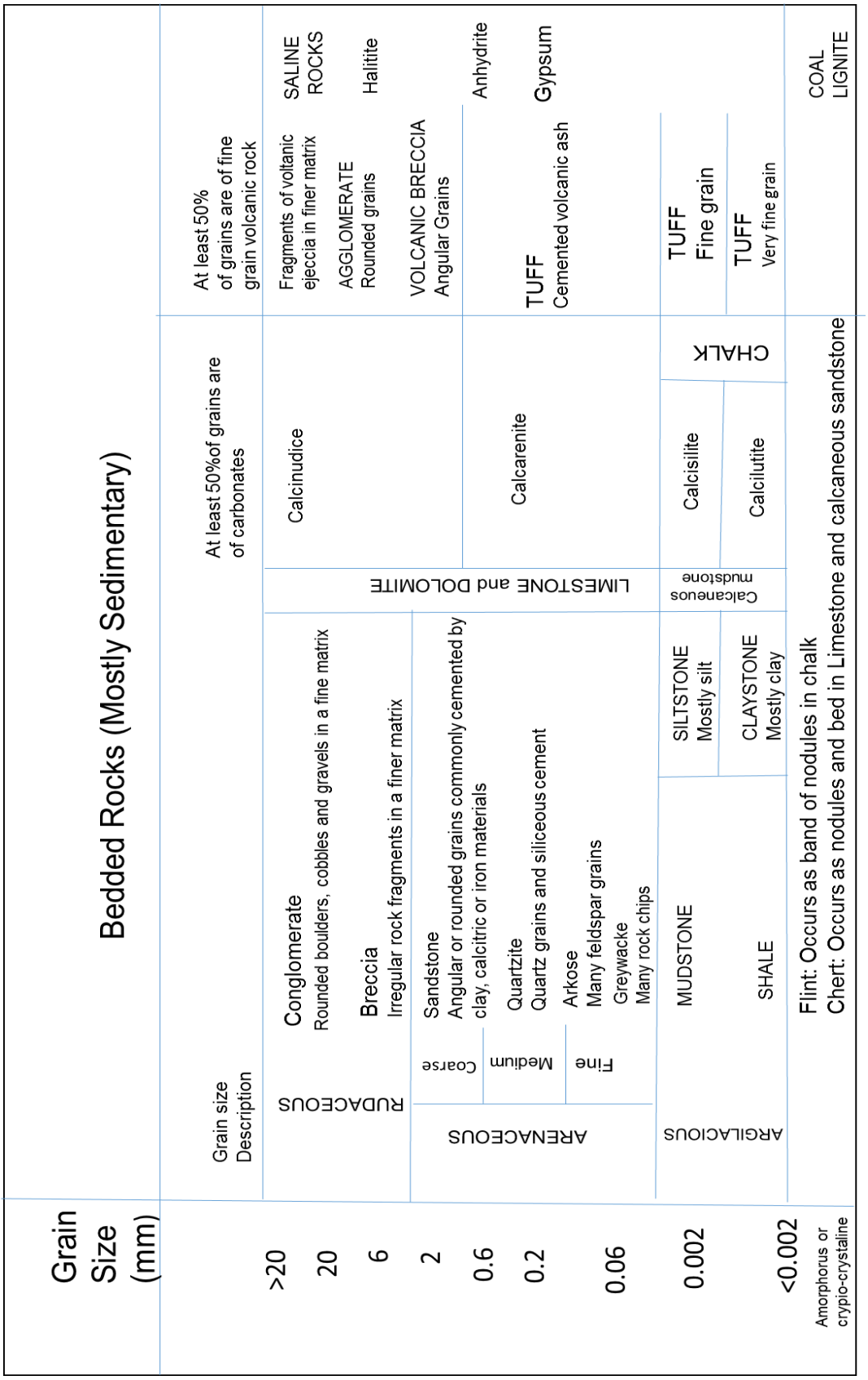

rock fragments or clasts and a cementing matrix (Bieniawski, 1967). The mechanical behavior of rocks is governed by the characteristics of both the clasts and cementing matrix. In mechanical testing, dilation of the materials basically draws a line between the granular and non-granular materials and provides a justification for this differentiation in natural rocks (Bieniawski, 1967). Granular rocks can further be classified based on their grain size and geologic origin (Picard, 1971)

Granular rocks which are mainly of sedimentary origins are the primary focus for this research. Fine grained granular rocks also known as argillaceous rocks have a grain size less than 0.06mm (Waldschmidt, 1941). This grain size cannot be viewed with the naked eye. Table 2.1 shows the examples of argillaceous rocks which are shale, mudstone, siltstone and clay-stone. Medium to coarse grained granular rocks which are also called arenaceous rocks are classified in Table 2.1. The sand sized grains are between (0.06 and 2mm). Sandstone is an example of arenaceous rock. The process by which arenaceous rocks are formed is partly mechanical and involves the breaking and deformation of parent rocks into re-lithified sand sized grains (Pidwirny, 2006). Rocks having a grain size greater than 2mm are classified as very coarse grained rocks, are also known as rudaceous or pebbly rocks. They are made up of quartz having a size greater than 2mm up to a boulder size (>20mm) enclosed in a fine grained matrix with particle size less than 2mm.There has been a lot of studies on arenasceous and argillaceous rocks such as mudstones and sandstones, while little work has been done on rudaceous rocks.

2.3 Sandstone formation

Sandstone is one of the most common type of sedimentary rock which is formed from cemented sand-sized clasts. The cement that binds the clasts ranges from clay minerals to calcite, silica or iron oxide (Tucker, 2003). Sandstone contains sand-sized grains of rock fragments and individual minerals broken down from other older rocks. The original rock which is made up of small grains of mineral that weathered when they are broken down are known as the source rock (Selley, 2000). The pieces from a source rock are eroded, or carried away from the source area. The longer chunks from a source rock are carried by wind, water, or ice, are broken down into very small fragments. Certain minerals found within rocks are also more likely to survive significantly longer journeys. After a source rock is weathered and eroded, the

resulting sand grains might fill a bowl-shaped basin on land or underwater. This phenomenon is coupled with the pressure from more sediments landing above finer particles carried by the movement of water through the grains, the sand becomes sandstone. Finer grains of rock and new mineral growth fill the spaces between the grains thereby cementing the new rock (Krause and Nelson, 1984). The pore spaces are visualized by the scanning electron microscope (SEM).

2.3.1 Scanning Electron Microscopy-Energy Dispersive Spectroscopy (SEM-EDS) or micrograph of sandstone

The grain and pores are made visible with the SEM-EDS micrograph. The near points of grain contacts are revealed. With the incorporation of the EDS, the mineral specific to major component are identified. These mineral include quartz, feldspar clay mineral and Mica. The technique is capable of revealing the pore content within the major grains (Welton, 1984). It has the capability of identifying even the smallest mineral within the pores. It works at a greater depth of view and resolutions. For rock analysis, the grain boundary is revealed at 10X to 20000X magnifications.

Sandstone consists mostly of quartz, feldspar and lithic fragments (Shao et al., 2001). The locations of these minerals are made visible and identified by their elemental components. There are other minerals in the composition of sandstone depending on the mineralogical maturity of the sandstone, which are identified by the elemental matching of Energy Dispersive Spectroscopy (EDS) with the X-ray diffraction of sandstone.

Results from SEM-EDs has shown that quartz is made up of more than 66% of the minerals found in sandstone (Blatt et al., 2006). This is due to the fact that quartz is the most common mineral in crystalline rocks. It is mechanically durable because of its high hardness and lack of cleavage. It occurs as both mono-crystalline and poly-crystalline grains and they usually show un-dulatory extinction. Feldspar makes up of only 10 – 15% of all the minerals in sandstone and it is generally plagioclase and alkali feldspar (Stoffler and Hornemann, 1972). Lithic fragments are generally unstable in sedimentary environment, yet if present, they indicate a provenance (Blatt et al., 2006).

2.4 Composition of sandstone and the cracking process (cementation)

The cracking process will occur in sandstone because the grains are cemented by various agents including quartz, calcite, clay minerals, and hematite, although other minerals such as pyrite, gypsum, and barite can also form cements under special geologic conditions (Keller, 1961). During the first deposition of sediment, there are many open spaces or pores that are later filled by the deposition of a matrix. The matrix can affect the amount of pore space that remains in a rock as it lithifies. Sandstones normally have significant voids and therefore, are usually good reservoir rocks for ground water, natural gas and petroleum (Akram et al., 2010).

2.4.1 X-ray fluorescence (XRF) and cement content of sandstone

X-ray fluorescence analysis of whole rock ranges from magnesium to uranium. It is capable of light element detection and trace metals. While X-ray diffraction (XRD) gives the mineral, XRF is more efficient for elemental detection. Major elements are determined using fusion disc of sandstone particles which have been ground and mixed with lithium tetra-borate and lithium meta-borate. Quartz cement is very common in nearly pure quartz. Pressed powder pellets are used to obtain the trace element which is a semi-quantitative analytical procedure. The minerals are identified by the elements e. g. Si indicates quartz. Overgrowth on quartz is called quartz cement which is derived from the grains. This overgrowth grows as crystals which extend the original quartz grains (Bryant and Blunt, 1992). The overgrown cement grows outward from the original grain until it runs into cement growing outward from an adjacent grain usually visible with computed tomography scan coupled to X-ray fluorescence Thus, the rock is characterized by a texture of interlocking grains with cement particle within the interphase. If the grain has small amount of clay or other fine grained dirt forming an irregular coating on its surface, the overgrowth may be preserved and show the original outline of the grain (Blatt et al., 2006).

Calcite cement is the most common cement/overgrowth in sandstone, although it does not tend to fill all pore spaces completely when present. They are identified by the patchy particles of overgrowth on quartz. Cements in calcite cemented sandstones are slightly dissolved (Blatt, 1979) which results into secondary porosity. Calcite is identified by the element calcium in the XRF data. Carbonate ion

also occurs in abundance in surface and groundwater, but is derived by dissolution of carbonate minerals (Blatt et al., 2006). Hematite is a cement present in some less common rocks.

2.4.2 X-ray Diffraction (XRD) and the identification of kaolinite

Kaolinites are phyllosilate minerals which are commonly found in sedimentary rocks including sandstone. Rocks with abundant kaolinite are kaolinite rock (Anderson, 2013). The mineral is detected by XRD technique. Chemically kaolinite are hydrated alumina-silicates ($Al_2Si_2O_5(OH)_4$), a minor component which often cannot be seen with the SEM. Thus, they are usually identified by their distinctive peaks of the XRD. Kaolinite is identified in sandstone by distinctive peaks of about 7.15Â and may also be identified at about 3.58Â (Hillier, 2002). In some cases, weaker peaks indicate the presence of kaolinite in the sandstone. This is equally useful especially when the peaks coincide with other minerals. Thus, the intensities of the mineral may also be used for its identification if they are coinciding with other minerals like chloride.

2.4.3 Drilling, rock fractures and rock composition

Rock is cemented grains and can be stressed by loading. Accidental or unexpected response of rock to stress is usually the cause of drilling difficulties, leading to increased drilling time, cost and even loss of the oil well. When cemented granular minerals in rock are disaggregated, the rock becomes unstable. Wellbore instability is a regular challenge (Awal et al., 2001) which results in annual cost-ineffectiveness to drilling operations in the petroleum industry (Bradley, 1978). Therefore, the utmost concern of drillers is to maintain the aggregation of the grains, thus preventing fragmentation of the rock (Ferla et al., 2009). Major surveillance involves keeping track of the lost in drilling fluid and the mechanical procedure involved in the drilling operations aim to minimise these lost expenses. There is no well drilled without a unique challenge. The consequence of most drilling problems is wellbore instability which is still challenging (Willson et al., 1999). Hence, the huge concern for drilling through the rocks is to eradicate fracture of the cemented quartz.

Mechanical operations have been employed to address these challenges such as re-entering of some well drilled with horizontal techniques, higher pressure jet drilling, under-balance drilling, etc. (Tan et al., 2004). These techniques are good but they are still 'medicine after event' solutions which have not stopped drilling problems (Kristiansen, 2004). Therefore, achieving well stability is critical but it is still a big challenge (Martins et al., 1999). Schemes used to mitigate the danger of well collapse may compromise some of the other elements in the overall design for example penetration rate, differential sticking or hole cleaning (Martins et al., 1999) Therefore, it might be necessary to employ predictions that can, perhaps help to mitigate the loss (Bowes and Procter, 1997). These methods were targeted at mud chemistry, density and rheology optimization. Sensitivity analysis had also been employed to assess if there are risk related to well inclination and trajectory (Moos and Barton, 2008). A Predictive model of well stability has been useful for well completion (Nygaard and Nævdal, 2006). This solves the problems associated with inflow complications where the hole collapse and sand production sets in (McLellan, 1996). For instance, in wells characterized by high permeability of interconnected grains with weak granular consolidation, the predictive tools are usually employed for choice of linear-casing (perforated/slotted). In some cases, the hole is left opened (McLellan and Wang, 1994). The causes of well instability (Chen et al., 1998) have been adequately illustrated by (Mohiuddin et al., 2001). Few causes of well instability are illustrated in Figure 2.2.

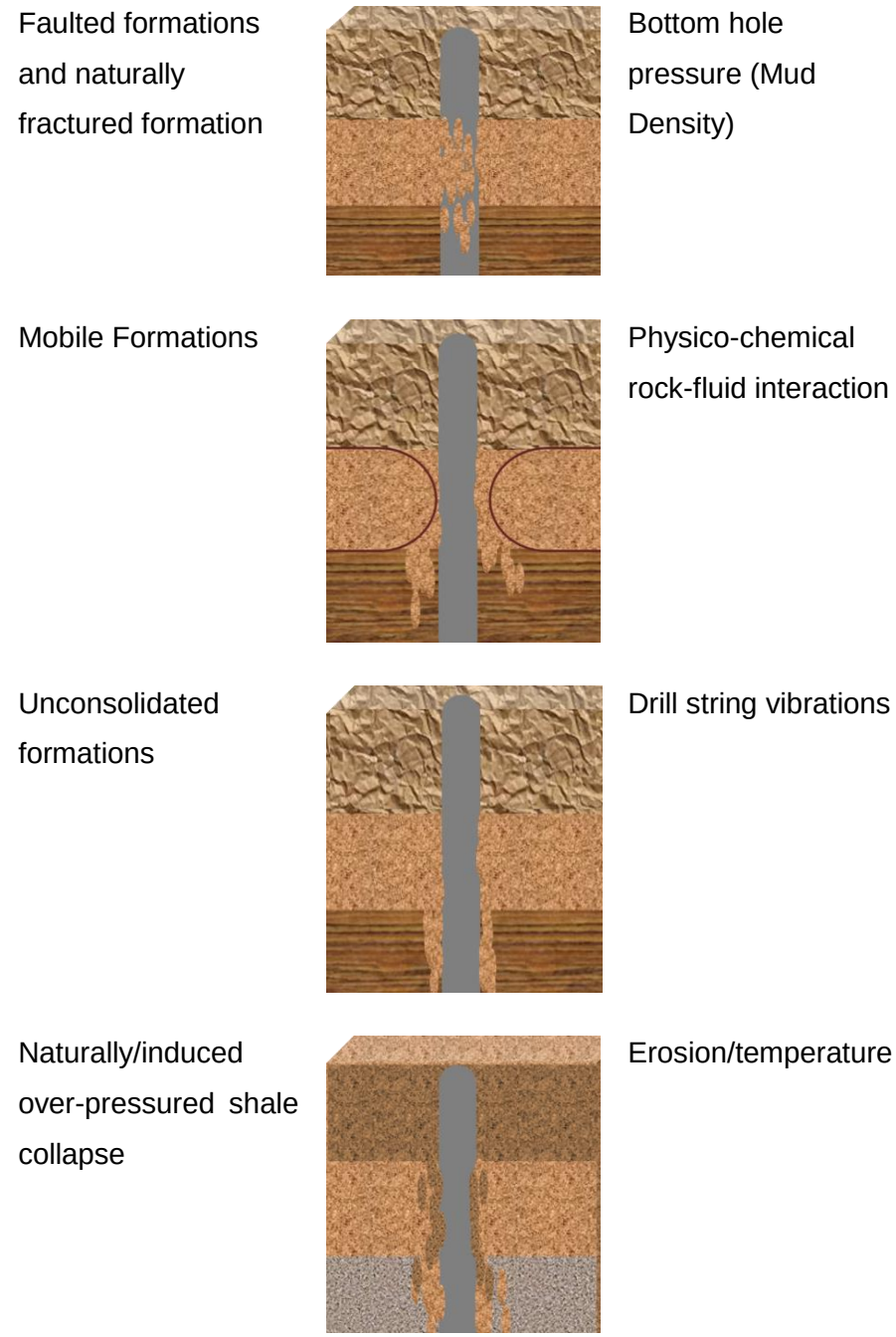

Figure 2.2 Causes of wellbore instability (Pasic, et al., 2007)

2.4.4 Cracking process in sandstone

Cracking takes different forms (Pininska, 2000), depending on the mineral composition and structure of the rock medium (Cundall and Fairhurst, 1986). Strength experiments conducted in the laboratory reveal that the primary factors responsible for destabilization of the rock structure under compression are the size, geometry

and strength of the mineral components of the rock. These and many other properties of heterogeneous rock influence cracking (Pininska, 2000). Simulation of cracking process in media having varying structure was explained at microscopic scale Napier and Peirce (1995). It showed that the level of advancement of tensile and shearing process during cracking is a function of the rock and the dynamics of its deformation. The process of cracking has a discontinuous character and varying dynamics as a result of the heterogeneity of the rock structures. The cracking process can be increased or reduced depending on the local characteristics of the rock structure and the actual stage of stability (Pinińska, 2008). In order to analyse the mechanism of cracking and evaluate its dynamics and its acoustic emission path, it is necessary to study the features of the structure in relation to the observations of the shape at the centre of cracking. This require their initial orientation and its modification during their compositional development (Pinińska, 1997).

2.4.5 Significance of strength characterization studies to field work

Detection of rock failure threshold is important because drilling operations involve compression on rock mass, the induced stress on rock sometimes exceeds the rock strength and the rock failure leads to a catastrophic event. However, fracture predictions can be made by applying damage threshold criteria into compressional simulation of rock.

Prediction of rock strength using drilling data and sonic log is feasible. This will require a correlation of UCS with crack initiation and crack damage stresses. By applying micro-damage analysis, generated with UCS we can measure rock strength from a drilling program. Sonic travel time is a property of rock used to evaluate source rock. The property is also used for mechanical analysis. A drilling process is coupled with log data which are recorded as sonic travel. This is usually received as lithology, porosity or fluid content. In some drilling process, neutron density log is coupled to drill string to receive strength data for rock. These drilling data is though useful to predict rock strength. This requires the use of drilling models (Amani and Shahbazi, 2013; Palchik, 2010) the equation that correlates the petrographic and strength parameter of rock is limited to UCS. Thus the micro-damage thresholds obtained in

is correlated to porosity to obtain a constant. This constant is a controlling factor useful for fracture prediction.

2.4.6 Factors influencing the mechanical behaviour of sandstone

The factors affecting the mechanical behaviour of clastic rocks have been studied. Dhakal et al. 1993 found that the mineral composition and structural features affect the mechanical behaviour in argillaceous clastic rocks. The influence of grain or clasts size in sandstones (Hirth and Lothe, 1982) and crystalline rocks have been observed on peak strength in uniaxial testing (Meng and Pan, 2007). Lindquist (1994) has also observed that the mechanical behaviour of heterogeneous materials is substantially affected by the proportion of larger clasts. Similarly, other factors responsible for increasing the strength of clastic rocks include increase in the clast-cement contact area (Ulusay et al., 1994), the strength of the cement, also known as the quartz content (Sabatakakis et al., 2008) and the clast packing density (Bell, 1978). Andriani and Walsh (2002) also discovered that the mechanical and petro-physical properties of clastic rocks are influenced by their size, shape and packing of grains, the cementing matrix and porosity. These are all controlled by the rock's depositional history. Therefore, failure in such rocks is controlled by the collapse of cemented grains which provide the zones of stress concentration at the clast-matrix interface (Handy, 1990). This is due to the stiffness contrast with cracks generally initiating and propagating away from such zones (Pollard and Aydin, 1988).

Table 2.2: Summary of mechanical parameters of sandstone.

Location	Test	Parameter	Value	References
Green river Basin Wyoming, USA	Triaxial compression test	E,GPa V UCS,MPa C, MPa T, MPa	13.37 0.25 61.7 13.36 6.9	S.J Wilkins (2007)
Lithgow Australia	Not known	UCS,MPa E,GPa V T, MPa C, MPa	7 7 0.25 1 1.5 55^0	Haque, A Chan, K Christie, D (2003)
Hawkesbury Sydney Australia	Uniaxial Compression test	UCS,MPa	23.8	Pells P.J (2004)
Not known	Uniaxial Compression test	UCS,MPa E, GPa v	44.56 23.28 0.161	Peng S. Zhang J (2007)
North Sea	Triaxial Compression test	E, GPa V UCS, MPa	2.228 0.07 15	E. Papanichas E.M Malmanger (1999)

* UCS- Uniaxial Compressive Strength, E- Young's Modulus, v - Poisson's ratio, σ_t – Tensile strength, φ – Angle of Friction, c – Cohesion.

2.4.7 Effect of grain arrangement

Apart from the physical and mechanical properties of quartz grains, their arrangement, distribution and proportion in the matrix are also important factors that have been investigated to influence the mechanical response of sandstone (Hawkes and Mellor, 1970). For instance, Moon (1993) has shown the influence of the loading axis on the compressive and tensile strengths of rocks in relation to the orientation of the quartz present in the matrix (Moon, 1993). His results were confirmed by Ozbek (2009) who investigated sandstone with the Schmidt rebound hammer and found out that the hammer rebound values changed in relation to, the preferred orientation of the embedded quartz. The change is due to the variation of the quartz-covered area (Johansson, 1976) and the random distribution or preferred orientation of the quartz and matrix ratio (Özbek, 2009).

Furthermore, laboratory testing on natural and synthetic sandstone rocks showed that the overall strength and deformation properties of composite heterogeneous rock such as sandstone can be estimated by the strength and deformation characteristics of the infill matrices and quartz (Cecconi et al., 1998). The strength of sandstone depends on the volumetric proportion of quartz (Kobayashi, 1995). It is not practicable to completely disintegrate quartz for the estimation of the particle size distribution and volumetric proportion of quartz in well-cemented rock. This is a function of the scale used for testing (Bjørlykke, 2015). It implies that only a low value of coefficient of variation can be determined at any scale by putting a restriction on the maximum quartz size to the sample size ratio, as suggested by ISRM (1983).

Savanick and Johnson (1974) conducted an investigation on calumet conglomerates to uncover the tensile strength of interface boundaries between the quartz and infill matrix. Their findings show that the interface bond only occurs on a portion of the contact area and the strength of the adjacent materials.

The literature referred to above indicates that the mechanical response of rock to stress is a result of a complex combination of composition and mechanical properties. Some of these properties are quartz and matrix, size distribution, arrangement of the quartz and the micro mechanisms occurring at the grain scale. Therefore, deformation of natural rock depends on specific parameters describing the microscopic behaviour of the rock. This implies that discrete examinations are justified because of the many contributing factors and parameters which are discrete mineral component. The cemented matrix may have properties which are directional. That is they could be anisotropic in their natural or stressed state. The stress loads on rock is crucial and need to be measured to obtain clues on their strength characteristic before mechanical handling.

2.5 Anisotropy and challenges with stress measurement

This section discusses the challenges in determining the microscopic geo-mechanical characteristics of rock which serve as the research gap in this work.

2.5.1 Micro mechanical damage and micro measurement

An undisturbed rock mass can be subjected to natural stress such as gravitational stress because of the overburden pressure. The disturbance are probably tectonic stress as a result of the straining of the earth's crust or they may be caused by the resultant stress due to past tectonism (Amadei and Stephansson, 1997). Micro measurement stress field must be considered in any rock engineering design together with general rock mass properties such as strength, permeability, deformability and time dependent behaviour (Amadei, 2012). For instance, the choice of the best direction and shape for complex underground works can be controlled by the direction and magnitude of the micro stress field, if it is necessary to minimize stress concentration problems. The possible hazard of an earthquake may be evaluated by the long term variation of the micro measurement of parameters within the stress field (Amadei, 2012). Thus the gap in field or industry is to understand and explain the magnitude and direction of the stress field at a point within a rock mass. This will provide the early detection of pending rock fractures. However, there is no known technique for the accurate measurement of the state of stress at a point even when the currently existing measuring instrument is remotely located (Amadei, 2012). In the drilling industry this includes neutron logging, uniaxial compressive strength (UCS) log, porosity-log received by drillers when they employ the technique of logging-while-drilling.

Generally, measurements are made on the internal surface of underground cavities and most of the measurements are done by deliberately disturbing the state of the stress in a rock. Then the resultant strains and displacements are measured. The measured strains and displacements are then compared with the stress having made some assumptions about the material behaviour (Baldi et al., 1988). A common method is to assume that the rock mass is linearly elastic, isotropic, continuous and homogeneous (Amadei, 2012). Apart from the error in measurement which can be reduced by taking proper care when taking the measurements, another major cause of error is the inadequacy of the analytical formulations that is used to convert data into rock stress (Amadei, 2012). The reliability of the micro stress determination can be improved by increasing the accuracy of the mechanical model used for the analytical formulation (Papanastasiou and Zervos, 2004). Typically, a rock is anisotropic and/or heterogeneous and/or discontinuous and deformation, even when elastic is somewhat non-linear in nature (Amadei, 2012). A medium is anisotropic if

its properties changes with direction, it is heterogeneous if its properties changes from point to point, while it is discontinuous if there is a separation or gap in the stress field (Nemat-Nasser and Hori, 2013).

A medium is said to be elastic if the deformation relating with its loading is fully recovered during unloading (Karner et al., 2005). In terms of load deformation or stress strain curve, there is a direct relationship between stress and strain. If the stress and strain are linearly related, the material is said to be linearly elastic. An important characteristic of the linear elastic theory is the principle of the superposition effect. Furthermore, the applicability of the theory of elasticity is dependent on the duration of loading. Elasticity assumes an immediate response upon application or removal of loads (Amadei, 2012).

Anisotropy is the main characteristic of schist, slates, gneisses, phyllites and other metamorphic rocks consisting of parallel arrangement of flat or long minerals (Hakala et al., 2007). Bedded rocks such as sandstone consisting of interlayered mixtures of different components also display anisotropy. Also some isotropic rocks such as granite and limestone will behave anisotropically if they are cut by regular joint sets. A general classification of rock anisotropy was proposed by Barla (1974). It consist of classes A and B rocks. Class A rocks show anisotropic characteristics despite apparent isotropy. Some granite rocks fall within this category. While Class B rocks show clear evidence of anisotropy and display apparent direction of symmetry (Barla, 1974).

The purpose of this research is to utilize the anisotropic property of rock to measure micro-stress and strain/displacement from a single point location in a rock. It is thought that the rock can exhibit anisotropy based on observation of the stressed model under a polariscope.

2.6 Exploration drilling of sandstone and suggested solution

Exploration drilling suffers loss by sustaining significant financial loss and even human loss of lives because of the lack of the knowledge of the strength

characteristics of the rock with respect to its inherent petrography. The crumbling nature of the reservoir rock may be both advantageous and disadvantageous. It is advantageous in the sense that it enhances more crude oil flow at production. This is because the generation of the fines widens pore throat. But grain crumbling is disadvantageous because they are accidental occurrences which could cause a kick. If the exploration drilling is not drilled for a kick, then, a blow-out may occur (Mouchet and Mitchell, 1989). The quality of drilling is therefore dependent not only on the formation pressure (Mouchet and Mitchell, 1989). It is necessary to incorporate a flexible program including monitoring the petrographic strength characteristic of the rock, so that as the drilling progresses, there would be consistent and continuous evaluation of formation pressure. Thus, the strength characteristic that accompany the petrology of the rock layer encountered can be captured while drilling. An example of UCS logging has been presented by some driller (Mouchet and Mitchell, 1989).

This research primarily provided stress threshold of Niger delta sandstone to a drillers. It contributes to the prediction of cracking in the sandstone layers. It is relevant to petroleum engineers because it helps them to incorporate the phenomenon that leads to the formation of crumbing and disintegration to their rock. This is because the damage threshold that will be obtained can be correlated to UCS logging and the early indication of onset of rock damage is realistic. By utilizing the existing sonic and UCS log data, which is currently used to monitor the lithology in every depth as the drilling progresses, we can correlated damage parameters. Therefore, this work evaluates the crack initiation stress and crack damage stress which can be and serve as damage thresholds in a UCS log data. This is then used as indicators for crack predictions in the sandstone layer. It may further be utilized to predict cracks in other layers too. Figures 2.3 shows a schematics logging data plot of the oil bearing sandstone data in one of the oil well in the research area.

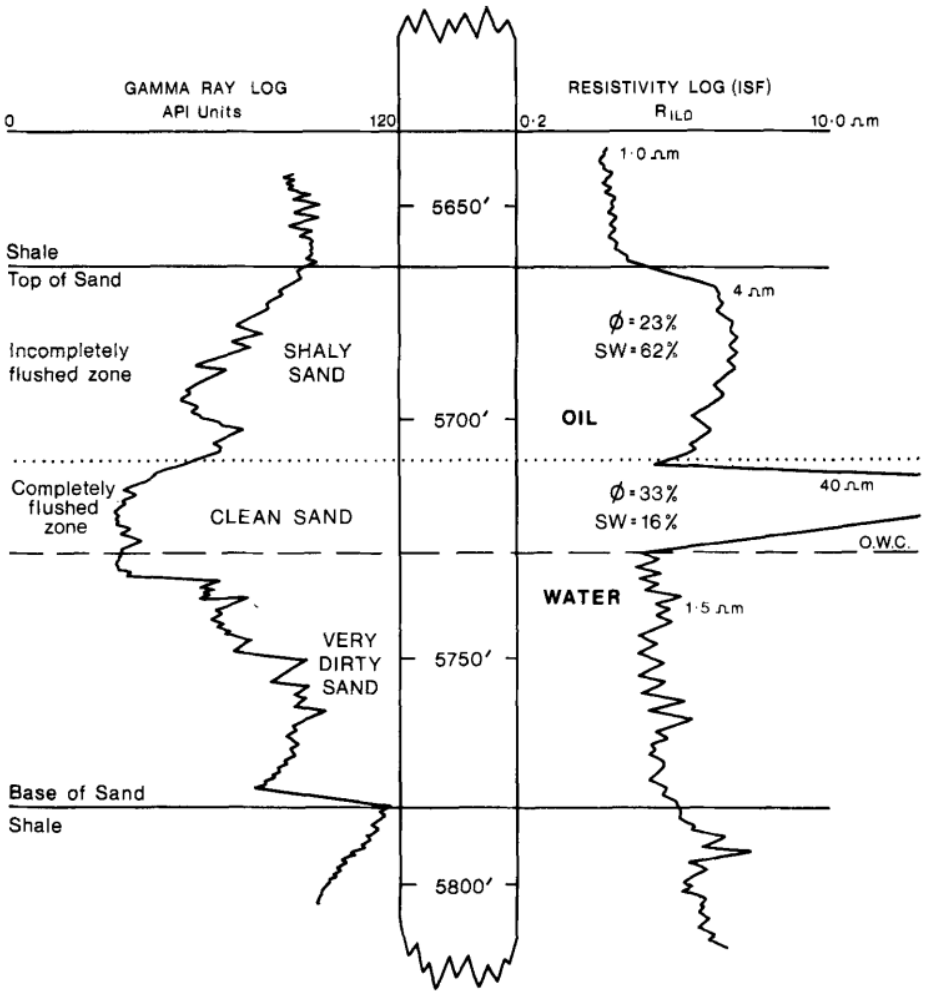

Figure 2.3 Schematic representation of the log through a hydrocarbon and water-bearing sandstone of the Agbada formation after Lambert and Shaw, (1982).

2.7 Strength characteristics of sandstone and log data

The strength characteristics of rocks in-situ are determined by fluid pressure. The pore pressure in the formation may exceed the rock strength, the axial drill stress may also exceed the strength of the rock; either of these can cause rock failure**.** Sonic travel time is a physical property of rock used for mechanical study of rock. It indicates the fluid content, porosity and the lithological effect. Similarly, neutron density log is employed for conveying rock strength from logs. They have been used for rock property estimation during drilling operations as substitutes for rock sample. some correlations between rock properties and the strength have been discussed (Chang et al., 2006).

In recent practice, the general rock failure criteria have been reduced to a few parameters which rely on lithology and compressive strength. Lithology is routinely derived during logging by estimating porosity or sonic velocities using pre-determined compressive strength. In granular rocks, porosity will only influence strength, if and only if grain, mineralogy and texture, are constant. This implies that a low porosity means greater strength if other factors are constant. A degree of micro-deformation has been observed in several sandstones and has been correlated in terms of grain contact models. Many petro graphical properties such as quartz, clay content, or feldspar have significant influences on strength while drilling of rocks with varying mineral content. Therefore, this inclination of porosity from strength may not work. Hence relating the petrography to the lithology becomes very vital.

Drilling operations require reliable estimates of formation pressures in order to use appropriate weight of drilling mud and design wells for project optimization. This is because if pressure data are wrong, well-instability is most likely to occur. Other side effects include stuck pipe, poor return of mud leading to kicks and influxes and eventually blowouts. Consequently, inappropriate pressure strength data could damage the formation and lead to the loss of the well (Nwozor and Onuorah, 2014). In the absence of accurate pore pressure prediction, the stress threshold of the formation rock can serve as a fracture indicator.

This is important because product of weathering and mica are found in the shale layer; this has been said to be deposited due to reactions of illite with oil in the formation (Pevear, 1999). Illite is mostly found as clay in sandstone. Its occurrence increases with depth and temperature in the Niger delta formations due to their geologic age (Eslinger and Pevear, 1988).

An industrial application involves obtaining a correlation between crack damage stress and Uniaxial Compressive Strength (UCS) obtained from drilling log data. This is used to explain the micro-mechanical response of the sandstone layer from the drilling log data. Some authors have shown that the drilling log data from the wellbore can be employed to evaluate UCS along the borehole (Militzer and Stoll, 1973). Many equations have been developed to correlate the petro-physical properties of rocks to

their strength (Golubev and Rabinovich, 1976). What is evident in the equations is that lithological properties are diverse and each of these properties affects rock strength differently (Militzer and Stoll, 1973). They are more complicated because the petrological properties that affect the strength also affect other physical properties of the rocks. Although the equations predicted UCS, strength characteristics vary with every single physical property which is prune to affect drilling log data. This implies that existing equations can be improved by accompanying the equations with micro-mechanical strength data in order to improve the existing equations. The experimental data on core sample is provided here. However, the correlations to micro-mechanical data can improve the log data because rocks of similar lithology may exhibit different strength characterization. This is due to the differences in depositional environments which invariably causes differences in composition. Therefore each empirical equation should be accompanied by micro-mechanical parameters for drilling though a borehole. Thus, different equations results for a specific region of rocks as a result of specific petrological properties. This culminates in the significance of local calibration for equations before they are initiated to predict UCS. Thus it is recommended that the addition of indicators like the damage threshold e.g. crack initiation stress, crack damage stress and the yield point to together with the UCS drilling data can help early crack detection. This is because they are micro-mechanical data that are sensitive to lithology and have lower values which are detected before the compressive failure point (Brace and Byerlee, 1966). The determination of this failure indicator will be done in chapter seven and eight.

The investigation on the strength characteristics of rock will be carried out in Chapters 3 to 8 by methodological identification of the different phases in the strain response of rock to compressional stress.

2.7.1 Grain matrix and stages of rock failure in the field

Sandstone is a rock of significant porosity that bears hydrocarbon fuels in them. Studies on the deformation mechanism have been done by researchers including Holyoke and Rushmer (2002) and Vyacheslav et al (2007). The mechanism of deformation involves initial closed fissures within the rock, next is the linear elastic deformation stage followed by the crack steady expansion process, and thereafter, unsteady expansion occurs. The first obvious step is the crack initiation

and is theoretically significant to understanding the stress state of the mass structure. It is a useful tool for in situ rock strength investigation which is very important while drilling through sandstone containing crude oil. Oil well drilling deformation leads to well instability. Well instability simply means the strain in sandstone formation due to prevailing in-situ stress. The fracture in the direction perpendicular to drilling string creates an aperture for stress gradient between the rock stress and the stress in the hole. This response is usually instantaneous at the time of drilling (Mohiuddin et al., 2001). An investigation into the strength show that the deformation process began with the grain expansion under crack closure.

The grain arrangement changes through elastic expansion as the grain dilates to initiate crack which then propagates to form fractures. The investigation tool is the crack initiation stress, crack damage stress and peak stress of the sandstone which are indicators of possible factures that result into borehole instability. The grain and bond properties are used to identify possible crack initiation stress, grain cohesion, internal friction angle and the elastic properties of the rock mass at large (Potyondy and Cundall, 2004). The grain properties are fundamentally significant data which explain the route to well instability, these properties can be useful tools for preventing the occurrence of the well instability (Cho et al., 2008). Therefore measurement of grain scale is important.

The challenges with point measurement in rock will be tackled in this work by using discrete element modelling (DEM) as a tool. The micro-properties of point data will be compared with the data from micro-measurement techniques, using ultrasound measurements and Photo Stress Analysis Tomography (PSTA) which is discussed in the next section. The next section explains the role that (DEM) plays in order to tackle the challenges of obtaining micro-measurement at single point in rock.

2.8 Discrete element modelling (DEM) and grain contact linkage

The particle-based model was originally developed to simulate the micro-mechanical behaviour of non-cohesive media, such as soils and sands (Cundall and Strack, 1979b). With this technique, the granular micro-structure of the material is modelled

as a statistically generated assembly of rigid circular particles of different diameters. The contacts between particles are typically assigned normal and shear stiffness as well as a friction coefficient. The commercially available code Particle Flow Code (PFC) represents an evolution of previous particle-based codes such as BALL and TRUBAL (Cundall and Strack, 1979b), which applies cohesive bonds between particles to simulate the behaviour of solid rocks. The resultant model is commonly referred to as the Bonded-Particle Model (BPM) for rock (Potyondy and Cundall, 2004). In a BPM, crack nucleation is simulated through breaking of internal bonds while fracture propagation is obtained by coalescence of multiple bond breakages. Blocks of arbitrary shape can form as a result of the simulated fracturing process and can subsequently interact with each other (Lisjak and Grasselli, 2014).

The two types of bonds normally used in PFC are contact bond and parallel bond. In contact bond model, an elastic spring with constant normal and shear stiffness, acts at the contact points between particles thereby allowing only forces to be transmitted. While in the parallel bond model, the moment induced by particle rotation is resisted by a set of elastic springs uniformly distributed over a finite-sized section lying on the contact plane and cantered at the contact point as shown in Figure 2.3. This type of bond model reproduces the physical behaviour of a cement-like substance gluing adjacent particles together (Lisjak and Grasselli, 2014).

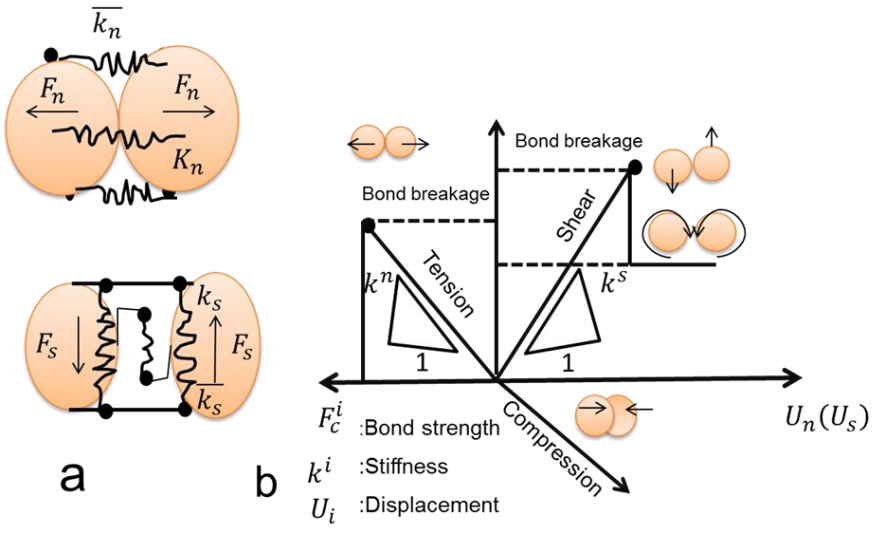

Figure 2.4 The parallel bond model implemented in PFC. (Cho, et al 2007)

From Figure 2.4, (a) represent normal and shear stiffness between particles. The contact stiffness, k_n and $k_{s,}$ remain active even after the bonds break as long as particles stay in contact. The bond stiffness (per unit area), $\overline{k}n$ and $\overline{k}$s, are suddenly removed. The bonds break regardless of whether particles stay intact or not. (b) Represents constitutive behaviour in shear and tension$(i = s, n)$.

However, one of the major disadvantage of this type of model is the unrealistic low ratio of the simulated unconfined compressive strength to the indirect tensile strength for synthetic rock specimens (Kazerani and Zhao, 2010); the straightforward adoption of circular (or spherical) particles cannot fully capture the behaviour of complex-shaped and highly interlocked grain structures that are typical of hard rocks (Cho et al., 2007). Moreover, low emergent friction values are simulated in response to the application of confining pressure. To overcome these limitations, a number of enhancements to PFC were recommended. Potyondy and Cundall (2004) showed that by clustering particles together as illustrated in Figure 2.4a, more realistic macroscopic friction values can be obtained. Specifically, the intra-cluster bond strength is assigned a different strength value than the bond strength grain cluster boundary. Cho et al. (2007) showed that by applying clumped-particle geometry as illustrated in Figure 2.4b. A significant reduction of the aforementioned deficiencies can be obtained. Hence strength ratio and non-linear behaviour of strength envelopes and frictional coefficients can be reproduced. These values are comparable with laboratory values. Potyondy (2012) recently developed a new contact formulation known as the Flat-Joint Model (FJM), which is aimed at capturing the same effects of a clumped BPM having more computationally efficient method as illustrated in Figure 2.4c. The partial interface damage and continued moment-resisting ability of the Flat-Joint Model allow the user to correctly match both the direct tensile and the unconfined compressive strengths of rock.

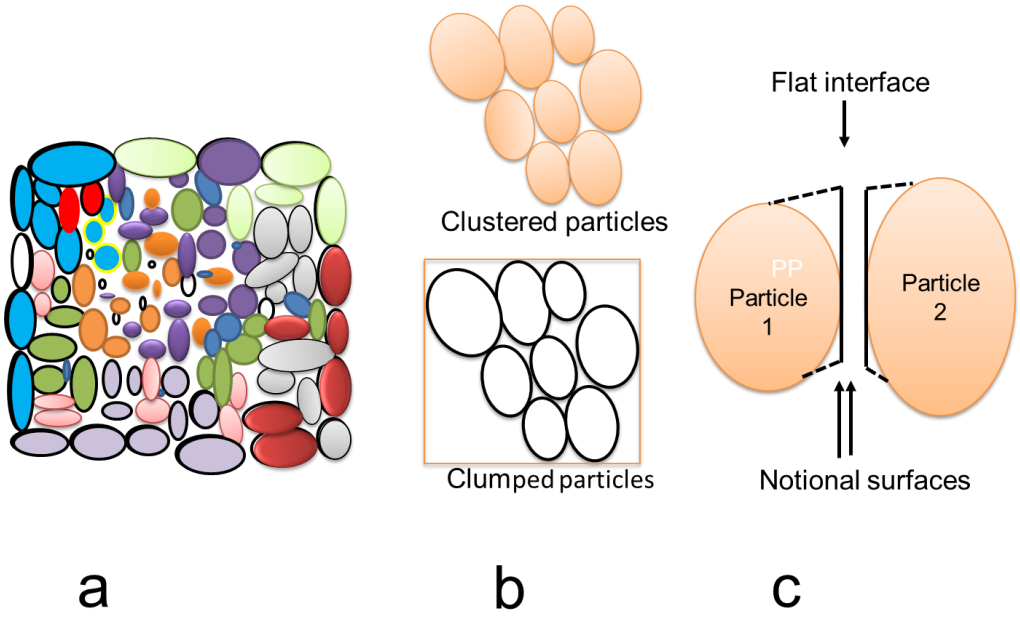

Figure 2.5 Proposed enhancements to the original BPM to capture realistic values

In the proposed enhancement to BPM of Figure 2.5 above, (a) represent Particle Clustering (Potyondy and Cundall 2004), (b) represent Clustered particles (Cho et al. 2007) and (c) represent Flat-Joint Model contact (FJM) showing the effective interface geometry (Potyondy 2012).

Another issue emanating from the particle-based material representation of PFC is the inherent roughness of interface surfaces representing rock discontinuities is illustrated in Figure 2.5a.This roughness typically results in an artificial additional strength along frictional or bonded rock joints. The problem was solved by the development of the Smooth-Joint contact Model (SJM). This enables the user to simulate a smooth interface regardless of the local particle topology as illustrated in Figure 2.5b (Mas Ivars et al., 2008). The ability of the BPM to capture the behaviour of intact material with the SJM for joint network leads to the development of the numerical rock mass. This aims at numerically prediction of rock mass properties. The solution include scale effects, anisotropy and brittleness, which cannot be obtained using empirical methods (Ivars et al., 2011).

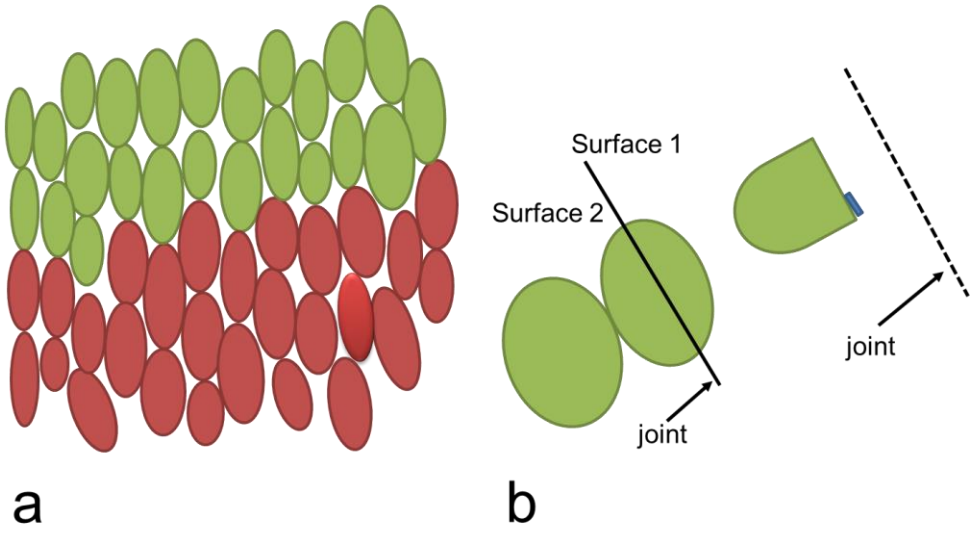

Figure 2.6 Representation of rock joints in PFC (Ivars et al., 2011)

Figure 2.6 (a) represent Traditional representation with rough surface and (b) represent Smooth-joint contact model (Ivars et al., 2011).

The particle-based code Yade developed by (Kozicki and Donzé, 2008; Kozicki and Donzé, 2009; Šmilauer et al., 2010), was recently introduced as an alternative modelling platform to the commercial software. The primary aim of the Yade project is to provide enhanced flexibility in terms of adding new modelling capabilities. It promotes code improvement through open-source development and direct feedback from the scientific community (Lisjak and Grasselli, 2014). In its basic formulation, the contact laws implemented in Yade share the same principle as those available in PFC. Small deformation is captured by linear elastic interaction forces between contacting discs/spheres. Rock fracturing is captured by ruptured bonds, whose strength is characterized by a constant maximum acceptable force in tension and a cohesive-frictional maximum acceptable force in shear. The shear strength drops instantaneously to a purely frictional resistance after failure. Conversely, in tension, after the maximum force is attained, the stiffness can be varied by a softening factor (ζ), controlling the energy released due to bond breakage as illustrated in Figure. 2.7a. Rock discontinuities can be treated in Yade by using a contact logic analogous to the SJM of PFC. Specifically, the interactions between bonds crossing a prescribed discontinuity plane are identified. It was re-oriented according to the joint surface. This ensures a frictional behaviour that is independent of the inherent roughness

induced by the particle topology. Applications of Yade to the investigation of the fundamentals of brittle rock failure have led to the implementation of an interaction range coefficient (γ). It can be used to join particles not directly in contact one with the other, yet closely located as illustrated in Figure 2.7b. By this, the degree of interlocking between particles can be effectively controlled. Therefore modelling of high ratio of compressive to tensile strengths can be numerically done. This approach represents an alternative to the clumping logic and the Flat-Joint contact model of PFC.

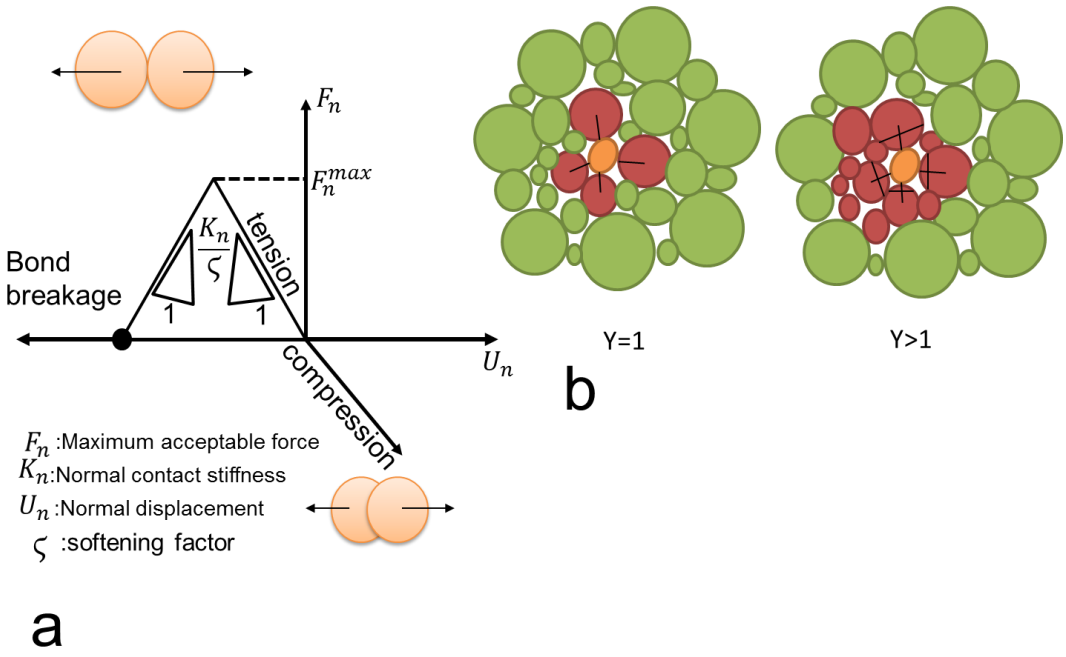

Figure 2.7 (a) represent the Interaction law between particle in tension and compression, (b) represent the effect of the interaction range coefficient on the simulated contact fabric (Scholtès and Donzé, 2013).

The advantages of the particle-based modelling methodology include the simple mathematical treatment of the problem. The complex constitutive relationships are replaced by simple particle contact logic, and the natural susceptibility of the approach to account for material heterogeneity. Due to the high level of simplification introduced, extensive experimental validation is needed to verify that the method can capture the observed macroscopic behaviour of rock. Furthermore, an extensive calibration based on experimentally measured macro-scale properties is required to

determine the contact parameters that will predict the observed macro-scale response (Lisjak and Grasselli, 2014).

2.8.1 Applications of DEM to rock mechanics

PFC has been used within the rock mechanics community to numerically investigate the fundamental processes of brittle fracturing in rocks by means of laboratory-scale models (Lisjak and Grasselli, 2014). The first proposed synthetic PFC model that could reproduce modulus, unconfined compressive stress, and crack initiation stress of the Lac du Bonnet Granite was developed by Potyondy et al. (1996) and Lisjak and Grasselli, (2014). Extended results were illustrated by Potyondy and Cundall (2004) with the simulation of the stress–strain behaviour during biaxial compression tests for different confining pressures. Several features of the rock behaviour emerged from the BPM, including elasticity, fracturing, damage accumulation producing material anisotropy, dilation, post-peak softening and strength increase with confinement. PFC simulates quasi-static deformation by solving the equations of motion, elasto-dynamics effects, such as stress wave propagation and cracking-induced AE, can be explicitly simulated. In this context, Hazzard and Young (2000) developed a technique to dynamically quantify AE in a PFC model. This technique was validated by simulating the seismic value of a confined test on granite. The technique was further improved by introducing moment tensor calculation based on change in contact forces upon particle contact breakage and was applied to the micro-seismic simulation of mining by experiment in a crystalline rock (Hazzard and Young, 2002) and of an excavation-induced fault slip event (Hazzard et al., 2002). Hazzard and Young (2004) proposed 3D simulations of acoustic activity using PFC3D. Diederichs (2003) used PFC simulation to analyse the aspect of grain-scale tensile damage accumulation under both macroscopically tensile and compressive conditions. A BPM was developed as numerical analogue to study the effects of tensile damage and the sensitivity to low confinement in controlling the failure of hard rock masses within the proximity of underground excavations. Analyses of failure and deformation mechanisms during direct shear loading of rock joints was carried out to obtain original insights into rock fracture shear behaviour and asperity degradation (Lisjak and Grasselli, 2014). Rasouli and Harrison (2010) investigated the relationship between the Riemannian roughness parameter and shear strength of profiles comprising symmetric triangular asperities sheared at different normal stress levels. Asadi et al. (2012) improved on the previous results by considering the shear

strength and asperity degradation processes of several synthetic profiles using triangular, sinusoidal and randomly generated profiles. Zhang and Wong (2012) numerically simulated the cracking process in rock-like material containing a single flaw under uniaxial compression, while Zhang and Wong (2013) investigated the coalescence behaviour for the case of two stepped and coplanar pre-existing open flaws. The effect of confinement on wing crack propagation was studied by Manouchehrian and Marji (2012).

BPM has been successfully applied to the study of damaged zones around underground openings. The spalling phenomena noticed around the Atomic Energy of Canada Limited's (AECL) mining by experimental tunnel were first simulated by Potyondy and Cundall in 1998, (Martin et al., 1999). Further analysis of the notch formation process in terms of coalescence of ruptured bonds was developed by Potyondy and Cundall (2004) using a PFC2D model embedded in a continuum finite-difference model as illustrated in Figure 2.7a. Hazzard and Young (2002) provided a micro-seismic simulation of the same excavation by comparing the actual seismicity recorded underground with the simulated spatial and temporal distribution of events. The effect of low stiffness spray-on line of fracture propagation based on in situ conditions of the above mentioned mine-by experiment was numerically studied by Tannant and Wang (2004). Similarly, Potyondy and Autio (2001) employed PFC2D to predict damage formation adjacent to a circular excavation in an anisotropic gneissic tonalite at the Olkiluoto deep geological repository. Furthermore, Fakhimi et al. (2002) showed that a BPM could match failure load, crack pattern, and spalling observed during a biaxial compression test on a sandstone specimen with a circular opening as illustrated in Figure 2.7b. Numerical study on thermally-induced fracturing around an opening in granite was carried out by Wanne and Young (2008) and Wanne (2009) for a laboratory-scale heater experiment. The AECL's Tunnel Sealing Experiment was carried out on the same rock.

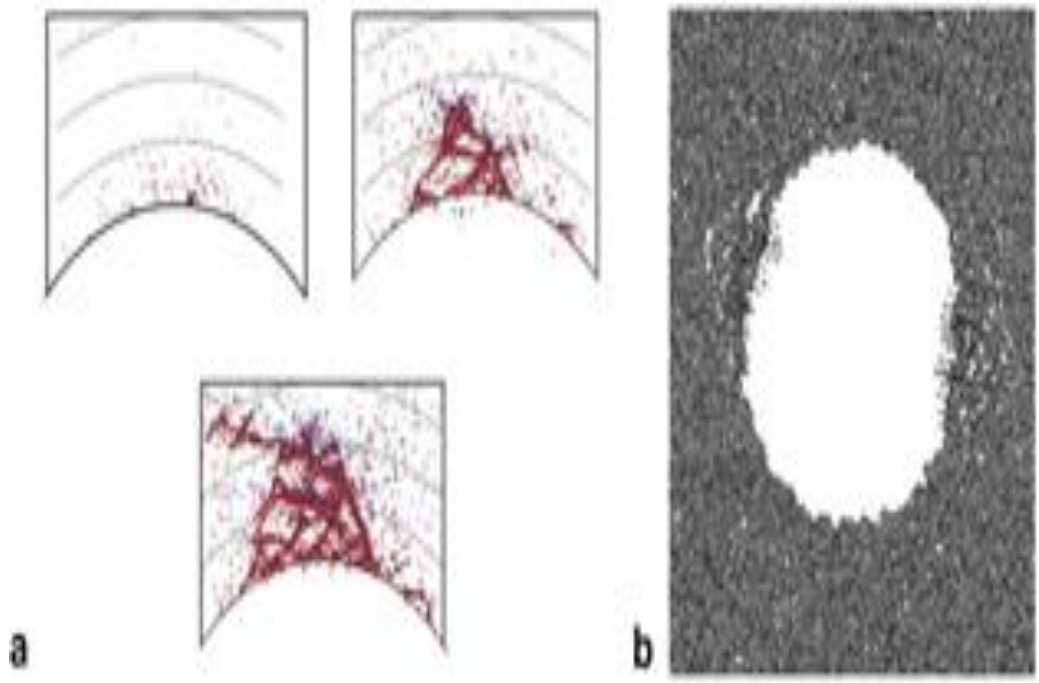

Figure 2.8 Simulation of fracture development around underground excavation using PFC. (Potyondy and Cundall, 2004)

Figure 2.8 (a) represent modeling of notch formation around the AECL's mine by experiment tunnel (Potyondy and Cundall, 2004) and Figure 2.8 (b) represent Damaged notches around a hole under biaxial compression (Tarokh et al., 2012). Simulation studies using the open-source code Yade have focused on the role played by Discrete Fracture Networks (DFNs) (Scholtès et al., 2011), this was done by Scholtès and Donzé (2012). The grain interlocking behaviour controls the mechanical responses of 3D rock samples.

2.8.2 Solutions to micro-data generation from alternative numerical methods

In this section an overview of alternative techniques that are considered to have the potential for modelling the mechanics of granular rocks, such as sandstone is presented. Several numerical methods have been applied in rock and soil mechanics to solve the problems (Jing and Hudson, 2002). The two main alternative techniques are continuum mechanics and dis-continuum mechanics. The techniques which are based on continuum mechanics are Finite Difference Methods (FDM), Finite Element Methods (FEM) and Boundary Element Methods (BEM). Dis-continuum mechanics mainly consist of Discrete Element Methods (DEM) (Jing and Hudson, 2002). The

two main techniques have associated advantages and disadvantages and their applications primarily depend on the properties of the materials to be modelled.

Unlike the continuum method, DEM is an approach to numerical simulation where statistical measures of the global behaviour of a phenomenon are computed from the individual motion and mutual iterations of a large population of elements. It is mainly used in situations where theoretical knowledge has not provided complete understanding and mathematical equations to model the physical system. This method has been implemented in various forms based on the geometry of discrete bodies and the mode of deformation representation. The most important advantage of DEM is to model granular media with particle shapes and rock mass incorporating discontinuities which was not effectively possible using FDM, FEM and FBM. The macro behaviour of a granular system based on the interaction and movement of the discrete particles can be modelled using DEM. It is relevant to utilize it for the studies of sedimentary rocks (Jing and Hudson, 2002).

2.9 Overview of a bonded discrete assembly

Rock mechanics is one of the disciplines from which DEM originated (Cundall, 1974). The formulation of the method is based on the solution of equations of motion of rigid and/or deformable bodies using implicit (FEM discretization) and explicit (FVM discretization) formulations (Jing, 2003). This method has been widely used in soil and rock mechanics and in other disciplines, like structural analysis, granular materials, material processing, fluid mechanics, multi-body systems, and robot simulation and computer animation since its origin (Jing and Hudson, 2002; Jing, 2003). It is one of the most rapidly developing areas of computational mechanics and is still in the developmental phase.

The primary objective of DEM is to circumvent the complexity of a large assembly by considering many sample elements, the behaviour of which can be simulated accurately (Ferrez, 2001). After the theory proposed by (Cundall, 1971), various theoretical formulations have been developed to simulate discontinuous media and these became known as discrete element methods. Cundall and Hart (1992) proposed a formal definition for discrete element methods: “the numerical schemes

which can allow finite displacement and rotation of discrete bodies including complete detachment and can recognize new contacts automatically as calculation progresses". These two conditions must be fulfilled to qualify any computational scheme as discrete element methods (DEM) because these conditions produce the important mechanisms of the discontinuous medium for numerous discrete particles (Cundall and Hart, 1992). They also proposed three important aspects of DEM which can help in their classification, as described in the next three sub-sections.

2.9.1 Representation of contact in discrete models

The major difference between continuum and dis-continuum mechanics is the representation of a contact or interface between the discrete bodies that make up a system. This interface may be soft, allowing deformation along the interface/contact, or rigid, with no deformation along the contacts. The selection of contact type mainly depends on the physics of the system (Cundall and Hart, 1992).

2.9.2 Representation of solid material

The material of the discrete bodies in discrete element methods can be grouped into two main categories: rigid or non-deformable and deformable. In discontinuous systems where most of the deformation is along the discrete bodies/particle contacts, the assumption of rigid material can be used to model the system (Zhao, 2010). Early developments in discrete element methods were based on the use of rigid particles as building blocks. There are two approaches to obtain deformable particles. First, the direct sub-division of discrete body into elements of definite deformation zones (Cundall, 1980). The second approach is used to obtain a complex deformation pattern by the superposition of several mode shapes for whole discrete body (Shi, 1988).

Table 2.3: Attributes of the four classes of Discrete Element Methods and the Limit Equilibrium Method (Cundall and Hart 1992).

Attributes		**Class-1**	**Class-2**	**Class-3**	**Class-4**	**Limit Equilibrium, Limit Analysis**
Contacts	Rigid	---	---	xxx	xxx	Xxx
	failure	xxx	xxx	---	---	---
Bodies	Rigid	xxx	xxx	xxx	xxx	Xxx
	failure	xxx	xxx	xxx	---	---
displacement	Small	xxx	xxx	xxx	---	Xxx
	Large	xxx	xxx	xxx	xxx	---
Strain	Small	Xxx	xxx	xxx	---	---
	Large	xxx	xxx	xxx		
Bodies	Fewer	xxx	xxx	xxx	xxx	Xxx
	Many	xxx	xxx	x	xxx	X
Material	Linear	xxx	xxx	xxx	---	---
	Non-linear	xxx	x	---	---	---
No Fracture		Xxx	Xxx	Xxx	---	---
Fracture		x	xxx	---	---	---
Packing	Loose	Xxx xxx	Xxx x	--- xxx	Xxx x	--- Xxx
Static		xxx	xxx	xxx	x	Xxx
Dynamic		xxx	xxx	x	xxx	---

--- does not allow, or not applicable. X can model it, but insufficient or not well suited. Xxx can model it well

2.9.3 Detection and review of contact parameters

There are two tasks to be performed before the start of calculations. First, identify all pairs of bodies that can interact, and second, determination of the type of interaction, (i.e the edges, vertices, face etc, of one particle that is touching the corresponding

entities of the other). Different schemes have been formulated to perform these tasks in two and three dimensions with different computational time (Cundall, 1980). The capability of each class of discrete element methods in response to various attributes is given in Table 2.3.

Table 2.3 suggests that the distinct element methods can allow maximum modelling strength against the given attributes. This provides a more rigorous scheme to solve the problems in relation to a wide range of materials. An example of implicit DEM which can be obtained by upgrading FEM or FDM is Discontinuous Deformation Analysis (DDA). The Distinct Element Method is an example of explicit DEM which yield a macroscopic response of media based on the interaction of discrete bodies (Jing, 2003). The term “Distinct Element Methods” is normally used when DEM is applied in rock mechanics. Discrete Element Methods (DEM) is equally used in other areas (Jing, 2003). Therefore, the broader term “Discrete Element Methods” (DEM) will be used to denote all formulations of DEM that represent an explicit mode of deformation in “Distinct Elements Methods”.

2.10 Previous developments reported using DEM in rock engineering

Several researches have been conducted in the past in the formulations of DEM. These have led to the development of computer codes depending on particle geometry, contact detection schemes and inter particle cement.

2.10.1 Formulations of grains with shapes

Different formulations of DEM have been documented by Jing, (2003) and Bobet et al., (2009) based on particle geometry (i.e. polygonal blocks, circular discs or spheres, ovals and arbitrary shaped particles by overlapping particles to form clusters or clumping spherical particles. The choice of adopting a particular formulation for a given problem is influenced theoretical knowledge of the micro-mechanics of granular media, the nature of the application and the computational resources available (Jing, 2003). However, theoretical understanding of DEM is based on the formulation and solution of equations of motion of rigid or deformable particles (Jing, 2003). In deformable particles, particles are further discretized into finite elements using FEM or FDM formulations which also give deformation (implicit) of particles in addition to

explicit deformation along the particles' contacts. An example of this application is UDEC (Cundall, 1980).

Table 2.4: Examples of DEM computer codes

Authors	Computer Code	Dimension
Lisjak and Grasselli, 2014	PFC and YADE	2D/3D
Lin and NG, 2015	ELLIPSE3D	3D
Alassi et al,.2006	PFC	2D/3D
Cundall and Hart 1985	UDEC	2D/3D
Marketos and Bolton, 2010	PFC	3D
Potyondy and Cundall, 1996	PFC	2D

.

A dynamic contact pattern is the primary constituent of DEM formulations that differentiate them from continuum methods. General formulations of DEM consist of the following requirements (Jing, 2003):

- Distribution of particles within the defined domain (i.e. area in 2D or volume in 3D).
- Assumptions about particle material, e.g. rigid or deformable.
- Development of algorithms for contact detection scheme, e.g. Penalty function, Lagrange multiplier, or augmented Lagrange multiplier.
- Development of constitutive equations for the particles/blocks/fracture system.
- Solution of the integral equations of the motion of the particles.

These requirements remain almost the same irrespective of particle shape or geometry. The formulations of DEM, based on particle geometry are discussed in the following sections.

2.10.2 Polygonal blocks and particle formulation

In rock mechanics, DEM was developed using a two dimensional polygonal rock block system (Cundall, 1971) which was thereafter used for the development of computer code RBM (Cundall, 1974). The RBM then progressed to SDEM to model the deformation of a complex 2D geometry of blocks. A parallel version (CRACK) was developed incorporating the fracturing, cracking and splitting of intact blocks under loading, based on a tensile failure criterion (Jing, 2003). Furthermore, in 1980, UDEC (Cundall, 1980) was developed which had the capability to overcome the incompatibility caused in the SDEM when dealing with deformable blocks with complex geometries of blocks. UDEC was extended to 3D problems (Cundall, 1988) with the development of 3DEC(Hart et al., 1988)). In DEM with blocks, it is assumed that the medium is divided into a finite number of blocks by the intersection of the discontinuities. The technique of the explicit DEM for a block system is presented comprehensively in Cundall and Hart (1992).

2.10.3 Circular discs, spherical particles and particle formation

The potential of DEM to model natural structures was implemented on circular discs in the late 1970s with the development of the computer program “Ball” (Cundall and Strack, 1979b). Earlier works focused on granular assemblies of circular discs in 2D and spheres in 3D. The major motivation for circular discs and spheres was fast contact detection, which increases the number of particles that can be simulated in a reasonable time.

This technique was applied to many problems across a range of scientific disciplines. Major relevant applications include the fundamental investigation and application in cohesive and frictional granular soils and powders; rock mechanics; the experimental validation of DEM; modelling methods; incorporating smooth joints to simulate discontinuities at laboratory and large scale, and industrial applications of DEM (Sallam et al., 2004). For DEM with circular or spherical particles, the medium can be represented by the assembly of circular discs (2D) or spheres (3D) with a set of micro mechanical properties that indicates the contact and bond conditions. The frictional materials can be simulated by grouping circular discs and spheres with micro mechanical parameters, that is, contact normal stiffness (K_n), contact shear stiffness

(K_s) and friction (μ) along the particle contacts. The macroscopic response of the granular assemblies is governed by the interaction of circular or spherical particles.

The cohesive-frictional materials can be simulated by gluing the particles together with a definite set of normal and shear bond strengths (σ_b, τ_b) at particles contacts defined by contact stiffness (K_n and K_s) (GROUP, 2008) and inter particle friction (μ). Different fundamental laws have been proposed for the interaction between particles. The typical computer codes being increasingly applied to model circular discs in 2D and spheres in 3D are particle flow codes PFC2D and PFC3D (Manual, 1995) and EDEM (Solutions, 2010).

The concept of modelling geo-materials as a collection of discrete circular or spherical particles was initially introduced by Cundall and Strack (1979a). The concept was extended and implemented in PFC using a Bonded Particle Model (BPM) (Potyondy and Cundall, 2004). The main advantage of using circular or spherical particles in the modelling of geo-materials is that the computational speed and the efficiency of ordinary personal computers is as good as the contact detection scheme and is computationally straightforward (Brown, 2013).

2.10.4 Elliptical or ellipsoidal particles and rock mass formulation

As stated above, the use of circular or spherical particles allows excessive rotation of particles mainly due to the particle geometry and the point friction at their contacts. Therefore, the true peak strength and the angle of internal friction of the assembly cannot be achieved. In order to eliminate or reduce this rotation, elliptical and ellipsoidal particles are modelled in DEM formulations. Applying this principle, numerous studies were conducted using elliptical particles in two dimensional shape-base in effect (Rothenburg and Bathurst, 1991; Ting, 1991; Wei et al., 1991; Pradhan and Swada, 1992; Ng and Lin, 1995). Rock formulated with elliptical particles yield a model with little tendency for particle rotation. But as with discs or sphere, particle interlocking and angularity-induced dilation cannot be achieved using elliptical particles, which is a characteristic feature of natural granular materials with non-spherical particles (Arkam, 2010).

2.10.5 Polygonal particles and rock formulation

In order to obtain the interlocking of natural granular materials, polygonal shaped particle was studied to simulate the complexities of natural granular materials in both soils and rocks. Particles of arbitrary shapes were constructed joining circular or spherical particles (Ashmawy et al., 2003; Matsushima, 2004; Mouchet and Mitchell, 1989; Nakata et al., 2004; Sallam et al., 2004). Mouchet and Mitchell (1989) simulated “Clump logic”, similar to overlapping clusters, which was proposed in PFC to model rocks or granular materials, in order to obtain true interlocking of the materials, high bulk friction of the assembly (Fu, 2005; Cho et al., 2007; Cho et al., 2008) These studies revealed that macroscopic properties (i.e. peak strength and angle of friction) are greatly influenced by particle shape. The assemblies with polygonal or angular particles can simulate much higher strength and friction compared to assemblies with circular or spherical particles. However, polygonal or polyhedral particles have complexities, such as the generation of angularity, complex contact detection schemes (along nodes and surfaces), and increased computational cost (Sallam et al., 2004).

2.11 DEM simulation of granular materials

An important application area of the DEM is the simulation of the mechanical behaviour of granular materials. From the early application of DEM to granular materials in the late 1970s such as Cundall and Strack (1979a) and Cundall and Strack (1979b), different studies have been conducted to simulate the behaviour of natural granular materials by using different shaped particles (that is circular, elliptical, irregular and polygonal). At first, the behaviour of frictional granular material was widely studied and thereafter DEM was extended to cohesive-frictional materials by incorporating inter particle bonds of specific strengths (Akram and Sharrock, 2010). Consequently, DEM’S area of application is mainly comprised of two classes; first for “frictional materials” (i.e. granular assemblies with no inter particle bonds which comprise of natural materials like sands, gravels, assemblies of steel balls or glass beads). Second for “cohesive-frictional materials” which are simulated by gluing the particles with specific cementing materials so that the failure is always allowed to occur through the cementing material (i.e. along the contacts) and not through the particles, assuming the particles are rigid or deformable bodies. The class of cohesive-frictional granular materials is made up of natural materials such as

cohesive soils, granular rocks and concrete, artificially cemented assemblies (synthetic materials) of irregularly shaped particles, like sands, gravels etc., and uniformly shaped particles, such as glass, beads, steel balls, circular discs etc. Sandstones are rocks consisting of discrete clasts bonded together with a cement matrix, and hence are also categorized as cohesive-frictional materials (Donzé et al., 2009).

Apart from the cohesive-frictional materials, DEM's application to simulate crystalline rocks/materials using a Bonded Particle Model (BPM) after Potyondy and Cundall (2004) or Clumped Particle Model (CPM) after Cho et al. (2007) is also a form of cohesive-frictional materials such as the inter particle bonds specify the strength of cementing material.

2.11.1 Particle Flow Code (PFC) based on DEM methodology in rock mechanics

PFC based on DEM methodology in rock mechanics (Konietzky, 2002) has been extensively used across different disciplines (Shimizu et al., 2004). It is available in 2D and 3D simulation. The method of formulation was explained by Cundall (1988) and Hart et al. (1988). PFC is based on the simplified implementation of DEM which allows finite displacements and rotations of discrete rigid bodies (Cundall and Hart, 1992). It includes complete detachment and automatic detection of new contacts of the particles with the progress of calculations.

In PFC, the interaction of the particles is considered as a dynamic process with states of equilibrium developing whenever the internal forces balance. The contact forces and displacements of the particle assembly are traced by the movement of the individual particles. Movement of the particle is a product of the propagation of disturbances which is as a result of the wall and particle motion caused by, externally applied forces and body forces (Potyondy and Cundall, 2004). This is a dynamic process in which the speed of propagation is dependent on the physical characteristics of the discrete particle system. Calculations in the PFC vary between the application of Newton's second law (for the particles) and a force-displacement law (for the contacts). Newton's second law determines the translational and rotational motion of each particle resulting from the contact forces acting on it, while

the force-displacement law updates the contact forces resulting from the relative motion at each contact.

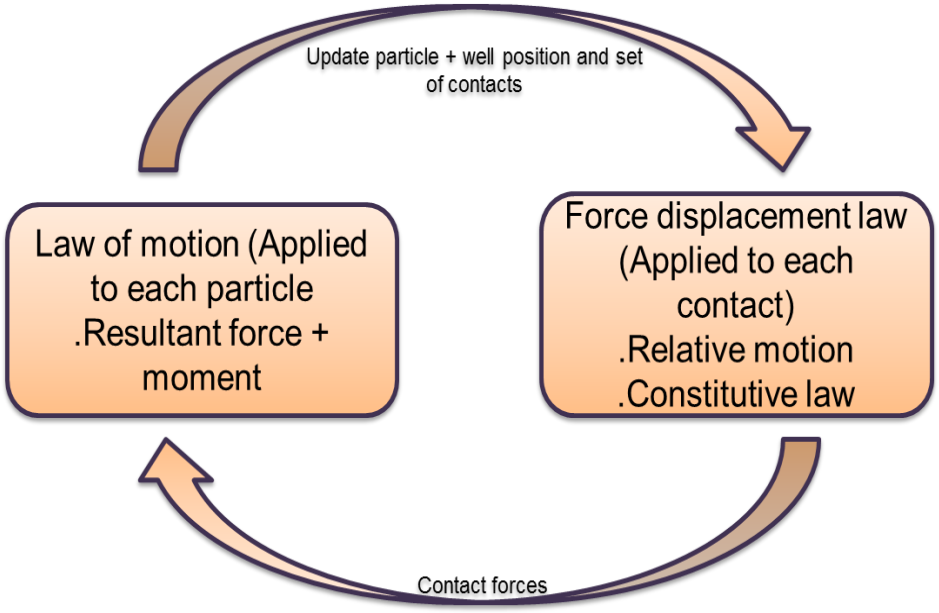

Figure 2.9 Calculation cycle in PFC3D (ITASCA, 2005)

This dynamic behaviour is expressed numerically by a time-stepping algorithm in which the velocities and accelerations are assumed to be constant within each time step cycle (Figure 2.9). Each time step is so small that, during a single time step, disturbances cannot propagate from any particle further away than its adjoining particles. Subsequently, at all times, the forces acting on any particle are determined exclusively by its interaction with the particles with which it is in contact.

2.11.2 Simulation of frictional granular materials

In the simulation of the frictional materials, the contact properties of the particles are specified. These include normal and shear contact stiffness and inter-particle contact friction. The stiffness can be linear, assuming particles as either rigid bodies or as the Hertz-Mindlin (Mindlin and Deresiewica, 2014) treating the particles as elastic bodies. In the simulation of frictional assemblies, it is preferable to use Hertzian contact theory to define inter particle contacts (Itasca, 2008). Besides the linear and Hertz-Minlin contact theory, some user defined contact models can also be implemented in PFC.

2.11.3 Simulation of cohesive-frictional granular materials

In the simulation of the cohesive-frictional materials, particles are cemented together with bonds at particle contacts. There are two types of bonding models; “contact bond” and the “parallel bond” (Bobet et al., 2009). The contact bond acts like a point of cementing material between two particles and is defined by normal and shear strength. While the other bonding model is the parallel bond model that is defined by normal and shear strengths and stiffness along with its extent (Cheung et al., 2013). The “parallel bond” acts like a cementing material between the two particles that can transmit forces and moments among the particles compared to contact bond model which can only transmit forces. The properties of the bonding models are specified in addition to the contact model’s properties so that after the breakage of the bonds, forces on the particles are specified by the contact models (Bobet et al., 2009).

2.11.4 Calibration process and inverse modelling approach

In PFC, for the simulation of granular frictional and cohesive-frictional materials, micro parameters are estimated to match the macroscopic behaviour with that of the actual physical materials. Therefore, for this purpose, numerical tests, including uniaxial, tri-axial and Brazilian tensile tests are conducted in PFC simulating the actual laboratory testing. During testing, the PFC’s input parameters are varied until the behavior of the numerical sample matches that of the physical sample. The corresponding parameters may then be used in a PFC2D or PFC3D simulation of a larger problem containing the same solid material as the sample. This approach has been named inverse modelling approach which include the following steps (Itasca 2004; 2005).

First, the matching of Young’s modulus is achieved by setting material strengths to a large value and varying the stiffness of the contacts and bonds. Then Poisson’s ratio is calibrated by varying the ratio of normal to shear contact and bond stiffness ratio. After obtaining the desired elastic response, peak strength in uniaxial testing is matched by varying the strengths (both normal and shear) of the bonds. Next, post-peak behaviour is matched by varying the inter particle friction. Thus, a complete strength envelope is obtained by performing a set of tri-axial tests at different confinements and Brazilian tensile strength test.

A comprehensive description of the calibration process by the inverse modelling approach can be found elsewhere (Itasca, 2004; Potyondy and Cundall, 2004; Itasca, 2005). This procedure is significantly based on a “hit-and-miss”, approach and includes test iterations to obtain a similar macroscopic response of the numerical assembly in terms of peak strength, Young’s modulus, tensile strength, cohesion and bulk friction. As soon as a reasonable calibration in the assembly response is achieved against a set of micro parameters, these parameters can be used for subsequent large scale modelling. Using inverse modelling approach, numerous studies have been conducted in the field of rock mechanics and geo-technical engineering (Konietzky, 2002; Shimizu et al., 2004). However, it has been observed that in both PFC2D and PFC3D (Potyondy and Cundall, 2004) a perfect calibration cannot be achieved using circular or spherical particles (Cho et al. 2007).

2.12 DEM simulation for granular materials in the context of the current research

Previous studies using DEM for the simulation of granular materials can be broadly classified into frictional materials, that is, unconsolidated materials and cohesive-frictional materials, that is, assembly of cemented particles or granules. These studies are very relevant to the present research as sandstone is a granular rock clasts cemented with matrix.

2.12.1 Cemented granular materials

The research to be conducted involving DEM for frictional materials was mainly focused on two objectives:

1. To simulate and understand the behaviour of grain contact of cemented grains in the assemblies using DEM, and

2. To validate the behaviour of the DEM simulation for contacting grains in the rock sample.

The scope was expanded to various horizons such as the simulation of natural heterogeneous and discontinuous materials. This is natural rock medium. The

studies include the understanding of the micro-mechanics with assumptions based on observed natural materials and similitude. This area is still under development and continuing research is being conducted. The pioneering validation of DEM was conducted by Strack and Cundall (1979). They compared the stress-strain behaviour of DEM simulation with that of Physical experiments on frictional materials. Cundall and Strack (1979a) compared the stress-strain behaviour of a numerical simulation by using computer code “Ball” with the corresponding response of 400 metal cylinders. Both numerical and physical rock mass responses demonstrated a reasonable agreement but with some minor differences. These differences were considered to be as a result of errors in the estimation of assumed parameters including density, friction between particles and walls and contact stiffness, which were not known in physical tests at that time.

Similarly, further attempts were made to validate DEM using a 16 disc static test and 1000 disc test with varying diameters (Sitharam, 2003). The DEM simulations were compared with experimental work on uniform sand for stress-strain plots at various confining pressure of both models. Load carrying capacity increases with the compressibility of the assembly with confining pressure. Numerical biaxial and hydrostatic tests were conducted on an assembly of 1000 particles and the results were compared with the published results of sand (Hakuno and Tarumi, 1988). A good qualitative comparison was noted in DEM simulations and experimental investigation on sand.

To explain the effect of particle shape in granular materials (O'Sullivan and Bray, 2002), an assembly of chrome balls was tested physically in shear box and tri-axial testing (O’Sullivan et al., 2004). The DEM simulation for the tri-axial test was performed by using spherical particles and overlapping sphere clusters based on Fourier shape analysis techniques. DEM simulations were also conducted for a shear box test in comparison with physical shear box tests. Physical tests were undertaken on approximately 1.0 mm diameter steel balls under 54.5, 109 and 163.5KPa normal load. DEM simulations were performed using known elastic parameters and the known friction of the steel balls following the physical test conditions. The numerical test results showed differences in responses in correspondence to physical test. That is, a stiffer response, stress dependency, no compression prior to dilation and an underestimation of overall assembly friction.

An experimental validation of PFC2D was conducted in tracking translations and rotations of angular grains of Fraser river sand due to external disturbances in a simple test (Sallam et al., 2004). Wooden pieces were produced in the shapes of sand particles to scale up the model. In PFC2D, angular particles were created using Overlapping Rigid Clusters (ORC) to simulate the sand particles. The results of the numerical simulations were observed to fall within the validation range of the physical tests and hence were considered reasonably (Ashmawy et al., 2003).

Recently, further work was carried out by Holt et al., (2005) who argued that numerical modelling can be used as a virtual laboratory that is basically identical to the physical laboratory. In order to implement this hypothesis, several tests were conducted on unconsolidated granular assemblies in a physical laboratory under controlled conditions and corresponding simulations were produced in PFC3D. The physical models consisted of glass beads to represent a frictional assembly. Stress dependent wave velocities were computed in the frictional assembly of glass beads in which particle contact stiffness was kept non-linear using the Hertzian contact model (Mindlin, 2014). PFC simulations reproduced the same response without the use of any fitting parameters.

Fu (2005) conducted a study by undertaking shear and compressions test on rock crush and simulated the same in PFC3D by modelling the spherical and polygonal particles. The micro structures of the rock crush particles were acquired by x-ray tomography imaging technique and employed in the simulations. The results showed that polygonal particles induced higher friction and dilation angles, and similarly, higher shear and compressive strengths, comparable to experimental results, than with spherical particles.

In summary, DEM simulations have been carried out to investigate and validate the response of frictional materials by using circular, spherical, elliptical, ellipsoidal and polygonal particles. These studies showed a reasonable achievement in understanding and modelling the mechanics of frictional materials. DEM simulation using circular or spherical particles showed less bulk friction owing to the excessive rotation of particles in the absence of interlocking, which is a characteristic feature of

natural frictional materials. The use of elliptical or ellipsoidal particles can produce a degree of interlocking and limit the rotation of particles; however, the bulk friction is less than that of physical materials. Polygonal particles require the complex contact detection scheme which results in a very high computation cost on a normal personal computer. In addition, to obtain the true angularity of natural grains is not possible as every grain is different in natural material and this affects the force chain or fibre.

2.12.2 Behaviour of DEM versus cohesive materials

In contrast to DEM's application on frictional materials, less work has been reported in literature with DEM's application and validation for cohesive-frictional materials. After the early DEM simulation for granular media (e.g. Cundall and Strack 1979a), researchers started looking into the cohesive-frictional materials using DEM. Like frictional materials, the initial objectives in the DEM's simulation of cohesive-frictional materials were to understand, investigate and validate the behaviour of material with that of the numerical simulation. Later, this work was extended to cohesive solids, concrete and natural rocks, and across various disciplines.

Deformation of elastic grains was used to investigate the particle assembly cemented at small areas (Digby, 1981). The work led the researchers towards the low and high strain deformations, including sliding along the grains.

The work on the effect of the cementation on the elastic and inelastic behaviour of the granular solids has been done. For example, Bruno and Nelson (1991) used a discrete element formation in 2D to look into the rock failure in tension, uniaxial compression and biaxial loading. Contact stiffness was assumed to be a linear function of the Young's and shear modulii of the cement, and the thickness and width of cementation bonds in the elastic domain.

An experimental study was conducted using synthetic cemented granular materials (Ottawa sand with halite and silica glass cement) in tri-axial compression tests (Bernabé et al., 1992). It was observed that a small amount of cement can significantly increase the strength of granular material if it is precisely deposited at previously formed grain-to-grain contacts.

Numerically, the behaviour of cemented granular materials was studied under low and high-strain loads using circular particles cemented together with elastic bonds (Trent and Margolin, 1992; Mouchet and Mitchell, 1989; Trent, 1989). The results showed that the macroscopic properties of the granular solids are governed by the properties and distribution of individual inter-granular bonds or the cementing material.

2.12.3 Behaviour of DEM versus behaviour of natural material

Dvorkin et al., (1991) investigated the normal interaction of two spherical elastic grains and an elastic cementation layer between them, for 2D and 3D cases. The results showed that a thin cement layer subject to normal and shear load can be approximately treated as an elastic strip. By this approximation, the problem of grain cement deformation (where the grains are deformable) was reduced to an ordinary integral equation for the normal stresses at the cemented interface, assuming the deformable grains and the width of the cemented zone was smaller when compared to the grain radius. They noted that the elastic response of the cemented system increased with the radius and stiffness of the cement layer. The contribution of the increase in the cement layer radius significantly increases the macroscopic stiffness of the bonded assembly. Furthermore, the response of a numerical model comprising of random identical spheres bonded with thin layers of cementing material, as in Dvorkin et al. (1991), was investigated for compressional-wave velocity measurements (Dvorkin et al., 1994).

Holt (2001) carried out a study to focus on the major differences between laboratory measured and micro-measurement virgin compaction using synthetic sandstone modelling. Synthetic sandstone samples were produced under stress with an injection of CO_2 in the solution of sand and sodium silicate contained in the tri-axial cell to replicate the micro measurement virgin compaction and to produce a stress released core by the removal of the sample from its container. The samples were then tested in uniaxial compression for micro measurement compaction and stress released core conditions. Acoustic emissions were monitored for numerical and synthetic sandstones. The numerical tests results reveal a good agreement in the

stress-strain response with that of physical tests, but with a deviation in micro-seismic activity.

Kulatilake et al. (2001) produced joint blocks from a mixture of plaster, sand and water and investigated their response under uniaxial loading. Numerical simulations were conducted in PFC3D including joints in cylindrical samples. The intact material's micro properties were adopted by the inverse modelling approach comparing the macroscopic responses of numerical and physical samples. The numerical simulations were found to be in agreement with the findings of laboratory testing in classifying the failure modes against same joint geometry configurations.

Narayanasamy also conducted a calibration study using PFC3D by examining the wave propagation and distribution of stress around the hole in sand material representing the borehole in cohesive material (Narayanasamy, 2004). The medium was artificially glued (i.e. round grained) sand named "Hickory sand". The micro mechanical characteristics were estimated by inverse modelling. The numerical simulation and experimental results showed almost identical particle displacements and rotations at small displacement, while large discrepancies were noted at high displacement.

The summary of studies on the behaviour of cohesive-frictional materials has revealed DEM's capability of replicating many features of granular solids and rocks. Therefore, no effort was made to model the behaviour of sandstone using DEM simulation. The simulation of quartz supported sandstone can be conducted in DEM by cementing the discrete particles with bonds such that DEM's discrete particles represent the sandstone quartz, while inter-particle bonds represent the cement matrix.

2.13 Micro to macro behaviour of cemented granular materials

Several theoretical formulations have been developed in the micro to macro mechanics of cohesive-frictional materials to illustrate the macroscopic response of the granular solids based on the interaction of the properties of the particles and the inter-particle cement. Two methods have been used to derive the macroscopic response of granular solids or cohesive frictional materials (Akram and Sharrock, 2010). First, there are homogenization theories in which strength and elastic

characteristics have been extensively studied within the frame work of composite mechanics. These theories were historically developed for a matrix-inclusion system and have been applied to porous media by considering voids as inclusions in a solid matrix. However, the application of homogenization theories has been found inadequate for a densely packed granular material (Chang et al., 1989).

The second method based on micromechanics was used to derive the elastic response of granular materials based on the behaviuor of two particles in direct contact. In this area, work has been done by Digby (1981) for porous rock Chang et al. (1989) presented the link between grain contacts and stiffness. The modulii of granular media that consist of unbounded particles has been studied by Cambou et al. (1995).

On a grain scale, several theories of the elastic inter-particle deformation such as Mindlin (2014) and Mindlin and Deresiewica (2014) or those considering particles as rigid bodies (distinct element methods) and the contact laws for frictional granular materials have been extended towards cohesive-frictional materials. In numerical simulation of the cohesive-frictional materials, most existing DEM formulations incorporate a piece of cementing material between the two particles which is called a bond or a bonding model. This bond cements together the particles and transfer forces and moments across the particles. In DEM, various bonding models have been carried out to obtain a representative cohesive-frictional material, such as rocks, concrete, granular solids, etc.

The proposed relations for determining the elastic and shear moduli was determined for concrete made of aggregate and binder (Portland cement). The results showed a reasonable correlation of the moduli with that of the experimental experience. However, the interplay of inter-particle friction and the effect of interface characteristics were not determined.

Jiang et al. (2006) studied the effect of bond rolling resistance by incorporating surface resistance in the bond model, in the inter-particle contacts as well as the surfaces. Using the developed DEM computer code (NS2D), a total of 86 (at constant stress ratio) biaxial compression tests were conducted on the bonded granular samples with different densities, bonding strengths and rolling resistances. The numerical test results showed, firstly, a larger internal friction angle, a larger yielding

stress, more brittle behaviour and a larger final broken contact ratio than the original bond model. Secondly, the yielding stress increases non-linearly by increasing the area of rolling resistance. Thirdly, the first yield curve (initiation of bond breakage), which defines a zone of no bond breakage and whose shape and size are affected by the material's density, was amplified by the bond rolling resistance and is analogous to that predicted by the original bond model.

2.13.1 Limitations encountered in developing macro behaviour from of micro behaviour

The Discrete Element Methods (DEM) is an approach of numerical simulation where the macroscopic behaviour of a particle assembly is computed from the individual motions and mutual interactions of the particles. It has been used in situations where state-of-the-art theoretical knowledge has not provided complete understanding and mathematical equations to model the physical systems, such as the mechanics of natural granular materials and rock masses (Ferrez, 2001).

Because our understanding about the complex and heterogeneous nature of these materials is incomplete, DEM is considered a very good aid to simulate, understand and investigate the factors and mechanisms controlling the mechanical behaviour of these materials including sandstones. However, DEM simulation is always based on assumptions that limit the accuracy of the model outputs. Among the various assumptions, are those commonly made with regards to the geometry and material type of the particles.

DEM with circular or spherical particles is the most commonly used simulation technique for rocks or granular materials due to the attractive computational cost. In contrast, polygonal particles take much longer time to simulate, even in laboratory scale models with a limited number of particles. Such large-scale simulations are even more computationally demanding along with memory, online storage, pre and post-processing, etc. (Ferrez, 2001).

The particle material is treated as rigid and deformation is allowed to occur at the inter-particle contacts. In crystalline and hard rocks, this assumption can produce similar behaviour if there are a reasonable amount of contacts, that is, if large number of particles is used in comparison to sample dimension (Potyondy and Cundall 2004).

In this case, deformation along the contacts can result in a reasonable behavioural similarity as per natural rock. This assumption is also tenable for the simulation of real granular materials with very weak cementing materials (compared to particle materials) in which deformation always occurs through the cement or cement-particle interface.

However, for granular solids with almost the same strength and elastic characteristics of particles and cement, the net mechanical response of the system will be contributed by the properties of both particles and cement. Therefore the use of rigid particles with a linear contact model will result in the response of such materials being misleading. This problem can be addressed by implementing Hertziann contact models (Mindlin, 2014) where particle contacts are treated as elastic bodies and can only undergo elastic deformation. Nevertheless, simulation of particle breakage or its plastic deformation cannot be achieved using this contact model.

Furthermore, in DEM even with circular or spherical particles, the selection of micro mechanical parameters, model dimensions for the calibration process and particle size as well as size distributions are the basic constraints for rigorous use of DEM in rock mechanics (Koyama and Jing, 2007). Recently, Koyama and Jing (2007) and Esmaieli et al., (2009) have carried out studies to overcome these problems especially by using a statistical approach to determine a set of mechanical parameters and a representative volume of the model with suitable particle size and size distribution. These studies, although helped in achieving a model representative of a rock or rock mass (by incorporating joints) based on representative elementary volume (REV) that estimates the relative effect of model dimensions, particle size and size distribution, the relation of DEM's parameters with that of real life physical models still remains a challenge that limits DEM's successful and rigorous use in predicting the response of natural materials whose mechanics is not well-understood such as sandstone. Therefore, DEM requires a careful calibration and validation with real experiments to better understand and overcome its limitations.

2.13.2 Calibration and validation of micro and macro data

Calibration and validation are two separate terms that are normally confused with each other in DEM's field of applications. Validation refers to the macroscopic behaviour of simulation, which is similar to physical systems having a similar

microstructure, while calibration is purely a mechanical macroscopic response, which can be gained from a simulation, such as that of a physical system that may or may not have the same microstructure (Akram et al., 2010).

In calibration, concrete, crystalline rocks or brittle materials can be modelled using DEM with the inverse modelling approach. The Bonded Particle Model (BPM) (Potyondy and Cundall, 2004) and Clumped Particle Model (CPM) (Cho et al., 2007) are typical examples. The resultant behaviour is the interaction of micro-mechanical parameters, which are normally assumed or estimated rather than measured. It has been observed that by using the inverse modelling approach, a similar mechanical response of a model can be gained with more than one combination of various micro parameters (Akram et al., 2010). For example, the calibration of peak strength and elastic modulus in uniaxial testing does not mean that the simulation is calibrated with that of the physical material. Over estimation of the tensile strength in the Brazilian test and underestimation of the angle of friction in uniaxial and tri-axial testing are inherent problems observed by many authors (Potyondy and Cundall, 2004; Cho et al., 2007). These problems cast doubt on the calibration process and the validity of the adopted micro parameters for subsequent problem-solving simulations.

In contrast, validation refers to a discrete modelling approach that determines how much quantitatively realistic behaviour can be obtained using physical or laboratory measured parameters. Although DEM has been validated to yield many features of physical materials (Potyondy and Cundall, 2004), to what extent real behaviour can be achieved using DEM simulation, is still a question.

Therefore, to obtain a test for successful validation, either the DEM simulations should be micro-structurally equivalent to the physical materials or the physical materials should be simpler so that an equivalent microstructure can be obtained in DEM simulations. The geological materials are naturally not very uniform and there are practical constraints that limit the amount of information that can be determined about the geology and the behavioural properties of the materials. Hence, simulating or validating the behaviour of such materials will pose difficulties in obtaining micro-structural equivalence in simulations and determining micro mechanical parameters (Akram, 2010).

Alternatively, a physical system can be developed whose simulation can be obtained in the DEM simulation with an equivalent microstructure, physical properties and model dimensions. All the physical and mechanical properties of such a system, for example, particle and cement based parameters, should be measured and used in DEM simulations. The comparison of the macroscopic responses of both systems in equivalent loading would validate the DEM simulation against a real physical system (Akram, 2010).

2.14 Preparation and testing of rock materials

Preparation and testing of rock material is another useful option for understanding the essential mechanics of natural granular materials, such as sandstones. Natural materials are non-uniform, anisotropic and heterogeneous. In order to understand the behaviour of these materials experimentally, the results will be an interaction of various factors such as, particle shape, size distribution, packing, elastic properties, characteristics, composition and distribution of cementing materials and, most importantly the void ratio and natural heterogeneities (Akram, 2010).

To get an understanding of the influence of a specific parameter on the overall results is very difficult. For example, two samples collected and tested from one location with different loading directions will differ in results and hence limit the accuracy of the results. Although the laboratory testing of the rock specimens under various loadings tends towards the basic understanding of the mechanics of the rocks, the net failure and peak strength seem to be governed by the aforementioned factors whose dependence cannot be investigated without keeping other parameters constant. In addition, practical considerations limit the amount of information that can be determined about the geology and behavioural properties of the materials (Wiles, 2006).

In order to overcome these limitations and obtain an understanding of the mechanisms occurring in the natural materials comprising rocks, an approach of physical modelling has been adopted in rock mechanics, which includes the characterization of rock to adequately describe the micro-structure of natural rocks. The two major advantages of this technique are the controlling of the heterogeneities that occur in natural materials and obtaining the reproducibility of the test results

(Wiles, 2006). This is very difficult in testing natural materials, such as rocks. However, this has been included in this research

Furthermore, the texture and structure of the material, that is, the grain size, porosity and cementation, can be controlled (den Brok et al., 1997). This approach has led to the understanding of the various properties and mechanics of the rocks such as stress-strain behaviour, pre and post peak dilation, fracture propagation, role of cementing materials and dependence of the particle size. This approach was specifically considered in the laboratory investigation of sandstones, which are naturally very heterogeneous and anisotropic rocks. The laboratory study of sandstone is very difficult because of the practical problems associated with the sampling and testing of such rocks. Hence, it is more appropriate to understand and investigate such rocks using a physical modelling approach. However, an important factor in the physical modelling of sandstones is to obtain similitude in the prepared physical model with that of the sandstone both in behaviour and structure. Different modelling materials, both natural and artificial have been used in the past for understating and investigating the mechanics of rocks and soils. A detailed discussion on similitude and modelling materials is provided in the following sections (Akram, 2010).

2.14.1 Application of studies to simulation similitude

In rock mechanics, similitude refers to the physical or behavioural similarity of a rock system with that of another system which could be a physical (synthetic rock) or an analytical or numerical model. In other words, two systems that have the same physical characteristics (features, parameters) and have the same reaction in response to some action, for example, loading, are said to have similitude.
The two basic conditions of similitude are:

1. **Geometric similitude**: Which is geometric similarity between two systems; it could be on a macro scale, that is, dimensions of the model and scaling and micro structural equivalence. However, it should be noted that it is not the only necessary condition of similitude (Sziics, 1980).

2. **Phenomenon similitude**: Two systems are similar if their corresponding properties are connected by bi-unique (one-tone) mapping

(representations). It mainly encompasses the responses of two models, that is, their strength and elastic characteristics (Akram, 2010). The similitude is based on mathematics. Hence, the sufficient and necessary condition of similitude between two systems is that the mathematical model of one is related by a bi-unique transformation of the other model (Akram, 2010).

Similitude is measured in terms of its credibility, which is the degree of similarity (Sargent, 2004). The credibility of similitude defines the limit of the acceptance of a system showing simulation as that of the actual system. The similitude studies in rock mechanics can be divided into two main classes: similitude between synthetic rocks (physical models) and natural rocks, and similitude between numerical models and natural rocks (Figure 2.10).

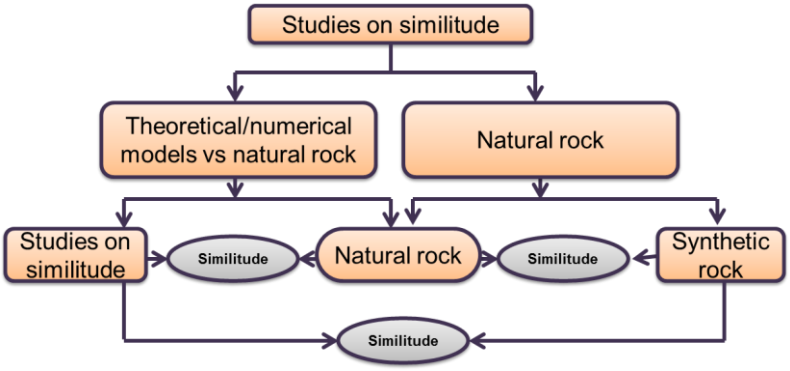

Figure 2.10 Diagram showing the main areas of the similitude studies in rock mechanics. (Akram, 2010).

In the study of rock mechanics, physical modelling has been an essential approach to understand the dependency of various parameters that are nearly impossible to examine in natural rocks owing to their inherent heterogeneities. Several researches have been conducted to study and understand the mechanics of the natural materials involving the preparation and testing of synthetic rocks having similitude with natural rocks. In this work, the similitude credibility represents the level of acceptance of the similarity between the elements of the two systems (i.e., physical materials and the natural rocks). For example, similarity in behaviour (e.g., mechanical parameters), micro texture and/ or structure, model scaling and dimensions.

Numerical methods have been progressively applied in rock mechanics to understand and predict the behaviour of natural materials. In the application of the numerical methods, theoretical knowledge of the mechanics of the materials has been introduced to simulate the behaviour of the rocks (Akram, 2010). Both continuum and dis-continuum approaches have been employed in this respect in rock engineering. The dis-continuum approach, where rock can be simulated as the assemblage of discrete bodies (Cundall, 1971) has become increasingly popular with the advances in computer technology and computation speeds. It is a rigorous aid in understanding the mechanics of granular media where the macroscopic response of the system is derived from the movement and interaction of individual particles. However, numerical models are always based on theoretical formulations and simulate behaviour of material based on average input parameters and assumptions, which may or may not be true in natural materials. Therefore, to make numerical modelling an effective and rigorous tool, it must be calibrated and validated with the physical model for reasonable similitude credibility (Ferrez, 2001). Hence, similitude studies involving numerical modelling should focus firstly on obtaining sufficient similitude (in behaviour, structure, dimensions etc.) with that of simple physical models rather than with natural rocks. Afterwards, if numerical models and simple physical models obtain similarity in behaviour and structure, they can be used for natural rocks.

2.14.2 Rock samples

The characterization and extraction of micro-parameters from sandstone are required to simulate natural rock. In previous works on granular assembly, micro-parameters were estimated by building the rock material with artificial grain and cement (Stimpson, 1970). Employing the use of artificial grains did not directly provide the micro-structural data; rather dilation was used as a yardstick to obtain micro-parameter (Brace et al., 1966). The disadvantage of using the artificial granular assembly is obvious in that dilation are not observed in none representative sample, therefore they are not exactly suitable for extracting the micro-parameters as it would have been from the real rocks. Therefore, this research seeks to identify the microstructure of rock and take the advantage of the characteristics behaviour to understand the deformation mechanics by extraction micro-parameters based on the structural behaviour.

In the modelling of sedimentary rocks, physical models were developed by using cement and gravels (Kobayashi and Yoshinaka, 1994). These micro-structures were tested for mechanical parameters in the context of foundation engineering and reasonable reproducibility of test results was obtained by controlling the properties of the cement matrix. But the elastic properties are not exact.

In every modelling study, a key objective was to achieve the similitude between the micro-structure and the rock, that is, the micro-structure should have similarities with the rock that could be at micro level (at laboratory scale) – the micro structure and the texture. It is very necessary to have a macroscopic mechanical response – strength and deformation characteristics. To satisfy all the conditions of similitude is practically impossible as the knowledge of mechanisms involved at the micro level of a particular rock can never be completed (Stimpson, 1970). Hence, the preference for the fulfilment of the conditions of similitude varied with the target objectives of the micro-structure. For instance, in some laboratory studies the microstructure gained similitude with natural rock while strength and other parameters were given secondary priority. In the modelling of an underground opening, microstructure was not given priority as the stress field and the rock strength and deformation characteristics were considered more important.

A numerical sandstone comprised of spherical quartz (rather than natural gravels) with a controlled data of bond strength as a cement matrix is a good option to understand the mechanics of rock deformation. The equivalent micro-structure of such sandstones can also be developed using DEM simulations for further investigation and similitude. The use of spherical quartz in synthetic sandstone will rule out the effect of particle shape and will provide better understanding of the mechanics of natural rocks. The behavioural similitude of synthetic sandstone can be obtained by comparing its mechanical response with that of natural sandstones (Figure 2.11).

Figure 2.11 Conceptual illustration of the present research: a) macro structure of natural sandstone. b) Numerical simulation of particles and inter-particle cementing material representing the natural sandstone.

2.15 Numerical solution to micro-parameter measurement from rock

Series of experimental research have shown that the failure process in brittle rocks under compression is characterized by complicated micromechanical processes (Lockner et al., 1991), including coalescence of micro-cracks and the nucleation growth, which may result in strain localization in the form of macroscopic fracturing Fitts and Peters, 2013). The evolution of micro-cracking, generally associated with the emission of acoustic energy (AE), results in a distinctive non-linear stress–strain response, with macroscopic strain softening commonly observed under low-confinement conditions (Bieniawski, 1967; Eberhardt et al., 1999). Unlike other materials such as metals, rocks exhibit a strong pressure-dependent mechanical behaviour (Cook, 1976). The change in failure mode, from axial splitting to shear band formation, is often examined for increasing confining pressures (Horii and Nemat-Nasser, 1986). This change in the failure behaviour is expressed in a non-linear failure envelope (Kaiser and Kim, 2008) and a progression from brittle to ductile post-peak response (Wong et al., 2006). The failure process observed during laboratory-scale experiments is further complicated by the presence of discontinuities, such as joints, faults, shear zones, schistosity planes, and bedding planes, at rock mass level (Goodman, 1989). Specifically, the response of the intact rock is affected by discontinuities by reducing its strength and inducing non-linearities and anisotropy in the stress–strain response (Hoek et al., 2002). Discontinuities add kinematic constraints on the deformation and failure modes of structures in rocks (Hoek and Diederichs, 2006).

Apart from the peculiar difficulties associated with the determination of a reliable micro-measurement input parameters, the application of numerical modelling for the analysis of rock engineering problems are challenging due to the features earlier mentioned of the rock behaviour. In particular, the gradual degradation of material integrity during the deformation process, together with the influence of pre-existing discontinuities on the rock mass response, has represented a major drive for the development of new modelling techniques. In this context, the available numerical approaches are typically classified either as continuum- or discontinuum-based methods (Jing and Hudson, 2002).

The handling of the computational domain as a single continuous body is the main assumption of continuum-based methods. Standard continuum mechanics formulations are based on theories such as plasticity and damage mechanics, which adopt internal variables to capture the influence of history on the development of stress and changes at the micro-structural level, respectively (De Borst et al., 2012). Generally, the implementation of continuum technique is based on numerical methods, such as non-linear Finite Element Method (FEM), Lagrangian Finite Difference Method (FDM), and Boundary Element Method (BEM), with the integration of plasticity-based material models. Standard strain-softening fundamental relationships cannot capture localization of failure because the lack of an internal length scale. This is due to an underlying mathematical problem (De Borst et al., 1993). The main consequence of using a standard continuum to simulate strain localization is the fact that localization occurs in a region of zero thickness and consequently superior mesh sensitivity arises. To overcome this deficiency, the description of the continuum must account either for the viscosity of the material, by incorporating a deformation-rate dependency, or for the change in the material micro-structure, by enhancing the mathematical formulation with additional terms (De Borst et al., 1993). The recent technique, known as regularization, includes non-local model developed by Bažant and Pijaudier-Cabot, (1988), gradient model developed by Mühlhaus and Aifantis, (1991), and Cosserat micro-polar model developed by Mühlhaus and Vardoulakis, (1987). Alternatively, Cohesive-crack Model under the assumption that damage can be represented by a dominant macro-fracture grouping all non-linearities into a discrete line was proposed by Hillerborg et al., (1976) and Bažant and Oh, (1983). A fictitious crack concept is employed to represent the effect of a Fracture Process Zone (FPZ) ahead of the crack tip, whereby phenomena such

as small-scale yielding, micro-cracking or void growth and coalescence are assumed to take place. In case of heterogeneous rocks, strain localization has been successfully simulated by damage models with statistically distributed defects. Several variations have been made to this approach for numerical schemes such as Finite Element Method (FEM) (Pande et al., 1990), Smooth Particle Hydrodynamics (SPH) (Benz and Asphaug, 1995), Cellular Automaton (Feng et al., 2006), and Lattice Models (Potyondy and Cundall, 2004).

Two techniques are commonly used to account for the presence of rock mass discontinuities within continuum models (Amadei, 1996). Homogenization technique is often adopted if the number of discontinuities is relatively large. The most widely used homogenization approach entails reducing, within a conventional elasto-plastic model (Hoek et al., 2002), the rock mass deformation modulus and strength parameters to account for the degrading effect induced by the local geological conditions (Hoek and Diederichs, 2006). More advanced models can also include transversely isotropic elastic response induced by preferably oriented joints (Amadei, 1996). Alternatively, if the problem is controlled by a relatively low number of discrete features, special interface (or joint) elements can be incorporated into the continuum formulation (Duncan and Goodman 1968; Pande and Sharma, 1979; Bfer, 1985). This approach is also known as the combined continuum-interface method (Bfer, 1985).

Discrete (or discontinuous) modelling techniques which is commonly referred to as the discrete element method (DEM), treat the material directly as an assembly of separate blocks or particles. Cundall and Hart (1992) defined, a DEM is any modelling technique that (a) allows finite displacements and rotations of discrete bodies, including complete detachment; and (b) recognizes new contacts automatically as the simulation progresses. DEM was originally developed to efficiently treat solids characterized by pre-existing discontinuities having spacing comparable to the scale of interest of the problem under analysis and for which the continuum approach described above may not provide the most appropriate computational framework. These problems include: compact rock masses, ice plates, masonry structures, and flow of granular materials. DEMs can be further classified according to several criteria such as, the type of contact between bodies, the representation of deformability of solid bodies, the technique for the detection and

revision of contacts, and the solution procedure for the equations of motion (Jing and Stephansson, 2007). DEM implementations are broadly divided into explicit and implicit methods, depending on the adopted solution algorithm. The term distinct element method refers to a particular class of DEMs that adopt an explicit time-domain integration scheme to solve the equations of motion for rigid or deformable discrete bodies with deformable contacts (Cundall and Strack, 1979a). The most important implementation of these group are represented by the Universal distinct element code (UDEC) (Itasca, 2000) and the Particle Flow Code (PFC) (Itasca, 2012b). Similarly, the best known implicit DEM is the discontinuous deformation analysis (DDA) method (Goodman and Shi, 1988). Despite the fact that DEMs were originally developed to model jointed structures and granular materials, their application was afterwards extended to the case of systems where the mechanical behaviour is controlled by discontinuities that emerge as natural outcome of the deformation process, such as fracturing of brittle materials. Specifically, the introduction of bonding between discrete elements allowed capturing the formation of new fractures and, thus, extended the application of DEMs to simulate also the transition from continuum to dis-continuum.

According to Bićanić (2003), the original boundary between continuum and dis-continuum techniques is less noticeable because several continuum techniques are capable of dealing with emergent discontinuities associated with the brittle fracture process. In particular, the hybrid approach known as the combined finite–discrete element method (FDEM) (Munjiza et al., 1995) effectively starts from a continuum representation of the domain by finite elements and allows a progressive transition from a continuum to a dis-continuum with insertion of new discontinuities.

2.16 Kinetics of particles from Newton's Law

Particle acceleration is proportional to the magnitude of the resultant force, provided the resultant force is not zero and these particles move in the force direction (Jong and Rogers, 1990).Therefore, the resultant force or shear force is equal to ($\sigma_1 - \sigma_3$) in the photo image and is repeated in Newtons' second law. F = Ma. Moreover, the ratio of the magnitudes of the resultant force and of the acceleration can be used to define the mass of the particle (Cundall and Strack, 1979b). It has been demonstrated

that Newton's second law can be expressed in an alternative form relating the rate of change of the linear momentum with the resultant of the forces acting on that particle (Corben and Stehle, 1994). However, the resultant force is equal to the rate of change of the linear momentum while linear momentum is the product of mass and velocity. A single particle's momentum is defined by the Newton's second law which is the operation done to allow each particle of bonded particles to go into motion. By allowing the inter-particle force to move, the bond slip and stiffness can be used to investigate deformation mechanism (Cundall, 2004). If the normal force component on the bond is F^n, the total acceleration at overlap is U^n, and the contact normal stiffness is K^n, the stiffness normal direction is controlling force behaviour described by the relationship between these three parameters. While behaviour in when it is in the contact tangential direction is that which relates the increment of both shear forces (ΔF^n) and shear acceleration (ΔU^n) (Cundall, 2004).

The linear momentum is adapted to the contact to give a contact model independent of both shear and normal stiffness. The grain slipping is synonymous to the acceleration of particle given by equations of grain behaviour in Figure 2.13, the normal force reaches the maximum value before shear next contact force of known friction coefficient allow particle rotation.

2.17 Bonded grains response and micro-parameters

Sandstone is bonded quartz grains bonded together by clay which acts as cement. The grain – grain usually overlap and if the force and momentum in each contact bond is $F_i \ and \ M^n$, the grain responds to stress. The force –displacement law defines the grain responds at bonded contact with six micro-parameters which are normal and shear stiffness K_n and K_s, frictional coefficient (μ) and the corresponding parameters in tangential direction.

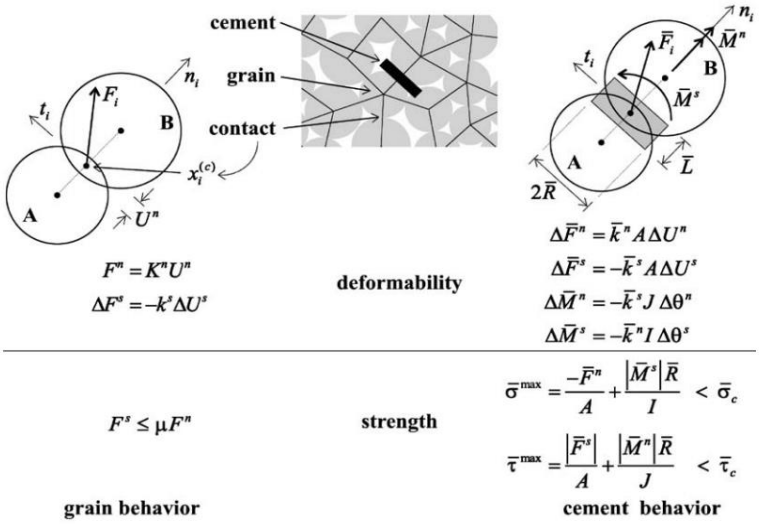

Figure 2.12 Force-displacement behaviour of grain-cement system (Itasca, 2000).

For the grain and bond respectively, these parameters are assigned to grain contact at the point of overlap $\boldsymbol{x}_{\boldsymbol{i}}^{(\boldsymbol{c})}$ along the line joining the grain centres. As represented in Figure 2.12, linear springs are assumed to be in the overlap, and act in series along the slider in the shear direction, therefore the contact force vector *Fi* which represents the action of grain A on B can be resolved into normal and shear components with respect to the contact plane as expressed in equation 2.4 (Itasca, 2000).

Going by the theory of grain-cement system discussed in this section, the next section takes advantage of the fact that deformation occurs even at a grain scale. Hence scaling deformation process in sandstone is likely possible. This is because grain-cement interaction at any two grain contact can be studied using photo stress technique. Techniques capable of grabbing information at a single point in any solid structure can possibly exhibit birefringence. This point information is explored by an experimental calibration process on sandstone.

2.18 Assumptions made in the experimental evaluation of micro parameters

The assumptions made to obtain micro properties from the sandstone model are inherent based on Newton's second law. These includes; (1) the contact bond is envisaged as two cement grains. Thus the grains interaction occurs solely at the cemented contact. (2) Each grain will slip from its position at bond if the forces at the contact exceed the maximum shear contact force. (3) The quartz grains are of finite

mass compared to the bulks sample. When the force applied on the sample strength exceed the bond strength of the weakest visible bond, the grain will move and distort the bond. (4) The photo elasticity techniques can measure micro strain in stressed points. And the strain measured will based on the contact interaction of the grains based on these stated assumption. A point measurement of diameter approximates to the diameter of quartz in sandstone provides the deviator stress data which defines the micro or single point strain information. (5) Sandstone sample is a bonded grain model in an isotropic state when it is not stressed.

When sandstone is stressed by loading, the motion of quartz grains will occur in the direction of stress. This is the strain which can be transferred to the coating in the same direction resulting in optical anisotropic behaviour. Therefore calibration involves gradual application of load on the sandstone specimen. The incremental load is expressed as a sequence of light and dark fringes on the coated sandstone sample. At the maximum light appearance, a dark contour is noticed as a fringe order. The first dark that appears is the first fringe order and the subsequent dark lines are the consecutive fringe order which provide consistency in calibration stages.

2.19 Grain stiffness detection by experimental technique

Several experimental approaches have been employed in detection of micro defect in materials which can be employed in deformation studies in sandstone. The techniques could be the ultrasonic detection or acoustic. An additional technique is the photo stress employed in Chapter 3.

2.19.1 Ultrasonic wave propagation through materials

Ultrasonic wave can be defined as physical vibrations in matter which occur at frequencies above 20Hz, which is approximately within the limit of human hearing. The waves can only exist in a material medium, such as air, water, rock (Halliday et al., 2001). There are so many users of ultrasonic sounds in nature. For instance, Bats are known to use ultrasonic sounds as a means for nocturnal navigation, while the Dolphins also use ultrasonic sounds for navigation, basic communication and detection of food in the underwater environment (Hazzard, 1998).

Ultrasonic sounds have been used in different facets of human endeavours. For example, in medicine, it is widely used in echocardiography, in engineering; it is commonly used for rock fracture detection, while in the military; it is commonly used for submarine sonar ping (Hazzard, 1998). Recently, ultrasonic sound has been developed for use in seismology, where it is commonly known as acoustic emission. An acoustic emission can be defined as a transient elastic wave emitted from small-scale cracks also known as micro-cracks, which are formed as a result of changes in stress (Hazzard, 1998).

Ultrasonic waves normally travel in longitudinal and transverse modes. A longitudinal ultrasonic wave can be described as a pressure wave or P-wave. This type of wave is the fastest moving ultrasonic wave. It propagates along a straight line as a result of particles on the molecular level oscillating parallel to the direction of propagation. A transverse wave also known as a shear wave or S-wave on the other hand is a wave which propagates perpendicular to the direction of travel due to a shear oscillation on the molecular level. The S-wave is slower than the P-wave due to the mode of oscillation (Johnson, 2005).

A horizontal variable represents transverse displacement of an element in the technique and time is significant. The amplitude is the magnitude of the displacement of the wave. The phase of the function is known as the angular motion with respect to a reference position. The phase changes linearly with time (Halliday, 2001). The repetitions of the pattern or shape of the function can be measured to determine the wavelength of the wave. A wavelength is the linear distance the wave travels in one cycle of the wave's function (Halliday, 2001). The onset of the wave across a material marks the arrival time of the wave. Ultrasonic waves depend on the elastic properties of a material (Halliday, 2001).

Ultrasonic waves can be propagated through any natural medium. The resonant frequency of a material is an important characteristic to note when attempting to pass ultrasonic waves through the material. This value is usually non-linear in rock. The resonant frequency of a rock can change with saturation or stress. Matching the resonant frequency of the rock to the transmitted ultrasonic signal will maximize the

amount of the wave's energy that is passed through the rock. The resistance to the flow of sound wave through the rock is known as acoustic impedance (Johnson, 2005).

Another concern when propagating an ultrasonic signal through a rock is refraction. Refraction is the incomplete transmission of a wave through an interface. When there is interplay between a wave and two materials that are not the same (i.e. mineralization, faults, or bedding planes inside of a rock). The wave splits into two and is said to be refracted (Halliday et al., 2001; Hazzard, 1999). A part of this refracted wave is reflected and the other part is transmitted at a different angle. This angle of refraction is influenced by the angle of wave incidence. The common theory ascribe to this technique is known as the Snell's Law (Halliday et al., 2001; Hazzard, 1999).

2.19.2 Mode conversion and application of wave measurement to this research

When sound propagates in a solid material, wave energy is transformed from one form to another form. For instance, when a longitudinal wave hits an interface at an angle, a portion of the energy can cause particle movement in the transverse direction to start a shear wave. Mode conversion occurs when a wave encounters an interface between materials of different acoustic impedances and the incident angle is not normal to the interface. It is imperative to note that mode conversion occurs each time a wave encounters an interface at an angle. This mode conversion occurs for both the portion of the wave that travels through the interface and the portion that reflects off the interface (Cobbold, 2007).

When sound waves pass through an interface between materials having different acoustic velocities, refraction takes place at the interface. The greater the difference in acoustic velocities between the two materials, the more the sound is refracted. However, the converted shear wave is not refracted as much as the longitudinal wave because shear waves travel slower than longitudinal waves. Therefore, the velocity difference between the incident longitudinal wave and the shear wave is not as great as it is between the incident and refracted longitudinal waves. Thus when a longitudinal wave is reflected inside the material, the reflected shear wave is reflected at a smaller angle.

2.19.3 Ultrasonic measurement of grain contact stiffness in normal and perpendicular direction

Monitoring and analysis of ultrasonic wave is another way that researchers are using acoustic emissions to study rock mass failure with the hope of predicting it someday (Luong, 2001). A major research area, which has invested heavily in ultrasonic/acoustic monitoring, is the search for non-accidental rock fractures in drilling, safe repositories for spent nuclear fuel, etc. The research on the fracture prediction from the beginning of microstructural deformation covers the estimation of stiffness parameters from the rock's microstructure which is one of the micro-parameter of geological rock applicable to rock simulations, in which the parameter can become a constant and would be kept in discrete simulation, which will be applied later for experimental validation (Luong, 2001). The problem caused by allocating normal stiffness parameter to discrete modelling is one of the major areas addressed in this research. The modelling must proceed with stiffness of grains in vertical and shear direction to minimize error in micro-measurement from rock during simulation. The advantage of this precaution is to avoid false failure prediction in field application. A realistic approach to the problem of reproducing rock behaviour is to build the model with physical micro-parameters that guarantee physical representation of the rock system. Photo stress analysis was employed to validate that acoustic monitoring in this study. Thus, an experimental contribution to discrete modelling of rock deformability is enhanced

2.19.4 Experimental challenges using ultrasonic wave technique for micro-measurement of mineral micro-structure

One of the aims of this research is to evaluate microstructural parameters of rock. Therefore, it is necessary to characterize the material. Usually, microstructures of materials are characterised with elastic wave properties. This should be limited to uncertainty of less than 0.1% (Colombo et al., 2003) but these limitation threshold is difficult to achieve. The ultrasound characteristic velocities are widely used as means of micro-structural detection. But there are some challenges regarding their measurements. These challenges include:

The ultrasonic wave technique does not allow direct measurement of the grain contact parameter. So the contact parameters from ultrasound are not measured with ultrasonic technique, they are obtained by correlations of wave velocities with the micro-data. The stiffness obtained is obtained by the correlation of the wave velocity with the stiffness parameter (Zadler et al., 2004). In this research, photo-stress technique has been used to measure directly the contact parameters which are independent of the assumed correlations of wave velocity with rock grains. Another source of difficulty is that the Eigen-frequency identification comes from the physical coupling of the sample to the apparatus. Therefore slight differences in the positioning of the sample between the transducers along with the force applied by the transducers contribute to this uncertainty. This error can be estimated by completely mounting and un-mounting the same sample several times (Zadler et al., 2004).

On the other hand, ultrasonic wave have been found successful in geological investigations and application therefore it has been employed in this study for the measurement of micro-parameters because it is sensitive to both surface and subsurface discontinuities and thee depth of penetration. For flaw detection or measurement, it is superior to other methods, only single-sided access is needed when the pulse-echo technique is used, it is highly accurate in determining reflector position and estimating size and shape, minimal part preparation is required, it provides instantaneous results, detailed images can be produced with automated systems, it is non-hazardous to operators or nearby personnel and does not affect the material being tested and finally, its equipment can be highly portable or highly automated (Zadler et al., 2004). The utilization of polarized light in tackling the present challenge of obtaining micro-measurement from rock is presented in the next section.

2.19.5 Utilizing polarized lights in micro-measurement techniques

Polarized light is an electromagnetic vibration employed to alleviate the challenges encountered in micro-measurement of rocks. The technique involves using an incandescent light source that emits radiant energy which moves in all directions and is made up of a wide spectrum of vibrations of different frequencies and wavelengths. A section of this spectrum which contain wavelength between 400 and 800 nm [15

and 30 x 10^{-6} in], is applicable within normal limit of human eyes. The direction of movement of the light is perpendicular to the vibration associated with the light. A train of waves is emitted by a light source which is made up of vibrations in all perpendicular planes.

If a polarization filter is introduced, only the component of the vibration that is parallel to the privileges axis of the filter will be transmitted. The vibration contained in one plane in an organised beam is known as polarized light or “plane polarized”. A complete extinction of the beam can be achieved when the axis of the two filters are perpendicular to one another and another polarizing filter A is placed in the path. The movement of light in a vacuum or in air is at a speed C of 3 x 10^{10}cm/sec, the speed (V) is lower in other transparent bodies and the ratio C/V is known as the index of refraction. This index is constant irrespective of the direction of movement or plane of vibration in a homogeneous body. However, the index depends on the direction of vibration with respect to index axis in crystals. Some materials such as plastics act isotopically when unstressed, but become optically anisotropic when stressed. The variation in the index of refraction is a function of the resulting strain, analogous to the resistance change in a strain gage. (Micro-Measurements, 2005; Mehta, 2008).

2.19.6 Photoelasticity techniques applied to rock mechanics

Many crystalline materials such as barium borate, beryl, silicate, quartz, etc. can exhibit uniaxial birefringent by nature because they exhibit double refraction. The frozen molecules in plastics allows plastics to possess birefringence property but polarizers are used to detect the stresses in plastics like polycarbonate, polystyrene, cellulose nitrate, epoxy resins, polymethacrylate, etc. Material selection is driven by the aim of the experiment to be performed. Birefringence occurs when rays of light travels from its source, incident on certain materials, split into two and transmitted through the material in different directions. Materials which are isotropic can be made optically anisotropy by mere application of stress. David Brewter (1816), was first to observe polarised light producing inference bands called isochromatics or stress fringes (Theocaris and Gdoutos, 2013). The stress fringes are defined by the locus of point of same maximum shearing stress normal to the incident rays which is in the plane of the material under investigation. Dark to bright colours form an optical cycle when the isochromatic effect is filtered by monochromatic filter. Zero fringe order is

assigned to the dark fringe, the second fringe is assigned the first fringe order and the subsequent fringe follow consecutive numbers called fringe order. The bands of colours usually show contours across the model sample depending on the irregularity in the sample. High stresses points are seen as closely spaced bands and low stressed points are seen as broadly spaced bands. The objective of this section is to evaluate stress magnitude across the model sample and to ensure repeatability procedure for the evaluation.

2.20 Calibration of sandstone and stress optic constant.

The material's stress optic coefficient is the measure of the susceptibility of the material to photoelasticity (Dally and Riley, 1991). Its unit has dimensions reciprocal to that of stress (m^2/N or 1/Pa). If a fixed value of wavelength is used for the calibration, then a constant can be maintained by relating the wavelength to the stress optical coefficient. Expressed in Equation (2.1) (Sampson, 1970).

$$\frac{\lambda}{c} = f_\sigma = \text{constant} \tag{2.1}$$

Where λ *is* the wavelength, c is the stress optic coefficient, f_σ is the material fringe value in m / (m^2 / N) = N / m.

The material fringe value can also be expressed as a function of principal stress difference in Equation (2.2) (Dally and Riley, 1991)

$$\sigma_1 - \sigma_2 = \left(\frac{N f_\sigma}{t}\right) \tag{2.2}$$

Where t is the material thickness, N is the fringe order; the principal stress difference is $\sigma_1 - \sigma_2$ *and* $f_\sigma$is the fringe value in N/m. This unit is the direct unit of stiffness of a material which is a similar to the definition as the elastic modulus of the materiel.

During calibration, careful precaution can be followed such that strains are made constant throughout the thin coating. Sandstone can become anisotropic under stress, but isotropic at initial state. It obeys a linear elastic behaviour which can be

observed for many samples before coating. Then it is convenient to incorporate the expression in Equation (2.3) (Khan and Wang, 2001). The strain in the sandstone can be expressed on the coated surface therefore the strains can be equal (Caputo and Giudice, 1983, Khan and Wang, 2001)

$$\varepsilon_1^s = \varepsilon_1^c = \frac{1}{E^s}(\sigma_1^s - v^s\sigma_2^s) = \frac{1}{E^c}(\sigma_1^c - v^c\sigma_2^c) \tag{2.3}$$

Where $\varepsilon_1^s and \varepsilon_1^c$ strain in the sandstone and coating are respectively E is the elastic modulus and v is the Poisson's ratio. Superscripts s and c are strain in sandstone and coatings respectively (Caputo and Giudice, 1983). Also to obtain the stress correlation of sandstone and coatings, Equation (2.3) becomes Equation (2.4) (Khan and Wang, 2001, Caputo and Giudice, 1983).

$$\sigma_1^s = \frac{E^s}{E^c(1-v^2)}[(1 - v^c v^s)\sigma_2^c - (v^c - v^s)\sigma_1^c] \tag{2.4}$$

Due to vertical and horizontal variation in stresses, the stress field in the sandstone is defined by Equation (2.4) and the difference in the sandstone stresses $(\sigma_1^s - \sigma_2^s)$ is defined by Equation (2.5) where the difference between the principal stresses in the photoelastic coating $(\sigma_1^c - \sigma_2^c)$ is utilized (Khan and Wang, 200; Caputo and Giudice, 1983).

$$\sigma_1^c - \sigma_2^c = \frac{E^c\,(1+v^s)}{E^s\,(1+v^c)}(\sigma_1^s - \sigma_2^s) \tag{2.5}$$

Equation (2.5) is the relationship between stress differences of both sandstone model and photo elastic coating. Since the light transmits through the photo elastic coating twice then we have the stress optic law definition for coated model as stated by (Khan and Wang, 2001; Caputo and Giudice, 1983).

$$\sigma_1^c - \sigma_2^c = \frac{Nf_\sigma}{2t^c} \tag{2.6}$$

Where $f_\sigma$the material fringe constant and the coating thickness is is t^c Or Equation (2.7) (Khan and Wang, 2001) can be employed since the sandstone material properties are different from the photo elastic coating properties. A plain strain condition fitted properly into Equation (2.6) since the coating thickness was far less than the sandstone specimen (Caputo and Giudice, 1983).

$$\varepsilon_1^S - \varepsilon_2^S = \varepsilon_1^C - \varepsilon_2^C = \frac{(1+\nu^c)(\sigma_1^c+\sigma_2^c)}{E^c} \quad (2.7)$$

The stress optic constant was determined as it was possible to calibrate the sandstone specimen using the photo stress equipment with the application of the elastic modulus of sandstone and the Poisson ratio of the sandstone such that data accuracy was maximized. The thrust of the particle kinetics of Newton's second law and the possible calibration of sandstone with the elastic properties can provide reasonable means to make assumption. The following assumptions are inherent from particle kinetic which applies to a single grain of the sandstone specimen under photo elastic stress analysis. A consistency in the theory of deformation can be conveniently stated in six assumptions used for experimental measurement criteria. The intensity of light emerging in the case of plane polariscope will be in Equation (2.8) (Micro-Measurements, 2005) and.

$$\mathrm{I} = b^2 sin^2 \frac{\delta\pi}{\lambda} \quad (2.8)$$

Here b is the amplitude, δ is the retardation, λ is the wavelength of the light, the light intensity (I) becomes zero when the crossed polarized analyser is parallel to the direction of principal strains. Therefore, a plane polariscope configuration is used to measure the principal strain directions.

Circularly polarized light can be produced by adding optical filters known as quarter-wave plates in the path of light propagation and the image observed is not influenced by the direction of principal strains. The intensity of the emerging light thus becomes (Micro-Measurements, 2005). The light intensity becomes zero in a circular polariscope when $\delta = 0, \delta = 1\lambda, \delta = 2\lambda$ etc. or in general Equation (2.9) expresses

the retardation measurable as a function of the wavelength of the light used Equation (2.9) (Lesniak et al., 1999).

$$\delta = N\lambda \tag{2.9}$$

Where N is 1, 2, 3, etc. The number N is also called fringe order and it indicates the size of δ. The selected wavelength is commonly at a value of 22.7 x 10^{-6} in $[575\ nm]$. The retardation or photoelastic signal is then simply describes by fringe order N. For example, If N is two, Retardation (δ) implies 2 fringes (Micro-Measurements, 2005) hence substituting 2 for N into Equation (2.15) we obtain Equation (2.10) with the retardation value of $45.4\ x\ 10^{-6}\ in\ [1150\ nm]$

$$\delta = 2\lambda \tag{2.10}$$

Once $\delta = N\lambda$ is known, the principal strain difference is derived using equation 2.11

$$\varepsilon_x - \varepsilon_y = \frac{\delta}{2tk} = N\ \frac{\lambda}{2tk} = Nf_\sigma \tag{2.11}$$

Where $\varepsilon_x - \varepsilon_y$ is the difference in strain between the horizontal and vertical direction respectively, t is thickness, δ is the retardation, λ is the wavelength of the light, the fringe value, f_σ, is a constants, and N is the result of measurements. The next section explains the possibility of obtaining the birefringence in bonded grains of rock using reflective polarization and coating techniques.

2.20.1 Application of grey field polariscope (GFP) to bonded grains deformation.

Sub-fringe Photoelasticity has been obtained with low loads by (Lesniak, 2000). Strains were measured directly from the Grey Field Polaris cope (GFP). The strain in the area/ point of interest are completely sub-fringe with low loads. The Red- Green – Blue (RGB) approach used in assessing multi-fringe data can be applied to obtain data elsewhere because the data obtained will be used to analyse the non-linear results of high strain seen at over ranged data (Lesniak, 2000).

2.20.2 Birefringence is obtainable in coated model of bonded grains using photo stress techniques.

The application of the photo stress technique to determine strain in cemented granular sample was done by making the surface of the sample photoelastic. First, stress was induced on the bonded grains; it is thought that material property is different at some location where the stress causes a change in the arrangement of the bonded grains. This stress in the material is transferred into the firm plastic coating on the bonded grain sample next birefringence occurrence is seen on the photoelastic coating. By implication, strain in the bonded grains is as a result of anisotropy (property measured at same point change with azimuth but not location) in the bonded grains. This occurrence of strain is transferred into plastic coating on the bonded grains of quartzite sandstone. Double refraction occurs on the coated surface of the sample. The light transmitted into the plastic coating on bonded grains model is reflected back as elliptically polarized light having its new major axis with orientation at π/4 off the direction of the initial principal strain (Figure 2.13) (Lesniak et al., 1999).

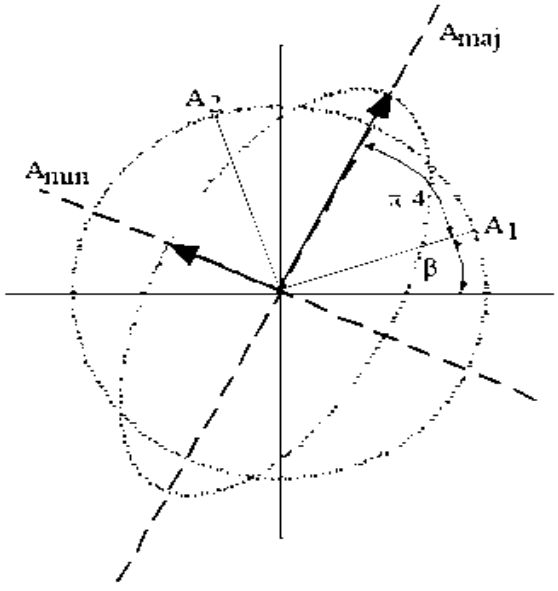

Figure 2.13 Response of Sandstone Sample Model to Birefringence/double refraction (Lesniak et al., 1999)

The response of anisotropy to birefringence is illustrated in Figure 2.13. If the rotation of the analyser at an angular frequency is (w) and the analyser is parallel at time t = 0, with a time input intensity is given by (I) in Equation (2.12) (Lesniak et al., 1999)

$$I = \frac{a^2}{2}[1 + sin2(wt - \beta)sin\Delta] \quad (2.12)$$

Where I is light intensity, a is the amplitude, w is the angular frequency, t is time, β is the reference direction, Δ is the angle made up to 90 degree from the reference direction. Since the Polariscope works using the equation above, if birefringence is zero (0) then a neutral grey colour is seen at the output also if birefringence occurs at the surface of the sample such as sandstone, due to the strain in the bonded grains, the signals' amplitude oscillates about its neutral-grey-level with time. The analyser's axis and the principal strain axis coincide when zero is read off at signals from oscillating portion. The reference (β) and principal directions are oriented. The oscillating light signal possesses both phase and amplitude which is a video lock- in algorithm of the Polariscope. In Figure 2.13, the angular direction shows results largely due to retardation angles because the grey produces perturbation which oscillates and normalized its light intensities or grey level. The experimental methodology employed in this research took advantage of the fact that strain in the bonded grains can be transferred from inside the structure to the surface of the bonded grains which was coated with reflective aluminum spray and photo-sensitive plastic respectively. The aluminum reflective surface under the coating function to retain polarization given out high intensity in which stress measurements and stress field were visible images. The fringe order expressed as contours obtained are seen in the photo stress fields. This is explained in the next section.

2.21 Analysis of photoelastic fringe patterns

Photo-stress can be used for the following types of measurements and analysis:

I. Qualitative measurements such as :
   a. The magnitude and sign of the tangential stress along free (unloaded) boundaries, and in all regions where the state of stress is uniaxial.
   b. The directions of principal strain and stress at all points on the photo elastic coating.

c. In a biaxial stress state, the magnitude and sign of the difference in principal strains and stresses at any selected point on the coated surface of the test object.

II. Full-field Interpretation of fringe patterns, allowing overall assessment of nominal strain/stress magnitudes and gradients.

2.22 Full-field interpretation of strain distribution

Photo stress has the capacity for immediate recognition of nominal strain (and stress) magnitudes, strain gradients and overall strain distribution. This is in addition to the ability to obtain accurate strain measurements at pre-determined test points. This very important characteristic of photo stress is known as “full-field interpretation” and it is peculiar to photo elastic methods of stress analysis. Photo elastic methods depend on the recognition of fringe orders by colour and an understanding of the relationship between fringe order and strain magnitude for its successful application (Micro-Measurements, 2005).

When a test object that is coated photoelastically is subjected to loads, the resulting stress causes strain to occur generally throughout the part and over its surface. The stress and strain on the surface is usually the largest and also the most important. Due to the fact that the photo elastic coating is uniformly and closely bonded to the surface of the part, the strain in the part is carefully transmitted to the coating. This strain produces a proportional optical effect which appears as isochromatic fringes when it is observed with a reflection polariscope (Micro-Measurements, 2005).

The fringe pattern produced by the photo stress is full of information and insight for a design Engineer. For instance, if a part is being stress analysed as a result of field service failures, the overall fringe pattern will usually suggest ways of preventing the failures. This normally involves material removal and weight savings. When a full-field picture of the stress distribution is generated, it shows that the overstressed zone responsible for the failures is surrounded by an area of near-zero stress. a small change in shape will redistribute the stress so as to eliminate stress concentration,

while forcing the under stressed material to carry its own share of the load (Micro-Measurements, 2005).

Similarly, in prototype stress analysis for developmental purposes, the pattern can point the way towards design modification to achieve the minimum weight, functionally adequate part, that is, the optimum design. Furthermore, full-filled observation of stress distribution clearly shows the effect of changing modes of loading, as well as the relative significance of individual loads and/or load directions. These examples shows the many ways by which full-field fringe patterns in photo stress coated test parts communicate with the knowledgeable stress analyst and provide a level of comprehension not attainable from “blind” strain measurements at a point (Micro-Measurements, 2005).

2.22.1 Fringe generation

Photo stress fringe pattern appears as a series of consecutive and adjoining different-colour bands (isochromatics) when they are observed with a reflection polariscope. The different colour bands represent a different degree of birefringence corresponding to the underlying strain in the test part. When there is an understanding of the unchanging sequence in which the colours appear, the photoelastic fringe pattern can be read much like a topographical map to visualise the stress distribution over the surface of the coated test part (Micro-Measurements, 2005).

The test starts by applying load or loads to the unloaded test part. When these loads are applied incrementally, fringes will appear first at the most highly stressed points. Next fringes appear as the load is increased, while the previous fringes are pushed towards the areas of low stress. Additional fringes are generated in the highly stressed regions and move towards regions of low or zero stress until the maximum load is reached. The fringes are ordinary numbers (first, second, third, etc.) as they appear, and they will retain individual identities throughout the loading sequence. The fringes are not only ordered in the sense of serial numbering, they are also orderly, that is they are continuous and never cross or merge with one another as they always maintain their respective positions in the ordered sequence (Micro-Measurements, 2005).

2.22.2 Fringe identification

White light is generally used for full-field interpretation of fringe patterns in photo stress testing. It consists of all the wavelengths in the visual spectrum. Therefore, the relative retardation which normally causes the extinction of one wavelength (colour) does not generally extinguish others. When with increasing birefringence each colour in the spectrum is extinguished sequentially according to its wavelength (starting with violet, which has the shortest visible wavelength), the observer sees the complementary colours. The simultaneous extinction of colours makes the fringes with the higher order to become fainter than the first, which falls in the transition area between red and green (Micro-Measurements, 2005).

2.23 Qualitative significance of fringe

Photoelastic fringes have characteristic behaviours which are very suitable for fringe pattern interpretation. For example, the fringes are ordinarily unbroken bands forming either closed loops or curved lines. The black zero-order fringes are usually isolated spots, lines, or areas surrounded by or adjacent to higher-order fringes. The fringes are ordered in such a way that they do not intercept one another so as not to lose their individual identities. Therefore, the fringe order and strain level are uniform at every point on a fringe and the fringes are always ordered in a continuous sequence both in number and colour. Consequently, if the first- and third-order fringes are identified, the second-order fringe must lie between them and the colour sequence in any direction must indicate whether the fringe order and strain level increase or decrease in that direction (Micro-Measurements, 2005).

This implies that the characteristics of photoelastic fringes are the same as those of constant-level contours on a coloured topographic map. Therefore, any photoelastic pattern can be considered, and visualized, as a contour map of the difference (without regard to sign) between principal strains or stresses over the surface of the test part. In other words, the magnitudes of the strain levels, as indicated by the fringe orders, correspond directly to constant-altitude levels on a topographic map. And the fringe pattern represents peaks and valleys, plains and highland, with “sea level” represented by the zero-order fringes (Micro-Measurements, 2005).

The zero-order fringe in the field of view is normally indicated by black colour. The stress will always be zero if the coated test part has a free square corner or a pointed projection, and a zero-order fringe (spot) will exist in the corner, regardless of the load magnitude, but shrinking in size slightly as the load increases. When there is zero-order fringe, the first-order fringe is normally recognised by the bright colours adjacent to the purple tint of passage. Alternatively, the test object can be loaded incrementally from an initial stress-free state and the starting zero-order fringe which covers the entire coating can usually be followed throughout the loading process as it decreases towards unstressed points and regions where the difference in principal stress is zero (Micro-Measurements, 2005).

Orders can be assigned to other fringes once one fringe has been identified, thereby making sure that the direction of the increasing fringe order corresponds with the correct colour sequence – that is, yellow, red, green, etc. The observer can quickly locate the highest fringe orders and the most highly strained regions by this process. The areas that have closely spaced fine fringes will usually attract the observer's attention, since the regions of steep strain gradient ordinarily signify high strain as well. The observer should also note that any large areas where the pattern is almost uniformly black or grey usually signify an under stressed region (Micro-Measurements, 2005).

Generally, the process of locating the highest fringe order will lead the stress analyst to one or more critical points on a free boundary. When this occurs, the observer knows that the non-zero principal stress at such a point is tangent to the boundary, and its magnitude can be obtained directly by multiplying the fringe order by a constant. The sign of the stress, positive or negative for tension or compression can also be determined very easily on a free boundary with the reflection polariscope (Micro-Measurements, 2005).

2.24 Measurement of principal strain directions

The principal strain directions are always measured with reference to an established line, axis, or plane. Therefore, the selection of a convenient reference is the first step for the determination of the direction or principal strain (or stress) (Metha, 2008). The

reference direction is then suggested immediately in most cases, like an axis of symmetry of the test part or structure; while in other cases, a vertical or horizontal line will suffice (Micro-Measurements, 2005).

When a plane-polarized beam of light travel across a photoelastic coating on a part subjected to stress, it divides into waves propagating at different speeds along the direction of the principal strains (Micro-Measurements, 2005). These two waves will be out of phase with one another after emerging from the plastic and will not recombine into a single vibration parallel to the one entering the plastic. However, at a point where the direction of the principal stress is parallel to the axis of the polarizing filter, the beam will not be affected and the emerging vibration will be parallel to the entering vibration (Mehta, 2008).

2.25 Measurements at a point

It has been established that in the first step of measurement, the stress analyst observes the whole area and assigns to each fringes its order (N= 1, 2, 3, etc.). If N is known at every point on a fringe, therefore a data of strain is obtainable by the correlations in Equation (2.13) for very incremental strain (Micro-Measurement, 2005).

$$\varepsilon_x - \varepsilon_y = Nf \tag{2.13}$$

Generally, the point of interest on the structure will fall between fringes and it will be necessary to establish the “fractional order” of fraction of a fringe. This method is called “compensation” (Micro-Measurements, 2005).

2.25.1 Measurements using the null-balance compensation technique

This technique operates on the principle of introducing into the light path of the polariscope a calibrated variable birefringence of opposite sign to that induced in the photoelastic coating by the strain field. When the opposite-sign variable birefringence is adjusted to precisely match the magnitude of the strain induced birefringence, complete cancellation will occur, and the net birefringence in the light path will be zero. The condition of zero net birefringence can easily be recognized because it

produces a black fringe in the isochromatic pattern where, before introducing the compensating birefringence, a coloured fringe existed (Micro-Measurements, 2005).

2.26 Conclusions

Physical models have provided a means to simplify and understand the complex mechanisms occurring in rocks on a micro to macro scale. But this comes with difficulties in accurate modelling, despite these challenges; physical modelling has been an important approach for investigating the behaviour of naturally occurring materials. Together with acoustic emission (AE), physical modelling can be turned into a very useful tool to study and predict the behaviour of sandstones which are very difficult, if not impossible to study in natural conditions even on a laboratory scale.

Sandstones are sedimentary rocks which comprises of gravels, cobbles and boulders embedded in a fine matrix or cementing material and they have been rarely studied in laboratory testing because of their inherent heterogeneities and the practical difficulties in sampling and testing. Notwithstanding, these rocks can be studied using indirect approach such as physical and numerical modelling.

Consequently, numerical modelling has been developed through a rigorous method for solving problems in rock mechanics. Continuum and dis-continuum approaches have been applied in rock and soil mechanics; however, discrete element methods seem to be more efficient and relevant for modelling the behaviour of granular materials because, in DEM, an overall assembly response is achieved by the interplay and relative movement of discrete particles.

Although DEM has been effectively used to predict many characteristics of granular materials, its calibration and validation is needed against the physical system. Several modelling techniques, such as bonded particle model (BPM) and the clumped particle model (CPM) have been proposed which, to some extent, reproduce the features of natural granular materials using simple circular, spherical or polygonal particles. However, DEM's validation and calibration remain a challenge for researchers and modelling professionals. In this area, work conducted both for frictional granular materials and cohesive-frictional granular materials (cemented

assemblies) were reviewed. The microstructural behaviour of sandstone may be viewed as that of a cohesive frictional material. The review of previous work on the DEM validation for cohesive frictional materials can be categorized as:

1. Modelling the macroscopic behaviour of natural materials, such as rocks and soils, in different loading conditions without taking into account the microstructure of the materials. Natural heterogeneities, anisotropy and scaling make it more complex to develop an accurate correlation between DEM simulations and real materials. Efforts have been centred on the development of complex shaped particles to achieve a similarity of the macroscopic response of the numerical simulation and natural materials.

2. Validations with synthetic materials were also aimed at comparing the macroscopic responses of the physical models and numerical simulations. Although synthetic materials controlled the material's heterogeneity and yielded reproducibility of the test results, similitude was not obtained at the micro level. As a result, there is no correspondence between the micro parameters used in DEM simulations and the microstructure of the synthetic materials. Only macroscopic responses in simple loading were considered sufficient when it is clear that the material's macro response is governed by the grain-cement interaction at micro level.

The importance of the microstructure and associated micro parameters for DEM simulations becomes more obvious when modelling coarse-grained rocks, such as sandstones. In such materials, numerical and physical microstructures have a one-to-one correspondence with each other and should produce similar macroscopic responses.

3. If micro structural similarity has been achieved, micro parameters detailing the grain-cement interaction were either estimated or assumed by the inverse modelling approach rather than through measurements. Furthermore, very few studies have been done experimentally on the micro level interplay between particle-particle and particle-cement interactions. Yet the effect of particle size and size distribution, the effect of inter-particle cement and micro to assembly friction for simple particles are still unsolved questions which ought to be investigated in relation to physical materials. The simulation of rock masses involving discontinuities, heterogeneities and scaling are the next challenges in this area that they can only be adequately

addressed when DEM simulations are validated for simple laboratory models and comprehensively tested.

The survey on sandstone shows that the rock can be made to exhibit plane stress. The property birefringent can be made possible by manipulation of the surface properties. Both discrete modelling and experimental modelling method are thought capable to obtain micro properties used to calibrate the resistance of a cemented quartz grain to displacement. In any deformation studies, when a single grain rotates, micro properties can be estimated in the physical structure. This concept can be employed to understand fractures in cemented granular assembly.

Chapter 3
Research Methodology

3 RESEARCH METHODOLOGY

3.1 Introduction

The deductive approach adopted for this research focuses on the development of advanced photo stress analysis techniques (PSAT) for the determination of micro properties of rock. This novel technique was carried out parallel to the well-known ultrasound measurement technique (Figure 3.1). Subsequently, the micro properties were used for the development of rock and the bulk strength characteristics.

The Griffith theory and the phenomenon of deformations of brittle materials was explored and tested under photo stress analysis and tomography. This approach was followed closely by the path of logic where the initial concept started with this theory and some hypothesis was adopted. Next, by confronting this concept with some preliminary results, the hypothesis was confirmed adequate for the development of an advanced experimental technique suitable for the micro properties determination in rock materials. Measurements were extracted from the natural rock under the control of Griffith theory.

For a perfect brittle material, the fracture strength of single quartz was reported by Griffith (1921). He proposed that a material contain many tiny flaws which cause localized stress concentration of significant magnitude at the flaw. Hence, the theoretical cohesive strength between discrete is obtained at points of stress localizations. This is at nominal stress which is well below the theoretical value. If any single crack propagates into a brittle fracture, the surface area in the sides of the crack increases. Therefore energy is needed to overcome the cohesive force of the discrete. The surface energy is increased by the elastic strain energy which is released as the crack propagates. Therefore Grifith (1921) clearly stated that, "a crack will propagate when the decrease in elastic strain energy is at least equal to the energy, to create the new crack surface" (Guest, 1967). This criterion was applied to determine the measure of the tensile stress which would just cause a crack of a certain size to grow into fracture (Was, 2007).

Therefore, the hypothesis made is that: 1.) any arbitrary point in rock is a grain contact for two or more quartz grains and 2.) the dis-association of the grains from their

contact is the onset of cracking. Scanning Electron Microscope (SEM) experiment was carried out in this current study to reveal rock as a granular assembly of quartz grains. By identifying crack nucleation which is derived from Griffith theory, the least micro-crack in a rock medium will likely allow stress to concentrate at crack tip where the crack concentration is maximum. In other words, this approach is concerned with the concentration of crack-tip stresses with originations and progression of micro-cracks. The deduction will begin with an expected pattern which will be first tested against the observed stress contours in sandstone coated with photo elastic material.

In order to test the hypothesis, the following steps were taken.

1. Taking note of the fact that fracture will occur after critical material stiffness is reached (Liu, 2005)

2. Expected pattern will be generated for consecutive stages of rock deformation to obtain models for grain contact which is a physical representation of the relationships between force and displacement in both longitudinal and transverse directions with respect to the point of examination.

3. Localized stiffness in defected points will be determined by deliberate strain induction of physical and numerical model with the application of stress on notched chevron.

4. Micro-parameters will be used to simulate the Macro-response of the rock material. A confined standard rock test will be employed to validate the outcome (point stiffness).

In order to obtain accurate measurement of the micro properties of Niger delta sandstone from the novel experimental technique developed, the research is made to flow in a circle that depends on Griffith theory as presented in Figure 3.1. The development of the advanced experimental technique was successfully achieved by the hypotheses based on Griffith's theory. Initially, the material was characterised to reveal the internal structure using XRD, XRF and SEM. Micro properties (which includes normal stiffness and shear stiffness of grain contacts) were measured from ultrasound measurement techniques using the fundamental concept of double refraction. These stiffness parameters were used to test the hypotheses of the existence of grain contact at any arbitrary point in sandstone, and the assessment of

the micro properties showed that the data extracted from the sandstone supported the hypotheses.

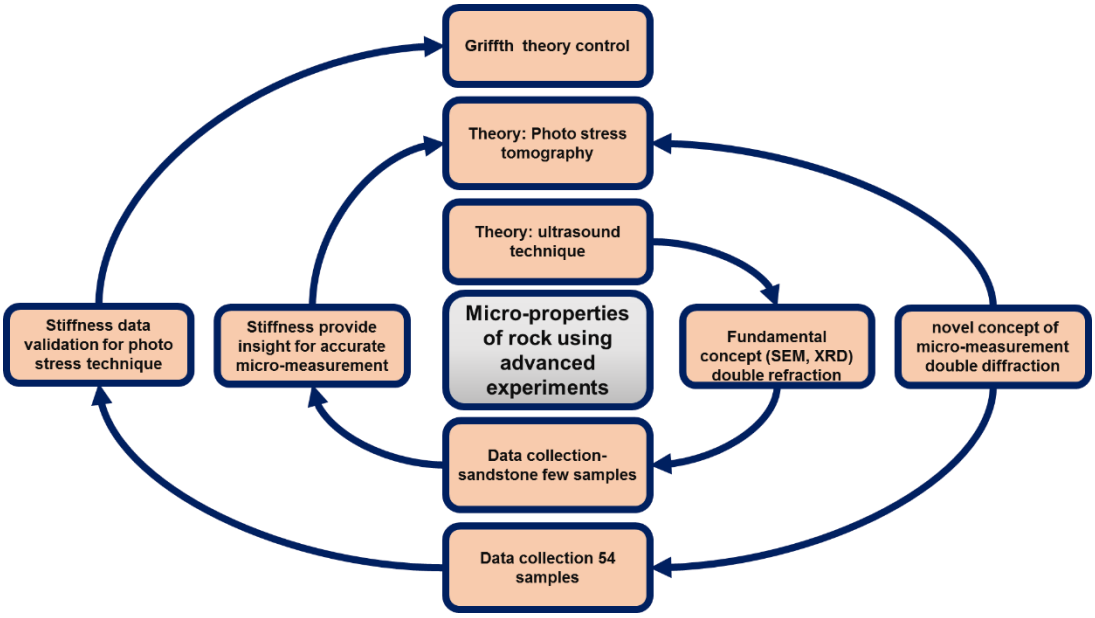

Figure 3.1 Deductive spiral methodology for dependence of micro-properties measured on Griffith theory

Rock characterization revealed the foundation on which the hypothesis of grain-to-grain interaction was conceived for this research. This first step provided the internal structure of the rock, thus micro-mechanical deformation in rock was determined from its micro-structure. While the ultrasound technique was used for micro parameter determination, the Photo Stress Analysis Tomography (PSAT) was employed for the extraction of micro-properties from rock under a single point examination. This arbitrary point was considered as the contact between two mineral grains. The resulting data was used to simulate the rock's mechanical response.

The standard method provided by International Society for Rock Mechanics (ISRM) was employed for the determination of macroscopic data (compressive strength, modulus, and Poisson ratio) of the rock. Subsequently, the micro-mechanical parameters from the rock were validated by comparing the elastic properties from DEM to those obtained by standard ISRM experiments. Information on the direct

relationship between crack-number obtained from DEM were employed to predict bulk strength characteristics of the material in Chapter 8.

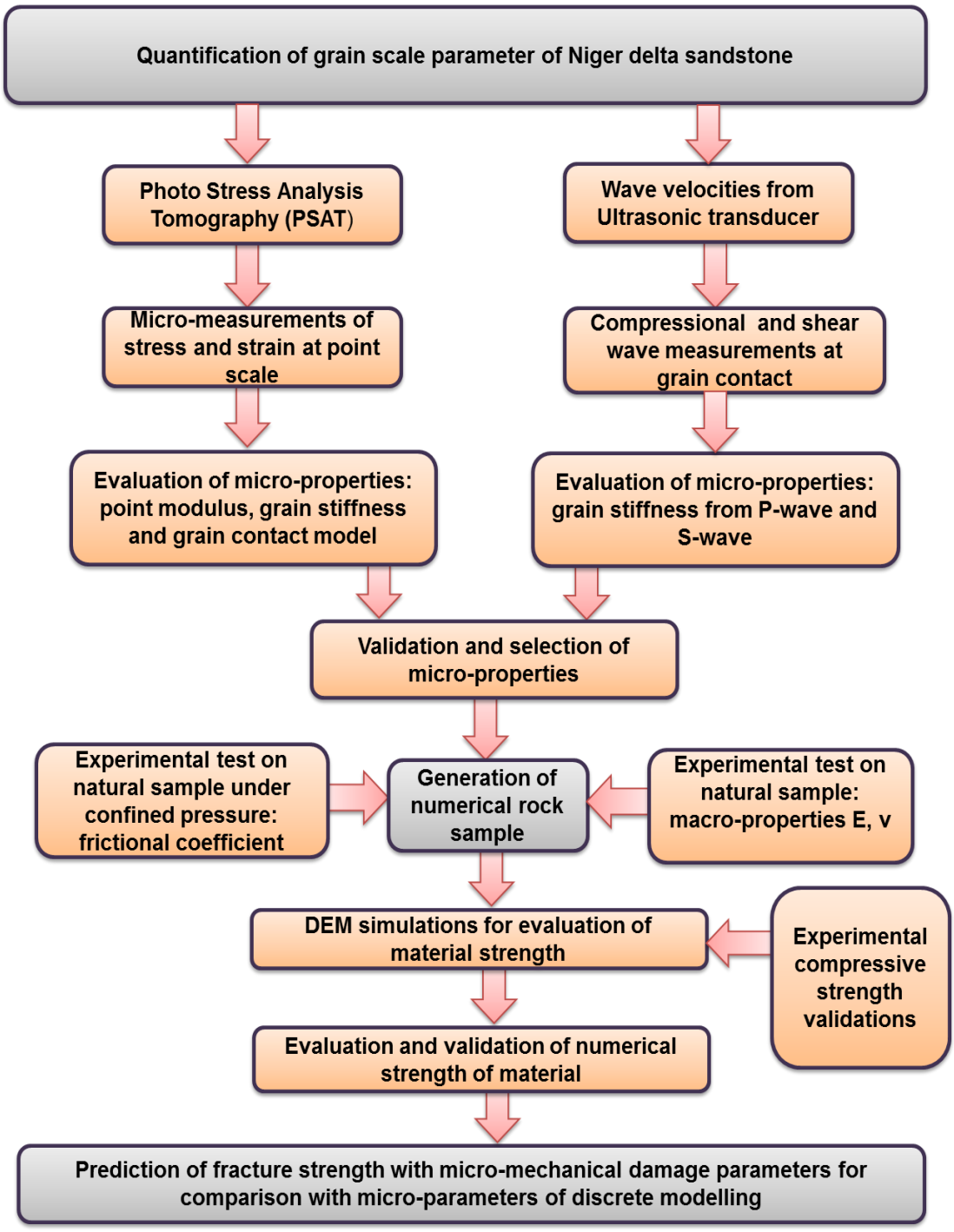

Figure 3.2 Framework of research method

An experimental and numerical approach was adopted which involved the details of the experimental-DEM hybrid carried out for the determination of micro-properties and simulation of rock as provided in three sequential stages;

Stage (1) characterization of rock for discrete modelling

Stage (2) determination of micro-mechanical properties from natural rock

Stage (3) discrete element modelling of rock and deformability in rock

3.2 Stage 1: Characterization of rock for discrete element modelling.

This approach involved identification of the constituent mineral and internal morphological structure of constituent grains in rock using X-Ray Fluorescence (XRF), X-ray Diffraction (XRD) techniques and Scanning Electron Microscope - Electron Dispersive Spectroscopy (SEM-EDS). By using these techniques, quantification and identification of the elemental composition of the rock was carried out. These characterization technique revealed the internal structure of sandstone. Thus visualising the grain-to-grain connection of the mineral composition of rock could be actualized.

The strength characteristics of the rock were thought to be dependent on their constituting mineralogical structures. Hence, rock properties were extracted from natural rock which are typically characterized by the inherent mineral composition, structural appearance, grain morphology, degree of grain interlock, density of packing, grain size and grain contact. These are attributes of the rock's constituent which comes with it from the oil field. It is thought that mineral composition of the grains should be identified for the purpose of relating mineralogy to deformation characteristics. However, theoretical facts have shown that rocks with quartz-particle cementation (Zorlu et al., 2008) are stronger than those with clay-particle cementations (Hardy, 1976).

3.2.1 X-Ray Fluorescence (XRF)

A non-destructive analytical technique was used for the determination of the constituent elements of sandstone. The chemistry of sandstone was determined by measuring the secondary (or fluorescent) X-ray emitted from a sample after it was

excited by a primary X-ray source (Figure 3.3) (De Viguerie et al., 2009). This procedure was followed to determine whether the sandstone contained mineral grains which controled its response to stress. A semi-quantitative analysis of Niger delta sandstone was determined for strength characterization purpose. The results are presented in Chapter 4

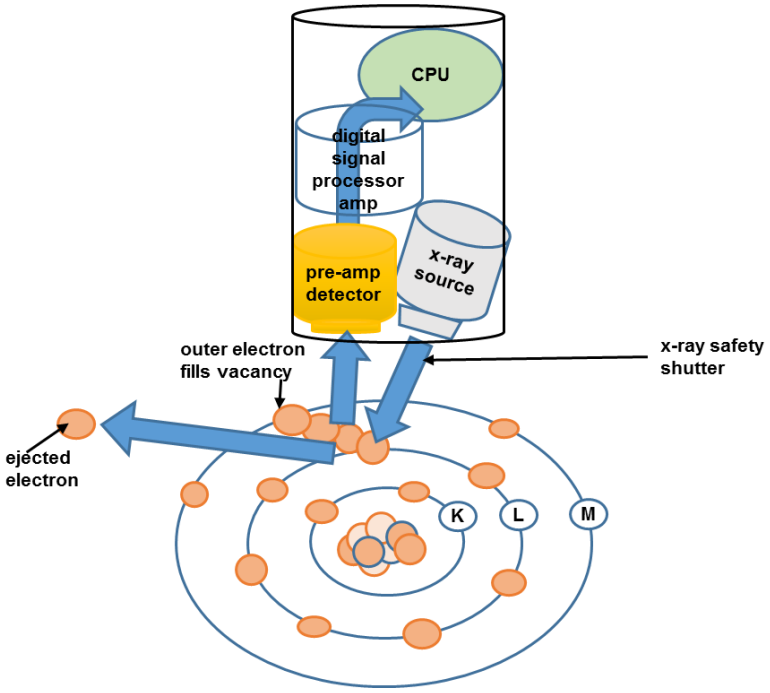

Figure 3.3 Procedure for obtaining X-Ray Fluorescence data from natural sandstone

3.2.2 X-Ray Fluorescence (XRF)

X-ray Diffraction (XRD) was carried out to identify the mineral content of the sandstone. The mineral content were thought to be responsible for the strain exhibited by rock. The minerals were probably responsible for the stiffness properties exhibited by the sandstone because of the likelihood cause of resistance to force exhibited by the cemented contact in the material. It was required to establish the effect of each mineral on the micro-properties and strength of the materials, therefore the XRD analysis was carried out. This procedure produced X-ray diffraction peaks which were formed by a constructive interference of X-ray beam at specified angles from every set of lattice planes in the sandstone specimen. The peak intensities were

determined by the distributed atoms which were within the lattice of the sandstone. The procedure is presented in the Figure 3.4.

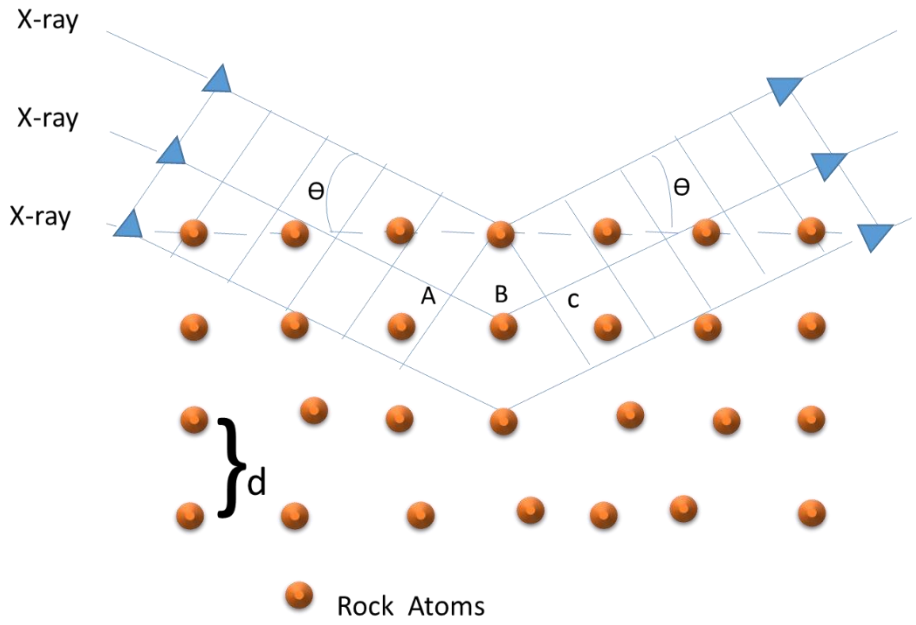

Figure 3.4 Procedure for obtaining X-ray diffraction peak data from natural sandstone

3.2.3 Scanning Electron Microscope – Electron Dispersive Spectrometry (SEM-DES) and Optical Microscope

It is required to determine the stiffness parameters at the grain contact. The application of stress are necessary to displace quartz grain per unit displacement. Therefore the overall strength of the rock depends on the stiffness distribution throughout the grain assembly. Hence, the bond strength will likely contribute to the deformation process. This is because stressing the sample will induce strain in the cemented contacts. Details on the grain and the contacting boundary of the grain will further reveal the nature of the strain occurring within the grain as a granular assembly. The Scanning Electron Microscope – Electron Dispersive Spectrometry (SEM-DES) procedure was employed for obtaining this internal structure as discussed in the next section. It was intended to view the grain shape and interlocking arrangements which are particular characteristics of the rock. In Figure 3.5 the mineral type and granular arrangements were determined by displacement of an

electron after an external excitation by another electron. The grains and the degree of roundness for each grain were identified corresponding to the mineral type. A quantitative contribution of the interlock effect was expected in the prediction of bulk strength characteristics of sandstone. The representation of the grains by a deviation from perfect spherical index has been reported (Zorlu at al., 2008; Bell and Lindsay, 1999). The SEM images are presented in Chapter 4.

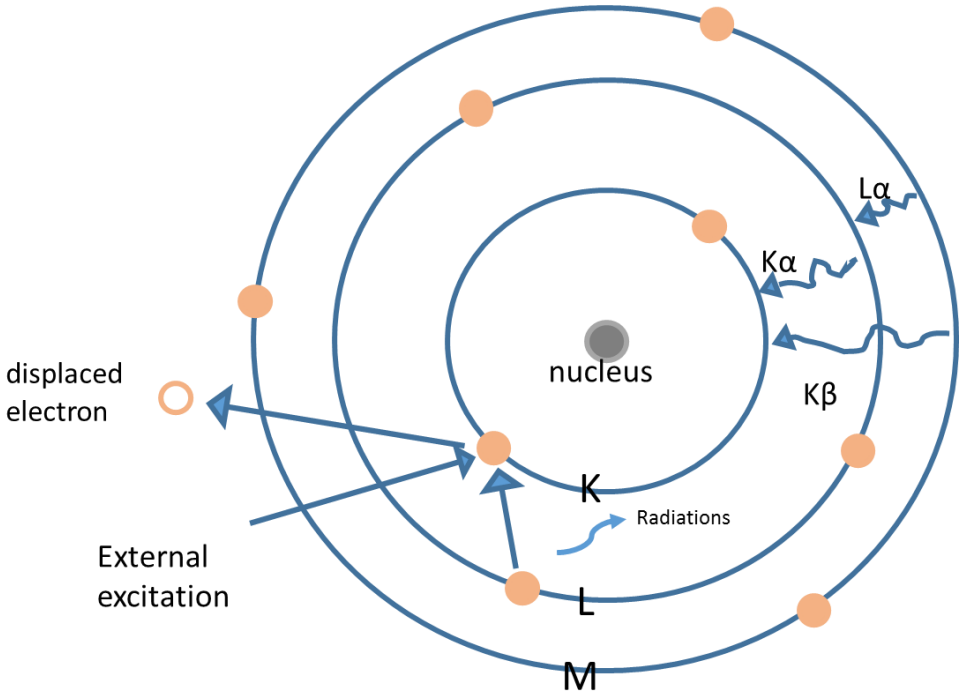

Figure 3.5 Procedure for obtaining mineral type and grain interlocking view from natural sandstone

The energy and number of the X-ray emissions from a sandstone specimen were measured by energy-dispersive spectrometer EDS. The energies of the radiations are characteristics of the differences in the energy between 2 shells and the atomic structure of the element emitted (Figure 3.5). The locations of minerals and the grains are obvious. The results are presented in Chapter 4. The clearer view of these boundaries were viewed by the optical microscope (Figure 3.6).

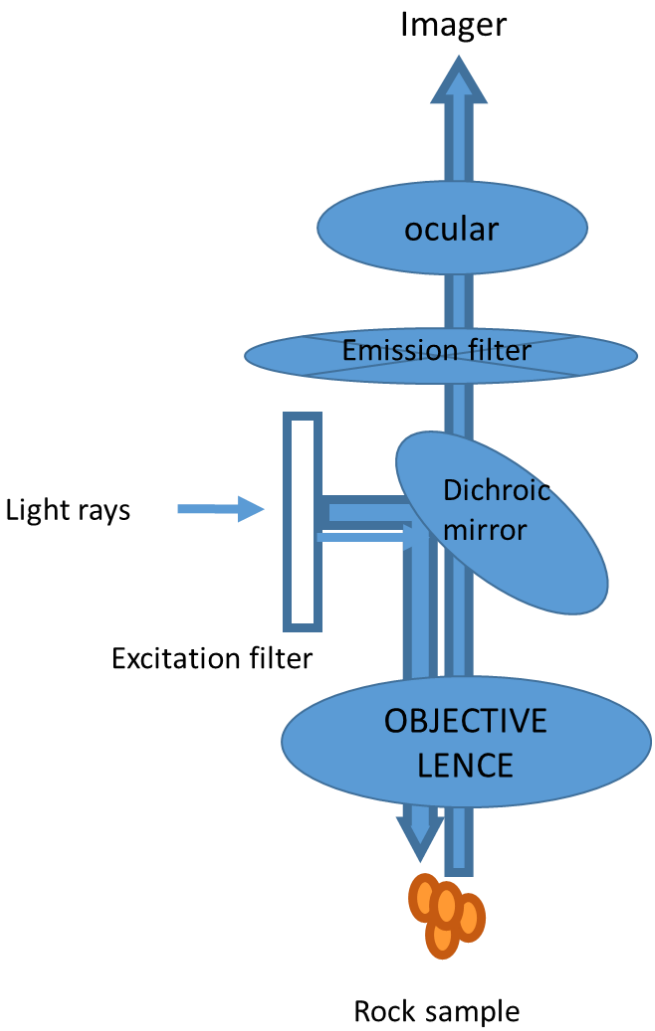

Figure 3.6 Procedure for obtaining grain contact interlocking view from natural sandstone

The microscope view was required to establish that the material under investigation was an assembly of discrete grain with finite clay – cemented contacts. Hence, grain boundary images were required. The hypothesis included the existence of grain contacts at any point in the sandstone. This is evident in previous sections where microstructural information has been provided. Therefore, increased levels of stresses could lead to disarrangement caused by displacement of grains from their contact location. This displacement could translate into strain measureable at any arbitrary point in the rock. Recall also that at the surface of the rock, strain and displacement within the granular assembly is more significant. This is because the grains are displaced easily than they are displaced within the bulk assembly.

In the second stage of this work, it was required to obtain grain contact stiffness. This was carried out by sandstone calibration. Calibration here implies the extraction of geometric figure from the contacting grains in the rock sample. Micro strain data were extracted and the corresponding stress results in a quantitative measure of the strain segmentation that describes grain displacement per unit force applied to the sample. The experimental micro-measurement is provided broadly in the next section.

3.3 Stage 2: Determination of micro-mechanical properties from natural rock:

This involved the development of the grain-grain contact model (i.e the physical representation of the displacement behaviour of a grain relative to another grain). Here, quantitative/geometric figures of grain displacement were used to establish representative equation. Both photo stress tomography and ultrasound techniques were used to capture contact stiffness (micro-parameters). Simultaneously, macro properties (elastic modulus and Poisson's ratio) were obtained using Standard method of test for elastic moduli of rock core specimens in uniaxial compression. Micro- parameters obtained from these experiments served as input parameters for discrete element modelling of rock. American Society for Testing and Materials (ASTM- Designation D 3148-72).

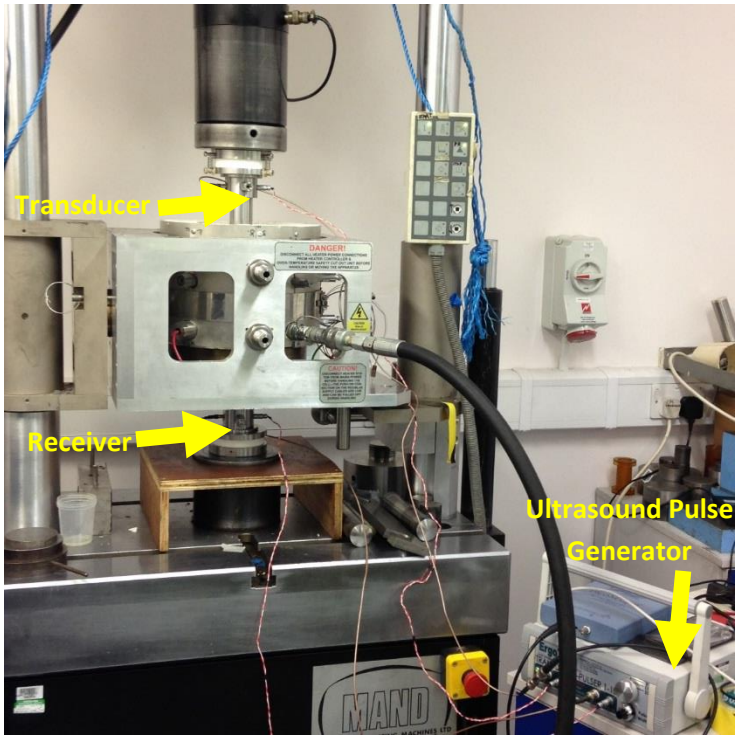

Figure 3.7 Set up of ultrasound measurement for determination of micro-properties

3.4 Double refraction techniques and micro-measurement

Rock deformation begins with internal structural damage which proceeds with continuous propagation of micro-cracks (Wibberley and Shimamoto, 2003; Koyama and Jing, 2007). Detection of these micro-cracks by experimental technique such as ultrasound measurement (Figure 3.7) and acoustic emission method (Momber, 2004) has been reported. The former produces amplitudes signal which are affected by the presence of micro-crack in the sample. Usually, this ultrasound generates electrical signal which is converted to mechanical energy by the micro-cracks. This energy spreads inside the rock medium in form of volatility (Tofel and Trcka, 2013). The micro crack in the sample changes the oscillation and returns it to the transducer to generate signal in the polarization direction. The resulting mechanical energy is reconverted to electrical signal. Hence the ultrasound travel time through the sample of height 50mm was recorded. Subsequently, the velocities were used to evaluate the micro stiffness at grain contacts.

In order to determine micro-properties from rock sample, PSAT is an alternative technique which is a novel approach involving measuring retardation with light wave. By implementing this technique, point stiffness in sandstone was estimated. Instead of ultrasonic wave, the method was made to use light wave for obtaining information at the least point in the rock. Defected grain contact produced anisotropy which resulted into light orientations of different velocities caused by different stress properties at a point in the rock. Usually, the light rays are polarized similar to ultrasonic wave. This has been presented in the study of strain in rock with photo-elastic coatings founded by ASTM (D-06). However, this principle was provided after Davis Brewster who discovered the first phenomenon of light which produce double refraction properties (Brewster, 1815). Later Dally and Riley, (1991) studied the reflected polarized light in solid structure. It was identified that, these authors did not provide the strain response of rock as due to grain contact interaction, which is fundamentally the onset of brittle rock deformation. Therefore, in this work, it was thought that the strain response in rock was evaluated at grain contact deformation state. This measurement procedure was followed instead of measuring the mechanical energy versus frequency as in ultrasound. Retardation of polarized light which was produced due to micro strain in the rock was measured. Subsequently the micro-parameter or grain contact was utilized to simulate the rock behaviour.

By using the elastic properties of the rock as basic inputs in PSAT, the tensional and compressional behaviour of the grains within the rock was represented. This was achieved by a sandstone sample with the notch made to enhance the concentration of load-stress on some targeted grains. Micro-fracturing was then be explained by obtaining point data using PSAT. The grain to grain contact was therefore monitored sequentially to extract displacement data from a point location in the rock.

Macro-parameters from ultrasound measurement technique were used to guide the point data extraction. The measurement for each step was simple with high prospect of reproducibility was adopted. (PSAT) technique can be used to image the progression of micro-fracturing process as controlled by the Griffith theory where expected pattern are to be obtained at points of micro-flaw in rock under the progression of force application on sandstone.

3.4.1 Theoretical view - refraction technique

When light passes through a medium, it can be refracted. This phenomenon is governed by Snell's law similar to the ultrasound technique. The law is illustrated in Figure 3.8. When the medium of transmission changes, the light is refracted. The refracted light is plane polarized. But when only a single ray of light passes through the medium, it is refracted. When sandstone sample was subjected to loading, the strain in the rock was transferred to the coated surface which exhibited an optical anisotropic property (called birefringence). A single ray was refracted which produce two refracted rays. These are known as ordinary and extra-ordinary ray (Figure 3.8).

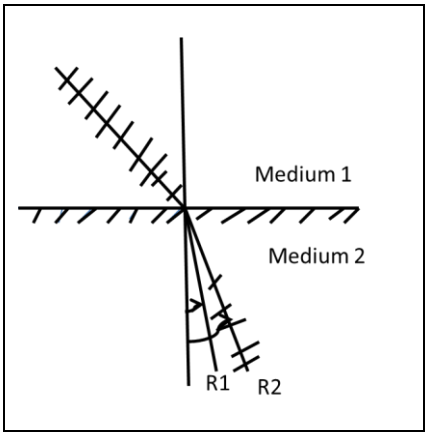

Figure 3.8 Schematic of the refraction process on photoelastic coated-sandstone showing the light refraction in anisotropic/strain localized point

Refracted ray is (r2). By comparing the ray with the ordinary ray (r1), it is clear that the rays passing through the anisotropic solid travels at different speed and direction (Figure 3.8). The optical axis was defined by a line drawn in the direction where no double refraction was seen. In this optical axis, a rotational symmetry in the camera was enabled so that the ordinary and extra ordinary rays are plane polarized where these planes are orthogonal to each other. (Usually if the material remains isotropic, both ordinary and extraordinary ray will travel same direction if the incident ray were parallel to the optical axis). But due to the occurrence of anisotropy, the optical axis and the incident ray are perpendicular. The extra-ordinary ray travels faster than the ordinary ray in the same direction. Thus the application of refractive technique for detection of point retardation was achieved. In the end, the rays were polarized perpendicularly.

The resulting rays from the medium had a phase difference which exhibited itself as fringes. Thus double refraction was not observed in some point where stress was not localized. For the full field view of strain localized points, it was observed that tensile and compressive fringes are significantly distributed throughout the stressed sandstone. It was thought that grains within the sandstone matrix can be compressed and enabled the coating exhibit compressive fringes whereas; the tensile fringes were exhibited due to tensed grains within the rock matrix (Figure 3.9). The schematic diagram of tension and compression of grains are illustrated in Figure 3.9. If the grains in sandstone are firmly bonded, then before compression, they resist the force load by the tension created at the grain contact. Both compression and tension are displayed by the fringes/contours. Since strain is not uniform in all direction, double refraction usually occurs.

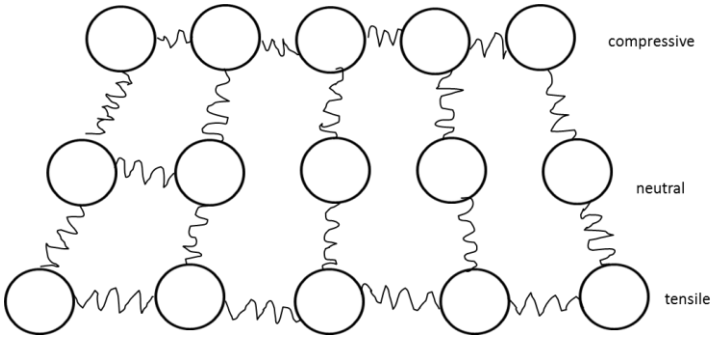

Figure 3.9 Schematic diagram of a granular arrangement of quartz and the cement bond under compression and tension

Preliminary view indicated that both compressive fringes and tensile fringes were uniformly distributed at the tip of the notch. Compressive fringes dominated after the tensile behaviour was exhibited in the perpendicular direction to shear direction. These two directions contributed to phase difference in the light rays. The notched sample obviate the need for cracking through the chevron.

3.4.2 Determination of normal and shear stresses

On a surface examination, the amount of stress particles impose on another particle can be in any direction relative to the surface. The stress can be measured in the normal direction as normal stress (compression or tension) perpendicular to the

surface as illustrated in Figure 3.10. It can also be measured in the shear direction as stress that is parallel to the surface (Hauke and Moreau, 2008).

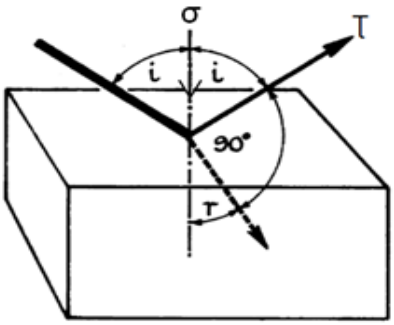

Figure 3.10 Polarized light at a surface "i" is the incident light, "r" is the refracted light "σ" and "Ƭ" are normal and perpendicular directions respectively.(Heywood, 2013)

Photo-elastic technique produced isochromatic fringes and isoclinic fringes which revealed stress location in structures. Isochromatic fringes were produced due to stressed points reflecting locus of points with constant principal stress difference. These isochromatic were identified by the light and dark fringes in monochromatic light source. If the light is an illumination of white light, they are identified by coloured fringes. The difference in principal stress is related to the birefringence or retardation with stress-optic law in Equation (2.14) and Equation (2.15). (Dally and Riley, 1991)

$$(\sigma_1 - \sigma_2) = k\delta = karcsin\left[\frac{I_{max}-I_{min}}{I_{max}+I_{min}}\right] \quad (2.14)$$

Where $(\sigma_1 - \sigma_2)$ is the principal stress difference which was evaluated for normal and shear direction, k is the optical constant for the photo elastic coat (0.06 from the manufacturer) and δ is the retardation $I_{max}\ and\ I_{min}$ are maximum and minimum light intensities respectively. The material thickness may be incorporated to obtain the corresponding principal strain difference $(\varepsilon_1 - \varepsilon_2)$ in Equation (2.15) (Vishay,2005).

$$(\varepsilon_1 - \varepsilon_2)k = \frac{\delta}{2t} = [(n_1 - n_2)] \quad (2.15)$$

Where $\varepsilon_1 and\ \varepsilon_2$ the principal strains, t is the coating thickness and $(n_1\ and\ n_2)$ are the refractive index in the corresponding directions of stain measured. The direction at the point of measurement was determined from the rotation angle. A black point was used to observe light extinguished presented in Figure 5.14

While the isochromatic are invariant even with model orientation, the isoclinic is identified by the changes in light intensity when the model is rotated. They are produced when the direction of any of the principal stress coincides with polarisation-axis of the polariser. The direction of the principal stresses in the sample is observed using the isoclinic fringes. By correlating stress difference with the isoclinic, two-dimensional stress analysis can be carried out (Ramesh, 2000). Isoclinic fringes are produced preferentially to reduce isochromatic fringes by placing small load per increment on the model under investigation. The isoclinic are also produced with the use of photo-elastic coating material of high material fringe constant (Ramesh, 2000).

3.4.3 Data point during micro-measurement

The setup consists of a white light source and a Polaris cope whose principle involves two polarizers. In the periscope, the source-light transmits through a polarizer which changes the light to polarized light. The ray travels through the stressed model/sample and further into every point in the model in the direction of principal stress. Next the light is reflected back, passes through the second analyser and the fringe pattern is produced. A high material fringe value photo-elastic coating material was selected to distinguish isoclinic lines.

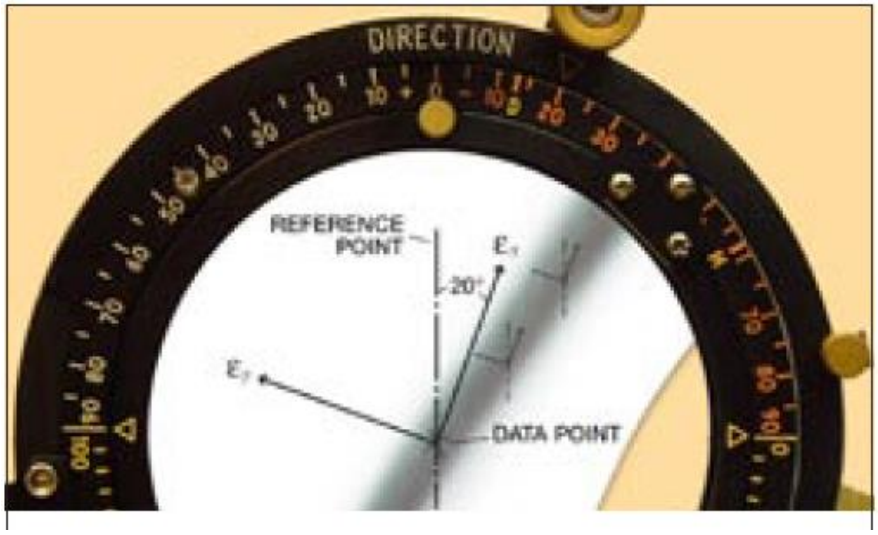

Figure3.11

Figure 3.11 Principal stress directions revealed by rotation of the polarizer/analyser axes (Micro-Measurements, 2005)

In order to produce complete extinction of light at the test point, a plane polariscope set up was used. Then, an isoclinic is positioned over the point and the directions measured with respect to an established reference. Note, with the Model LF/Z-2 Polariscope, a vertical axis was chosen and the principal strain directions were read from the calibrated dial.

The anisotropy behaviour of the rock enhances stress measurement (Amadei, 2012). This property has been employed to explain linearity of the stress and strain relationship of brittle rock whose deformation was not linear with load force. Here by inducing strain into the rock, the anisotropy response was transferred to the photo-elastic coating which allows retardation in both normal direction and shear direction to be captured (Figure 2.17).

3.5 Single point data hypothesis in research method

Single point stress information exists in rock (Amadie, 2012). But some authors say it is very difficult to measure. However, it is important for discrete modelling of rock. Therefore, an attempt is made in this current work to estimate a point parameter which is referred to micro-parameter.

Based on the findings in the previous procedures state in section one and two, experimental determination of micro-properties was carried out using Photo Stress Analysis Tomography (PSAT) and Ultrasound measurement technique. The micro-parameters were compared. Subsequently, these parameters were used as inputs for rock simulation using DEM. Thus, deductive approach allowed the stress concentration and enabled stress measurements. It infers that stiffness property at a single point location in the sample can be estimated directly. At each point in the sandstone, the grains are contacting one another. The plot of maximum shear stress versus corresponding fringe order was used to evaluate the material fringe value. The force acting between two contacting grains (Equation 3.6) was derived from the stress/pressure applied (P) to the pack of contacting grains. By correlating the incremental stress acting on the pack of quartz grains with the surface area of each grain, the number of contacting grains and porosity, the external force was evaluated. (Mavko et al., 2009; Bachrach and Mukerji, 2004).

$$F = \frac{AP}{C(1-\phi)} \tag{3.6}$$

Where the surface area A is given by $4\pi R^2$, P is the stress applied to the sandstone granular assembly, C is the number of contacting grains and ϕ is the porosity of the sandstone.

Using Equation 3.6 both tensional force and compressional force were estimated data extracted from Photo Stress Analysis Tomography (PSAT) technique and the plot of the forces versus displacement was used to estimate contact stiffness.

Grain displacement was estimated using the fringe (or wave) distance from the point where fringe originate in the sample. The displacement corresponds to strain in the granular pack. The magnitude of the distance was multiplied by the real length per length of the sample under investigation. The corresponding stress that produces each fringe was also recorded to estimate fringe constant. The vertical displacement and horizontal displacement at each point was estimated by measuring retardation in both directions respectively. The results are presented in Chapter 6.

3.6 Stage three: Discrete element modelling of rock and deformability in rock: hypothesis validation

In order to carry out a validation of the stiffness data recorded from experiments, the data were entered as inputs data for numerical modelling. The macro-properties derived as response from the simulated rock was used for the validations of micro-property estimations which were hypothesized in stages one and two.

Observe that the sandstone examined in experiment was a brittle homogeneous rock of discrete grains (with a degree of spherical index). The experimental results discloses deformation trend as the quartz grains overlapped under mechanical load. Also, stress contours were generated due to grain displacement. It is thought that the quartz grain probably interacted probably at grain contacts having a measure of spherical inter-layer.

During close observation of SEM, the grains were observed to be arranged in an overlapping manner. Each overlap was finite compared to the grain diameter hence contacts size was only a point captured by the micro-measurements. The clay was finite in the quantitative analysis of the sandstone. By recording force magnitude and the corresponding displacement at each point of examination, a contact mode was established as the stress contours were clear indications of the relative motion of the grains which were attributed to moment and force at the point of examination. The contact of the discrete grains was stiff even when bonded with small contact. Hence, a significant amount of force was required to displace the grains. It means the bond will break down before the final large crack opens.

The particle flow code (PFC) is a software package which was developed to numerically synthesize rock. Some assumptions that were found very satisfactory to fundamental experimental findings on rock deformability, (stage one and stage two) these assumptions include.

1. Representation of grains with particles which were spherical hard object with a finite mass.
2. Each particle’s motion does not depend on another’s and can change position and spin.

3. Interaction of these particles occurs only at their contacts; since these particles are round, only two particles touching points are considered as contact.

4. The point of particle overlaps are called contact which are small compared to particle size hence contacts cover a small area.

5. The rule governing force-displacement at each contact correlates relative particle motion to gain momentum and force at the contact with neighboring particle.

6. Particle clusters are formed by the small contact bonds, carry load and can deform.

7. Grains can be represented by gluing two or more spherical particles to form the desires grain spherical index.

The PFC package was therefore employed to carry out discrete modelling in two different stages.

The first stage involved the development of the synthetic model sandstone and the second stage was the numerical testing of the synthetic sandstone. The rock was built numerically using the normal and shear contact behaviour to incorporate particle contact model. Next the tri-axial compression test was carried out for the evaluation of the micro-parameters from the macro-elastic properties. Further, the tri-axil test allowed the detection of the crack number synonymous to the acoustic emission counts. The crack numbers are provided in Chapter 8. Acoustic events directly indicated damage localization. Hence, the overall research aim was achieved because subtle fracture in sandstone was successfully identified via replication of micro-mechanism of deformation in experiments by discrete models.

The objectives to help in achieving the overall aim of prediction of bulk strength included;

1. Measuring stress transmission through the cementitious rock materials. The stiffness parameter was incorporated first into simulated model. This is addressed exhaustively in Chapter 7.

2. Sensing shear stress distribution and using its nub at micro-scale to simulate its bulk fracture strength. This is addressed in Chapter 6 and 7.

3. Influence of grain shape properties on the micro-mechanical damage was carried out. The crack number generated was used for the damage analysis. This is addressed in Chapter 8.

3.6.1 Measuring stress transmission through cemented materials.

Information on the measurement of stress transmission through cementitious materials is provided in Chapter 7, however, the summary of the procedure is provided in this section. By incorporating the micro-scale data obtained from experiment, normal displacement and shear displacement was measured experimentally. By incorporating force chains between each contacting grain, force transmissions through granular matrix were simulated. In previous reports, micro-parameters (e.g. grain modulus and stiffness ratio) were obtained numerically by calculations that reproduce the macroscopic elastic properties (young modulus and Poisson's ratio). This research seeks to improve simulation inputs by utilizing the detailed micro and macro properties of real sandstone. Hence, this provides the detailed normal and shear force localization using force chains. Simulation codes were applied with direct input techniques to improved replication of the real rock behaviour.

DEM: At this point, discrete model was developed based on the observed internal stress distribution of the sandstone under photo stress analysis. The numerical solution was top down simulations limited to pre-peak stress point. The assumptions of discrete modelling itemized above were incorporated in the modelling. In addition the following assumptions were included.

- Two concrete observations have shown that the normal stiffness was experimentally validated to be right, (ultrasonic technique and the photo stress technique). The parameter of concern was the discrete particle shape. However, the SEM image and the optical microscope indicate spherical indices that could be approximated to be two to three spherical particle clumped-shapes. Therefore the clump particles were generated and the mixed clumps were varied until the desired property of the sandstone was obtained. Clumped particles were used to make adequate the effect of particle morphology on the mechanical behavior of the rock.

- Contact model were experimentally developed and fixed into simulations. In order to make adequate the rock behavior, the exact initial extensile internal response during initial stages of mechanical loading.
- The degree of force transmission in the grain assembly depends on bond strength connecting grains. Sensitivity analysis was used to obtain the adequate bond strength.
- Validation of models was easily carried out with normal displacement and shear displacement data from the numerical model. A point pressure was applied to a notched sample to target stress application to a point. Both experiment and modelling test were limited to a point application of stress concentration.
- Corporate analysis with tested homogeneous sandstone sample (Berea sandstone) was used to make adequate uniform microstructural distribution.

3.6.2 Crack nucleation and identification in discrete modelling of rock.

In order to identify the onset of crack growth, crack nucleation process was monitored during initial loading stages in the discrete model. The bonds were installed between contacting grains. Force applications were directed on the bond until the load magnitude attained elastic limit of the bond so that crack nucleation was captured. Contact bond model obtained from experimental model were installed and the elastic spring between particles were drawn as force chains having both the normal and shear stiffness quantity. These springs acted at contacting points between grains and were used to reflect forces transmitted through the network of the grain matrix. Since the sandstone contained cementitious material gluing contact particles together, simultaneously, the parallel bond properties were specified to monitor the moment caused by grain rotation which could be resisted by the installed spring at the same finite contacts. Only the bond strength was varied until the rock properties were reproduced.

From Figure 2.4 and 2.7 (a.) represent Normal and shear stiffness between particles. The contact stiffness, Kn and Ks remain active even after the bond breaks as long as particles stay in contact. The bond stiffness (force per unit area), $\underline{K^n}$ and $\underline{K^s}$ are suddenly removed when the bond breaks regardless of whether particles stay in contact or not. (b.) represent Constitutive behaviour in shear and tension (i=s,n).

3.6.3 Development of notched sample with point data from experiment

These require the experimentation targeted at testing the hypothesis used to obtain the micro-properties. The contacting grains were cemented; they exhibited tension and compressional stiffness properties under stress. Therefore analysis of stress at any point below the loaded notch in the rock sample was thought of to provide grain displacement and strain dependence on stress level. Experimental and numerical data were compared. The significance of this procedure is its usefulness in solving the problem of stress analysis of the complicated geometrical composition of rock.

The thrust of this procedure is to obtain inputs for the DEM with a block procedure. The force transmission was to be observed in synthetic sample which was notched by excavation so that the notch/crack tip is used to study bond deformation. The flow diagram shows the algorithm of procedure followed during the simulation of compression on the bond at the notched numerical sandstone (Chapter 7)

By introducing the contact-model, the force distribution in natural rock was included into the sample. The chain network of force was composed of linked cylindrical symbol located at each contact in the sample with the centre of the cylinder located at the contact. The cylindrical symbol axis was aligned with the contact-model force vector (F). The radius of the cylinder which is proportional to the magnitude of vector magnitude (F) saved as history data.

The result of the force distribution is provided in Chapter 7. The tensional and compressive stress fields in the sample were presented. The code for this section is provided was written as a fish which was limited to identification of deformation nucleation at onset. The same effect of tension and compression caused by force chains in the real sandstone is significant. This is due to the fact that the outcome of the tension and compressive behaviour of grain contacts in discrete model could validate the success of the experimental point stiffness. This stiffness property was used to build and replicate behaviour of the rock. Next, synthetic model was made cylindrical for proper evaluation with standard test (ISRM test).

3.6.4 Development of cylindrical sample and using its nub at micro-scale to simulate its bulk fracture strength

The development of cylindrical sample was achieved which aided the determination of the bulk strength of the rock. In the previous procedure, the contact and bond model of an experimental point were used to replicate the grain contact behaviour of the sandstone under elastic regime. The procedure in this section involved calibration of the macro-scale models to obtain the micro-parameters of the rock in Chapter 7. The framework developed in view of the hypothesis that; any point data within the rock surface will estimate the grain contact behaviour.

3.6.4.1 Stage one: input parameters for model development of numerical sandstone subjected to standard test

During the development of the simulated sample of sandstone, the procedures utilized the direct modelling method which generated particles replaced with clumps. Individual clump was connected with parallel bond and the breakage of the bond was represented with contact bond damage.

3.6.4.2 Specimen specification with grain generation using PFC

Clumps were cemented together in a vessel with walls made to form an isotropic well-connected system at 1MPa confinement pressure. Refinement level was connected with each region so that high refinement level lowers the grain size. Each sandstone region had a set of microscopic properties which were peculiar to the grains so that all grains and bonds locations mapped into the sandstone region. Micro properties were assigned to these locations in a sample of height 98mm by diameter 38mm. When a specified isotropic stress was installed, floating grains with less than three contacts were eliminated and the final group of grains were bonded together by installation of parallel bond. The vessels were then removed from the specimen ready for boundary- value simulation and specimen testing.

3.6.4.3 Numerical tri-axial test and formulation of deformability parameter during DEM

Using the Equations 3.12 to 3.17, the installed linear contact model were used to deform in-between particle contacts. After stress equilibrium was established, a

servo-mechanism was applied as in the laboratory experiment. At any contact for two discrete clumps *A* and *B,* which usually overlapped at contact in the discrete element model. The radii of these clumps could be denoted by rA and *Rb*, while *xA* and *xB* were used to denote their corresponding vectors in the global set of axes for positioning. The vector *F* of the forces interacting denoted the reaction between particle *A* and particle *B.* This was separated into normal *Fn* and shear vector *Fs*. These forces were automatically connected to relative displacements U^n, with normal stiffness K*n* and shear stiffness K*s.* Where U^n is the relative normal displacement between two particles denoting normal contact vector with *n*, we can denote Δ*Us* with the incremental tangential displacement. The shear force *Fs* was obtained by summing the Δ*Fs* increments. The normal and tangential stiffness were defined by Equation 3.12 and 3.13 (Potyondy and Cundall, 2004).

$$F_i^n = K_n U^n \tag{3.12}$$

$$\Delta F_i^s = -K_s \Delta U^s \tag{3.13}$$

Where $K^n$and K^s are the input values of normal and tangential stiffness for both contacting clumps (particles) A and B connected with a radius multiplier.

To reproduce the behaviour of sandstone under deformation of contacts, the pure axial and pure shear loading were used. These correspond to the normal and shear behaviours which were uncoupled, and the contact normal and shear stiffness were used as expressed in Equation (3.14) (Potyondy and Cundall, 2004).

$$K_{n=} \frac{AE_c}{L} \tag{3.14}$$

$$K_s = \frac{12IE_c}{L^3} \tag{3.15}$$

Where, E_c is the contact Young's modulus, which is greater than the ensemble Young's modulus. Since the experimental model revealed a linear contact model, the contact stiffness, K^{ξ} were computed by assuming that the stiffnesses of the two contacting particle K_A^{ζ}, and K_B^{ζ}, were in series as stated in Equation 3.15 and 3.17(Itasca, 2004) (Potyondy and Cundall, 2004).

$$K_{\xi} = \frac{k_A^{\xi} k_B^{\xi}}{k_A^{\xi} + k_B^{\xi}} \quad 3.16$$

Where ξ = (normal, shear)

$$K_n = K_n^A = K_s^B \quad 3.17$$

Since the two particles were assigned the same normal and shear stiffness. It follows that the relationship between these stiffness and the modulus at a single contact bond was found by substituting Equation 3.16 into Equation 3.17 above to obtain Equation 3.18 (Potyondy and Cundall, 2004).

$$K_n = K_s = 2E_c\{2\dot{R}\} \quad 3.18$$

In the scripts, based on Equation 3.18 the modulus at a single contact bond is directly proportional to particle stiffness, and inversely proportional to particle radius.

The absence of Poisson's ratio in the link between particles in equation 3.18 implies that at microscopic scale, no relationship exist between Poisson's ratio and particle stiffness. However, a macroscopic Poisson's ratio was observed for the assembly of the arbitrarily packed particles. Usually the normal to shear stiffness ratio was correlated to macroscopic Poisson's ratio affected the amount of load carried in the shear and normal modes at contacting points, hence influenced the macroscopic failure mechanisms. The deformability micro-parameters were specified in order to achieve a consistent means of setting deformation: the two parameters specified were the Young's modulus at every particle-particle contact, E_c; as well as the stiffness, ratio K_n/K_s.

Using Equation 3.18, the normal stiffness and shear stiffness could be evaluated since the scripts set a particle radius to be of equal magnitude with the mean radius. This simulation has been implemented in the particle flow code (PFC) (provided by Itasca consults). PFC employs a force-displacement approach with the Newton's second law of motion to control the motion of each particle as the summation of forces applied on particle contact. The dynamic behaviour of the computation involved a time algorithm in which the velocities and the accelerations were constant at each time step.

During deformation by reduction in the magnitude of R, it mimicked the effect of reducing the strength of the cementation material at the grain contact in the sandstone.

The complete set of the micro-parameters included the stiffness ratio k_n / k_s , the Young's modulus at each particle-particle contact Ec, the Young's modulus of each parallel bond $\bar{E}_c$, the particle friction coefficient μ, the normal strengths, $\bar{\sigma}_c$, shear strengths $\bar{\tau}_c$, of the cement-like material represented by a parallel bond. The radius multiplier which sets the radius using Equation 3.19: (Potyondy and Cundall, 2004)

$$\chi = \frac{E_c}{E_c + \bar{E}_c} \qquad 3.19$$

Where χ is modulus-damage index which is a local measure of the damage, in terms of modulus reduction, that occurred when a parallel bond broke. E_c is the Young's modulus at each particle-particle contact; $\bar{E}_c$ is the Young's modulus of each parallel bond. The overall modulus at a parallel-bonded contact (at which the two bonded particles have a non-zero overlap) was calculated as the summation of E_c and $\bar{E}c$, When a parallel bond broke, the overall modulus at the same contact is reduced by $\bar{E}c$, Next, the relationship between macroscopic modulus and deformability's micro-parameters were estimated using Equation 3.20: (Potyondy and Cundall, 2004).

$$E = \frac{E_c}{\zeta} + \frac{\bar{E}_c}{\bar{\zeta}} \qquad 3.20$$

Where E is the macroscopic modulus, ζ and bond$\bar{\zeta}$ are the ratios of micro-modulus to macro-modulus contribution for the particle-particle contacts and the parallel bonds, respectively.

3.6.4.4 Variation of particle shape and parameter matching:

In order to compare the stiffness ratio and the micro-elastic modulus obtained from experiments with numerical modelling, grain shape was investigated. This was because, a wide range of grain sizes of 80-120μm was observed in SEM image. To achieve mixed particle representation, all the clumped shape were mixed at ratio as follows (1) 0.95:0.05 for 2-particle clump, (2)0.45:0.55 for 2-particle clump and 3-particle clump mix respectively and (3)0.05:0.95 for the 3-particle clump to build the

synthetic. The grain density and bulk density were inputs that catered for the rock's porosity.

3.6.4.5 Effect of confined pressure on the rock:

Overburden pressure is referred to the in-situ stress around rock. It is one major factor that may limit the application of micro-structural estimation in understanding macro-response of rock's deformation. Hence, the influence of the overburden pressure on the macro-properties will be presented in Chapter 6. The study included the application of confined pressure on rock.

Parametric study was done under confined pressure on the sandstone. The macro Young modulus and Poisson's ratio calculated from tri-axial experiment on real rock were determined. These values were compared to the simulated tri-axial test on synthetic rock of same geometry and dimension as in the natural rock. The particle contacts in the natural rock and simulated rock responded to load stress. By introducing similar load pattern, the force displacement data of both samples was determined. This data were captured due to strain localization induced by the loading. Therefore, the discrepancies between the elastic property of the natural and synthesized sandstone can be discussed.

3.6.4.6 Utilizing micro-mechanical damage to predict bulk strength

Influence of petrographic properties on micro-mechanical behaviour was studied in Chapter 8. The corporate samples (Berea sandstone and Doddington sandstone were used to represent sandstone of different minerology). This included the effect of mineral content on the mechanical strength of the rock. The crack number was generated numerically. It provided crack damage threshold data. In Chapter 8, the crack damage indicators were obtained experimentally as volumetric stiffness. The damage indicators were compared and they provided clues for preventive strengthening of sandstone. The same sample used to identify damage threshold (crack initiation and crack damage) for comparison fracture predictions purposes: crack number were used for the prediction of fracture. In summary the three stages identified above for the determination of micro properties of rocks and the numerical validations is illustrated in Figure 3.12

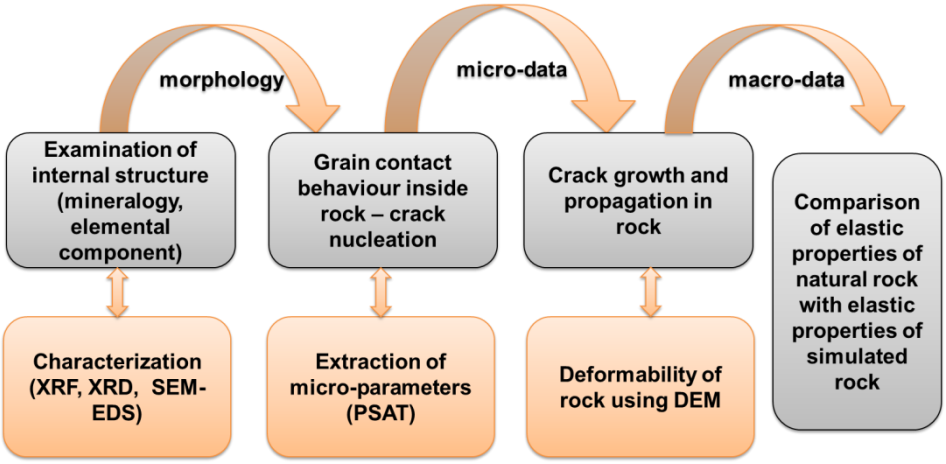

Figure 3.12 Stages of the research methodology

3.7 Conclusion

A coupled physico-mechanical characterization was used to visualize the composition and arrangement of quartz in sandstone, and the sandstone was found to be a granular system. In sandstone, the standardization, development and implementation of a new grain contact modelling were established. The adopted mechanisms of deformation in the granular assembly constitute strain obtained due to stress-mediated cemented-quartz-grain compacted together, hence, grain-to grain contact model was obtained. By the inclusion of state-full grain to grain contact, the model was found applicable to numerical algorithm which simulates the exact grain assembly of the physical material suitable for valid numerical compression test.

Actualization of envisaged three sequential methodologies (characterization, experimental modelling and numerical modelling) established a full understanding of contact modelling. Here, a rigorous calibration based on the conceptual idea of coupling elastic properties from the ultrasound technique with the imaging system of the photo elasticity was employed. This reveals the same mechanism of deformation for rock in the granular assembly. The grain displacement was directly related to Newton's second law in the numerical modelling.

Granular assembly with two and three particle clumps system was used to explore the role of grain morphology in discrete modelling. With the inclusion of the grain

density and bulk density, which results in a porosity of 22% for granular assembly under investigation, coupled with a grain size of 80 -100microns, porosity and packing density was catered for in numerical assembly. Hence, the physical sandstone was well represented numerically. The inclusion of the cementation due to the clay cementing particle observed in characterization was also involved.The observed value of elastic modulus and Poisson's ratio confirmed the accuracy of the grain contact models established in this research. Although some factors such as loading rate affect models, however, the grain contact stiffness parameter derived from the experimental model is constantly stiffness parameter. This requires cementation of each contacting grain which exerted a significant influence on the bulk modulus of elasticity and Poison's ratio.

The achievement in this research is that numerical tri-axial test and unconfined test-experiments show the progression of rock deformation. Deformation mechanisms followed the changing mode of macroscopic elastic properties.The displacement of grain from contacts reduced the material strength under compression within the numerical granular assembly. Hence, macro-properties were in line with the applied stress, not awkward, but a right validation.

In the next section on results of findings, it is envisaged that the coupling of the real physical rock micro-properties results in a feedback of exact mechanical behaviour of the granular under compression. This makes numerical modelling of mechanical behaviour of rock less complicated. It ultimately depended on the strength characteristics of the grain contact and the cementation which had an impact on the establishment of elastic property.

In the next chapter, particle clumps variation will be examined to establish the effect of grain morphology on the elastic properties of rock. Less complex shape particle represent the rock, while uniform clumps or mixed clump system represent the rock. The higher bond strength affected the rock and the degree of interlock affected the elastic behaviour during mechanical loading. The second Newton's law was still assumed but the significance of incorporating the real grain contact model in this work was evident by the simulation time and the accuracy of elastic properties which has been a discrepancy in all rock modelling research.

Chapter 4

Experimental Characterization of Niger Delta Sandstone

4 EXPERIMENTAL CHARACTERIZATION OF NIGER DELTA SANDSTONE

4.1 Introduction

This chapter focuses on the experimental characterisation of grain-scale properties (chemical and physical) and evaluating the bulk mechanical strength properties of Niger Delta sandstone. These experimental measures serve as input into DEM, as well as to compare the experimental bulk strength measures with corresponding DEM simulations where applicable in the chapter following later (Figure 3.1). It is important to provide a petrographic property (detailed description of rock) before carrying out any mechanical test on rock material. Under mechanical loading, the resistance exhibited by rock is determined by its inherent petrographic properties which are usually micro-scaled-parameters. These properties determine damage threshold which is of fundamental importance in describing the stages that leads to rock deformations. Here, the petrographic properties of Niger Delta sandstone were extensively determined using experiments. For this, X-ray fluorescence (XRF) was used to carry out a semi-quantitative elemental distribution analysis of the elements present in sandstone. X-ray diffraction (XRD) was used to determine the mineral content. Scanning Electron Microscope-Electron Dispersive Spectrometry (SEM-EDS) was used to identify the mineral content by mapping the minerals observed by X-ray. A view of the optical microscope was used to verify boundary contact in the rock. In order to obtain the cohesive strength and the internal frictional angle, multi stage tri-axial compression test were carried out on the same sandstone sample at four stages of confined pressure which are 5MPa, 10MPa, 15MPa and 20MPa. The elastic properties of the grain behaviour under compression were determined using the standard ISRM- compression test. During the determination of the elastic properties, the damage thresholds were identified on the stress-strain curve. Experimental determination of damage thresholds was also provided. For information, the mineralogical characteristics and damage threshold properties of Niger Delta sandstone were compared with that of other two commonly found sandstone, which were Berea sandstone and Doddington sandstone.

4.2 Characterization of rock for discrete modelling

The characterization of natural rocks was carried out using X-ray fluorescence (XRF), X-ray diffraction (XRD) and Scanning Electron Microscope - Electron Dispersive Spectroscopy (SEM-EDS). These are standard characterization techniques employed to obtain internal structural view, elemental and mineral composition of the sandstone (Potter et al., 2011). The sandstone used in this research was taken from Niger-delta sandstone petroleum formation in Nigeria. The petro-graphical properties were determined to obtain classical view of the grain boundary morphology, micro-parameters and the elastic properties of the natural rock (Figure 4.1). This helps to link the experimentally measured micro-scale parameters with discrete element modelling in the subsequent chapters.

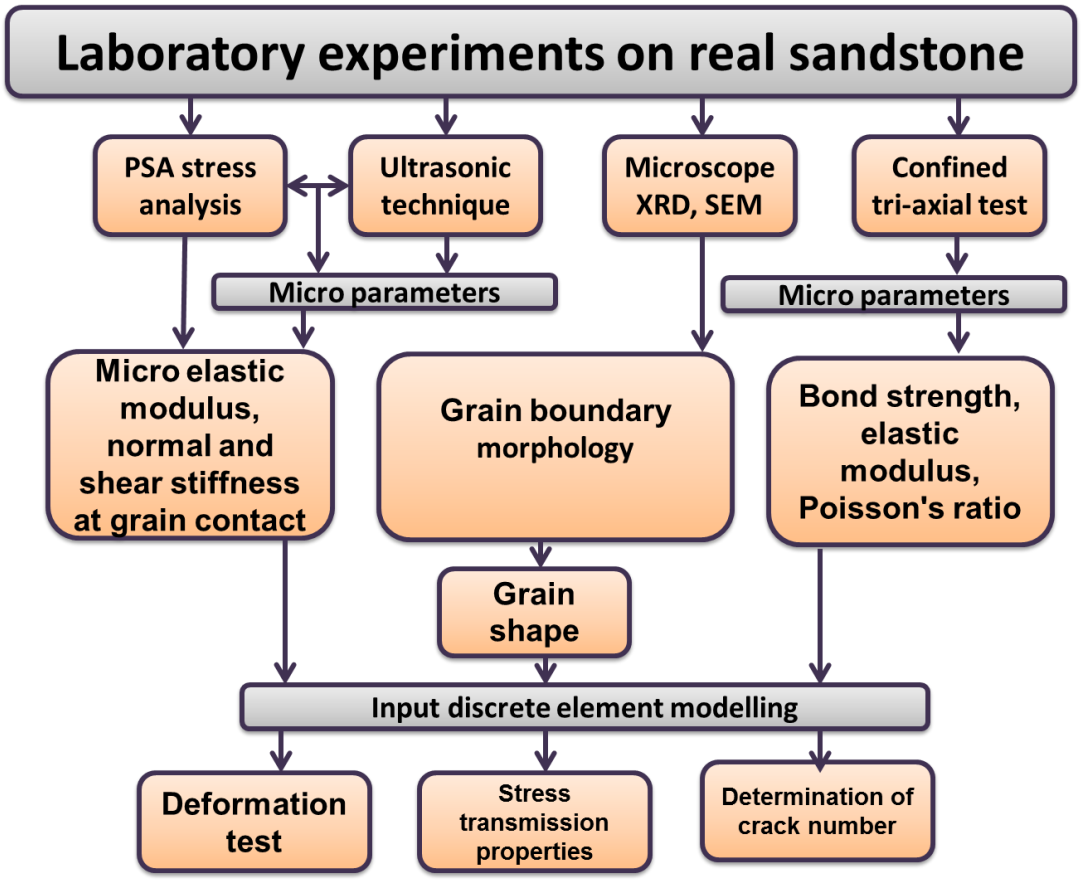

Figure 4.1 Block diagram for the determination of grain- scale parameters and their links to DEM simulation work.

The strength characteristics of the rock largely depends on the inherent mineral composition, grain morphology, degree of grain interlock, packing density, grain size and the grain contact characteristics of the matrix. The deductive approach adopted required that mineral composition of natural rock should be identified for the purpose of relating mineralogy to rocks deformation characteristics. Theoretical studies have shown that quartz particles binding grains together in sandstone (Zorlu et al., 2008) are stronger than clay bonded grained rocks (Hardy, 1976). Therefore, sandstone contains mineral grains which control its response to stress. Here, a semi quantitative analysis of the rock mineral was carried out with XRF analysis.

4.3 X-ray Fluorescence (XRF) analysis of natural rock

The procedure adopted for the XRF analysis of natural rock is similar to the method provided by Boyes (2009). A high energy source was used to excite each atom in a material under investigation. The excitation caused X-ray photons of a characteristic energy (defined by wavelength) to be emitted. By counting the number of photons of individual energy emitted from the material, the elements present were quantified. Elemental detection involved picking specific photons. The semi-quantitative analysis of Niger delta sandstone is presented in Table 4.1. They were sourced from the same oil field at Ughelli. The XRF analysis presented in Table 4.1 shows that sandstone was silica based because of the significant composition of silicon. Clays were identified in the chemical composition of the rock with the presence of; Fe, K, Al and Ca. The other elements present in traces are depositional materials associated with the origination of the rock formation. A similar analysis carried out on Berea sandstone by Lai et al., (2015) showed that the quartz content was between 74.7% and 89.5%, the feldspar content was between 3.5% and 9.5%, the clay content was between 1.3% and 4.8% other component was between 0.4% and 16.6% with porosity variation from 9.8% to 16.2%.

4.4 X-ray Diffraction (XRD) analysis and cementation between discrete grains in natural rock

The technique adopted for X-ray diffraction involved bombarding the rock sample with finely oriented monochromatic rays. X-ray with reflected beams can be described

theoretically as spherical waves which produce a diffraction pattern of regular spaced spots (Phillips and Phillips, 1980). The reflected beam scatters and are usually arranged symmetrically with d-spacing.

Table 4.1 Semi quantitative elemental analysis of Niger Delta sandstone using XRF

Element	**Concentration %**		
	Sample A	Sample B	Sample C
Si	73.1	51	62
Fe	10.1	17.9	12.4
K	5.48	8.18	9.19
Al	4.33	7.66	9.85
Ca	2.71	3.68	0.815
Ti	1.55	3.81	2.36
P	0.768	0.423	0.466
Zr	0.684	5.51	1.11
Cu	0.375	0.152	0.19
S	0.197	0.159	684
Mn	0.163	0.402	971
Mg	0.157	0.2	327
Rb	0.156	0.164	0.23
Cr	0.112	0.671	0.102
V	0.865	0.518	0.50
Sr	647	0.125	0.243
Ni	0.517	0.227	0.132
Ba	-	0.307	0.593
Y	-	0.132	-
Nb	-	610	-
Cl	-	-	655

When these reflections synchronize, they are directed such that Bragg's law (Suryanarayana and Norton, 2013) defines their path length difference to be the same as a multiple of wavelength. This law relates the wavelength of electromagnetic

radiation to the angle of diffraction and the regular lattice spacing in the rock specimen. These are diffracted X-rays. A range of 2θ angles were used to scan the sample through diffraction directions of the lattice converted to d - spacing. Mineral content was identified by the set of d-spacing and were characterized based on the International Centre Diffraction Data (ICDD).

4.4.1 Mineral content and strength analysis

Mineral content was qualitatively determined using XRD and SEM-EDS. X-Ray Powder-diffraction was carried out with BRUKER machine set at 40mA and 40kV. Ni filter and the Cu, K-alpha radiation was used. This procedure ran from 2^{o}2Ɵ to 70^{o} - 2Ɵ at a scanning speed of 5^{o} -2Ɵ/min. Figure 4.2 presents the XRD analysis of the Niger Delta sandstone. The sample showed significant peaks of quartz as the most significant component. Other component information was provided by the XRD analysis. Thus, a further analysis was done using the SEM-EDS.

From the results, quartz (SiO_2) content was identified as the most significant mineral in the XRD analysis (Figure 4.2). This agrees with the highest proportion of silicon elements observed in the XRF analysis (Table 4.1). Figure 4.2 shows characteristic peaks of quart and kaolinite present in Niger delta sandstone. Kaolinite is a cement-like clay mineral. Hence, the presence of cementing mineral is thought to be a criterion which determined the sample strength. This was because the strength and stiffness of the cement bindings of one grain to another was distributed throughout the bulk sandstone.

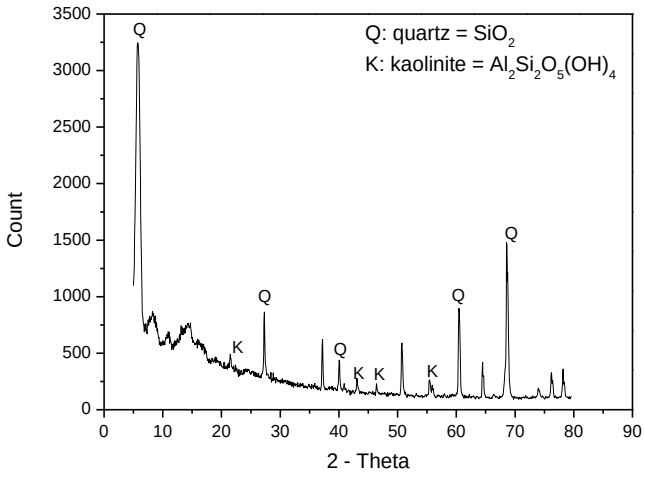

Figure 4.2 XRD analysis showing the quartz and kaolinite content.

Thus, the Niger delta sandstone was comparable to Berea sandstone because it contains distinctive peaks of quartz and kaolinite which are shown in Figure 4.2. Although quantification of clay and quartz was not obtained in this research, the peaks show the dominance of quartz content. A quantified data for Berea sandstone was carried out by Churcher et al. (1991). The data was compared with the analysis done by Daniel and Kaldi (2012). Their studies showed that Berea sandstone was predominantly quartzite with about 10% clay of kaolinite and illite, because the distinctive peaks of quartz and kaolinite were seen in them. In order to obtain more information about the content of sandstone, a further analysis was done using SEM-EDS method to characterize the Niger delta sample.

4.5 Scanning Electron Microscope - Electron Dispersive Spectrometry (EDM/EDS) and optical image analysis

The procedure adopted for SEM-EDS technique was similar to the method provided by Hafner (2006). A beam of electrons was directed at the rock specimen. Electrons in the inner shell of atoms were excited by external electron and were displaced. A hole was created in the space where the electron was displaced. The space created was occupied by another electron from the higher shell energy. The differences in the energies of the shells were released as X-ray (Hafner, 2006). By matching E.D.S. data from the emitted x-rays, the elements present were identified by the atomic structure with characteristic energy levels.

Figure 4.3 presents the SEM image of Niger Delta sandstone. It shows the arrangement of grains which are all of silicon-oxide components. This dominance of quartz grains agreed with the XRF and the XRD analysis. Other minor elements which were in between the quartz grains were in small traces. The clay particles in between grains are obvious in Figure 4.3.

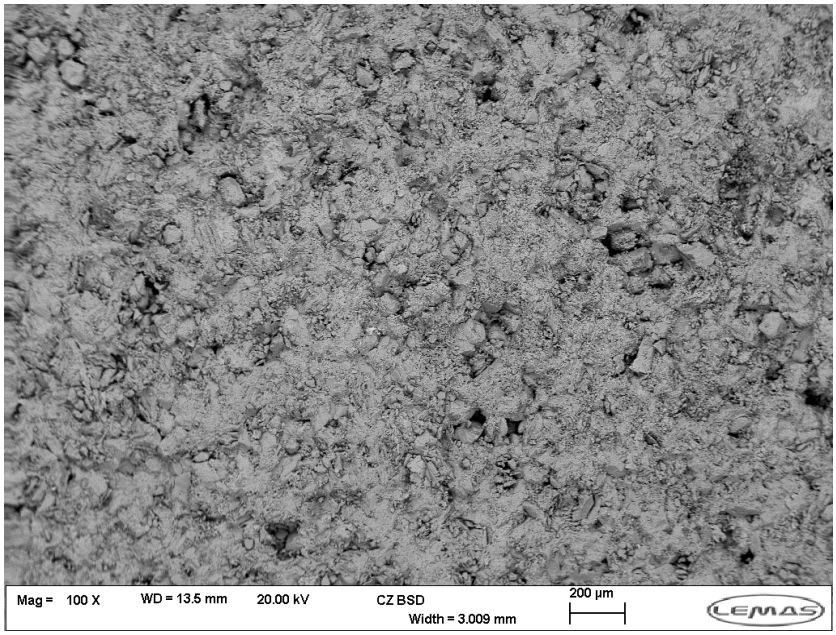

Figure 4.3 Granular arrangement in Niger delta sandstone

In order to verify the presence of basic elements in XRF and XRD analysis, the SEM result was mapped by X-ray characteristics data in Figure 3.4. Quartz grains were found to be dominant because both oxygen and silicon elements were observed in the mapped SEM image. By setting windows around peaks of all possible elements present in the scanned sandstone, the digital image was mapped out for each element. Here, dots were placed on the screen as the X-ray count of specific element was received. The black portions imply the absence of the element in those locations.

The grain shape and interlocking arrangements are characteristics of the microscopic structural view (Figure 4.3). Thus, the degree of roundness could affect the quantitative strength characteristic of the sandstone. In the numerical simulations, the representation of sandstone grains involving deviation from perfect spherical index has been reported (Zorlu et al., 2008). The grain shape can be described with a degree of spherical property (Bell and Lindsay, 1999). This is particularly due to the fact that the quartz grains are not perfect sphere (Figure 4.3 and Figure 4.4).

The quartz or the visible grains are presented in Figure 4.3. It is clear that quartz to quartz are the grain to grain contact in sandstone. The clay bond may break inside the sandstone, so that bonded quartz grains could lose cementation effect. Due to

these possible occurrences, a stiffness property can be obtained for the rock. This is regarded as the resistance of the cemented contact to external force, necessary to displace a quartz grain per unit displacement (Stephenson et al., 1992). Therefore, the overall strength of the rock depends on the stiffness of quartz or the contacts which are distributed throughout the grain assembly. The bond strength between the grains will be involved in the deformation process. The strength of these basic minerals determines extent of strain in the cemented contacts for a rock under stress.

In order to visualize the elemental points in the SEM image, the sandstone sample was gold coated and the thin sheet of sandstone was epoxy filled to reveal the grain boundary and interlock arrangement (Figure 4.5). In Chapter six the mapped out SEM image of Niger-Delta sandstone for elemental composition will be provided and discussed in details. The description of the micro-displacement within the grain assembly is also presented.

4.6 Natural micro-cracks and crack propagation in sandstone

The SEM-EDS results show that inherent micro-crack/vacancies exist in sandstone (Figure 4.4). In general under tri-axial compression, crack in orthogonal direction to compression closes under confined pressure. Some micro-cracks are not inherent but are newly formed by compression under load. Heterogeneous properties of strain localized points in rocks are concentrated around grains of different modulus value. Crack propagation can define the line of fracture. It is facilitated by pore spaces, grains with lost interlocked properties at the boundaries and intra-crystalline weakness. Observed average porosity for the Niger delta sandstone was 20.65% (Table 4.2), hence, the pore spaces were obvious in the samples.

4.7 Effect of clay particles in pore space on strength characteristics

Non-cementation may exist in some points. These are also clay contents which have significant effect on the strength of sandstone because they sustain the pores space and induce secondary mechanical properties. Clay content has been found to reduce the coefficient of friction (Corbett et al., 1987). The clay content affects frictional characteristics of grain assembly in rock (Dowla et al., 1990). Therefore, compressive strength increases with decrease in clay particles found within the pore space. The pore space in the sample can influence the compressive strength (Corbett et al.,

1987). An inverse relationship between porosity and the compressive strength of rock has been reported by Dowla et al. (1990).

.

4.8 Effect of cementations and mineral composition on mechanical properties of rock

Clay particles fuse up in some pores and form cementation between quartz grains (Fisher et al., 2009). This cementation was observed in Niger-delta sandstone under the SEM image. The resin impregnation of sandstone sample was to aid identification of grain boundary and void space. In order to obtain the constituent mineral, points were counted in each specimen. Each point was matched with the XRD and the mineral was identified. The locations of mineral point were then determined (Figure 4.4)

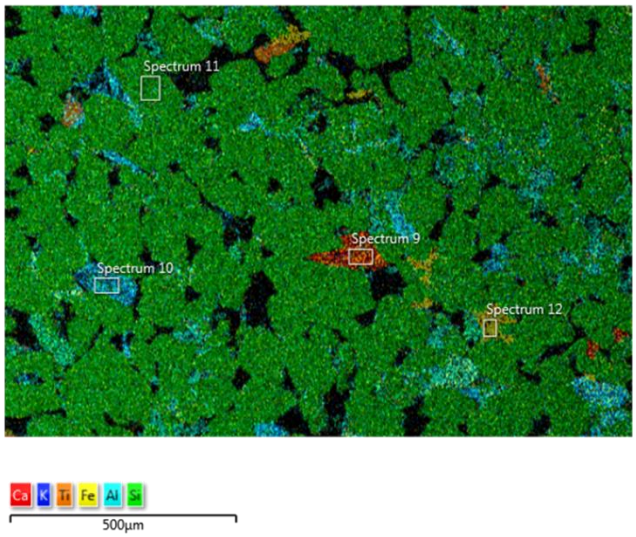

Figure 4.4 SEM-EDS Basic minerals in sandstone

Note that in Figure 4.4, the black colour indicates absence of element or empty space. A semi-quantitative elemental analysis was carried out on Niger delta specimen. The elemental data revealed the presence of quartz, feldspar, clay and Mica which are the basic minerals in the sandstone sample. Kaolinite is an example of common clay mineral found in sedimentary rock (Gill et al., 1977). Quartz and kaolinite have been reported as basic minerals in sedimentary rock (Bevins, 1994). Basic minerals in Berea sandstone have also been provided by Lai et al. (2015) (Table 4.4 and 4.5).

4.8.1 Quartz

Niger delta sample is a quartzite-sandstone which are identified by Si element, (Table 4.1, Figure 4.1-4.5). Quartz in sandstone has been defined as silicon oxide (Allaby and Park, 2013). Silicon elements are found in spectrum 11 in Figure 4.4. This indicates the presence of Quartz in Niger Delta sandstone.

4.8.2 Feldspar

Feldspar or plagioclases are groups of rock mineral-forming content. The elemental combination could be $KAlSi_3O_8$ or $NaAlSi_3O_8$ or $CaAl_2Si_2O_8$ (Deer et al., 1992). In Figure 4.4, Ca and K shows that Feldspar was observed in spectrum 12 for Niger – delta sandstone.

4.8.3 Clay

Clay is a binder found at quartz contacts which is in-between discrete quartz grains. The particles are hydrous aluminium phyllosilicate containing cations. Berea sandstone has its feldspar content associated with clay minerals because of the K and Ca elements (Huggett, 1986). A similar description of identifying mineral in sandstone with SEM-EDS is reported in literature (Huggett, 1986; Huggett, 1982; Huggett, 1984), following these authors' observations. This research adopted similar method for rock analysis using Niger delta sandstone, the feldspar is (Figure 4.4) similar to Berea sandstone examined by Huggett, (1984).

4.8.4 Mica

Mica is the component that contains almost all the mineral that make up the rock. They are identified by the perfect cleavage of related mineral (Deer et al., 1992) in sandstones. Table 4.1 presents a list of the minerals presents in the Niger delta sandstone which describe the Mica peculiar to the sample examined. These entire elements affect the strength of the rock Table 4.2 and Table 4.3 present studies on the effect of mineral on the strength of sandstone.

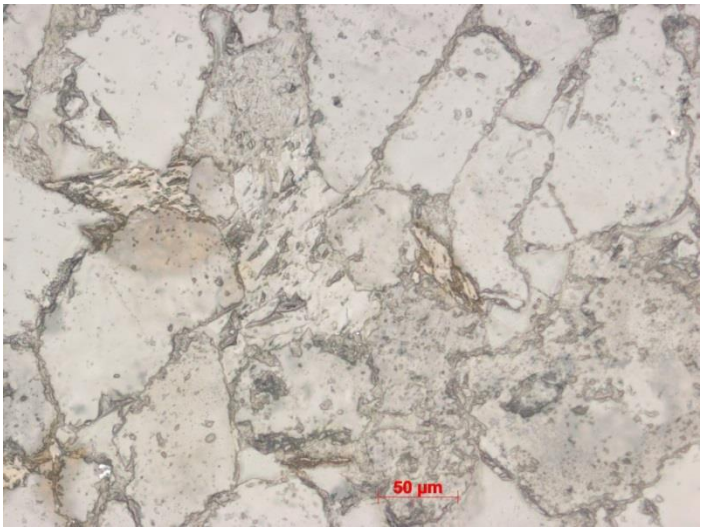

Figure 4.5 Optical microscope of Niger delta sandstone

4.9 Optical microscope image analysis of natural sandstone

The optical microscope technique was adopted for the boundary imaging. This is similar to the technique provided by Kino and Corle (1996). The objective lens was brought as low as 2mm to the rock sample so that light from the sample is brought to a focus inside the microscope tube. Next, an enlarged image was formed. The inverted image was captured by the microscope by using the in-built post-processing control of the microscope. The optical image of the thin section epoxy filled specimen is shown in Figure 4.5 for the sandstone which ranged in grain sizes from coarse to fine grains, grain boundaries between grains within the sandstone revealed contacting boundaries. It shows clearly the arrangement of quartz grains and the existence of packing in the assembly. Here resin was used to impregnate the sandstone on a Plexiglas sheet. The observed grain shape and sizes were not uniform. Therefore the grain varied in sizes between 80µm to 129µm which was classed as coarse to fine grains.

The compressive strength is thought to depend on petrography (or grain shape). This was because interlocks exist between the grains. It can be observed that the grains are in firm contact (optical view in Figure 4.5). Hence, it is necessary to take into account grain-contact stiffness in this microscopic study. With the knowledge of the inherent properties of the sandstone, the grain to grain contact displacements are due to the interactions of the quartz constituents. The optical image shows clear contact between constituent grains. Hence if the grains are compressed, there should

be a behavioural trend controlling relative displacement of grains at contact. The grain property and the bond properties at grain contacts are expressed as point (grain) scale properties or micro-properties in this research. By subjecting these grain assemblies to mechanical loading, under birefringent experimental procedures, quantitative data can be estimated from the strain response as presented in the Chapters 6 and 7. The experimental technique applied for evaluating macro- strength measurement is presented in the next section.

4.10 Standard methodology provided by International Society of Rock Mechanics (ISRM) for the strength, modulus and Poisson ratio

Validation of macroscopic response of rock (strength, modulus, and Poisson ratio) to mechanical loading was carried out using ISRM. These macro-properties were determined with uniaxial and tri-axial tests (Koyama and Jing, 2007). These properties include Young modulus, Poisson's ratio, and frictional coefficient of the rock. The essence of these tests was to compare macroscopic response of DEM and physical experiments which were the counterpart macroscopic data of natural sandstone. It was intended that similar experimental procedures will be replicated in numerical simulation to obtain mechanical responses of the sandstone. This is usually achieved by carrying out similar tests (uniaxial and tri-axial tests) on simulated sandstone. These macro-data served as validations for understanding the link between grain-scale properties (micro-parameters) and macro-strength characteristics. By using the same sandstone core of 96mm high and 38mm in diameter subjected to a strain rate of 0.6MN/m^2/sec, in a multistage tri-axial test (Zhang et al, 2012), the experimental data for Young modulus (E), Poisson's ratio (v), cohesion (c) and internal frictional angle (μ) were obtained (Figure 4.5).

4.10.1 Determination of bulk compressive strength, Young modulus, Poisson's ratio: Uniaxial Compression Test (UCS).

The Young modulus, compressive strength and Poisson's ratio were determined by the ISMR procedure provided by Fairhurst and Hudson (1999a). The cylindrical specimen dimension was 90mm height by 38mm diameter (Figure 4.6).

The tangent modulus was determined at a stress level of 50% of the uniaxial compressive strength (Dyke and Dobereiner, 1991). The Poisson's ratio was taken as the ratio of the diametric slope of the lateral-stress-strain to axial slope of the axial-stress-strain curve. The compressive strength (78MPa) was observed at the maximum stress recorded (Table 4.2). Five samples of Niger delta sandstone were tested for the mechanical properties and observations were similar due to the similar composition and micro-structural properties of the rock.

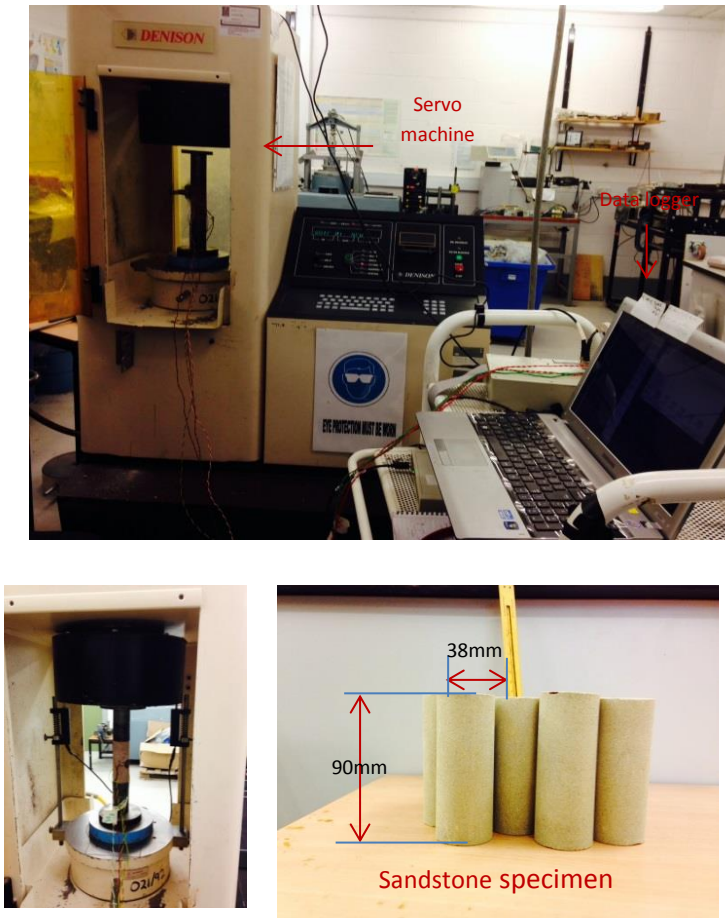

Figure 4.6 Experimental set up for uniaxial compressive test: rock engineering laboratory, University of Leeds

4.11 Determination of compressive strength, frictional coefficient, and elastic properties under confined pressures: tri-axial compression test

A specimen of dimension of height, 90mm and diameter, 38mm diameter was used to carry out a tri-axial compression test following the ISRM technique. The sleeve tri-axial kit was used to confine the specimen to a pressure of 5MPa, 10MPa, 15MPa, 20MPa, 30MPa, 40MPa, 50MPa and 60MPa (Figures 4.7 and Figure 4.8).

Figure 4.7 Experimental set up for confined pressure compressive test: rock engineering laboratory, University of Leeds

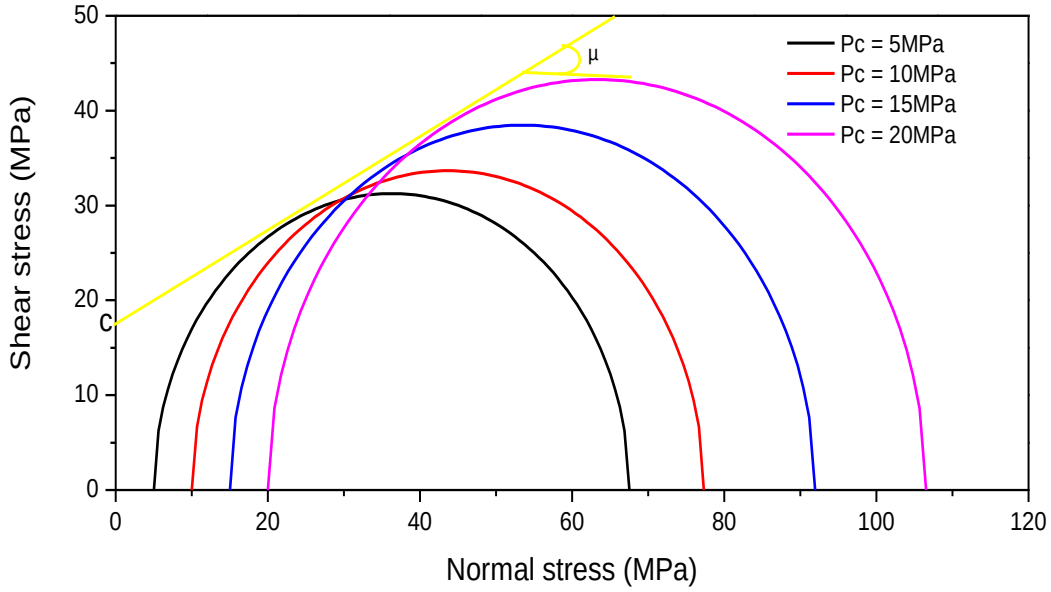

Figure 4.8 Cohesion (c =18MPa) and frictional angle (μ =22.0^{o}) for Niger Delta sandstone at 5MPa, 10MPa, 15MPa and 20MPa confining pressure (Pc).

The value of Young modulus increased linearly until the critical strength of sandstone was reached. The Niger delta sandstone was both siliceous and kaolinite cemented. A study conducted by Nemcok et al. (2009) illustrates the sensitivity of modulus to internal deformation of sandstone is dependent on mineral composition. For example, some mineral type characterize rock with crack density, this is because higher crack densities indicate lower Young modulus property of the rock. Therefore, cohesion and internal frictional angle are important to characterizing the strength of rock. The shear strength of sample is stress dependent. This is due to cohesive nature of contacting aggregates. Cohesion is said to be the property that results from the stress imparted to the aggregates which are electrostatically bonded as discrete grains. Hence, the shear strength of rock reveals the stress dependence in orthogonal directions. This is because the cohesive nature of the aggregate is controlled by cementation. Cementation determines the rheology of sandstone because the cementing minerals fills the pore space and thus raise the yield strength (Nemcok et al., 2009) and cohesion. Therefore, the movement of each grain is referred to as deformation. The cohesion of Niger delta sandstone was 18MPa with an internal frictional angle of 22degree (Figure 4.8 and Table 4.2).

Table 4.2 Macro-properties of Niger delta sandstone

Macro properties	Niger delta sandstone
Modulus (GPa)	20.7
Poisson's ratio	0.29
Cohesion (MPa)	18
Internal frictional angle (^{o})	22 ^{o}
Compressive strength (MPa)	78
Porosity (%)	20.65
Grain density(kg/m^3)	2590
Bulk density(kg/m^3)	2055

4.12 Mineral type and mechanical behaviour

Niger delta sandstone consisted of a high quartz proportion, small amount of Feldapar, characterized by mica. This made the sample distinct from other sandstone sample. The uniaxial compressive strength and modulus were 78MPa and 20.7GPa respectively (Table 4.2). For the sample examined, the presence of mica and feldspar could affect the strength magnitude. These minerals could either lower or raise the compressive strength and Young modulus. Specifically, higher quartz content contributed to higher strength magnitude in rock, this observation was made by Makani and Vidal, (2013).

On the basis of distinctive peaks of X-ray diffraction of the Berea sandstone and Niger delta sandstone, as presented in Figure 4.4 it was found that quartz is the major mineral type of the rock, followed by feldspar. Kaolinite clay mineral was observed. Other mineral types were present in small amount. These minerals were therefore the mineral supports that are responsible for the 78MPa yield stress and the 20.7GPa elastic modulus that characterized the material strength. Coarse nature and granular orientation were characteristic properties of the sandstone as presented in the SEM and optical image (Figure 4.3 and 4.4). The mechanical behaviour was determined by these properties. The average grain size for Berea was reported as 0.15mm (Hiltl et al., 1999) whereas the average grain size for Niger Delta sandstone was 0.148mm.

Quartz and mica mineral are found in the Niger delta sample. The porosity is 20.65% (Table 4.2 and 4.5). The sample is porous (mineral support is at a strength of 78MPa), with very high pore space observed in the sample; the compressive strength is also dependent on the porosity of the sandstone. Young Modulus is 20.7GPa and the Poisson's ratio is 0.29. The mineral type distinguishes the mechanical behaviour for Niger delta sample from other types of sandstone (Table 4.3). (Adeyanju and Oyekunle, 2010)

4.13 Comparison of petrography and mineral support in sandstone

For the purpose of comparison, the mineral-type in Doddington sandstone is presented in Figure 4.9. It differ from both Niger delta and Berea sandstones because Feldspar and clay mineral are not present. Doddington sample does not have similar mineral composition that could be compared with Berea and Niger-delta sandstone. Close examination shows that the sample is relatively weaker then both Niger delta and Berea sandstone. Therefore, the mineral composition in each sample serves as support for the external load on the sandstones because they form the building blocks. Although all samples are quartz-dominant they differ in strength characteristics because of their different proportion of clay and mineral composition. The yield point of Niger delta sandstone was higher than the reported yield point of 58MPa of Berea sandstone (Evans, 2012). It implies that the Niger delta sample contained higher quartz compared to Berea sandstone but it also contains less clay particle in its pores. The Berea sandstone contained more feldspar than Niger-delta sandstone. This may account for the lower yield strength in Berea sample when compared to Niger delta sandstone. The crack closure and damage stress is discussed in the later part of this chapter. For comparison purposes, Table 4.3 shows that mineral composition in sandstone would affect the mechanical strength of the material.

During deformation test, Niger delta sandstone exhibited a significant brittle deformation. This high brittle behaviour could be due to the high mica content which allows a non-uniform distribution of load on the matrix. Although this contained high proportion of quartz, it contains low degree of cementation which makes it a well bonded granular pack. If the quartz content is high in a sample and contains very low

percentage of clay, then the sample has well sorted grains and it will exhibit a low strength magnitude compared to samples with less clay particles in the pores.

Table 4.3 Basic component and mechanical properties of sandstones

References	Mineral composition	Sample	Uniaxial compressive strength(UCS)
Kalimov, et al., 1971	% Carbonate = (dolomite, CaMg(CO3)2, +calcite)	22Sandstones, 39siltstone	Increase in carbonate increases UCS
Kalimov, et al., 1971,	Clay = (Illite +beidelite+kaolinite)	22 Sandstone, 39 siltstone	Increase in clay decreases UCS
Steiger and Leung, 1989	Clay = smectite	Sandstone	Increase in clay decreases UCS
This research	Quartz	Sandstone	Increase in yield point
This research	Feldspar	Sandstone	Decrease yield point

4.14 Mechanical behaviour of Niger Delta sandstone compared with Berea and Doddington sandstones.

Niger delta sandstone was used to carry out the study of micro-mechanical damage. Berea sandstone was chosen for comparing the results obtained in Niger-delta sandstone. This is because Berea sandstone is recognized as a reference rock for strength analysis for oil-bearing rocks (Evans, 2012). Unconfined compression test was carried out on both Berea and Niger delta sandstone. For each test sample, axial and radial strains were recorded. The strain behaviour were not so different, therefore the two samples were compared. The unconfined compressive stress for the sample is found as 68MPa for Niger-delta sandstone and 52MPa for Berea sandstone (Table 4.5). The comparable strength observed in Niger-delta and Berea is due to the cementation in both samples. In general, Niger-delta sandstone and Berea sandstone indicated very typical properties of sandstone, but Niger delta sandstone had a higher cohesive property peculiar to the grains. This property is indicates the higher strength and stiffness property of Niger Delta sample when compared to Berea

sandstone. Its degree of deformability was also higher. The cohesive behaviour exhibited by the grain to grain depended on grain shape and the degree of interlock within the grains. Berea sandstone was used as an analogue for reservoir rock (Hart and Wang, 1995; Menéndez et al., 1996). The elements in Berea sandstone and Niger delta is provided in Table 4.4. The similarities in samples (Niger delta and Berea sandstone) was considered. Thus, the two samples were compared in on the basis of mechanical properties as provided in Table 4.5.

Table 4.4 Comparison of elements present in Berea and Niger delta sandstone

Sample	Si (%)	Al (%)	K (%)	Fe (%)	Ca (%)	Ti (%)	Mg (%)	Na (%)	Author
Berea sandstone	84.88	5.33	3.49	2.49	2.11	1.11	0.36	0.23	Lai et al., 2015.
Berea sandstone	81.84	5.04	3.57	3.88	4.16	1.03	0.61	0.22	Lai et al., 2015.
Berea sandstone	62.00	9.85	9.19	12.40	0.82	2.36	0.33	0.13	This research
Niger Delta sandstone	73.10	4.33	5.48	10.10	2.71	1.55	0.16	0.52	This research

Table 4.5 Macro properties of Niger delta sandstone and Berea sandstone

Macro properties	Niger delta sandstone	Berea sandstone
Modulus (GPa)	20.7	20.6
Poisson's ratio	0.29	0.32
Cohesion (MPa)	18	24
Internal frictional angle (^{o})	22	26
Compressive strength (MPa)	68	52
Porosity (%)	20.65	21.92
Grain density(kg/m3)	2590	2631
Bulk density(kg/m3)	2055	2077

4.15 Mineral content and strength analysis of Niger delta sandstone compared with other sandstone

The XRD analysis of Niger Delta sandstone, Berea sandstone and Doddington sandstone is presented in Figure 4.9 a - c respectively. Each sample shows significant peaks of quartz which indicates the most significant component. The characteristic peaks show that Niger delta sandstone and Berea sandstone are closer in mineralogy compared to the third sample (Doddington sandstone). Observe that, clay mineral was probably in negligible quantity in Doddington sandstone. The peaks of mineral point are identified in Figure 4.9a-c.

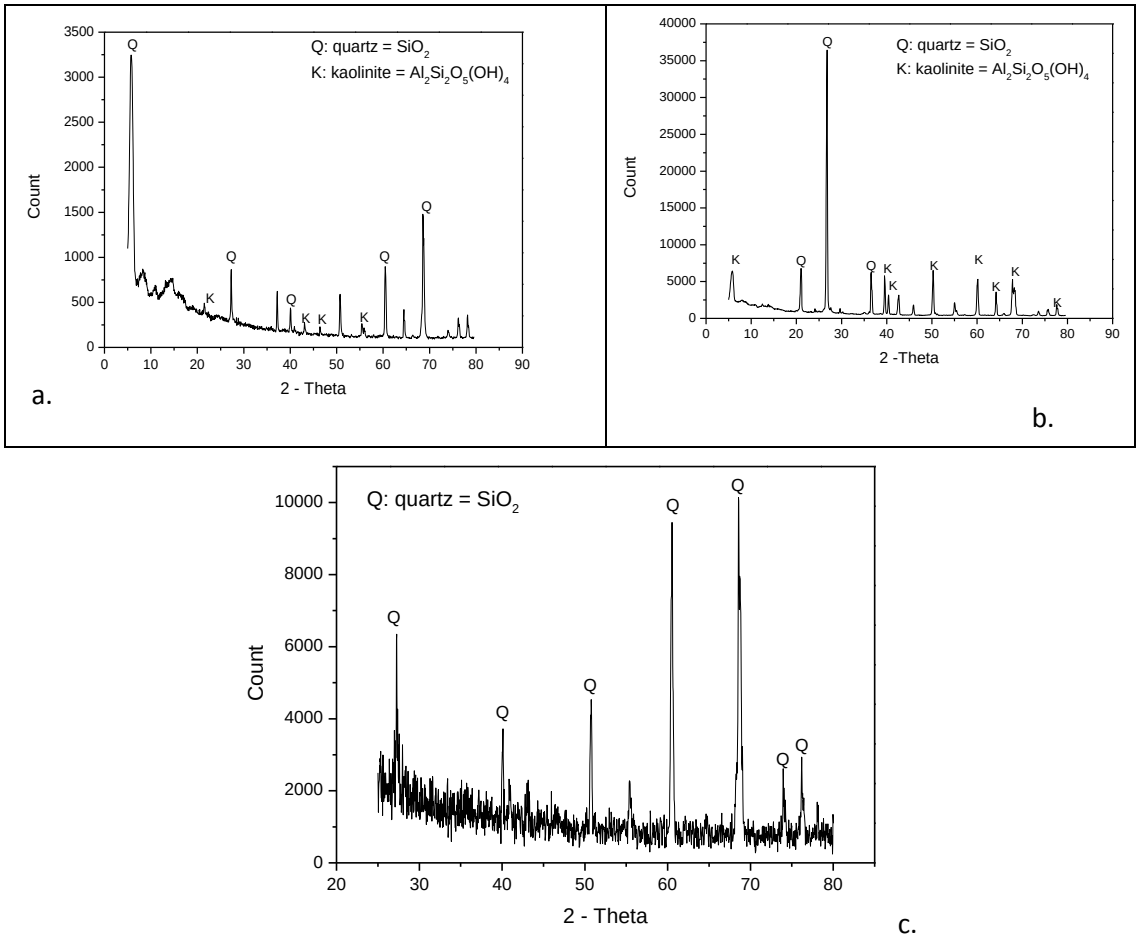

Figure 4.9 XRD analysis of ;(a)Niger Delta sandstone (b) Berea sandstone and (c)Doddington sandstone

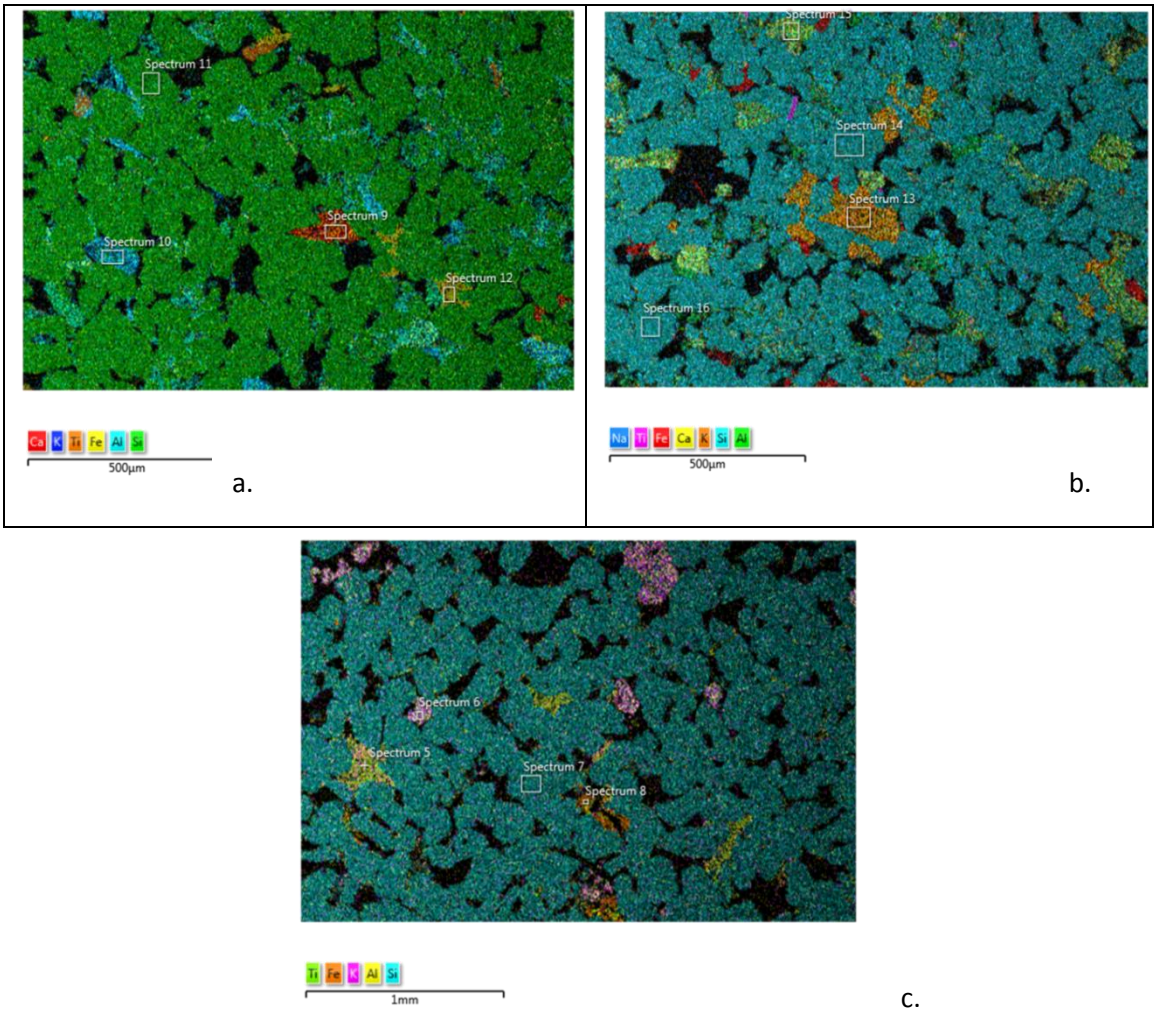

Figure 4.10 EDS- Layered Image analysis of Niger Delta Sandstone (b) Berea sandstone and (c) Doddington sandstone

4.16 Basic minerals in the sandstones

Semi-quantitative analysis was carried out on three sandstone samples: (a) Niger Delta sandstone, (b) Berea sandstone, (c) Doddington sandstone. Quartz, feldspar, clay and Mica were the basic minerals in the sandstone samples. Generally, Kaolinite clay was found in sedimentary rock (Gill et al., 1977; Bevins, 1994). Quartz was the silicon elements which were found in spectrum 11, 14 and 7 (Figure 4.10 a-c). This indicates the presence of Quartz in Niger Delta sandstone, Berea sandstone and Doddington sandstone respectively.

In Figure 4.10 Ca and K indicate that feldspar was present in Niger delta sandstone but not as rich in alkali-elements as that found in Berea sandstone. Berea sandstone contained quartz with subordinate feldspar which is identified with the presence of the Na, Ca and K, elements in Figure 4.10b. Feldspar was observed in spectrum 12, 15 and 5 for Niger Delta sandstone, Berea and Doddington sandstone respectively in Figure 4.10a-c respectively. Berea sandstone specimen had the highest feldspar in its specimen.

4.17 Petrography and mineral support in sandstone

The result of Doddington sandstone is presented in Figure 4.10c. It differ from both Niger delta and Berea sandstones because Feldspar and clay mineral were not present in the sample examined. Doddington sample was different in mineral composition compared with Berea and Niger Delta. Close physical view shows that the sample is relatively weaker then both Niger Delta and Berea sandstone. The granular arrangement is sorted as presented in Figure 4.11c. Therefore, the mineral composition in each sample serves as support for the external load on the sandstones. Although all samples are quartz-dominant they differ in strength characteristics because of their mineral composition. Niger delta sandstone contained higher quartz content compared to Berea sandstone but it contained less clay particle in its pores. This makes the yield point of Niger Delta sandstone higher than Berea sandstone (Figure 4.12a-c). Berea sandstone sample contained more feldspar than Niger Delta sandstone and this also accounted for the lower yield strength in Berea sample. The crack closure stress (20MPa) and the crack damage stress (140MPa) are higher in Niger Delta sandstone (Figure 4.12a) than Berea sandstone with 18MPa and 110MPa respectively (Figure 4.12b). Doddington sandstone is relatively weaker with sorted mineral support, its crack closure stress (8MPa) and the crack damage stress is not distinctive because it exhibits a significant brittle behaviour at yield point. This behaviour can be attributed to its no-clay content.

4.18 Micro-cracks and crack propagation in sandstone

The SEM results show that inherent micro-crack exist in sandstone, Figure 4.10a-c presents the link between the void space as the micro-cracks, Figure 4.11.a-c shows

the micro-cracks in between the grains. Under tri-axial compression, crack in orthogonal direction to compression closes under confined pressure. The initial crack closure implies that some micro-crack was not inherent but were formed by compression under load. Heterogeneous properties in rock stresses were concentrated around grains of different Young modulus. This value results due to the characteristic exhibited by the inherent micro-cracks peculiar to the sample. Crack propagation can define line of fracture. It is facilitated by pore spaces, grains that have lost its interlocking properties at the boundaries and intra-crystalline weakness. The average porosity of Niger delta sandstone was about 20.68% (Table 3.5). The pore spaces are obvious in the samples.

4.18.1 Effect of clay particles in pore space on strength characteristics

Pure un-cemented clay content (Figure 4.11 a-c) has a significant effect on the strength of sandstone because they sustain the pores space and induce secondary mechanical properties. Clay particles in the pore space has been found to reduce the coefficient of friction (Corbett et al., 1987; Dowla et al., 1990). Therefore, compressive strength increases with decrease in clay particles found within the pore space.

The pore space in Berea sample is more than the observed pore space in Niger delta, indicating higher porosity. While Berea sandstone has an average porosity of 21.92%, the Niger delta sandstone is 20.68%. The most porous sample is Doddington sandstone with 23% this is followed by the Berea sandstone and then the Niger-delta sandstone. The compressive strength follows the same trend. Therefore, an inverse relationship exists between porosity and the compressive strength of the samples with Niger-delta having 160MPa, followed by Berea sandstone with 152MPa and Doddington sample with 122MPa.

4.18.2 Effect of cementation and mineral composition on elastic properties and strength

The clay particles fuse up in some pores and form cementation between quartz. This cementation was observed in Berea sandstone and Niger Delta sandstone. But

negligible cementation was observed in Doddington (Figure 4.11a-c). Thus under loading surface, more grain contact exist in the other two samples than Doddington.

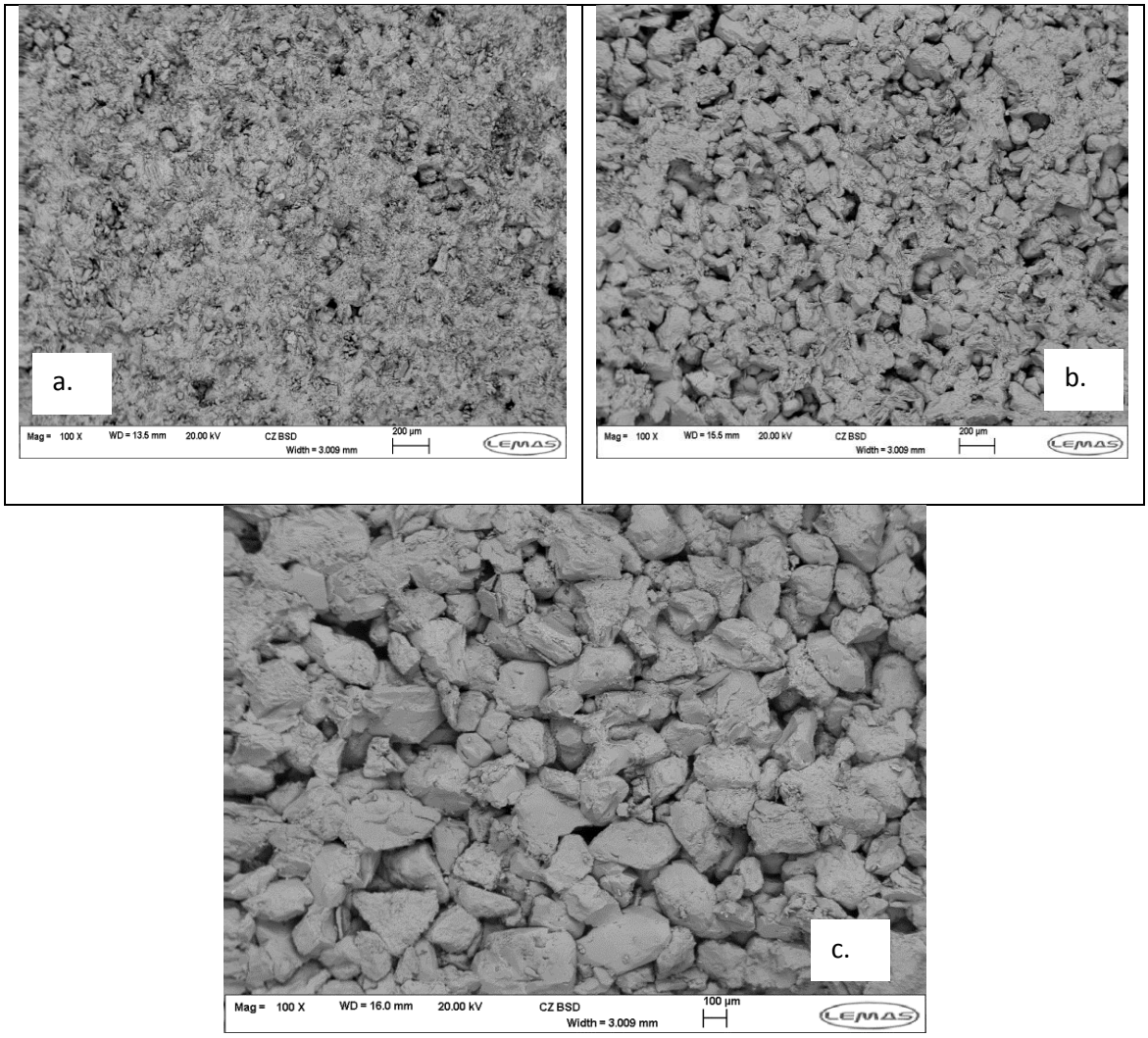

Figure 4.11 Granular arrangements in (a)Niger Delta Sandstone (b) Berea sandstone and (c)Doddington sandstone

By using the same sandstone core of 96mm high and 38mm in diameter subjected to a strain rate of 0.6MN/m^2/sec, in a multistage tri-axial test, the experimental data for Young modulus, Poisson's ratio, cohesion and internal frictional angle were obtained. The crack volumetric strain is provided by the DEM (Potyondy and Cundall, 2004) in Equation (3.1).

$$\varepsilon_{cv} = \varepsilon_v - \frac{(1-2v)(\sigma_1-\sigma_3)}{E} \quad (3.1)$$

Where ε_v and ε_{cv} are volumetric strains and crack volumetric strain. E is the Modulus of elasticity and v is the Poisson's ratio, σ_1 and σ_3 are the axial and confining stresses respectively. At confined pressure of axial test was carried on numerical model later in Chapter 8. From the results obtained for a numerical model, the micro-mechanical behaviour was identified with the crack initiation stress, crack damage stress and yield point.

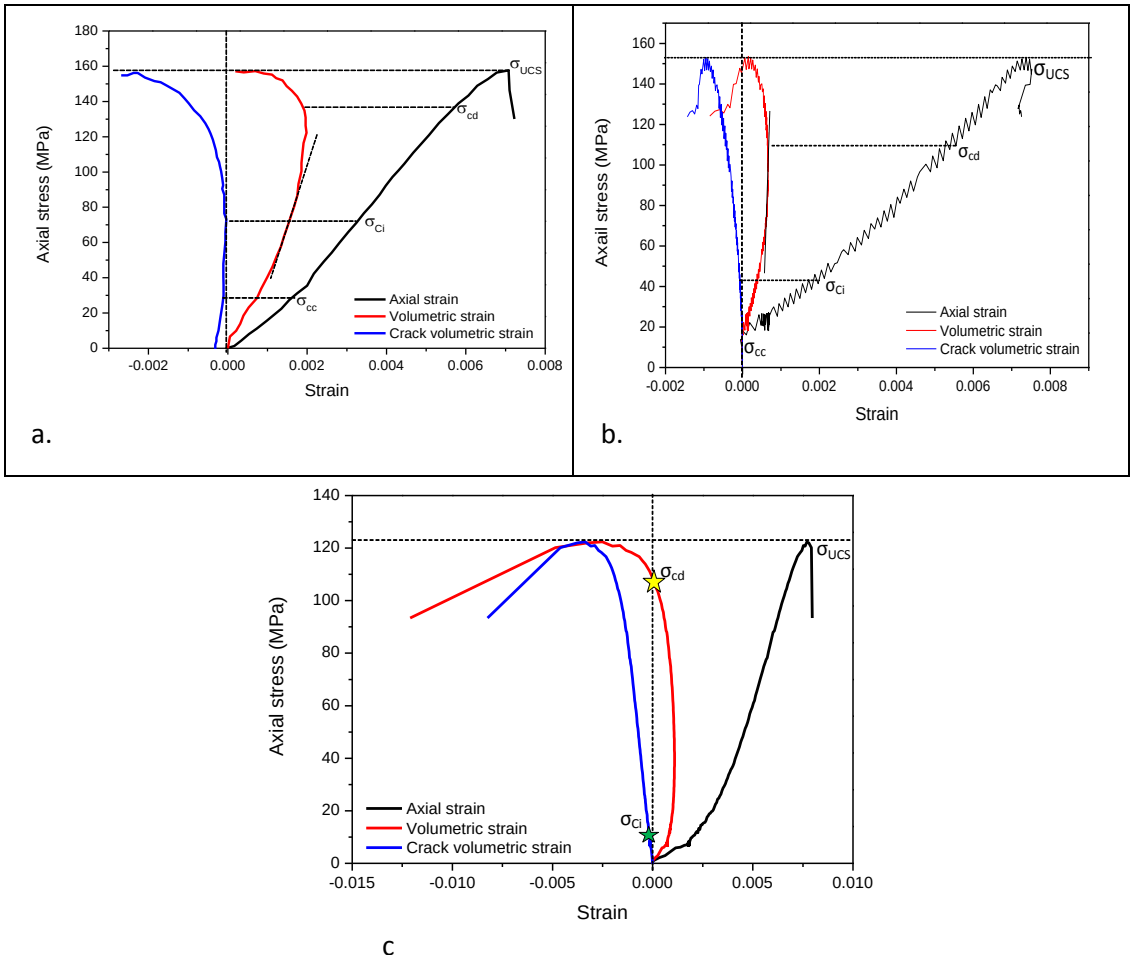

Key: σ_{cc}, σ_{ci}, σ_{cd} and σ_{UCS} are stresses due to crack closure, crack initiation, crack damage and uniaxial compression respectively.

Figure 4.12 Experimental result for the stress-strain curves for Niger Delta Sandstone (b) Berea sandstone and (c) Doddington sandstone under tri-axial test at 15MPa confined pressure

4.19 Conclusions

Mineralogical compositions determine the strength characteristics exhibited by rock. For sandstone, the proportion of quartz and feldspar are major content which control

the mechanical behaviour under compression. Each mineral type determines the strength characteristics of the rock. For the Niger delta sandstone, a high quartz content relative to low feldspar content was present with other proportion of mica and clay. These compositional properties distinguishes the mechanical properties of the rocks.

The yield point exhibited by Niger delta sandstone is determined by the quartz content, mica content and the characteristic cementation properties. These minerals are elastic property determinants. Sandstone is composed of almost spherical-shaped grains which characterized its porosity, grain contacts and the degree of interlock. The grain stiffness determine the compressive strength of Niger delta sandstone. The internal frictional angle and cohesion are also affected by these properties. The characteristic smaller grain size, lower porosity, higher clay-content, higher stable mineral, higher quartz content, higher feldspar, all leads to higher compressive strength and a high value of elastic properties.

The Niger delta sandstone is a granular system with characteristic internal frictional angle and cohesive properties. Thus, strain response under mechanical load characterizes the mechanism of deformation, which is due to the motion of quartz grain within the grain assembly. Such strain data can be utilized to obtain microscopic data which include normal stiffness, shear stiffness and bond strength at grain contacts.

The displacement of grain from intact state reduces the material strength under compression. The observed value of elastic modulus depends on the cohesive property of the aggregate of quartz in the sandstone. Although some factors such as loading direction relative to crack direction affect the modulus. Grain contact possess non-homogeneous stiffness property. This is due to the variations in the cementation of each contacting grain which exerts a significant influence on the modulus of elasticity.

Chapter 5

Experimental Evaluation of Micro-parameters of Niger delta Sandstone: Stiffness Ratio Using Ultrasound Tests

5 EXPERIMENTAL EVALUATION OF MICROPARAMETERS OF NIGER DELTA SANDSTONE: STIFFNESS RATIO USING ULTRASOUND TESTS

5.1 Introduction

Rock grains such as in the case of sandstone, have non-homogeneous mineralogical properties. This could result in variation in the stiffness measure, which is perhaps the most important microscopic variable in characterising the rock. The focus of this chapter is to evaluate the stiffness ratio (ratio of normal to tangential stiffness) of Niger Delta sandstone using ultrasound experiments. This would help later to feed as input parameters in the DEM simulations.

Analytical explanation of micro-structural deformation of strongly bonded (rock-like) granular materials has been provided by Holt (2005) and Li (2011). However the concept of accounting grain scale interactions within cementations structure such as rock is not sufficiently developed for formulating contact models for cementations materials. This Chapter will provide a novel insight into the behaviour of grain-to-grain contact of sandstone rock is presented in this Chapter. Grain contact stiffness (normal and tangential) was obtained by measuring P-wave and S-wave data using ultrasound probes. The corresponding elastic properties of the rock were subsequently used to determine bond strength.

The material under investigation is an assembly of discrete grain with finite clay – cemented contacts in Niger Delta sandstone. Grain contacts can exist at any point in sandstone. Deformation is said to be the displacement of grains from their contact location. These displacements translate into strain measureable at any arbitrary point in the rock. The rock exhibit maximum strain at the surface, because the grains move freely at the surface while the displacement is inhibited in the inner core of the bulk assembly.

5.2 Ultrasound measurement and natural rock

Sound wave propagation depends on the vibration or oscillatory motion of a grain inside the rock (Wang et al, 2006). Ultrasonic wave produces signal even when an infinite mass or a grain oscillates. The grains are connected to each other in the rock with an envisaged elastic springs (Cho et al, 2007). Each grain motion is relative to the contacting grain connected to it. As inertial and elastic force of restoration acts on each grain, only one resonant frequency will be associated to the grain of mass M on a spring. Normally, the relationship of the force on the grain (mass M) is controlled by the spring resistance called stiffness. The force of restoration of the elastic spring per unit length is regarded as the spring constant (Makse et al, 2004). We know from Hooke's law that within the elastic limit of a material, the relationship between the particle displacement and the force of restoration of a grain to its equilibrium position is linear (Petroski, 1996; Herrmann, 1991). Hence, grain to grain contact stiffness was quantified based on the assumption that Hooke's law holds as the quartz grain deforms.

5.3 Micro-parameters and requirement for numerical computation

DEM requirement involves setting material deformability by specifying elastic modulus and stiffness ratio at grain contact. If these two most important parameters are determinable, the simulation of the natural rock can be improved. This concept is better than iterative calibration of the macroscopic parameters in DEM in relation to a microscopic data which is complex (Wang and Tonon, 2010). Thus the benefit of extracting micro-parameters from natural rock is that, the complexities in DEM could be greatly simplified by using realistic experimental data as inputs. The next section explains how the ultrasound technique is adopted to obtain micro-parameters (stiffness ratio).

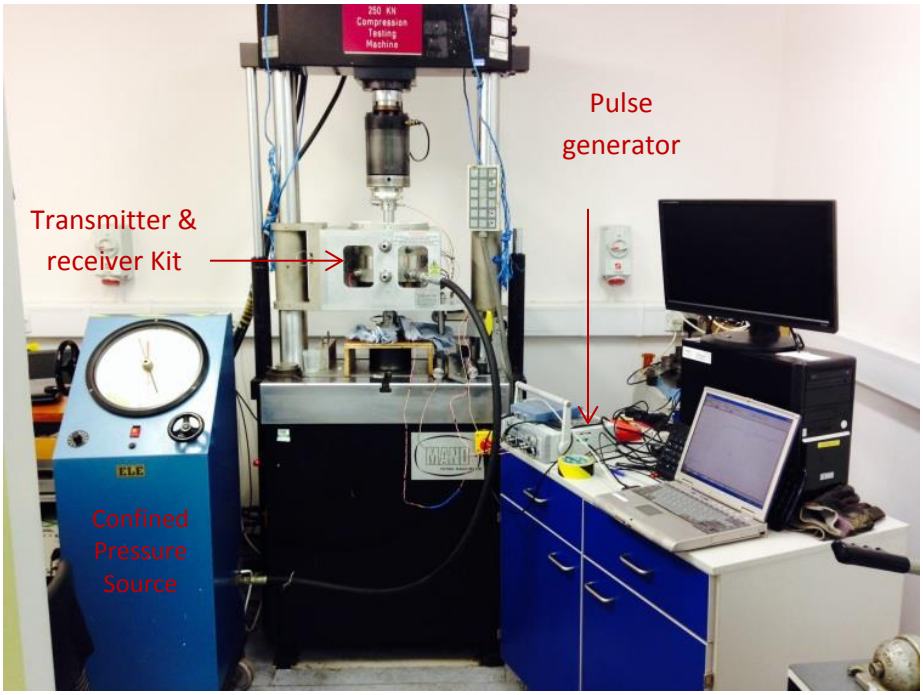

Figure 5.1 Experimental set-up for determination of compressional and shear wave velocity using ultrasonic techniques

5.4 Ultrasound measurement: wave velocity through Niger delta sandstone

First of all the stress strain data were obtained using the strain gauge and the procedure provided in Chapter 3. By following the procedure in the standard test (Figure 5.1) of the International Society of Rock Mechanics (ISRM) (Ulusay and Hudson, 1974), the P-wave velocities and S-wave velocities were determined. Subsequently, the grain contact stiffness was evaluated. Figure 5.1 shows the experimental set up which consist of a pulse generator that sent the ultrasound signal at specified frequencies through the sandstone. Transducers were placed on both ends of the sandstone. The procedure allows the sonic signal to travel through a sample size of 38mm diameter by 50mm in height. The velocities were measured by sending pulse ultrasound through the sandstone. The frequency of excitation was 1000 kHz. The waveforms were transmitted at frequencies ranging from 300-400 kHz based on the stress applied with the corresponding compressive and tangential forces.

Grain-contact-stiffness was evaluated separately as normal stiffness and shear stiffness with the measured P-wave and S-wave velocities respectively. These normal and shear grain contacts stiffness (micro-parameters) were used to develop the contact law governing grain interaction as each grain contact deform under compression.

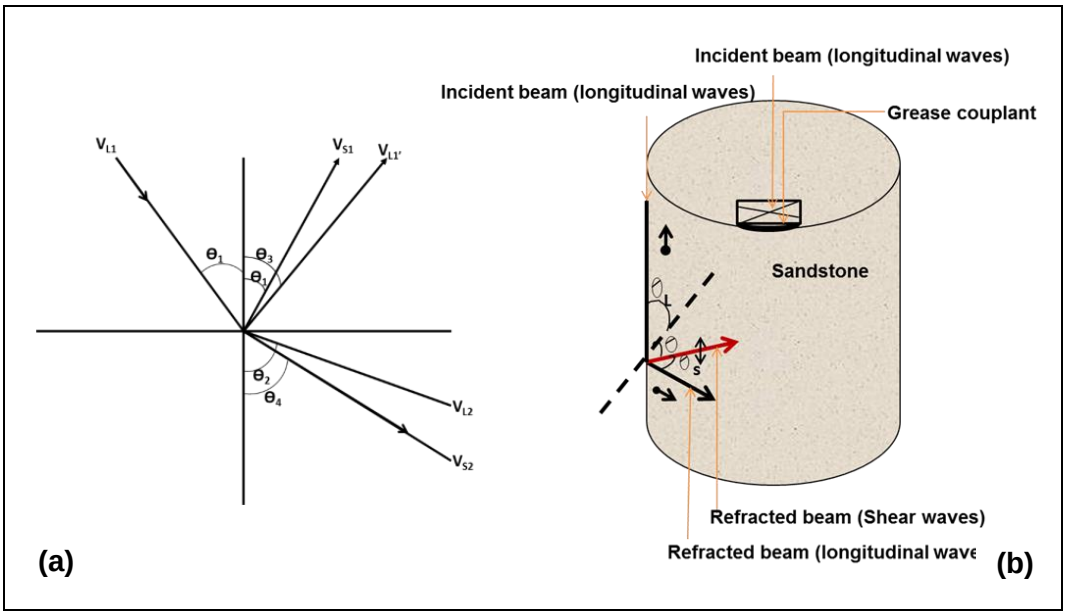

a.)Snell's refraction (Bryant, 1958) b.)Longitudinal and shear waves

Figure 5.2 Ultrasound measurement technique (Jiles, 2007).

Note that: V_{L1} is the longitudinal wave velocity in material 1, V_{L2} is the longitudinal wave, velocity in material 2, V_{S1} is the shear wave velocity in material 1. V_{S2} is the shear wave velocity in material 2.

5.4.1 Deductions made from ultrasonic measurement by refraction

A wave is refracted when ultrasound wave passes through an interface or micro-defect in rock matrix (Bryant, 1958) (Figure 5.2). The same phenomenon occurs when light passes through an interface. Refraction occurs in rock because of the velocity difference between the gel medium and the rock medium (Jiles, 2007). The larger the difference in the acoustic properties of the two media, the greater the refraction produced. The angle of incidence at which the sound wave enters the rock and their velocities can be correlated. This correlation is called Snell's law (Figure

5.2a). By this technique, both shear and longitudinal wave are refracted (Figure 5.2b).The refractive beam for longitudinal and shear waves were shown in Figure 5.2b.

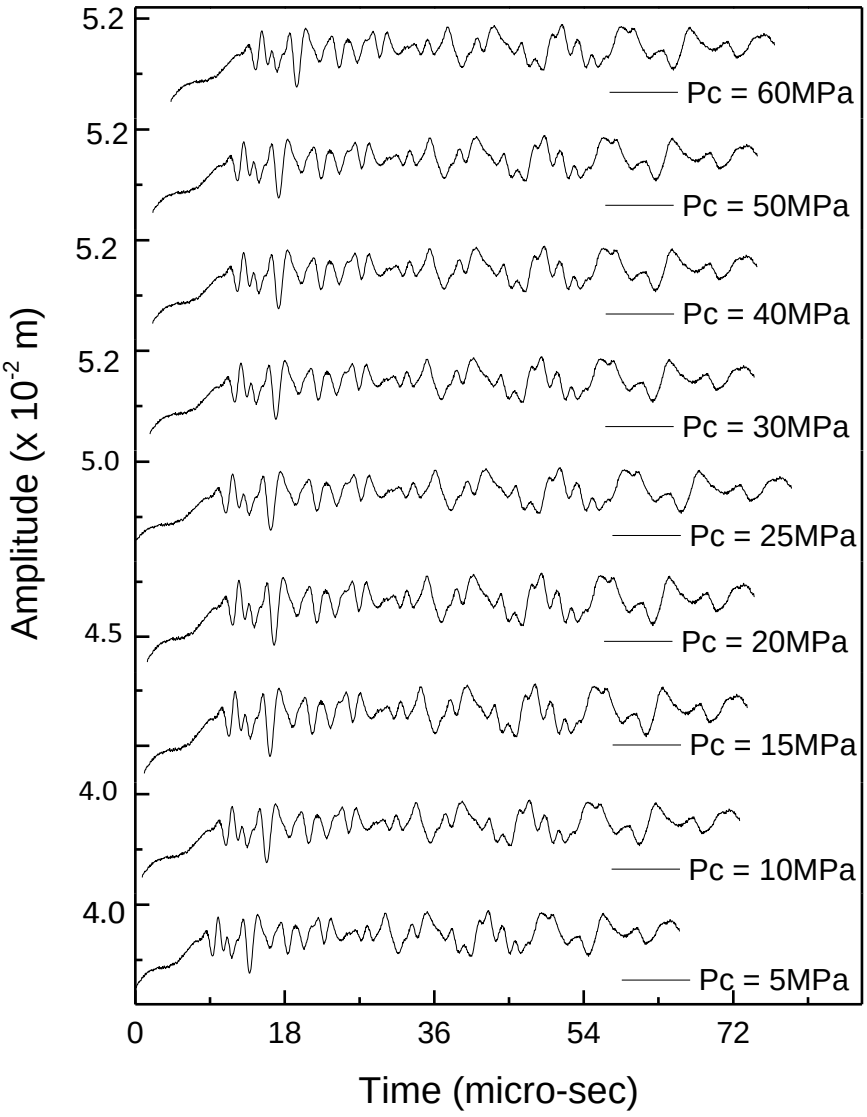

Figure 5.3 Compressional wave signature for Niger delta sandstone at various confined pressure (Pc).

5.4.2 Measurement of longitudinal and shear wave velocities

Grain displacements inside rock matrix were captured in both longitudinal and shears directions to obtain longitudinal and shear wave respectively (Figures 5.3 and 5.4). The refracted waves appeared as oscillating curves. Wave propagation could depend on the elastic properties of the rock. Thus, the waveform obtained on the data acquisition shows plots of acoustic amplitude versus time with distinctive peaks of longitudinal and shear characteristics. For the Niger delta sandstone, compressional wave arrivals were followed by the shear waves (Figures 5.3 – 5.5).

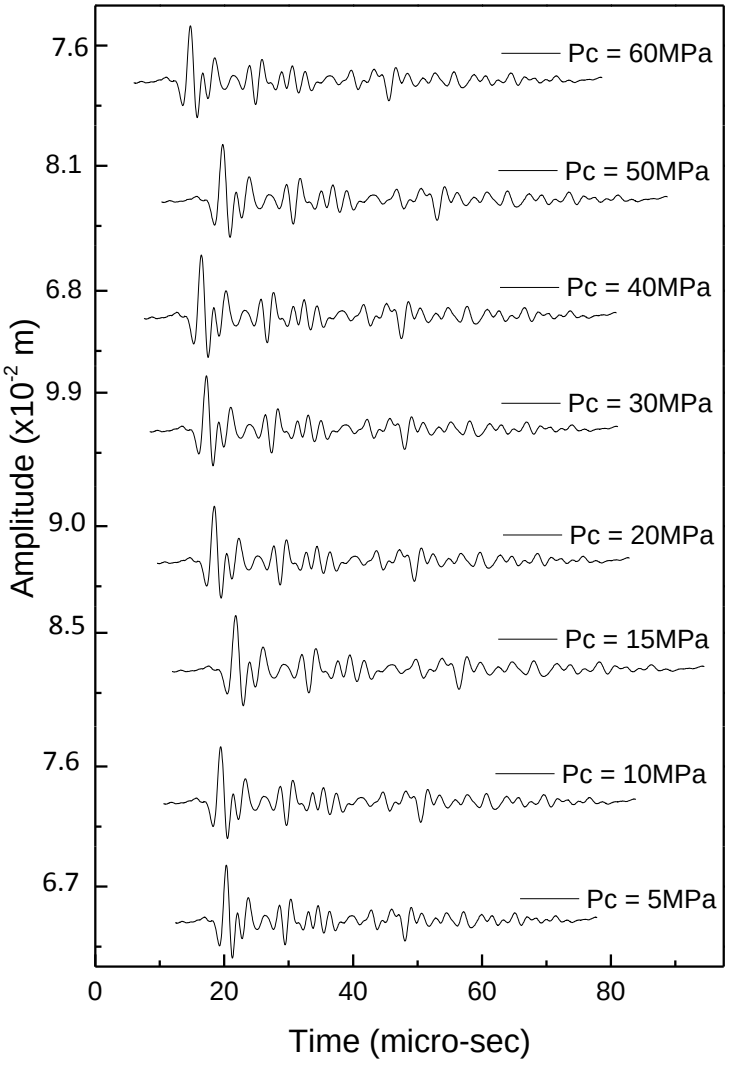

Figure 5.4 Shear wave signature for Niger delta sandstone at various confined pressure (Pc).

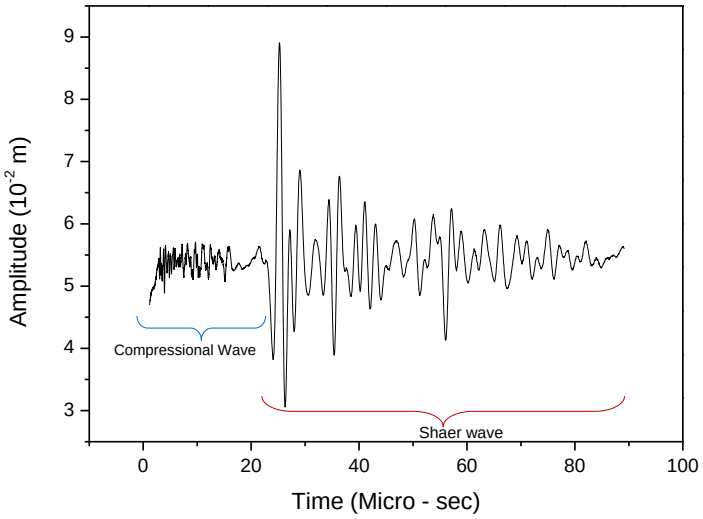

Figure 5.5 Wave signatures of compressional and shear wave in the acoustic waveform

5.4.3 Acoustic wave and direction of grain displacement

During sample compression at some confined pressures of 5MPa, 10MPa, 15MPa, 20MPa, 30MPa, 40MPa, 50MPa, and 60MPa, ultrasound wave was made to pass through the rock sample of height, 80mm and diameter, 38mm. During this experiment, each grain vibrated round its mean central position. The acoustic characteristics showed that, the wave released by the pulse-system pass through the sample and produced a characteristic signature. The acoustic wave received was recorded as compressional (Vp) wave, which recorded the grain displacement in the direction parallel to the direction of wave propagated (Figure 5.3). Next, the shear-wave (Vs) was recorded by virtue of the displacement of the grain when the wave travels in the transverse direction (Figure 5.4). The normal and shear wave properties in longitudinal and transverse direction due to grain displacement were determined. Figure 5.5 is the signature of the combination of the two waves received.

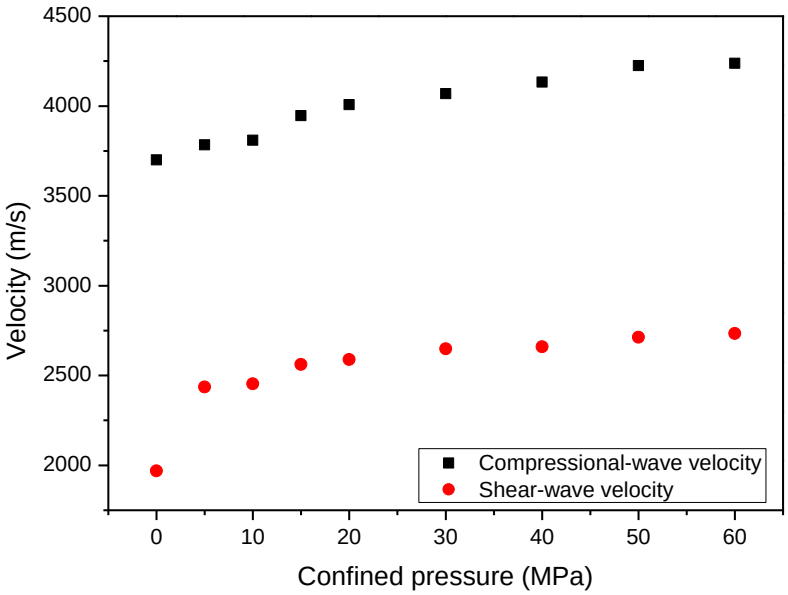

Figure 5.6 Averages for compressional velocities (Vp), shear velocity (Vs) used to obtain; normal stiffness (Kn), shear stiffness (Ks), Poisson's ratio (v) and modulus (E) of Niger delta sandstone samples.

Table 5.1 Averages for compressional velocities (Vp), shear velocity (Vs), normal stiffness (Kn), shear stiffness (Ks), Poisson's ratio (v) and Young modulus (E) of Niger delta sandstone sample at 5-60MPa of confined pressures (Pc).

Pc (MPa)	Vp (m/s)	Vs (m/s)	Vp/Vs	Kn (MN/m)	Ks (MN/m)	Kn/Ks	v	E (GPa)
5	3784	2437	1.55	5.92	2.15	2.77	0.146	27
10	3809	2454	1.55	5.99	2.19	2.77	0.145	28
15	3946	2561	1.54	6.31	2.52	2.52	0.136	30
20	4007	2589	1.55	6.58	2.50	2.66	0.141	31
30	4069	2648	1.54	6.66	2.76	2.42	0.133	33
40	4132	2660	1.55	7.07	2.55	2.80	0.146	32
50	4225	2713	1.56	7.43	2.60	2.88	0.149	34
60	4238	2734	1.55	7.40	2.74	2.71	0.144	34

It has been established that acoustic waves are affected by rock mineralogy, fluid composition, porosity, texture, clay content, cementation, confined pressure, and temperature (Kassab and Weller, 2015). In this sample, the strain in the grain contact resist passage of signal during compressional test and the perturbation data was recorded as a grain contact data from the observed velocity in Figure 5.6. This yielded a mean velocity ratio (Vp/Vs) of 1.55 presented in Table 5.1 which was an average of 6 experiments for each confined pressure. In Figure 5.6 at confined pressure of 30MPa, the velocity ratio was almost constant up to 60MPa. Hence, for this sample, the confined pressure necessary to obtain normal and shear contact behaviour was 30MPa (Figure 5.6).

5.4.4 Grain contact stiffness from compression and shear velocities

By using the Winkler correlations (Winkler, 1983), the normal stiffness and shear stiffness of the grain contact were evaluated using the compressional and shear velocities respectively. The elastic modulus and grain densities were evaluated and the value obtained was between 18-26GPa. The variation in the modulus value implies heterogeneity in the sample with a corresponding range of Poisson's ratio from 0.133 to 0.302. The acoustic wave velocities were correlated with coordination number and grain density using Equations (5.1) – (5.3). The normal stiffness and shear stiffness served as a basic micro-parameter measured for the elastic characteristic data of the rock sample. The statistical analysis of the stiffness modulus and Poisson's ratio for 54 sample tested are provided under statistical section at the end of this chapter.

$$K_n = \frac{12\pi R\phi}{C}\left[V_p^2 - \frac{4}{3}V_s^2\right] \tag{5.1}$$

$$K_s = \frac{24\pi R\phi}{C}\left[V_s^2 - \frac{1}{3}V_p^2\right] \tag{5.2}$$

$$\frac{K_n}{K_s} = \frac{3\left(\frac{V_p}{V_s}\right)^2 - 4}{6 - 2\left(\frac{V_p}{V_s}\right)^2} \tag{5.3}$$

Here, Kn ans Ks are normal and shear stiffness respectively, Vp and Vs are the P- and S- wave velocities respectively, R is grain radius and ϕ is the porosity and C coordination number. In Figure 5.6, the average velocities are plotted against confined pressure. Next the contact stiffness was calculated and plotted in Figure 5.7. The average stiffness ratio turns out to be 2.68 with a standard deviation of 0.3048, for normal stiffness and shear stiffness of 6.5373MN/m and 2.4564MN/m respectively. The standard deviation for the normal and shear stiffness is 0.5595MN/m and 0.2632MN/m respectively.

Velocity ratios (i.e., ratio compressional velocity to shear velocity) were plotted in Figure 5.8 to compare possible ratio for stiffness data in Figure 5.9. The average ratio of normal to shear stiffness was 2.68. In Figure 5.8, a reflection of the stiffness ratio (Figure 5.9) was observed for velocity ratio (Figure 5.8). This was a simple validation for consistency in the evaluation of the stiffness data.

A near constant value of compressional and shear waves were maintained at about 30MPa confined pressure up to 60MPa. Stiffness ratios were within the range of the stiffness ratio obtained from the Photo Stress Analysis Tomography (PSAT). The PSAT experiments will be presented in Chapter 6.

Qualitative data extracted from the micro-structure of rock are normally obtained from measuring elastic wave velocities (Nur and Wang, 1989). These elastic waves are actively influenced by grain deformation, therefore, the characteristics of these wave velocities during grain distortion can be employed to evaluate contact parameter. Winkler's evaluation of normal stiffness and shear stiffness is directly based on measured wave velocities. It is observed that this correlation is not based on any pre-defined grain contact model.

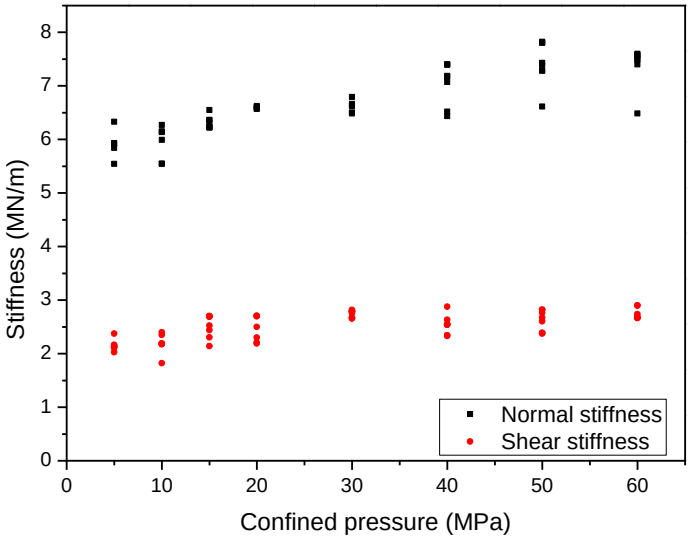

Figure 5.7 Grain to grain normal stiffness (Kn) and shear stiffness (Ks) of the sandstone sample from ultrasound measurement technique.

5.5 Micro-fracturing and micro-measurement

Micro-fracturing of rock can be explained by interaction between the grain and cement components which constitute the material. The grain displacements that result in fracture can be very difficult to quantify as the grain interact relatively with each other. This quantification has been evaluated for dry grain assembly with force transmission through grain contacts (Shukla et al., 1988; Oda et al., 1982)

Recent advances in numerical modelling of rock fracturing require the building of rock with its micro-mechanical properties which are derived from displacement allied quantities. These quantities are obtained by numerical calibration of the macro-scale elastic parameters. The micro-properties are important and should not be neglected because failures in rocks are peculiar to their micro-behaviour. Rocks may exhibit behaviours which include; the elastic non linearity, plasticity and complex features which characterized rock's response to stress. In order to compare micro-data from simulated rock behaviour, this work seeks to quantify the micro-mechanical properties by estimating the grain and cement data from an arbitrary point in natural rock.

It is understood that deformation begins at cemented contact (Dvorkin et al., 1991; Dvorkin et al., 1994). Under stress, the grains in contact are usually separated and possess a single point contact (Dvorkin, and Yin, 1995). Recall that the sandstone has been characterized (Chapter 3) which shows discrete grain cemented at contacts. From these facts, we can assume that when; the cemented granular grains of rock are loaded the behaviour is elastic; the cementation at contact is finite therefore, grain data corresponds to cemented contact data; the grain remains intact but remain elastic until after a critical stress is reached. With these three assumptions, we can identify the tensional region and the compressive behaviour of the grain contact behaviour as the grain move from its position under stress.

5.6 Directional measurement

Illustrations of the directional measurement at a point in the sample are illustrated in (Figure 5.8 and Figure 5.9). This was draw by Amadei, (2012). In Figure 5.8, the different inclination of the anisotropy is illustrated. Also the oblique incidence initiates the value of the principal strain. Thus, the corresponding stresses can be evaluated. Typically stress will induce strain in all directions. Figure 5.9 shows that with axial stress (Y) applied to the sample, strain (Ɛx, Ɛy, Ɛz) occurs in all directions corresponding to the anisotropy in rock.

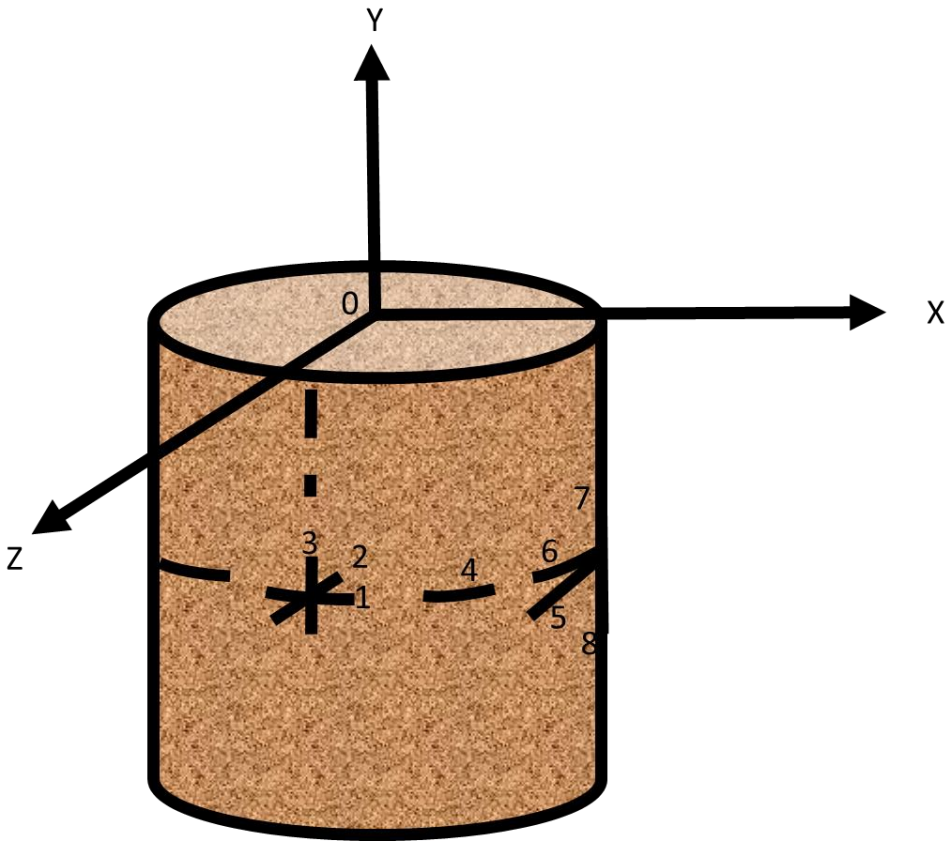

Figure 5.8 Illustrations of the directional measurement from the sample showing strained localised points (Amadei, 2012)

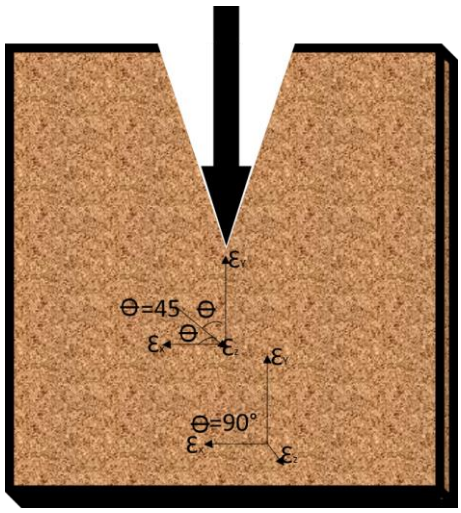

Figure 5.9 The two and three different inclination of the anisotropy is illustrated (Amadei, 2012)

5.6.1 Determination of stiffness of a single point

Stiffness of a single point was evaluated. The ultrasound yielded velocities in the axial direction and perpendicular directions of loading. Due to the occurrence of double refraction, displacement in the normal and shear direction at that point was recorded. At the point location in the sample, applied forces were recorded and corresponding arrival time was measured. The point stiffness in both normal and shear direction was hence estimated.

5.7 Statistical analysis of normal and shear stiffness data

Linear regression was used to ascertain the validity of the micro-parameters measured. The statistical descriptions are also presented based on the experimental data Table A1 and A2. 54 samples were tested. Six assumptions were required for the data to be found valid for regression model. The statistic package for social science (SPSS) was used to carry out the statistical evaluation. This was because the macro-parameter data was obtained simultaneously for all the stiffness data observed. Hence, applying linear regression model is satisfactory. Also, the data fulfilled the entire requirement for linear regression validation.

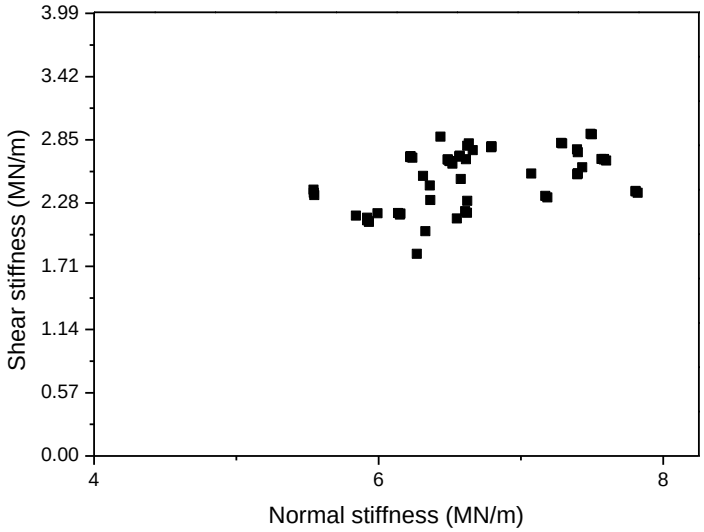

Figure 5.10 Plot of shear stiffness versus normal stiffness

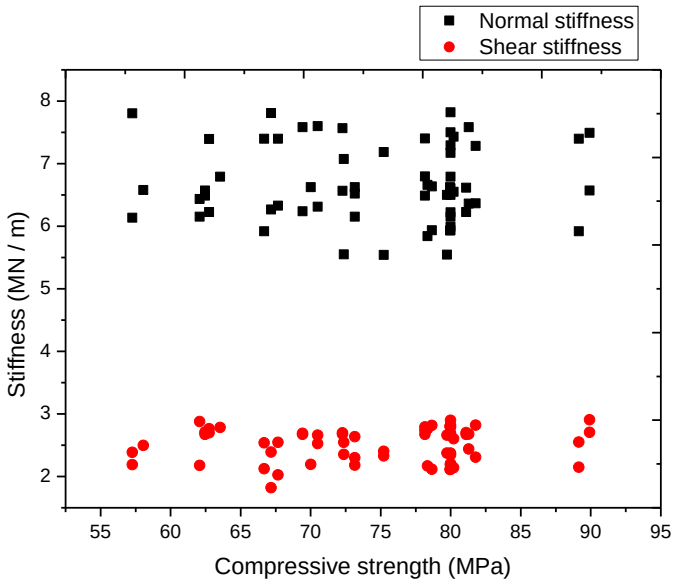

Figure 5.11 Stiffness versus compressive strength of sandstone

These requirements include:

1. No significant outlier was found on the vertical or dependent axis. The outliers usually have large residuals which may have negative effect on the predicted model. For example, it may affect the accuracy of the regression equation and hence affect the value of the predicted model. However in there are few cases the criteria exist to cater for outlier detection and with case- wise diagnostics.
2. The data show strong independence of observation which was checked with Durbin-Watson statistics (Azzalini and Bowman, 1993) to evaluate autocorrelation in regression models.
3. The data shows homo-schedasticity. That is the variances along lines of best fittings are similar.
4. The residual errors in the regression line were approximately normally distributed. This was achieved by using the superimposed normal curve on the histogram plot. It should be noted that this test should be coherent in order of this list above.

If all these assumptions are true then the model used for prediction is valid. This was tested with Poisson's ratio and elastic modulus plots with stiffness data in Figure 5.12 and Figure 5.13.

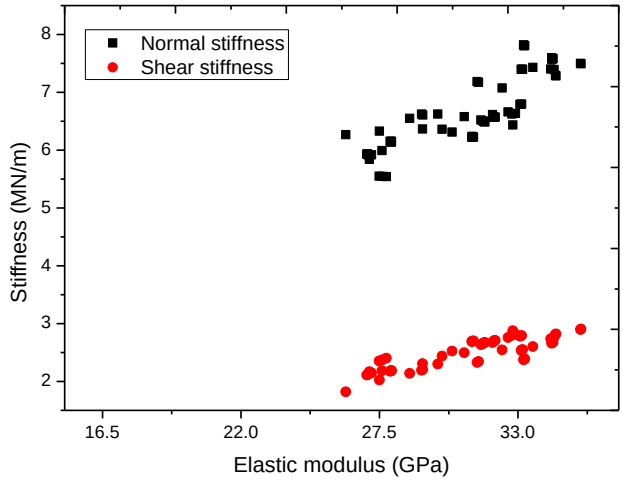

Figure 5.12 Analysis of stiffness with elastic modulus

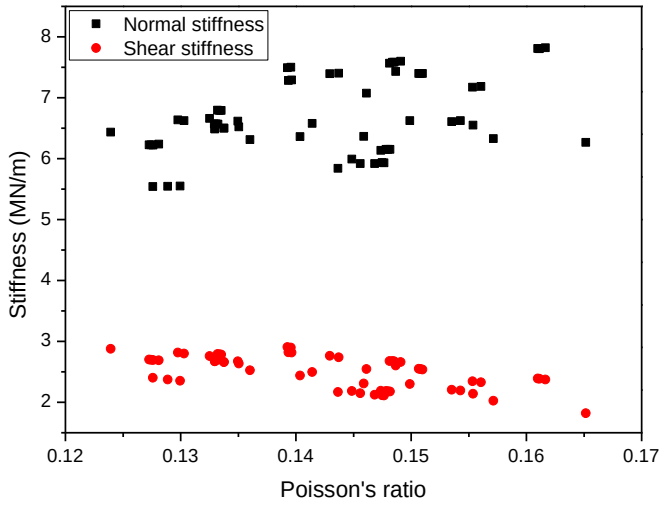

Figure 5.13 Analysis of stiffness with Poisson's ratio

5.7.1 z-test for normal stiffness and shear stiffness

The z-test was carried out in order to ensure that the measurement of normal stiffness and shear stiffness are consistent in yielding the same stiffness ratio (Table A1 and A2). This was done using the SPSS (Statistical Package for Social Sciences) software. It processed the experimental stiffness data and generated the expected value of normal stiffness against their actual value. In order to carry out the z-test (Table A3), it was confirmed that the parameters were normally distributed. The assumption of normal distribution was checked by plotting a Q-Q graph (Figure A1 - A3). The plot presents the experimental data lying within their diagonal lines. This is an indication that the stiffness measured is normally distributed. The significance

level is 0.05 (Doane and Seward, 2011) (i.e. α=0.05) . Under the ultrasound measurements, the normal stiffness, the Z-value-Skewness and the Z-value-Kurtosis are 1.698 and 0.055 respectively. For the shear stiffness measured, the Z-value-Skewness and the Z-value-Kurtosis are 0.695 and 1.667 respectively (Table A3 and Table A4).

Since the population variance are known for normal and shear stiffness measured (Table A4), then the stiffness are approximately the same for all points in the sample. This is due to the degree of cementation, pore spaces at grain contact and mineral type.

Shapiro-Wilk's test (Shapiro and Wilk, 1965) shows that the p-value = 0.000001<0.05 (Table A5), it means we reject the null hypothesis. At significance level of 0.05, there is enough evidence to conclude that the mean stiffness of 6.5373 MN/m and 2.4567 MN/m have a ratio of 2.66 from all the experimental data. Therefore since we reject the null hypothesis for the confidence interval of 95% (Groeneveld and Meeden, 1984).

5.7.2 Statistical confidence of the stiffness ratio

The standard deviation of the data set was employed to express the variability of the stiffness data, it is indicative of a confidence in statistical conclusions. The observed small standard deviation implies that the values of stiffness ratio data set are close and highly concentrated to the mean stiffness ratio. The experiment was strictly controlled by Griffith theory because a small standard deviation was aimed. This is because, the stiffness ratio is restricted to the contact stiffness obtained from measured velocity. Many authors have derived the micro-structure (stiffness ratio) of sandstone (Dvorkin and Nur, 1996) by calibrating the experimental Poisson's ratio and young modulus of rock samples (Potyondy, 2013). Their results shows that magnitude of stiffness ratio for sandstone is within the minimum and the maximum range obtained from the experimental work in this research. In specific terms, the magnitude of stiffness ratio has a standard deviations that provided insight for adequate experimental repeatability. Consequently, the deviation between data measured between 5 MPa and 60MPa fluid pressure is justified because of the large range in confined pressure did not produce large difference in stiffness ratio.

5.8 Conclusions

Rock deformation starts when grains are displaced from their intact position. This implies that, crack localization and the onset of crack formation are due to grain motion. The data obtained at this localized points are grain-scale data. Although the grains are cemented, a cement contact is finite compared to the grain size, thus the contact stiffness is approximately equal to the grain stiffness. Therefore the statistical description of the grain contact stiffness is a description for micro-mechanical deformation.

Velocity ratio of 1.5 to 1.7 has been reported for sandstone (Castagna et al., 1985; Shillington et al., 2008; Pickett, 1963). A similar data was observed for Niger delta sandstone with a characteristic coordination number 9 and a porosity data of 20.65%. This velocity ratio serves as indicator for stiffness ratio because the velocity ratio is a reflection of the stiffness ratio.

Previous attempts made for the determination of grain contact stiffness involve the use of artificial grains and cement to build rock (Dvorkin and Yin, 1995; Holt et al., 2005). This stiffness data from natural sample can be compared with parameter evaluated in DEM. The DEM uses contact model whereas the natural data reflect the natural contact behaviour.

An average value of 2.5 was obtained by ultrasound method for the stiffness ratio of sandstone which was approximately the same as the value provided by Winkler (1983), hence the stiffness ratio of 2.5 were validations for other measurement techniques.

By using data extracted from natural sandstone, the complications of computation can be simplified in the numerical simulations. In this context, a scheme of procedure is suggested to include identification of fracture process zone (FPZ), determination of micro-parameter and the development of the granular assembly in Chapter 6.

Overall, the stiffness ratio of the sandstone was evaluated successfully. The tests also revealed experimental measure of Poisson's ratio and inter-particle friction of sandstone grains. These parameters can form a reliable input to DEM modelling work in the subsequent chapters where applicable.

Chapter 6

Sensing Stress Distribution on Opaque, Anisotropic Materials and Using its Nub in the Multi-scale Simulation of its Fracture Strength

6 SENSING STRESS DISTRIBUTION ON OPAQUE, ANISOTROPIC MATERIALS AND USING ITS NUB IN THE MULTISCALE SIMULATION OF ITS FRACTURE STRENGTH

6.1 Introduction

Fundamental level understanding on the strength and fracture properties of opaque and anisotropic materials require accounting for key multi-scale characteristics, from single-grains scale to bulk scale. This task remains as a stiff challenge in a wide range of science and engineering fields including geotechnical, petroleum, mining, minerals, advanced materials and particulate engineering. Here is the generic multi-scale framework for simulating the strength characteristics of real sandstone samples using a combined measurements and modelling strategy. Using photo-stress analysis methodology, first we sense the shear stress (or strain) distribution and its components along orthogonal directions on the surface of a V-notch sandstone sample under mechanical loading. Using this and applying a classical grain-scale model, the stiffness ratio of the sandstone is evaluated at grain scale. This is also compared with using ultrasound sensors independently and a good level of agreement is obtained. Thereafter, the grain-scale stiffness ratio which characterises the signature of material anisotropy is fed as an input in to the discrete element modelling of cylindrical sandstone rock samples subjected to axial compression. Physical experiments are also conducted to evaluate the load-displacement characteristics and bulk fracture strength of cylindrical sandstone sample. A good level of agreement is obtained between the simulations and experiments. Thus the current multi-scale framework can be applied in future to evaluate the mechanical properties of such complex and anisotropic materials in a reliable manner.

6.2 Sandstone and inherent anisotropy characteristics

Rocks have inherent granular arrangement and bonding at grain level (Burnley, 2013). A common feature of an anisotropic fractured rock is the discontinuity of fracture path within its structure induced by shear localisation (Burnley, 2013). Fracture path within sedimentary rock are identified by irregular interlocking pegs and sockets where insoluble minerals concentrate (de Andrade Ramos, 2000). Mineral sorting of rock samples have shown compositional differences at grain scale, identified by irregular

interlocking pegs and sockets where insoluble minerals concentrate (de Andrade Ramos, 2000). As a result, they display anisotropic material properties at bulk scale (Hudson and Harrison, 2000). Fracture in rock occurs along weaker stress planes (Park, 2013). The grains are displaced in directions perpendicular to least principal stress under external loading (Secor, 1965; Vander Pluijm and Marshack, 2004; Singhal, and Gupta, 2010).

A major challenge in characterising the mechanical response of anisotropic rock media and its links to mobilising bulk strength characteristics is the identification of stress (/strain) distribution in rocks especially when they are opaque. Existing strength measurements of rock media are done either at macro scale using bulk strength testing devices, or at micro scale using strain gauges though some whole field optical techniques such as speckle interferometry is emerging (Razumovsky, 2011). However, for using conventional strain gauges, it is not always easy to pre-locate the positions of weak strain (or stress) propagation paths in anisotropic rock samples (Lawn, 1993). Ideally, one would like to track the distribution of stresses and strains inside three-dimensional rock samples under mechanical loading, but the scientific community is still far away from accomplishing this task more easily. This could be responsible for the lack of accurate theories for defining the strength distribution in deformed complex materials. Attempts to track the fracturing process by visualising whole-field strain or stress distribution patterns and linking the grain-scale behaviour to bulk scale strength characteristics of anisotropic materials (Lawn, 1993) are generally scarce in the literature. The relative displacement of the grains in them culminates into crack propagation under mechanical loading and accounting for such micro effects in predicting their bulk strength is not yet well established. If single-point measurements of grain stiffness could be measured even on the surface of suitable rock samples, grain stiffness at orthogonal directions can be estimated. Such realistic point scale inputs into a higher scale modelling could help to evaluate their multi-scale strength characteristics more reliably. This forms the motivation of the current work.

6.3 Experiments and modelling

In order to measure the stress/strain magnitudes at macro-scale, strain gauges are usually applied limited to bulk data (Fairhurst and Hudson, 1999b), for example the results are average measures over several grains within gauge length. Other methods such as photo-elastic stress analysis have been reported in the past using strongly bonded optically sensitive birefringent disks mimicking the sandstone (Zang and Stephansson, 2009) and provided macro-parameters. The residual strain field within sandstone grains was mimicked using birefringent material to represent naturally shaped quartz grains while epoxy was used to represent the bonding cement (Zang and Stephansson, 2009). The quartz-cemented sandstone was simulated approximately so that nearly the same elastic modulus of the grains and cement of the experimental sample was the same as the real sandstone. Other probing tools such as ultrasound tomography and X-ray computed tomography were useful to measure some mechanical (Appoloni et al., 2007) and internal micro structural properties (Winkler, 1983) of the grains respectively. Such properties could significantly influence on the macroscopic strength characteristics of rock samples (Holt et al., 2005). However, stress (strain) measurements on real sandstone material were required at grain-scale to evaluate realistic micromechanical features, which is the focus of the current work.

On the computational front, a number of methods including finite element method (FEM) (Burnley, 2013) and discrete element method (DEM) (Cundall and Strack, 1979a) have been used to understand the strength characteristics of rock samples. For evaluating both the internal and bulk strength properties of rock samples, using DEM is relatively more suitable. The method models the interactions between the neighbouring grains as a dynamic process and the time step is advanced using an explicit finite difference scheme. The interaction between contiguous particles is governed by a number of ways, for example using linear spring-dashpot models (Cundall and Strack, 1979a) and theories of contact mechanics (Dvorkin and Nur, 1996, Hossain et al,. 2011). Though large scale sample representation in DEM is computationally expensive, some DEM studies have been reported for small scale rock samples (Hunt et al., 2003). However, DEM modelling fundamentally requires assigning initial value of micro parameters (e.g. stiffness parameters) of particle and inter-granular bond strength to build a rock sample. Such micro parameters are

either guessed or obtained through a calibration processes in such a way that at first, the tuned parameters result bulk strength values of rock samples comparable with physical experiments using real samples (Yoon, 2007). Thereafter, internal characteristics such as velocity and displacement patterns inside the samples at different stages of the loading can be probed in detail (Fakhimi and Villegas, 2007; Cundall and Strack, 1979a)). Experimental design and optimisation strategy had been reported to build discrete model which was subsequently used to calculate micro-parameters of grains in order to reproduce macro-properties (compressive strength, young's modulus and Poisson's ratio) of the rock during compression test (Yoon, 2007). Some discrete models employ the technique of calibrated circular particle interaction to obtain a suitable dimensionless parameter for building rock models (Fakhimi and Villegas, 2007) such that granular bond models produce the micro-properties (normal/shear stiffness, normal/shear bonds, and frictional coefficient) during the calibration procedure. Micro-properties were evaluated (Fakhimi and Villegas, 2004) using a slightly overlapped circular particle interaction (SOCPI) to work out ratio of unconfined compressive strength to tensile strength as well as the failure envelope. However, the macroscopic strength was less in magnitude when compared to the real rock sample. Fakhimi and Villegas (2007) improved on the overlap technique (Fakhimi and Villegas 2004,) using dimensional analysis to calibrate the particle assembly for Pennsylvania blue sandstone through deformation characteristics in stress paths. In this, the micro-properties were found to underestimate the macro-properties of the real rock sample using theoretical contact models. Though previous iterative approaches have provided new insights on the internal behaviour of rock samples under mechanical loading, multiple combination of parameters, for example most importantly stiffness ratio (i.e., ratio of stiffness along the orthogonal directions to a given grain contact plane) in combination with other model parameters could match the bulk strength in a given test. Hence, it would be best to measure the stiffness ratio experimentally, especially in the case of anisotropic rock material such as sandstone to feed as a realistic input to DEM modelling for simulating its strength characteristics. This fundamental challenge, though not yet tackled, has been addressed in the present work.

The key steps of the present study are summarised progressively as follows: (i) Chemical and physical analysis of the sandstone sample (obtained from Niger Delta) was performed to get grain-scale chemo-physical properties (Figure 5.1)

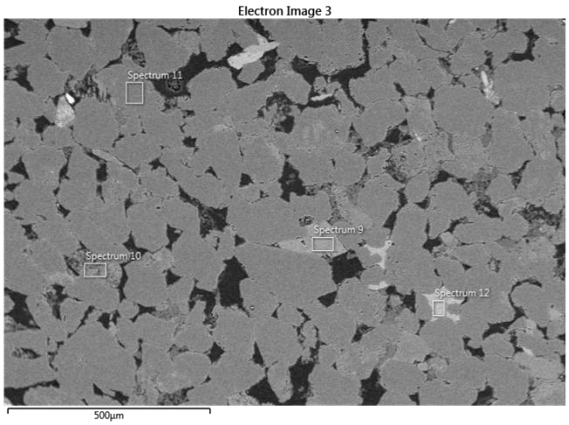

(a) Grain-scale image of sandstone

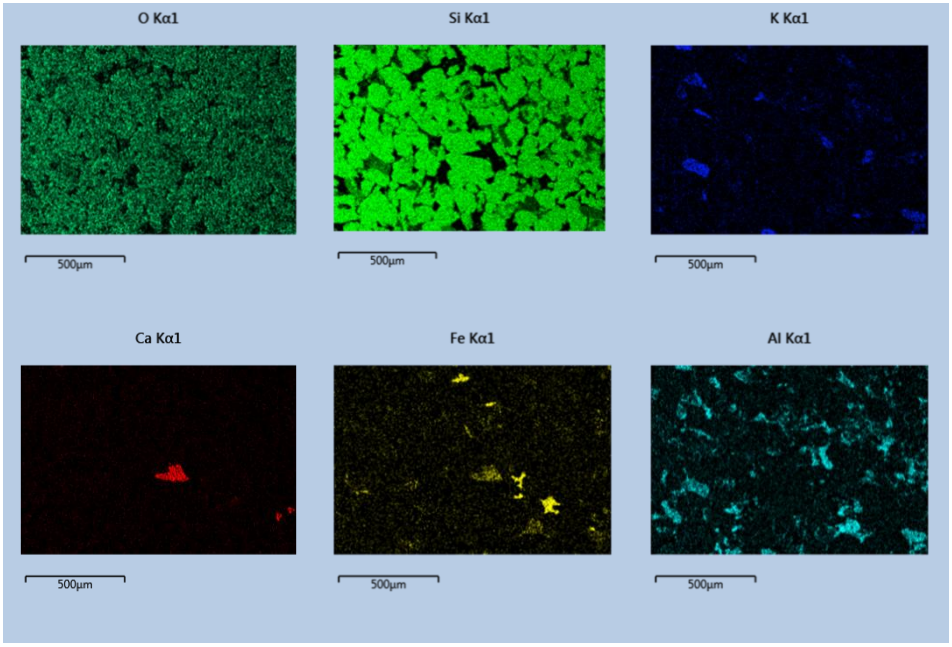

(b) Map of elemental composition in the SEM image of sandstone

Figure 6.1: Scanning Electron Microscope (SEM) Image of Niger Delta sandstone.

(ii) A Chevron sandstone sample (V-notched, Figure 6.2) was applied with a birefringent coating of uniform thickness 300±20 microns on its surface (iii) The V-notched sample was subjected to axial loading in stages. Using photo stress analysis tomography (PSAT, Figure 6.3) and considering that the material is elastic, the

whole-field shear strain (/stress) distribution profile (Antony, 2015) was tracked for different loading increments.

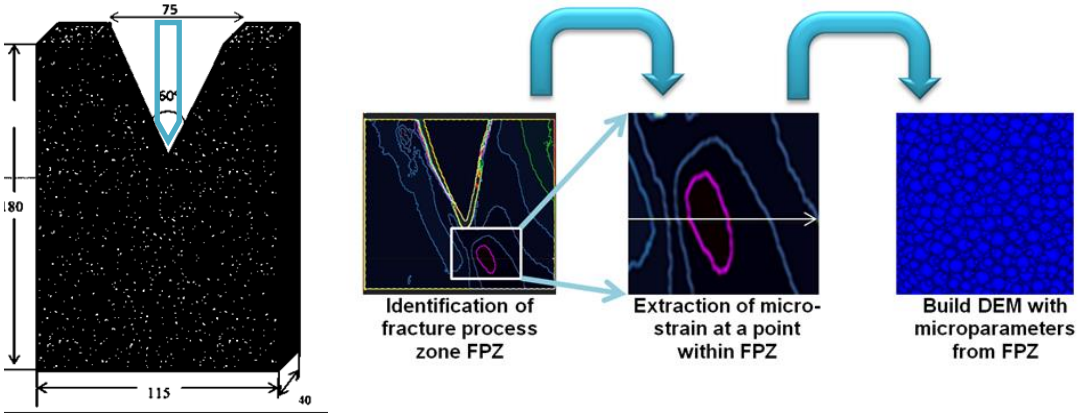

Figure 6.2 (a) Schematic diagram of V-notch sample used to extract micro-parameters and the simulated sample

Note that the steps involved in extracting micro-parameter from sandstone is presented in Figure 6.2; (a) Schematic diagram of V-notch sample. All dimensions are in millimetres (b) Typical contours shows the significant regions of positive and negative stresses below the tip of the notch, referred to as fracture process zone FPZ (c) Enlarged view of FPZ and along the scan line, the variations of positive and negative stress (/strain) profiles are probed to get grain-scale parameters (d) schematic diagram of a cylindrical particulate assembly which uses grain-scale parameters as inputs to simulate its fracture strength. Stress analysis is performed to resolve the two orthogonal component i.e., elastic stress components acting at 45^o to the horizontal and vertical planes (positive σ_1 and negative σ_2 respectively (Antony, 2015) and henceforth referred to as positive and negative stresses(/strains)) and the point of their maximum value is tracked in the V-notch sample progressively for each loading increment (iv) Assuming that the contiguous grains experience these measured stress components along orthogonal planes, and using a well-known inter-granular model, the incremental force and displacement components were tracked and their slope was obtained. The ratio of this pertaining to the regions of positive and negative strain reflects the anisotropy (stiffness ratio) of the sandstone (v) conventional ultrasound testing was also done to obtain the stiffness ratio of sandstone (which is due to the ultrasound wave responses in them along orthogonal

directions) and a good level of agreement is obtained between the two approaches (vi) The stiffness ratio obtained from step-iii, is fed as an input parameter (rather than commonly assuming as 1 pertaining to an isotropic and homogeneous material) and using clumped-spheres to reflect the shape and size of the grains of sandstone obtained from step (i), discrete element modelling (DEM) is performed to simulate the bulk stress-strain relation for a cylindrical sample subjected to axial compression. Evolution of some internal parameters such as the velocity distribution of grains is also done to get an idea of the discontinuities and the evolution of the fracture plane and (vii) finally physical experiments were also done for the sandstone cylindrical samples pertaining to the loading condition of the DEM simulations to get the bulk stress-strain relations and a good level of comparison is obtained between the experimental and simulation results to validate the present approach, which links experimentally measured point-scale information to bulk scale strength characteristics of complex material

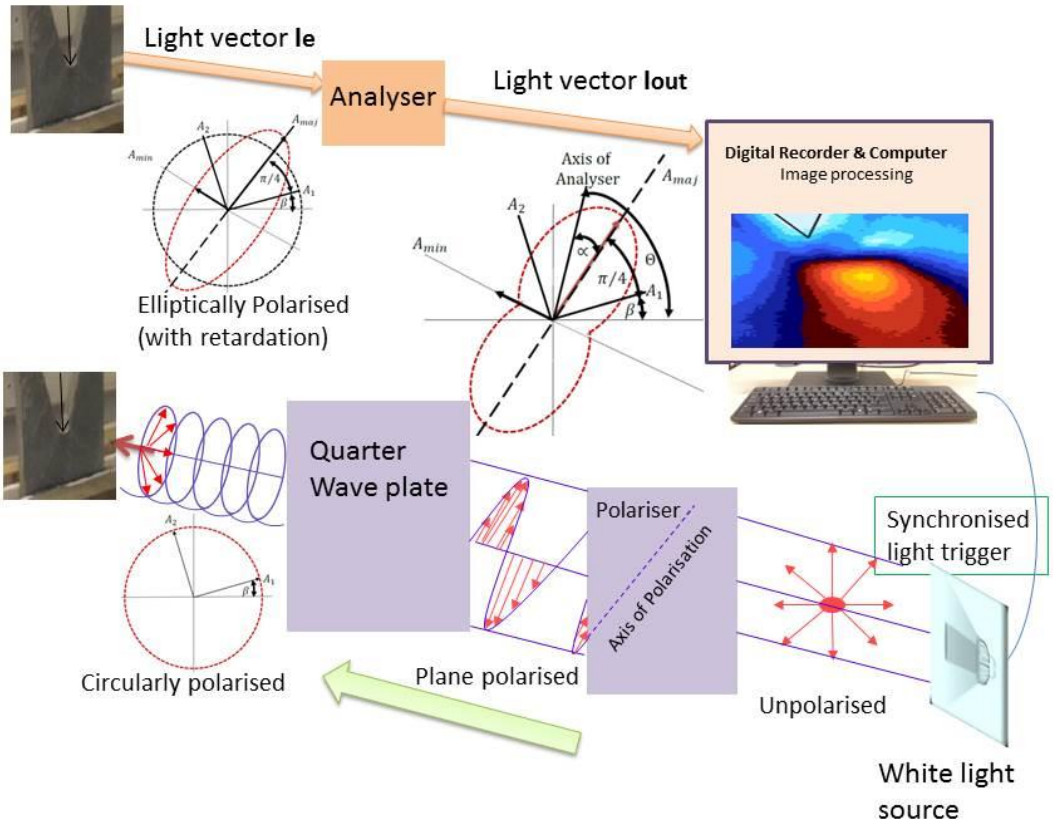

Figure 6.3 Basic optical elements of PSAT setup for sensing retardation of principal components of light and maximum shear stress distribution on the surface of sandstone under axial loading. The contours show different orders of fringes**.**

6.4 Results and discussion

Initially, the sandstone was experimentally characterised thoroughly as much as possible for understanding its grain-scale characteristics. Figure 1 shows the SEM image of the sandstone sample and X-ray mapping of its elemental composition. This shows the granular nature and structure of the quartz grains which are cemented at their contacts in the sandstone. The bond strength of clay cementitious material is relatively weaker than the strength of quartz (Waltham, 2001). The coordination number of the quartz grains mostly varies between 8-12 (average coordination number 9) and the grain diameter between 60-100 microns. Furthermore, previous studies on the deformation of the grains in rock have not rigorously accounted for the structural characteristics of the rock (Holt et al., 2005). However, considering that rock deformation is a multi-scale processes with potential links between material properties at different scales, using SEM and X-ray analysis of sandstone, we start with realistic information on the nature of strongly bonded grains in the sandstone. The SEM and X-ray analysis suggest that the examined sandstone is composed of well-sorted quartz grains with random sizes. It is a clastic rock with low degree of heterogeneity (Figure 6.1). This is consistent with sedimentary oil-bearing rocks such as Niger Delta sandstone with random distribution of grain bonding; the grain morphology is multiplex (Lambert-Aikhionbare and Shaw; 1982, Reimold et al,. 2014) with large pore space and low grain spherical index (Figure 6.2). Using the Saturation and Calliper Techniques (Ulusay and Hudson, 2007), the following properties of the sandstone were measured: porosity 22%, grain density 2120 kg/m^3 and bulk density 2135 kg/m^3. The friction coefficient of sandstone is obtained as 0.6 from the standard tri-axial test (Hoek and Franklin, 1967) under a confined pressure of 15MPa. These experimentally characterised material parameters are used later for simulating the strength characteristics of sandstone using DEM by modelling the individual grains as bonded discrete spheres (Figure 6.4).

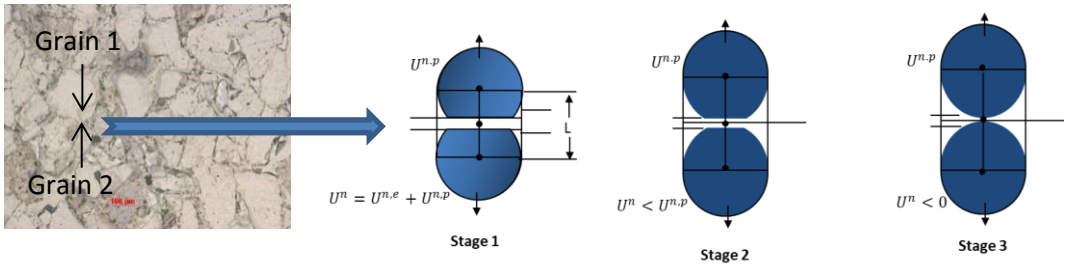

Figure 6.4 Illustration of progression of crack through two contiguous grains' contact.

The optical image and the illustrations of the progression of crack through two grains is presented in Figure 6.4. This is modelled in DEM using spheres (Ren, et al., 2012) with bond strength pertaining to the cementitious bond between the grains. The typical stages are as follows. Stage1: This corresponds to the initial stages of the loading where the load level is low. Cementitious bond and spheres sustain tension. Stage 2: For further increase in the load at this intermediate stage, the overlapped-grain tries to separate. The grains are still bonded and retain a tensional force. Stage3: At the verge of grain separation. The two grains are out-lapped, but the contact retains critical tensional force leading to compressional force. The bond strength of sandstone grains is about 120-140MPa (Rong et al., 2013). Standard tri-axial confined compression test (Ulusay and Hudson, 2007) of sandstone was also conducted experimentally under a fluid pressure of 15MPa, which resulted into the values of the bulk compressive strength (failure strength), elastic modulus and Poisson's ratio as 125MPa, 24.48GPa and 0.25 respectively. The bulk compressive strength and deviator stress was also compared between the experiments and DEM simulation later. Experimental unconfined compressive strength test (Ulusay and Hudson, 2007) of the sandstone was also conducted, which resulted the Young's modulus of sandstone as 18.6GPa. This is within the range of other studies reported values of this, for example 16.5GPa obtained experimentally for the Berea sandstone (Halleck et al., 1988) and 20GPa used in the simulations for China sandstone (Rong et al., 2013).

Figure 6.5 depicts a deformation contour for the micro-cracking mechanism of a single point for the following retardation values: 63nm, 71nm, 78nm, and 93nm. These retardation values correspond to the following list of optical-forces: 1MPa, 5MPa, 7.8MPa and 9MPa respectively.

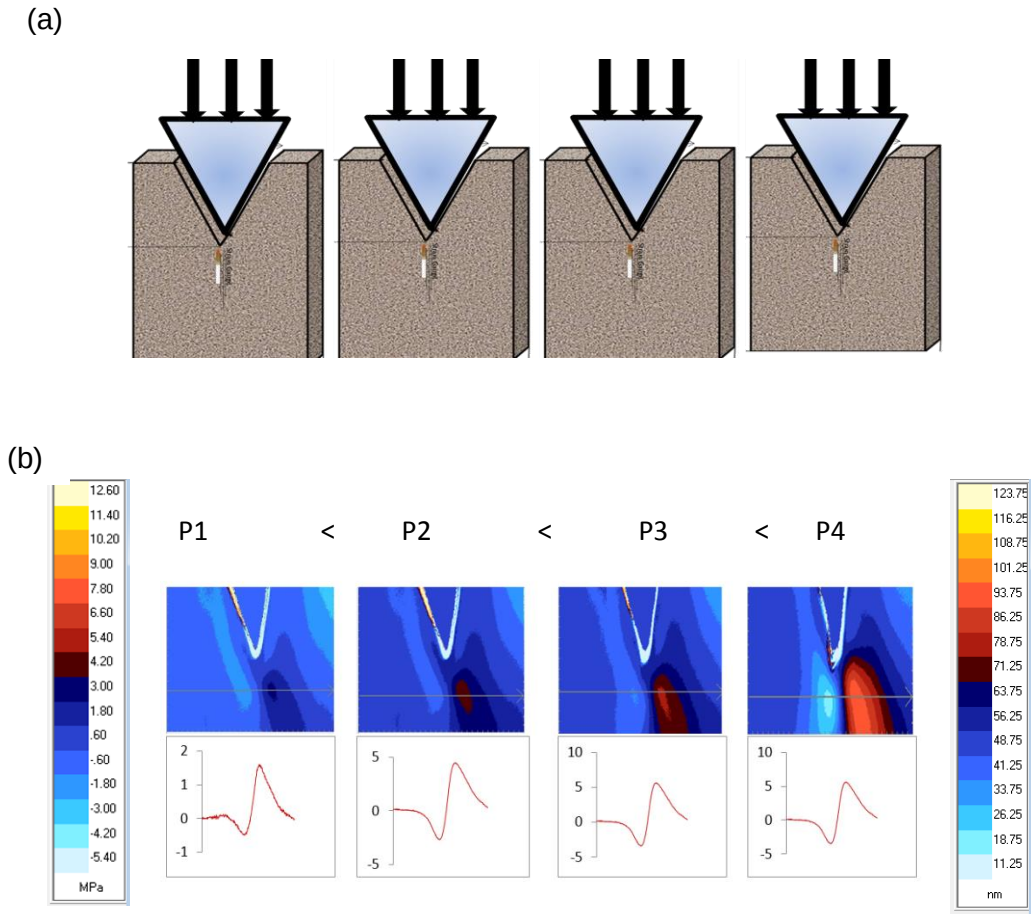

Figure 6.5 T(a)direction of load application (b) typical evolution of retardation map in the sample for an increase in external load levels (P1-P4), (P1<P2<P3<P4).

In Figure 6.5, typical evolution of retardation map in the sample for an increase in external load levels (P1-P4) is presented. Such maps are generated for a number of incremental loads and the outputs are analysed. Retardation information are scanned along the section (passing through the highly stresses point in the map). The positive and negative values of the retardation correspond to the positive and negative stress acting in orthogonal planes at the point of interest. The slopes of these two parts, as illustrated in the last image (P4) were tracked and their ratio

computed for different load levels. The distribution of retardation of light between the major and minor optical axis on the V-notch sample (which is proportional to maximum shear stress (Dally and Riley, 1991) is visualised using PSAT (Figure 6.3, details in the methodology section) for different axial load levels. This approach is most suitable to make point-scale measurements of retardation of light components along orthogonal directions.

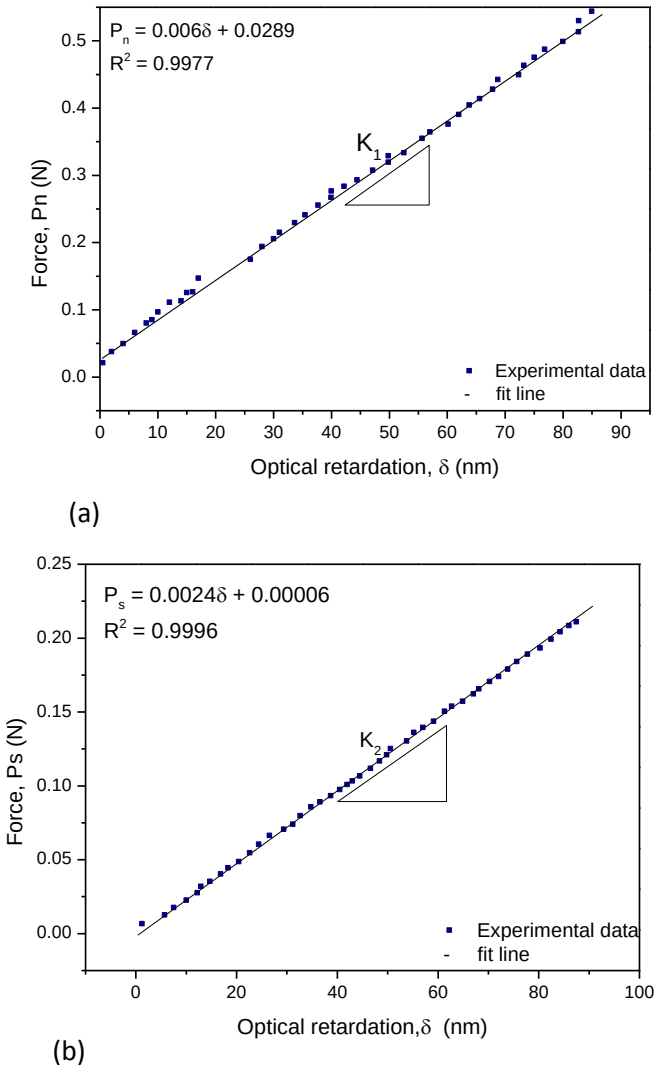

Figure 6.6 Experimental evaluation of stiffness (K) values (a) (K1) (b) K2

The origin of this retardation is due to the difference in the principal strain (/displacement) along orthogonal directions at the point of interest in the sandstone. As we could expect, highly stressed regions are sensed beneath the tip of the notch and the colour coding is done in relation to the magnitude of retardation and maximum shear stress. Suitable sections are chosen to analyse the nature of the

optical retardation as explained in Figure 6.5. The post-processing of the retardation data was done for locating the position of maximum positive and negative stresses and their evolution was tracked under different loading increments. Using the point-scale measurement of orthogonal stress components, assuming that the point is represented by contiguous spheres in contacts (Li and Fjær, 2012), Figure 6.3) and the approximation between stress-force at grain contact as used by Mavko et al. (2009), the grain force corresponding to the orthogonal components of measured stresses at the point of interest is obtained and plotted against the optical retardation in Figure 6.6. In this, a linear fit is made to the data and the slope of the line corresponds to K_1 and K_2. The ratio of these results the stiffness ratio K, equal to 2.5. The standard deviation in K was observed as 0.21 from a large number of repeated tests (about 50 tests). We also evaluated the stiffness ratio of the grains contact independently using the conventional ultrasound sensing methodology (Aydin, 2014) which resulted in a value of 2.68, which was comparable to the PSAT measure described above. However, the slight discrepancies in this between the PSAT and ultrasound-based results could be attributed to the fact that, the K measured from the ultrasound method was based on the average response due to the contributions of all contacts in the experimental sample whereas the current PSAT measure is point based. Furthermore, we also evaluated the value of K from the slopes of the initial optical responses as described in Figure 6.5 without the need to use the stress-grain force contact model*, and the result was fairly similar. Henceforth, we used the K value derived from PSAT, which is more realistic, as an input parameter into DEM modelling of the bulk strength of cylindrical sandstone sample at the later stage. Furthermore, it is interesting to note that existing DEM modelling studies on the strength characteristics of sandstone used the input of K in the range of 1.8-2.9 (Ren et al,. 2012, Rong et al,. 2013) However, unlike measuring K at microscale in the current research, most of the above mentioned DEM studies calibrated the value of K (trial and error) by matching the simulation response to the experimental bulk strength of sandstone. Also the optical output presented in Figure 6.6 result the individual values of K1 and K2 as 6MN/m and 2.4MN/m. This can be compared reasonably well with the values of normal and shear stiffness of sandstone reported earlier in the literature, for example 7.1MN/m and 2.9MN/m respectively for Berea sandstone tested using ultrasound sensor under a confining pressure of 17MPa (Winkler, 1983).

Using the experimentally evaluated grain-scale properties and packing density of the sandstone, DEM simulations using PFC3D software were performed to evaluate the variation of compressive strength and deviator stress. The loading condition pertains to the standard experimental confined tri-axial test (Ulusay and Hudson, 2007) under different levels of confining pressure. The input parameter to the simulations are summarised in Table 6.1.

Table 6.1 Grain Contact Parameters for the Niger Delta Sandstone

Parameter, unit	Quantity
Bond normal strength, mean (MPa)	120
Bond normal strength, std. dev (MPa)	10
Bond shear strength, mean (MPa)	120
Bond shear strength, std. dev (MPa)	10
Grain contact stiffness ratio, kn/ks	2.5
Grain contact Young's modulus (GPa)	18.6
Bulk density kg/m^3	2135
Grain density kg/m^3	2120
Grain radius ratio, Rmax/Rmin	1.66
Friction coefficient	0.6

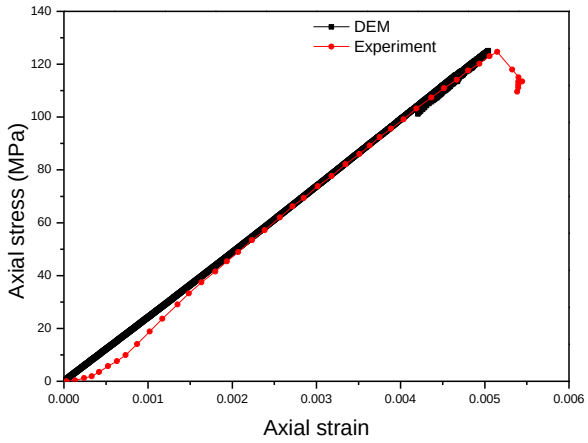

Figure 6.7 Variation of the compressive strength of sandstone obtained from the UCS test

The simulations results were compared with corresponding experimental tests as discussed earlier and the results are presented here. Figure 6.7 shows the variation of bulk compressive strength of sandstone under a typical confining pressure of 15MPa.

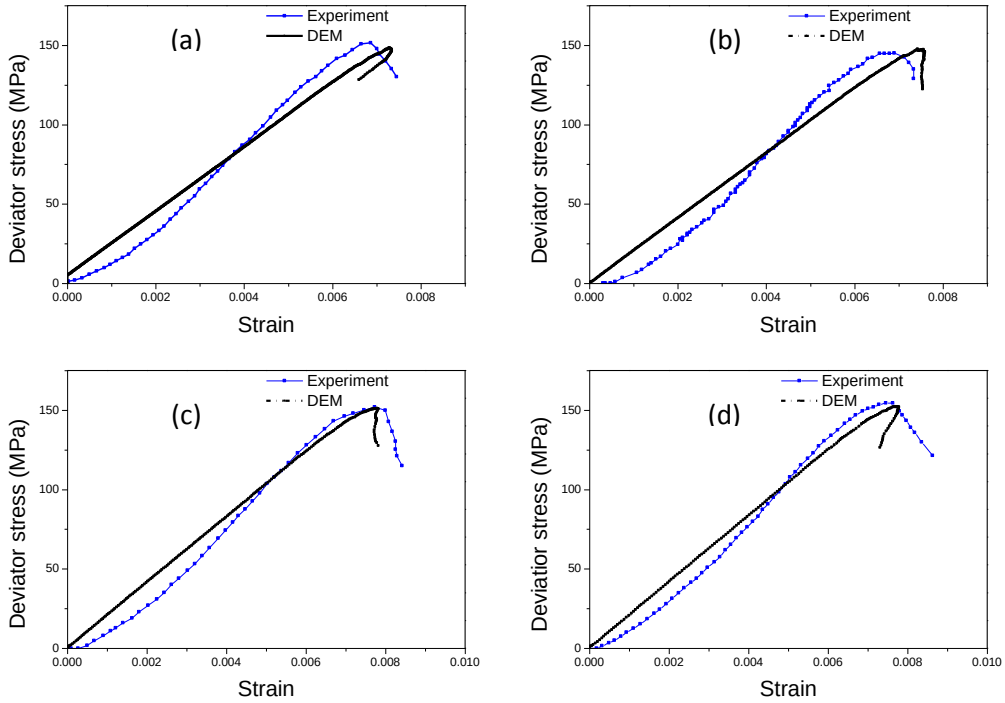

Figure 6.8 Variation of the macroscopic deviator stress during the tri-axial loading under different levels of confining pressure: (a) 5MPa (b) 10MPa (c) 15MPa and (d) 20 MPa.

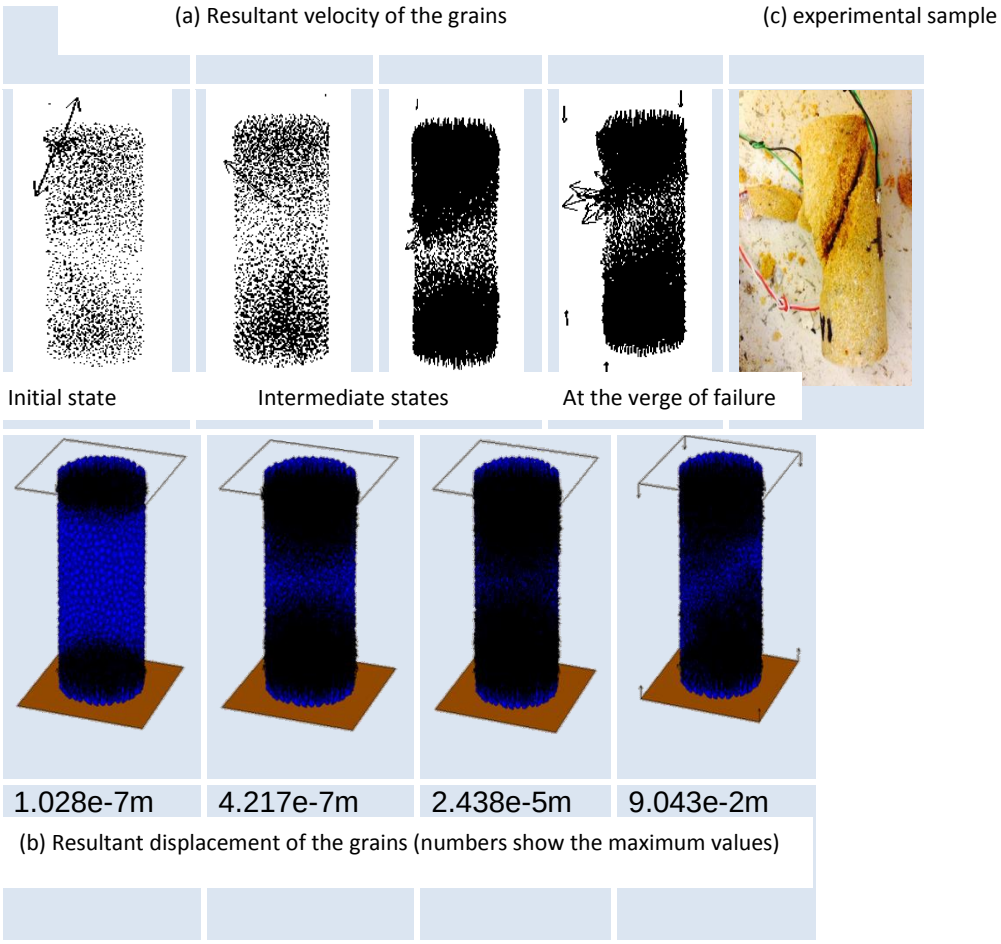

Figure 6.9 Variation of the (a) resultant velocity and (b) resultant displacement of the grains at different stages of loading (confining pressure 15MPa). The thickness of the arrows is proportional to the magnitude of the respective measures (c) a typical visual image of the experimental sample at failure.

In Figure 6.9, the pattern of the failure plan is similar to that of discontinuities in the simulation samples at the verge of failure (~45o) is presented. A good level of agreement is obtained from the simulation and experimental results, especially on the ultimate compressive strength of sandstone (about 125MPa). Further the shear behaviour (Timoshenkgo and Goodier, 1970) of the sandstone was studied by plotting the variation of deviator stress (Timoshenkgo and Goodier, 1970; Towhata, 2008) (this was the difference between the principal stresses) during the confined tri-axial test and presented in Figure 6.8. Again, by and large the more important ultimate deviator stress levels of the samples agree well between the experimental and simulations. This shows the usefulness of the current multi-scale simulations in which measured grain-scale parameters, including the PSAT measurement of

stiffness ratio were utilised. However the variation of experimental bulk deviator stress showed some non-linearity in comparison with the experiments. Considering that the DEM simulations used a simple grain-scale constitutive behaviour, the shear behaviour predicted from the simulations, mostly linearly until failure, is a fairly good average representation of the corresponding experimental data.

A detailed investigation on the DEM results of internal characteristics of sandstone under mechanical loading is outside the scope of the current investigations. However, having validated the DEM simulations with experiments here, the variation of the resultant velocity of the grains obtained from the DEM simulations are presented in Figure 6.9. In this, the visual image of the failed sandstone sample is also inserted for the comparison. It is quite interesting to note that the failure plane of the experimental and simulation samples agree fairly well and this further confirms the validity of the simulations and experiments reported in this multi-scale research programme.

Point stiffness parameter was estimated as inherent grain contact stiffness. Each data value depends largely on the load force applied on the sandstone sample which is assembly of grain.

6.5 Statistical analysis of point stiffness (K1 and K2) in natural rock using Photo Stress Analysis Tomography (PSAT)

Micro-parameters (stiffness) were determined by making the surface of the natural rock birefringence. Therefore it is important to provide statistical analysis of the test data obtained from the direct micro-measurement of the point response to load force in the natural rock. At resolutions of 70 micro-meters (data logger), the stiffness of 54 tested data is plotted in Figure 6.10.

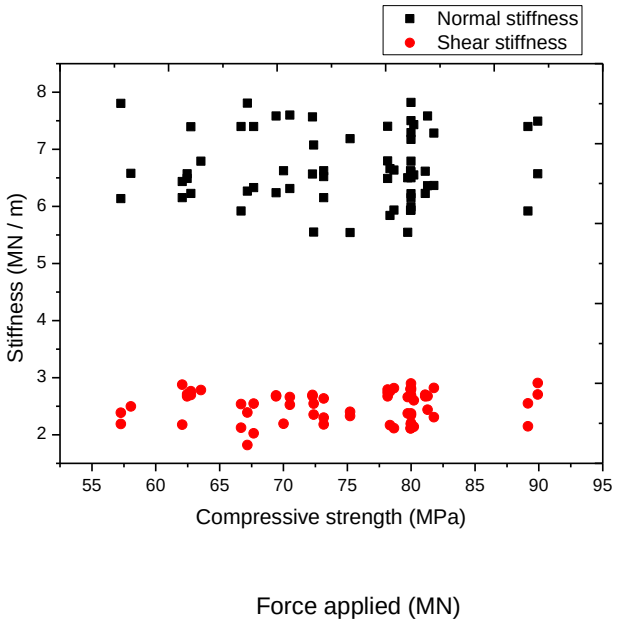

Figure 6.10 Stiffness and force data for Niger delta sandstone

Figure 6.10 shows that the corresponding compressive force reported in literature is in agreement with compressive data gathered in this experiment for sandstone. Under standard ISMR test, the compressive strength of sandstone is between 50MPa to 100MPa. This strength characteristic produces the common range of modulus and Poisson's ratio (Brahma and Sircar, 2014). At a unit area of load applied on sandstone, the force load on the sample that produces normal and shear stiffness is between 50MPa and 90Mpa Figure 6.10.

6.5.1 Descriptive statistics of point stiffness data

From Table B1, the point stiffness ratio of normal to shear direction is not a constant or fixed value, the average is 2.50, with a standard deviation of 0.30648. This analysis show that, the normal stiffness and shear stiffness is averaged 5.7001MN/m and 2.2735MN/m respectively. The standard deviation for the normal and shear stiffness is 0.93904MN/m and 0.21938MN/m respectively. The stiffness ratio is at a standard deviation of 0.30648 which shows that at a dimensionless scale the deviation from mean is small (Table B1).

6.5.2 Symmetry of distribution (skewness) and Sharpness of distribution (Kurtosis) in measured stiffness data.

The skewness and kurtosis are used to determine the z-value. This value has a span of -1.96 to +1.96. (Cramer and Howitt, 2004; Doane and Seward, 2011) it is obtained by dividing either the skewness or kurtosis by the standard error, r, (Table B1 – B3). Here K1 has a z-value- skewness of 1.5692 K2 has z-value- skewness as 1.0615. This shows that at the specified standard error in Table B2 and B3, the K1 and K2 data are normally distributed. Hence the data can be subsequently subjected to simple linear regression. The simple linear regression between force applied on the sample and the stiffness is presented as normal distribution curve in Figure B1. If a data is normally distributed, the P-P plot supports that the perfect diagonal characterizes the regression standardization. This occurs when the data points surround the diagonal (Figure B2).

Table B4 presents the mean of the data used to measure the normal and the shear stiffness of the rock material. Table B5 presents the normal stiffness measured, the Z-Value-skewness and the Z-Value-kurtosis are 2.37 and 0.285 respectively. For the shear stiffness, the Z-value-skewness and the Z-Value-kurtosis are 0.796 and 1.065 respectively. The standard requirement is that these values are between -1.96 and +1.96 (Groeneveld and Meeden, 1984; Doane and Seward, 2011) therefore the data are approximately normally distributed. Table B6 presents the coefficients of the Beta indicating the lower and the upper bond of the Beta evaluated at 95% confidence interval.

By using the z-test (Table B7), the Shapiro-Wilk's test was carried out to obtain the p-values Table B8). The p-values are indicated as “Sig” (Table B8) which are less than 5% ($p>0.05$) (Razali and Wah, 2011) the histograms for the force distribution used to measure the normal and shear stiffness is presented Figure B1. The corresponding normal P-P plots of the regression standardized residuals is presented in Figure B2. The normal distributions are indicators that the stiffness (shear) data were normally distributed. The normal stiffness also approximately normally distributed as indicated by the Z-value-skewness. The skewness of 0.771(Standard error = 0.325) and a kurtosis of 0.182 (Standard error =0.639) were obtained for normal stiffness. The skewness of 0.346(Standard Error is.325) and a kurtosis of

0.509 (Standard error of 0.639) for shear stiffness (Cramer and Howitt, 2004) .The p-values are less than 0.05 therefore we reject the null hypothesis (Cramer, 1998). The data are approximately normally distributed.

The mean force that produces a mean stiffness (K1 = 5.7001) is (70.6977MN) for 54 test data carried out on Niger delta sandstone (Table B4). The regression at a confidence interval of 95% of the variance in force data is responsible for the stiffness observed. The standard error associated with the model is 3.000 which is adequate for mean of the stiffness (Table B5). The adjusted regression squared is the percentage of the variance in the stiffness explained by the force applied on the sample. Therefore 1% variations existed in the stiffness data measured. This is depended on by the force applied to the sample.

In Table B4 the coefficient of variance in the measured stiffness is presented. The coefficient of stiffness is 3.906 for 1% variances in the measured stiffness. This means the magnitude of force that will yield any stiffness is 51.272+ (3.906*5.7001) MN or 70.005MN. This data is significant up to 47.5% at a t- test value of 72.0%. This significance is based on setting 95% confidence interval at a range of constant between 22 and 112.394 (Table B6). The range of stiffness is between -9.928MN/m and 2.117MN/m at a fixed confidence interval of 95%.

The residuals statistics of force applied on the sandstone for which this stiffness analysis was carried out is presented in Table B7.Data from ultrasound measurement are presented in Appendix A. The stiffness ratio was within the small standard deviation. Similar to photo stress technique, the ratio did not deviate beyond 0.30485 observed in the standard deviation obtained in the ultrasound experiment. This is expected because the photo stress technique uses input of elastic modulus and poison's ratio obtained from the ultrasound macro-elastic data. The resultant stiffness ratio is further validated statistically in the statistic section.

Although no current photo elastic data are available for comparison with the measured data from PSAT, ultrasound data were simultaneously obtained from same

sample used for photo stress analysis. The statistical analyses are presented in Chapter 4 (Table A1, Table A2, Table A3 and Table A4) for 54 measured acoustic emissions. The initial strain transfer is initially small. Thus statistical work done to clarify the fact that the strain transferred from the material to the coating might have results that decreases the magnitude of the actual strain. This value may be peculiar to the coating material. However the American Society of Testing and Materials (ASTM) has used the photo-elastic method to obtain strain in rock (Olsson and Peng, 1976). A strong indication of the validity of this data is that the stiffness ratio in PSAT is in agreement with the stiffness ratio observed for acoustic amplitudes. This is also an indication of a reliable fringe-contour that was observed.

6.6 Conclusion

PSAT has been successfully used to capture the sequences of deformation in the cracking process of natural rock from Niger delta. The stiffness properties of the rock have been included in the Formulation of numerical rock in DEM. Thus by defining stiffness property under numerical compressive test, the natural (stress-strain) behaviour of the rock was replicated numerically. This is improvement to the progressive research of modelling rock behaviour which is still a challenge.

DEM has been employed to simulate behaviour of sandstone as an assembly of particles interacting at their contact points. This was done to model crack as dilation of particle contact defined by complicated empirical law; this law can be replaced with simple contact law or stiffness parameter from natural rock. In this context, force-displacement characteristics of arbitrary points are regarded as contact. Thus the micromechanical stiffness characterizes macroscopic behaviour of the numerical rock.

The stiffness parameter is a quantification of the natural microscopic strength exhibited by the sample. In addition, the non-linear elastic deformation property is included into the stiffness parameter obtained from the natural sample. It is experimentally realistic that magnitude of the stiffness quantifies all complicated inherent physio-chemical support/strength of the material. Therefore, numerical

model using such a contact parameters reproduce the important feature of the mechanical behaviour of the material, including the strength characteristics and failure event.

The strains exhibited by rock under mechanical loading were captured as anisotropy which was translated into birefringence. This phenomenon enabled the determination of stiffness property at a point location in rock. Thus via Photo Stress Analysis Tomography (PSAT), the sample with plane stress displayed the birefringence property to enable micro-structural examination used to calibrate the resistance of a quartz contact in the cemented granular assembly under compression. The practical application occurs when sharp crack tends to tri-tensile plane strain and the crack-tip act as a plastic region, which is small compared to crack size and specimen dimension in the constraint direction. The point data can be estimated as a single grain motion in the rock which can be used to build any size of model numerically.

Stiffness measurement at point scale is reported here originally by PSAT. They compare well with the outputs from ultrasound methodology. Indirectly also, the stiffness ratio is validated by feeding them as input into DEM modelling to predict bulk strength characterization, which also agreed well with experimental bulk strength measured.

Chapter 7

Analysis of the Effects of Contact Stiffness and Bond Strength Characteristics of Sandstone using DEM Simulations

7 ANALYSIS OF THE EFFECTS OF CONTACT STIFFNESS AND BOND STRENGTH CHARACTERISTICS OF SANDSTONE USING DEM SIMULATIONS

7.1 Introduction

The focus of this chapter is to evaluate the influences of grain-scale parameters on the mechanical properties of sandstone using 3 dimensional DEM simulations. The analysis helps to provide further insights that are not easily visualized in using experiments only. The simulation is centred on building rock sample from the scratch. This includes representing each rock grain with a particle in 3 dimensions, and to the specified grain density. The interaction of each particle with other contacting particles was controlled by particle contact stiffness parameter which was determined experimentally at a point scale in Chapter 6. The force transmissions within these particles were recorded as force-displacement data during compressive numerical experiment. V-notch sample is used for simulations in this Chapter. The dimensions of the notched sample used here is the same as the one used in the experiments (Chapter 5). Particles were bonded at these contacts using parallel bond. The bond depends on the particle size chosen and was specified in terms of normal and shear strength. These distributed bond strength, were used to represent the heterogeneity which is peculiar to the natural Niger delta sandstone.

7.2 Approach to the study of particle contact deformation

The simulations in this research employ the use of micro-parameters (normal stiffness, shear stiffness, bond strength and frictional coefficient) from sandstone evaluated experimentally in Chapters 4-6. In order to facilitate the simulation of rock using experimentally derived micro-structural parameters, contact stiffness has been experimentally verified with statistical description in Chapter 4 and 5. This is because the force linkages to all individual grain contact are conveyed by normal and shear stiffness properties. However, this simulation is limited to the onset of crack nucleation through the identification of tensile and compressive behaviour of the particle assembly. These two characteristics are peculiar to the onset of deformation where the progression of crack is identified by the compressive stress increment preceding final fracture at peak strength (Rong et al., 2013).

The characteristics tension/compression was significant and revealed the grain contacts behaviour in rock under load (Kazerani, 2013). Micro-structurally, the presence of cementing clay at grain contact suggests that the contact stiffness quantified from the ultrasound measurement technique quantifies the entire attribute at the grain contact exhaustively. Therefore two types of bond were basically incorporated these include the contact bond (which cater for the stiffness properties) and the parallel bond (which cater for the cement/glue between the grains) (Jiang, et al., 2014). Nonetheless the contacts are assigned the stiffness estimated from experiment. This was declared in the DEM program script as the contact bond plus an elastic spring with both normal stiffness and shear stiffness using PFC 3D program (Itasca, 1997). These values were assigned to particle contacts and hence serve as micro-parameter inputs. They influence on the force transmission characteristics of the linked contact chain in the opaque cementations rock materials. The parallel bond detected moment which the particles exhibit as they rotate (Itasca, 1997). Under loading, the rotations are resisted by the elastic spring on the finite connection at the contact plane. Bonds therefore function to reproduce the physical behaviour of the grain contacts in the real material (Potyondy and Cundall, 2004).

7.3 Single points, stress localization and stiffness representation in DEM

Compression and tension exhibited at the stress localized points occur simultaneously and orthogonally (Egger and Pellet, 1990; Shimizu et al., 2009; Pollard and Fletcher, 2005). By identifying the normal and perpendicular direction of grain contact displacement experimentally, the stiffness data was determined in the normal and perpendicular-to-normal directions. The direction of loading determines the tangential force**.** The micro- properties of grain contact which are normal stiffness and shear stiffness parameters were estimated from ultrasound as presented in section 5.7 (Chapter 4). These values serve as fixed input/micro-parameters in the code used to build the bonded particle model because the microscopic input parameter into will generate the macroscopic behaviour of the rock (Potyondy, 2010). Bond strength was obtained by sensitivity analysis to produce the inter-granular characteristics of the rock. Thus, a compressive test was carried out with force targeted on the granular park at a notch (Figure 7.3). It is important to note that the simulation is limited to the initial response of the rock to compression. Figure 7.1 shows the study route.

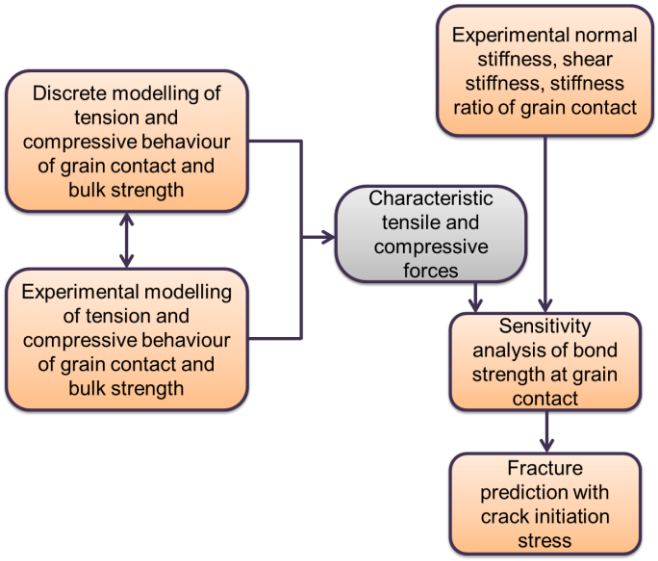

Figure 7.1 Flow diagram used to study deformation of bonded granular assembly

The assumptions made for modelling notch sample include;

(1)Force chains are capable of exhibiting the exact initial extensile internal response during initial stages of mechanical loading.

(2)Force transmission in the particle assembly depends on bond stiffness plus bond strength connecting the grains. For fixed stiffness property, sensitivity analysis on bond strength can yield adequate representation of bond strength in the model

(3)A point pressure applied to a notched sample can induce stress application to a point which will cause stress localization to occur around the notch tip.

(4)The connecting springs will acts at contacting points between particles and will be used to reflect force transmitted through the network of the grain matrix (Figure 7.2).

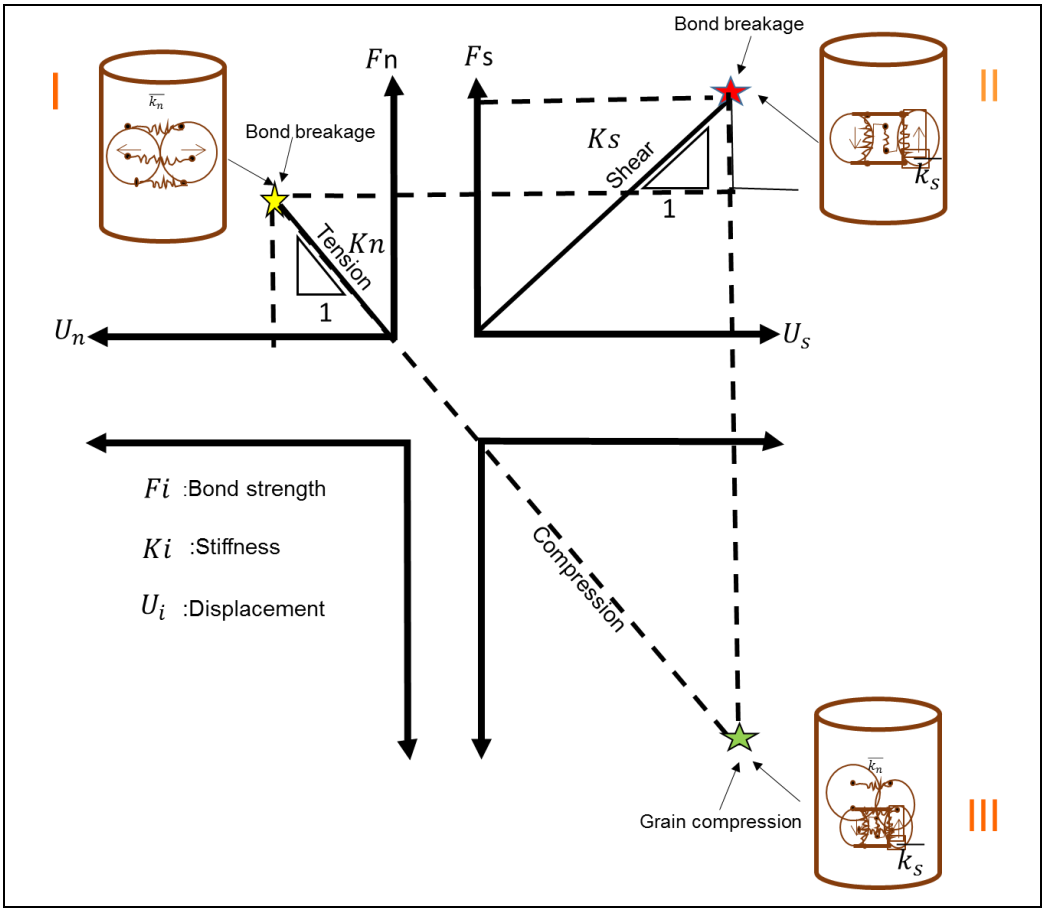

Figure 7.2 Bond and stiffness implemented in PFC

Note that section I, the yellow asterisk marks the beginning of the contact bond breakage due to a tensile behaviour. Next, the grain contact breaks at critical shear force on the contact (the red asterisk - section II). In section III at the green asterisk, the grains are compressed at a force application which is beyond the critical shearing force. The tensile and shearing behaviour are simultaneous interactive response of the grain contacts when the material is subjected to compressive Force (Fn). Illustrations in Figure 7.2 was drawn following the observations from the experimental work carried out in this Chapter and the result was in compliance with the theory of grain deformation provided by Potyondy and Cundall (2004); and Cho et. al. (2007). Section I also represent Normal and shear stiffness between particles. The contact stiffness, Kn and Ks remain active even after the bond breaks as long as particles stay in contact. The bond stiffness (force per unit area), Kn and Ks are removed when the bond breaks regardless of whether particles stay in contact or not; section II represent constitutive behaviour in shear and tension (green asterisk in section III represents granular compression due to shear property and normal property).

7.4 Development of notched sample with point data from experiment

The flow diagram show the process for the simulation of compression on the bond at the notched numerical sandstone (Figure 7.3)

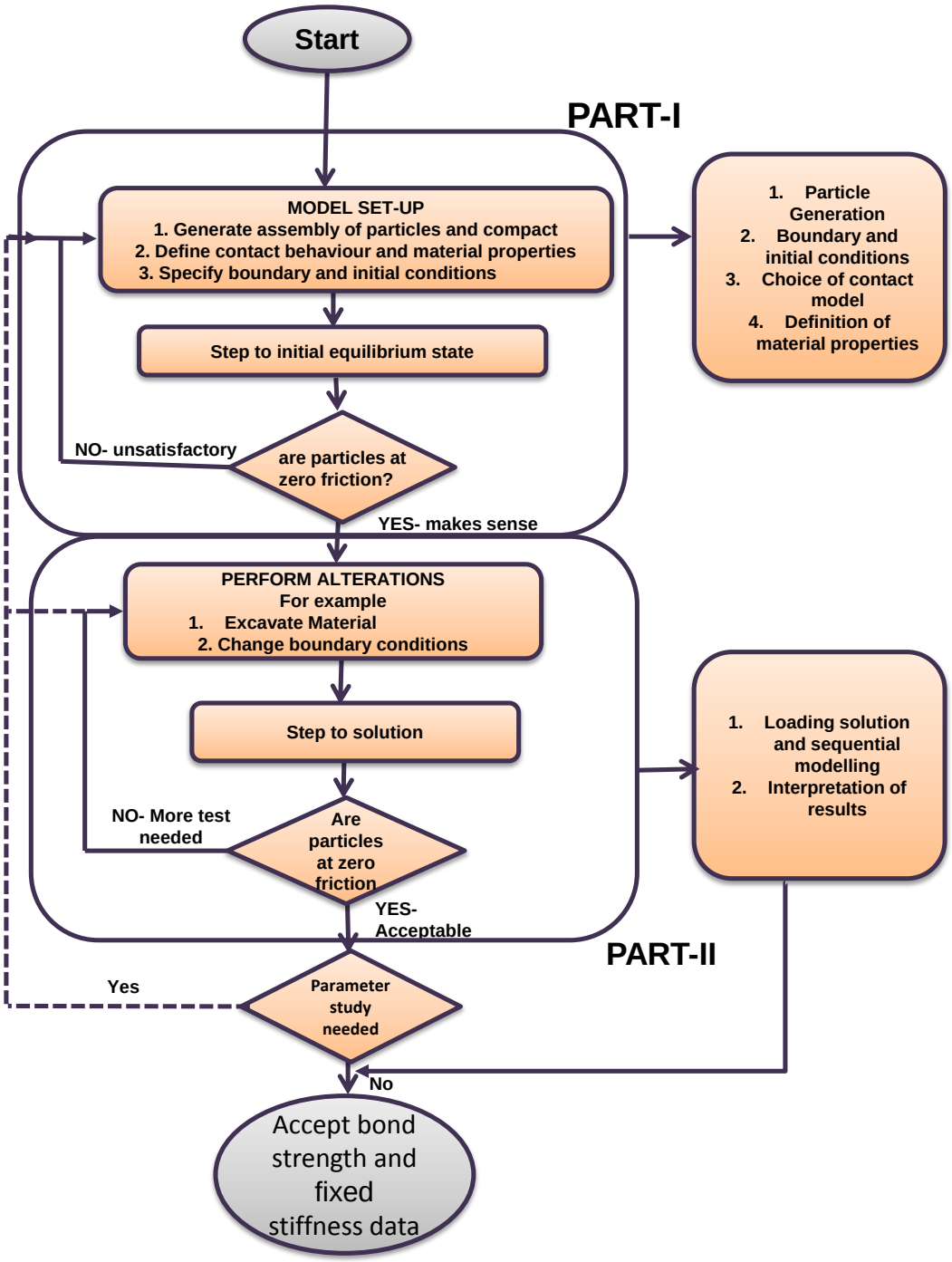

Figure 7.3 Development of rock model and loading sequence

The sequence of model development and loading is presented in the block flow chart (Figure 7.4). Particle Flow Code (PFC 3D) simulation package was utilized with a fish code to excavate particles from notch the specifications were included in the model. The notched model is presented in Figure 7.5. The contact-model for force distribution was included into the particle contacts. The distance between particle centres is the size of the bond cylinder (Figure 7.5). These serves as (pathway of force transmission (or force chains) connecting particles in the matrix. A platen was created to contact this contact force chains at the notch so that as the particles are displaced from their contacts, the force-displacement data can be recorded.

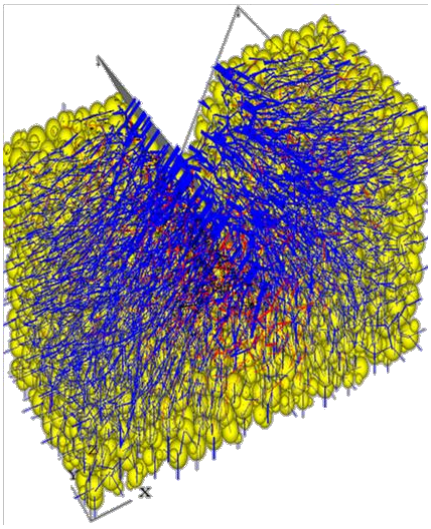

Figure 7.4 (a.) Platen in contact with the V-notch sample

7.4.1 Geometry and dimension

The dimensions of 180mm by 115mm by 20mm (LBH) were specified next, 60dgree notch was created for the purpose of contacting few particles at the notch with a compression platen. The specifications are presented in Figure 7.6.

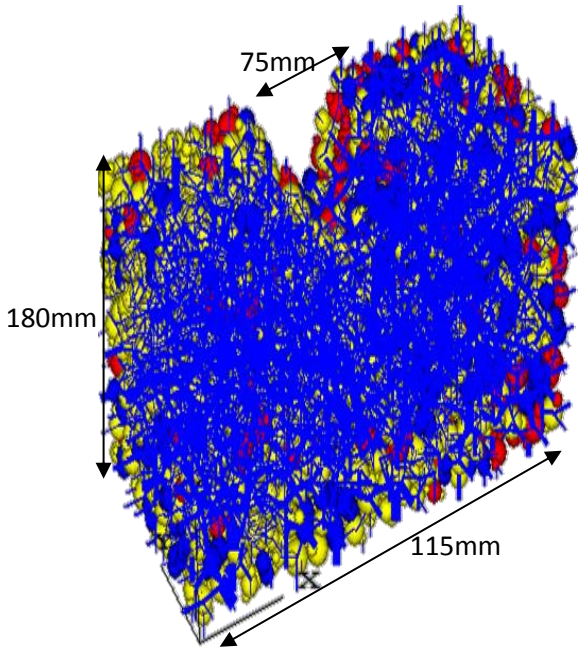

Figure 7.5 Sample specification in both experiment and DEM (all dimensions are in mm)

(Potyondy and Cundall, 2004). When less resolution was used, the particles at the notch were not visible for crack nucleation. The distribution of the particles was incorporated by defining a radius ratio of 1.66 and minimum particle size of 2microns.

Next the sample was made to maintain equilibrium with isotropic stress of the whole assembly. This enabled the replication of the interlock stress of the natural sample. To achieve this, the simulator mode in PFC was activated and thus particle number was chosen arbitrarily by the command Ba_rho equals 2200.0 (Kg/m^3). Porosity was specified by the input values of bulk and grain density of the natural sandstone. Table 7.1 presents the micro-parameter specifications.

Table 7.1 Micro-parameter input for notched model

Micro-parameters	Experimental Data	Numerically calibrated data
Normal stiffness of grain contact	5.7001MN/m	5.7001MN/m
shear stiffness of grain contact	2.2735 MN/m	2.2735 MN/m
Frictional coefficient of Grain	0.6	0.6
Stiffness ratio	2.5	2.5
Parallel bond normal strength	-	120MPa
Parallel bond shear strength	-	120MPa
Micro-modulus of parallel bond strength	-	18.6GPa

7.4.2 Compression test and behaviour of rock under elastic Limit

Force and displacement of loading platen on contact force chain were stored during numerical compressive test. The parameters in Table 7.1 were scaled with radius multiplier that spread round the sample volume. This radius multiplier works in the program environment to multiply or reduce the magnitude of the bond strength carrying the stiffness property.

As presented in Figure 7.7, the network of force was composed of sphere linked between each contact with connecting lines to the centres of the neighbouring particles. The thickness of the line is proportional to the magnitude of the contact force (F) saved as history data. To differentiate compression and tension, the cylinder colour represents tension or compression. ($\boldsymbol{F} \cdot \boldsymbol{n} \geq 0$ is compression, where $\boldsymbol{n}$ is the contact unit-normal vector). Thus, if F is negative it is tension.

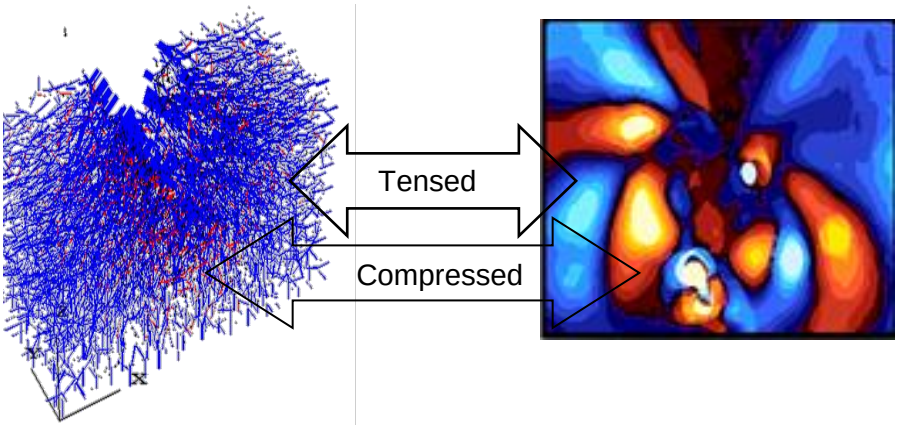

a.)Force distribution in DEM-simulated sandstone

b.)Countours of maximum shear stress in natural sandstone

Figure 7.6 Compressional and tensile forces for the same computational notched model, same geometry and 5MN load on Niger delta sandstone a.)red tensed and black compressed force chains b.) PSAT experimental contours of shear stresses in tension (blue) and compression (red)

In Figure 7.7 (a) Force chain in simulated sandstone shows tension as red force chain and compression as black force chain. The blue force chains are force chains installed during model development b.) Contours of maximum shear force in real sandstone shows tension in blue contours and compression in yellow through maroon contours.

7.5 Platen movement, contact stiffness and the behaviour of force chain contact

Platen (Figure 7.7) is made to displace the particle contact, the force on the contact is recorded for every displacement. The immediate particle contacts at the notch were compressed in the granular assembly and sample exhibit contact tension in red and compression contact force in thicker blue chains (Figure 7.7). The load platen is compressed downward at the notch. This was used to measure contact displacement. This data were recorded at a velocity of 0.005mm/sec.

7.6 Grain contact stiffness and cementation

Single point stiffness was estimated earlier in Chapters 5 and 6. The single point is assumed a grain contact point of linkage between two grains**.** This is because the microscopic image revealed the cemented grain contact overlap is distributed throughout the rock material (Figure 7.8). This contact is thought to be carrying a constant shear and normal stiffness

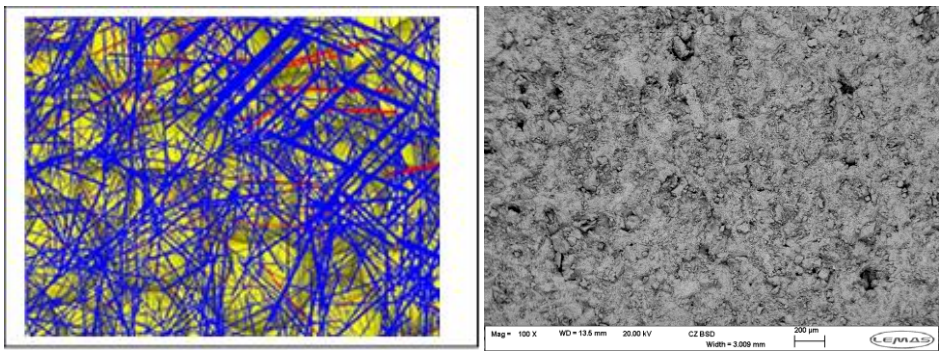

Figure 7.7 a.)Typical numerical view of particles beneath the tip of the notch b.) Scanning electron microscope view of grain in Niger delta sandstone

It is important to note that the particle contact displacement were restricted to very low load force application. This makes the contact exhibit tension and compression via particle frictional behaviour under elastic limit. The tensile and compressional displacement was based on the experimental input value of normal and shear stiffness data. With the platen force applied on the particle contact at the notch, the displacement was recorded (see appendix A). Thus compressive forces were supported by perpendicular tensile forces (Egger and Pellet, 1990). The result of the displacement versus force (compressional and tensional) is shown in Figure 7.9 where higher magnitude of force applications is shown with thicker blue force chains. The contacting grains were cemented; they exhibited tension and compressional stiffness properties under stress. Therefore analysis of stress at any point below the loaded notch in the rock sample was thought of to provide grain displacement and strain dependence in response to loading level. Figure 7.10 presents the characteristic tensional and compressive force distribution.

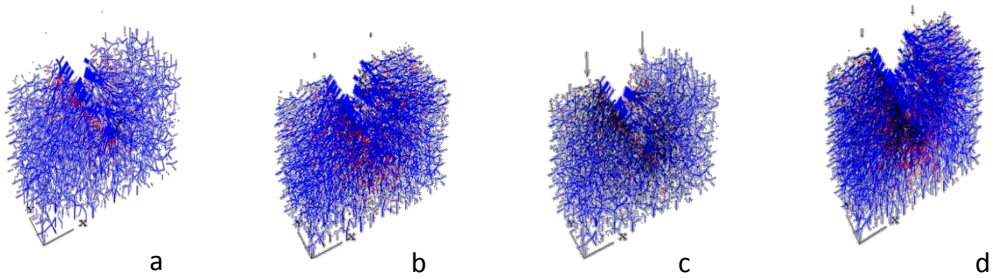

Figure 7.8 Distribution of tensional (red contact force chain) and compressive force (black contact force chains) transmissions during compression a)few contact in tension at 8MPa stress application b.)more contact in tension at 10MPa stress application c.)few contact in compression 12MPa stress application d) more contact in both tension and compression at 15MPa stress application.

Figure 7.9 a-d presents the initial force chain response occurring at the initial loading stages. That is, even if a sudden high magnitude of load is applied, the initial tension and compressive behaviour must first occur. Following this trend, the tensile and compressive forces at particle contact will be exhibited. At about 2MPa of pressure application, some force chains in the stressed pattern under the notch at the stress concentrated location, the particle contacts begin to compress and will eventually rupture. The next sequence of compression was observed in Figure 6.9b. As the high stress on the overlying force increases, the normal stress and the shear stresses are distinguished as mentioned earlier in the experimental observation (Chapter 6). As the simulation progresses, the stress dominate and concentrate at the notch line. Hence increase in the force on the line along the chevron notch increases the shear concentration which results a high value of shear stiffness. The fourth stage (Figure 7.9d) presents the concentrated stress under the notch. This is similarly to the stress localized points under the notch in the experimental findings in Figure 7.7b. The contours of the stressed points are compressive. Similarly the stressed point under the notch shows some compressive force chain under the notch. The similarity in the stressed points can be explained with the similarity in the load force concentrated to the notch. In both cases, force transmits down the notch point. This is expected for a notched sample undergoing a mode I fracture mechanism.

7.6.1 Force transmission in sample

The strains under the notch are caused by the rotation of each particle relative to connecting particles. Thus under mechanical loading, the shear force was

transmitted through the contact force chain as particles exhibits rotational displacement. The shear force transmission was visible by the rearrangement of the particles aiding displacement data.

The force pattern for experimental visualization (PSAT) in Figure 7.7b is not exactly the same as the simulated counterpart. These minor variations in the force transmission through the particle contacts are due to the fact that PFC uses discrete particles which are actually distinct. But the natural sample is decorated with photo elastic coating (a continuum system) in that, the shear stress data captured by the experiments are not discrete, but the strained pattern are results of transferred strain from the cemented granular assembly to the surface photo elastic coating. The data generated afterwards in Figure 7.7 is from continuum digital quantitative experimentations. However the strain in the cemented granular assembly are due to the tensile and compressive behaviour of the grains that make up the rock material.

Hence, it can be said that the normal characteristic of grain contact undergo tensile stretch. This continues to the point where the normal force becomes critical. The characteristics of grain behaviour undergo tensile stretch. The schematics in Figure 7.2 present the contact behaviour in the tension and compression. As normal force increases it is elastic up to the 0.6mm displacement Figure 7.10. The bond breaks in tension at negative force of – 0.2N (Figure 7.11). Although these experimental observations are specific to the consolidated sandstone sample of Niger delta, the material behaviour conform to the phenomenon explained by the simulated work on rock by (Ghazvinian et al., 2012) and (Cho et al., 2007).

On the other hand, the shear characteristics of the single point exhibits positive increase in magnitude as the retardation were measured. These characteristics were captured by the shear stresses until the shear strength of the contact becomes critical. At the critical force, the characteristic shearing property drops due to bond rupture illustrated in Figure 7.2 (Cho et al., 2007)., experiments are presented in Figure 7.11. The shear force measured beyond this critical shear force is yielded data. That is the data/fringe signal fades out (Figure 7.2 and Figure 7.11)

7.7 Discussion on discrete contact behaviour

The mechanism of bond deformation was explained by Potyondy and Cundall (2004) which forms the foundation for building discrete modelling of bonded particle model for rocks. The phenomenon of tension and compression of single point location in real sandstone has a direct numerical application. This is because the behaviour of particle within an assembly of particles in contact (called bonded-particle-model) has been used for several brittle rock simulations even when the micro-properties are not known (Rong et al., 2013). In order to obtain the micro- parameters, calibrations of macro-parameter were carried out. This approach was successful by employing the concept of the tensile and compressive contact behaviour in the bonded particle model developed (Kozicki and Donzé, 2009; Fakhimi et al., 2002). Bond breaks in tension at critical tensile stress whereas the bond breaks in compression at critical compressive stress (Cho et al., 2007).

The simulator is scripted to connect particles and diverse characteristic contact interaction (Potyondy and Cundall, 2004; Boutt and McPherson, 2002), This shows tension and compression response under compressive stress.

7.7.1 Stress concentration, particle contact force and increasing negativity during tensile response

The tensional and compressive behaviour of the few particles beneath the notch was recorded at an extended displacement of 5mm of platen. It was observed that the tensional force was negative. The negativity increases until tensile strength failed Figure 7.11. The red curve shows that the force data becomes increasingly negative until the highest possible negative force is reached. The highest point of negativity has been described to be the point of bond rupture in tension (Van Baars, 1996). It is also important to note that the tensile behaviour occurs at the initial loading stages. Thus the force load that corresponds to the tensile strength is about 2MPa.

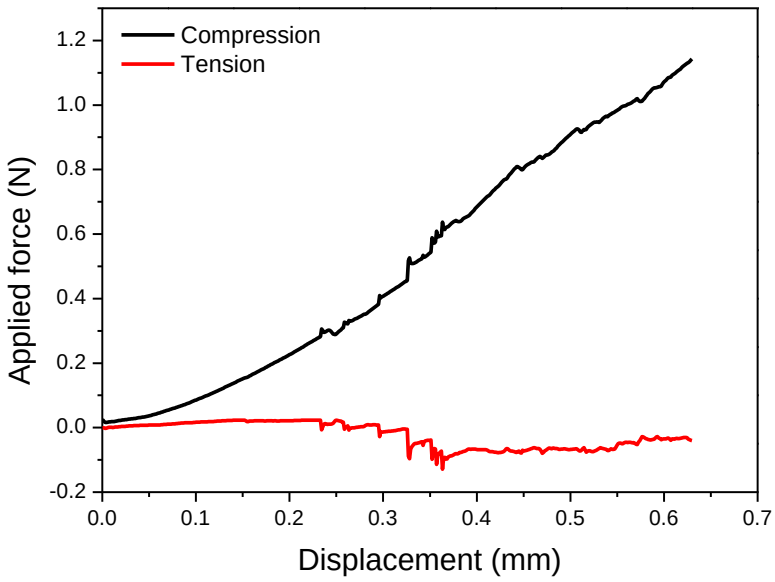

Figure 7.9 Contact force displacement of tension and compression (before bond rupture, displacement at 0.5mm)

7.7.2 Stress concentration, particle contact force and increasing positivity during compressive response of sandstone.

Force measurement during compression on force chain shows that the compressive data becomes increasingly positive until the bond fail under compression (Figure 7.11). The force at 2.4N is the yield strength of a contact bond at which bond rupture. The compressive force increases positively until the contact strength fail at 2.4N (Figure 7.11).

Discussion on contact deformation and crack nucleation

The direct implication of contact deformation is that crack has begun to form. These are micro- crack which forms due to the rupture of contact bonds (the yellow asterisk). The micro-cracks develop due to coalescence of raptured bonds. This particle displacement in shear is captured as crack nucleation. It is seen in the peak tensile stress (the purple asterisk) of - 2.02MPa at a displacement of 12mm (Figure 7.11). The previous application of using the discrete modelling to simulate this process was discussed in Chapter 2.

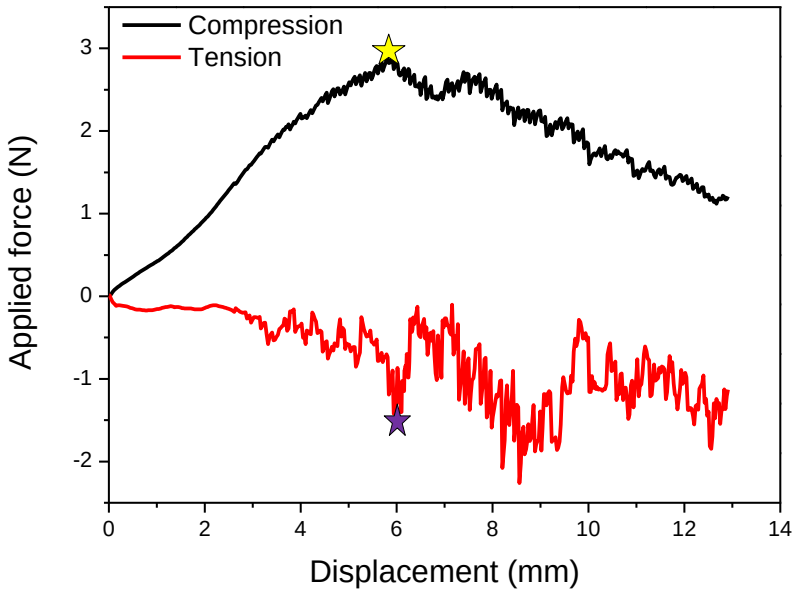

Figure 7.10 Stress-displacement behaviour at particle contact before 12mm Displacement bond breaks in tension (purple asterisk) bond breaks in compression (yellow asterisk)

Compression exerted on the contact force chain that link particles reduce the bond strength at grain contact. Hence micro-fracture is formed and the crack nucleation occurs. In this test, grain contact bond breaks at 2.4MPa (Figure 7.11). During the crack propagation represented by the coalescence of multiple rupture of contact bond, particles rotate as a representation of final shearing away from the glued contact. In Figure 7.2, however, the moment resulting from two contacting particles rotation is opposed by the surrounding elastic spring connecting other neighbouring particles. This network of force chain is distorted and the materials become deformed. The shearing in not uniform (Figure 7.11).

7.8 Discussion on cohesion at particle contact

Unconfined compressive test has been carried out and the shear strength within the inter-granular arrangement was reported (Price, 2008). Similarly, cohesive strength of 0.3MPa was reported for sandstone (Derski et al., 2012). The parameter of cohesion for the numerical sample and the natural sample can be explained with the

presence of contact between particles that exhibit cohesion and internal friction (Figures 7.16). During compression, rock strength is determined by the minerals they are composed of. This is because the strength of a rock mass depends on the packing, shape and sizes (Bell, 2013). It is important to note that material compositions are not uniform at every location in the sample examined. This is the reason for the variations in the value of stiffness and cohesion measured at a point location. Therefore a macroscopic examination is important (Derski et al., 2012). One significant observation is the cohesive property observed at 0.4909 MPa and 0.5001MPa for natural and simulated rock respectively (Figure 7.12).

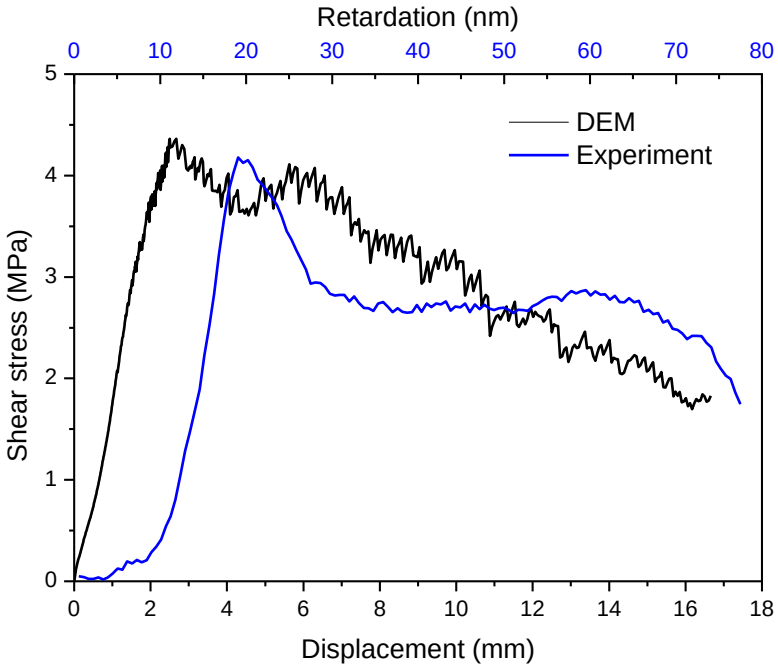

Figure 7.11 Shear stress behaviour in numerical and experimental sample

Experimental data was captured at stress application beyond rupture strength. This is because the macroscopic material is still intact. The critical shear strength at which a contact rupture is 4.5MPa, thus the ruptured bonds may not show macroscopic visible fractures but are micro cracks which constitute the onset of fracturing process in rock. For instance in Figure 7.16 the peak shear at 4.5MPa is a bond-ruptured point due to shear. This mechanism is not different from the bulk behaviour in shear. However minimal the microscopic crack is at a point, it is a separation of a particle

from the neighbouring grain which was initially intact. This leads to random or definitive multiplication of discrete separations which may be non-planar. This phenomenon can be referred to as interface shear transmission (Potyondy, 2010). That is, ruptured bond transmit sufficient shear through aggregate interlock (Rait and Bowman, 2010). Therefore if a shear displacement is supported by a normal displacement due to the irregular asperities of grains and mortar tips shooting across the shear points, (Hazzard and Mair, 2003) shear transfer is generated and stress is transmitted through grain interlock (Davies et al., 2007) Further this transmission through the grain interlock is friction-damped with compressive forces supplied by characteristic reinforcement within the grain assembly. Hence the shear resistance which is measured as shear force at a point regarded as grain contact (Anthony and Marone, 2005) were measured because of three contributions. These are granular cohesion, frictional shear and dilation. The resistance due to frictional damping is proportional to dilation, it increases with normal force. It is easily represented by relating the normal and shear force in a plot which rise with increasing normal force. The phenomenon of this physical change is provided in Chapter 8 where the grain contact models in PFC are implemented.

7.9 Effect of the bond strength on compressive strength

Higher bond strength results in higher peak forces. This conforms to the simulation carried out on Jastrzebie sandstone (Konietzky, 2002). In the sensitivity analysis on bond strength carried out in this section, a trend was observed with the method of fixing experimental stiffness ratio 2.5. By fixing an input for grain density (2590kg/m3) and bulk density (2055kg/m3) obtained from standard experiment, the porosity of the natural rock was fed into the simulated model. For simplicity, the normal and shear bond strength were effectively assigned the same value to clarify their effect on material strength (Table 7.2). This procedure was carried out to identify the trend of relationship between bond strength and bulk strength of the rock.

7.9.1 Standard compressive test (Experimental and DEM)

For the experiments, the medium grained rock was cored from the Niger Delta. A cylindrical shape with 90mm height and 38mm diameter was prepared for the uniaxial compression test. The sandstone was loaded at a velocity of 0.005mm/s due to the

displacement of the piston of the servo controlled compression machine. The axial, lateral and volumetric strain data were recorded. The resulting stress-strain relationships were used to determine elastic properties which allows the generation of the volumetric strain curve. The elastic volumetric strain was calculated using elastic parameters. These constants were obtained from second region or the linear section of stress-strain curves in Figure 7.13.

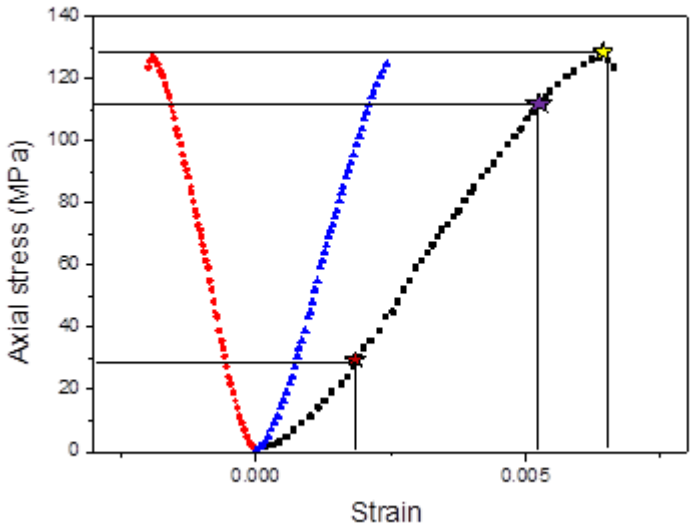

Figure 7.12 Experimental strain response of Niger delta sandstone at a confined pressure of 15MPa

Numerically, standard compression test was simulated and this uses the servo-controlled platens to compress a numerically generated model of sandstone. The model is of equal dimension as that of the natural sandstone. The generated model contains 5600 particles each of which were bonded to connecting particles by parallel bond. The frictional coefficient was 0.6. Its bulk and grain densities were 2055kg/m3 and 2590kg/m3 respectively. The bond strength was studied by observing the strain response of simulated sample which was assigned a magnitude of 80MPa, 120MPa and 140MPa in bond strength. The results shown in Figure 7.14-7.16 are a plot of both experimental and numerical strain response of the rock models. These include the axial strain, lateral strain and volumetric strains. The complete parameter that is used for the simulation of rock is provided in Table 7.3.

Table 7.2 Micro-Parameters used for building numerical model with fixed normal and shear stiffness

Parameter, unit	Quantity
Particle (grain description)	
Normal/shear stiffness	2.5
Bulk density, kg/m^3	2055
Grain density, kg/m^3	2590
Young Modulus, GPa	18.6
Frictional coefficient	0.6
Bond (Cement description)	
Normal/shear stiffness	2.5
Normal strength, MPa	120
Shear strength, MPa	120
Young Modulus, GPa	18.6

7.9.2 Influence of bond strength on compressive strength

The higher the bond strength, the more prolonged the detachment of the contacting grain at deformed location (Konietzky, 2002). The direction of maximum particle velocity is more pronounced. The parallel bond force distribution spreads out uniformly. At peak strength of 89MPa, 129MPa and 190MPa each sample loses bond strength at all bonded contacts. The nature of the failure of the natural sample was similar to the second sample simulated with 120MPa bond strength. The strain behaviour of the laboratory data is compared with DEM test in Figure 7.14-7.16. The strain responses exhibit a good level of agreement between them.

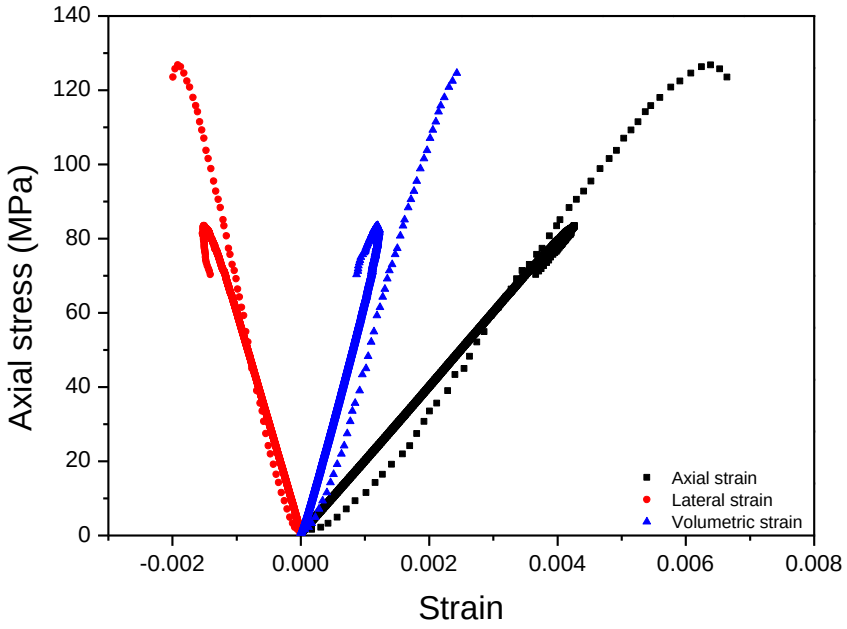

Figure 7.13 Strain response of Niger delta sandstone with 80MPa bond Strength. (Dotted marks are Laboratory result), (solid line are numerical results) under compressive test at 15MPa confined pressure.

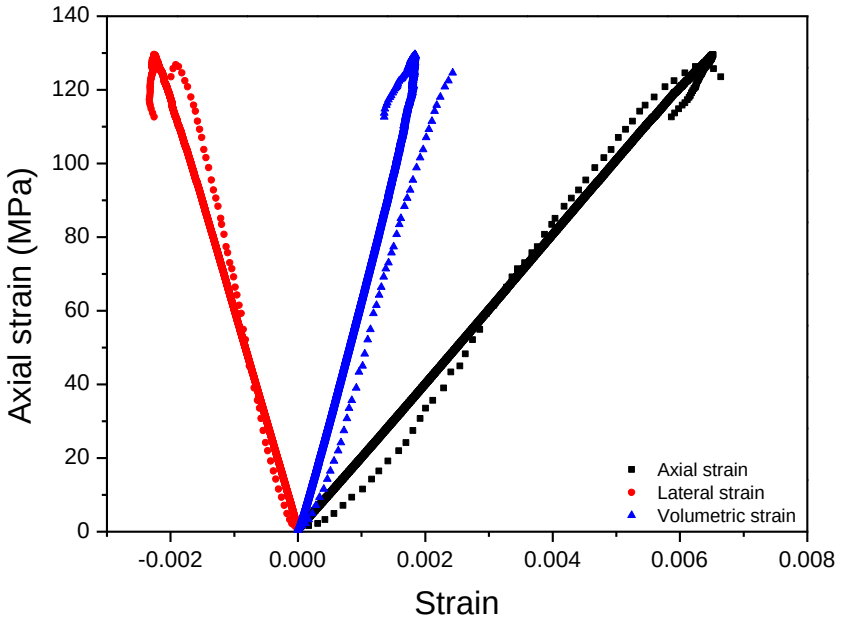

Figure 7.14 Strain response of Niger delta sandstone with 120MPa bond Strength. (Dotted marks are Laboratory result), (solid line are numerical results) under compressive test at 15MPa confined pressure.

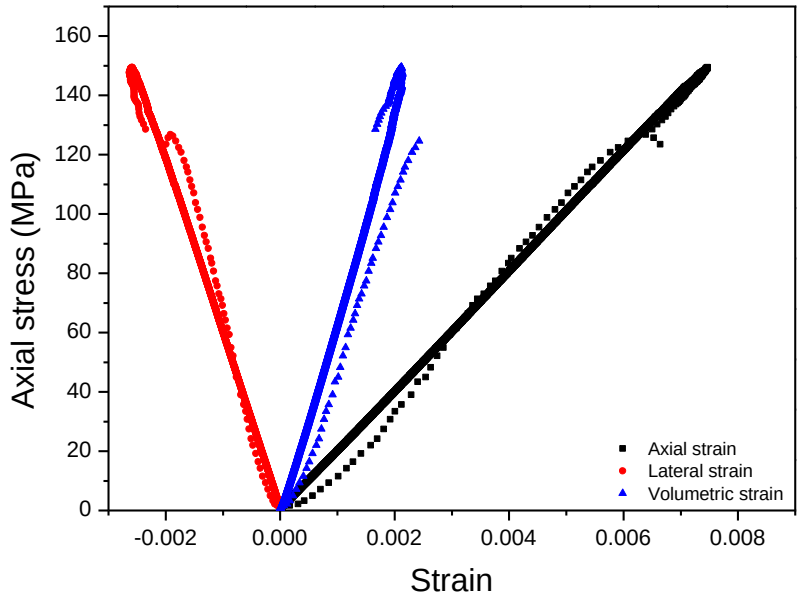

Figure 7.15 Strain response of Niger delta sandstone with 140MPa bond strength. (Dotted marks are Laboratory result), (solid line are numerical results) under compressive test at 15MPa confined pressure.

The strain plot for 120MPa bond strength presented in Figure 7.19 shows that slight difference were observed in the values of peak axial strain for laboratory (0.00766) and simulated (0.00798) data. But the lateral strain show relative a peak strain lateral with 0.00299 and 0.00598 for laboratory and simulated rock respectively therefore the volumetric strain becomes 0.00202 and 0.00129 respectively. The occurrence of strain difference in lateral direction is found in a similar material called Jastrzebie sandstone (Konietzky, 2002). The simulated model for Berea sandstone results similar response (Holt et al., 2000).

7.10 Comparison of the macro-mechanical parameters in DEM and natural rock

By comparing the natural sandstone behaviour to the numerical model it was clear that; if the bond strength is lower than peak strength, the characteristic strain and peak strength are lower than the strength of the natural rock (Figure 7.14 and Table 7.4). At a bond strength higher than the material strength, the material higher strain and peak strength was observed for the simulated model Figure 7.14. In Figure 7.16,

the strain and the peak value match the natural model when the bond strength of close value was used for the numeric model. Table 7.3 shows the average macro-parameters describing the behaviour of both the simulated and natural sandstone.

Table 7.3 Average macro-parameters observed for Niger delta sandstone

Macro-parameter at peak strength	Average Laboratory experiment	DEM Experiment at 120MPa bond strength
Axial strain	0.0060	0.0065
Lateral strain	0.0020	0.0022
Volumetric strain	0.0019	0.0018
Uniaxial compressive strength	124MPa	129MPa
Young modulus	24.10GPa	20.9GPa
Poisson's ratio	0.29	0.33

While the strain is influenced by particle contact stiffness, the bond strength determines the compressive strength of the material. The mean bond strength is related to the mean particle size which controls the tensile strength of the rock. These findings are similar to inferences drawn on the simulation of rock by (Potyondy and Cundall, 2004).

7.11 Statistical analysis of variance (ANOVA) with 2-way ANOVA analysis

A statistical correlation was established between ratio of standard deviation to mean and the stiffness ratio for the purpose of determining the crack initiation stress. This correlation explains the contribution of each parameter and their significance to rock deformability.

In Appendix C, ANOVA carried out here is a method of analysis that involves interacting two independent variable (Sokal and Rohlf, 1969). The variables are

(1)ratio of normal stiffness to shear stiffness) and (2) (ratio of standard deviation to mean bond strength) with a dependent variable (Peak stress). A high and low level of stiffness ratio was chosen for the ANOVA which are 2.6 and 2.2 respectively. These values were obtained from experimental data.

The parametric study carried out shows that the bond strength of the sandstone sample is between 80MPa and 140MPa and within these values, the model behaviour matched the laboratory test. By specifying standard deviation of 20MPa for bond strength of 80MPa, 120MPa and 140MPa, it turns out that 0.14, 0.16 and 0.25 respectively are ratio of standard deviation to mean bond strength used for ANOVA. The ratio controls the crack initiation in numerical modelling (Itasca, 1997).

It should be noted that this research is aimed at predicting crack initiation stress using experimental-DEM hybrid. This is because it is not clear on how to obtain this value with numerical test of similar physical laboratory test. It has been stated that the crack initiation stress is underestimated if the value is obtained from the axial stress in the physical laboratory experiment. This is because Martin (Martin, 1993) has shown that on the crack volumetric strain curve, the on-set of dilation is the crack initiation point. This is not applicable to the discrete model (Lajtai et al., 1991) because crack initiation was conceived based on a homogeneous material, while most rock are heterogeneous. This implies that crack initiation can occur severally before the peak stress is reached on a stress strain curve and both lateral and volumetric strain may curve at low stress value. Secondly at the grain boundaries, low stress fracture initiation may occur. Therefore crack initiation data is characterized by a wide range of data. This is not so far from the peak strength data.

In numerical modelling, the choice of crack initiation point is different, the crack initiation stress is identified in the simulated model by specified fraction (pk_ci_fac) of the total number of cracks (Potyondy and Cundall, 2004). At specified fraction of crack initiation stress (pk_ci_fac), a bond can break. Therefore if the predicted crack initiation stress exceeds the peak strength, then fracture is predicted. This is because beyond the peak point, the crack is initiated; post peak behaviour set in and finally the sample fractures.

7.12 Determination of crack-initiation stress: prediction of bulk strength

For the numerical test, crack initiation is controlled by the ratio of standard deviation to mean bond strength (ROSD). 54 experiments were carried out at 5MPa confined pressure test to obtain the peak axial stress at material failure. Further the data were subjected to ANOVA for the prediction of crack initiation stress from the estimated marginal means obtained from statistical variance.

7.12.1 ANOVA for estimated marginal means of crack initiation stress

Figure C1- C3 shows that crack initiation are at 40MPa, 50MPa and 57MPa, with corresponding peak fraction of 0.48, 0.56, and 0.67. The crack initiation stress is about 15% of the peak stress observed from the volumetric strain. This was achieved with stiffness ratio of 2.2 and 2.6 which are the minimum and maximum stiffness ratio respectively.

7.12.2 Between subject and factors

In Table C1 and C2, the levels of ratio of standard deviations to mean (ROSD) were used for the analysis of variance. These levels were the ratio that simulated the behaviour of the materials with the yield point at 50MPa strength. The low and high levels for ROSD are presented in the Table C1.

7.12.3 Levene test of equality or error

A suitable test for 2-way ANOVA is presented in Table A.3 as the Levene test. Thus if the null hypothesis is violated, the 2-way ANOVA is best carried out to obtain a valid model and variance analysis. The “0.0000” shows that the hypothesis is rejected. The value is less than 0.5, which rejected the null hypothesis. For this analysis, the data violate the assumption of homogeneity of variance. Therefore error variance of dependent variable is not equal across group. This explains the application of the 2-way ANOVA is good for this violation.

7.12.4 Test between subject effect

RODS is statistically significant because it is less than 5% (Table C4 and C5). The statistical significant difference is presented on dependent and independent partial

Eta square. 14.2% of Eta square of the variance of dependent variable is attributed to ROSD. Kn/Ks is not significant. Hence it contributes little or no difference to the dependent variable (peak stress).

7.12.5 Pairwise interaction

In Table C6- C10, the interaction of stiffness ratio and ratio of standard deviation to mean material strength (ROSD) are presented. Table C6 presents the intercept of 98.5% at ROSD of 14.2%. Kn/Ks is 2.8%. the product of ROSD and stiffness ratio is 3%. All all values of the adjusted R squared of 0.077. The first pairwise comparisons I (Table C8) and and second pairwise comparison II (Table C9) estimated are presented. These values are obtained for the univariate tests which yielded a p-value of 0.026 (Table C10) which is less than 0.05.

7.12.6 Estimated marginal mean of peak stress and predicted crack initiation stress.

In Table C6, at the stiffness ratio of 2.2, the ROSD, are close and the crack initiation stress obtained from the peak stress is equal. Therefore we can predict crack initiation to begin at 57MPa for the sample under 15MPa confined pressure test. In Table C11 - C15, the estimates of the stiffness ratio shows a strong statistical significance (Table C11). The pairwise comparison for the stiffness ratio I and II are presented in Tables C21 and Table C13. Table C14 –Table C16 presents the validations of the experimental significance of the relevant peak stress value. The final plots of the peak stresses are presented in Figure C1 –Figure C3 as the estimated marginal means of ROSD. These peak stress values are between 72MPa and 75MPa.

7.13 Conclusion

Overall, the studies indicate the effect of contact stiffness and bond strength on the force-displacement relationships of grain contacts in rock. Thus the evolution of both tensile and compressive behaviour of the grain contact when the samples are loaded in DEM reproduced the natural behaviour of the sandstone. The axial and lateral strain components under compression at a confined pressure of 15MPa yielding a

bond strength of 120MPa for Niger delta sandstone, strengthen the fact that the behaviour generated for simulations and experiments are similar when parameters from natural material are used in the DEM simulations as input data. For the Niger delta sandstone, the tensional curve are plots on lower force magnitude than the compression curve. These two properties are simultaneous characteristic behaviour of the grain contact during initial loading stages.

Chapter 8

Parametric Analysis on the Influence of Grain Shape on Micro-Mechanical Behaviour of Sandstone using DEM Simulations

8 PARAMETRIC ANALYSIS ON THE INFLUENCE OF GRAIN SHAPE ON MICRO-MECHANICAL BEHAVIOUR OF SANDSTONE USING DEM SIMULATIONS

8.1 Introduction

The DEM simulations reported in Chapter 6 is for particle cluster matching the average coordination number of the experimentally characterized Niger-delta sandstone. However, the present chapter critically evaluated the effects of grain shape on the mechanical properties of sandstone using DEM simulations. Here, the rheology of natural and simulated rock was examined during crack propagation under tri-axial compression. In order to study the effect of particle shape, three numerical samples were generated with different particle shapes. Brittle deformation was examined based on relative rotation and clay-resistive disposition of rigid mineral grains. The damage thresholds were determined for the purpose of detecting the specific strength characteristics of the rock. Particularly, the crack initiation threshold and the crack damage threshold were detected. The implications of these crack damage are explained. The yield criterion of peak strength versus confined pressures and the associated frictional parameters (cohesion and internal friction) were used to explain strength characteristics. For comparison purpose, experimental analysis has been provided for the description of the strength characteristics using the popular Berea sandstone where applicable.

8.1.1 Background on the method of analysis, the micromechanical strength characteristics of rock

The importance of micro-examination is due to the fact that the peak strength of some rocks are false (Eberhardt et al., 1998). This is because the mineral support would have been lost long before the applied load data can indicate the point of crushing. Therefore the crack initiation and crack damage stress are better indicators of the strength characteristics of the rock than the data generated by the applied load logger. The common indicators that are used for discussion in this present work are the crack closure stress (σ_{cc}), the crack initiation stress (σ_{ci}), the crack damage stress (σ_{cd}). The crack closure is the stress level which causes the closure of pores or pre-existing micro-cracks which are oriented at any angle to the applied load. This is the initial non-linear response observed in the axial strain. The extent of the non-linear

stretch is dependent on the pre-existing crack densities. This stage is followed by the linear elastic behaviour of the rock material on the axial strain (Eberhardt et al., 1998). Crack initiation stress is the stress sustained by the sample where micro-fracturing begins. It is the point of deviation from linearity observed on the lateral and volumetric strain. Crack propagates at stress level sustained by the material which is beyond the initiation point followed by the crack growth which may be stable, if the crack is unstable, it is indicated by the reversal point in the volumetric strain. At this point, critical energy is released and the material damages at the point called the crack damage stress (σ_{cd}) (Figure 8.1 and 8.2). However Martin (1993) and Bieniawski (1967) regarded the crack damage as the point that peaks the unstable crack propagation which occurs due to the undefined relationship between applied stress and crack length. Other occurrence in the material during crack propagation includes crack growth velocity. The unstable crack growth can also continue until a point is reached where micro- crack coalesced. This is the point where the rock loses all its mineral support.

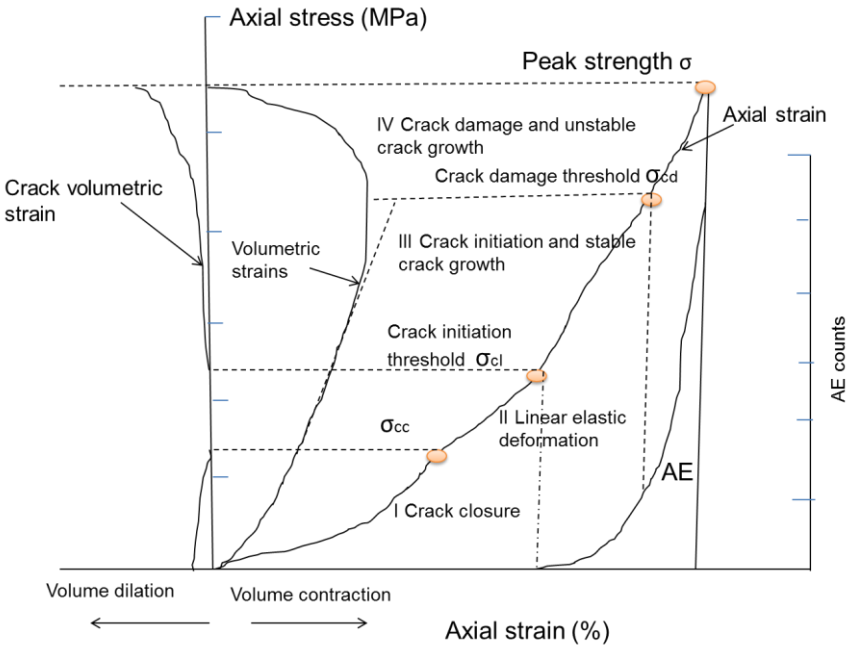

Figure 8.1 Schematic diagram of stress-strain typical curves of rocks. (Martin, and Chandler, 1994)

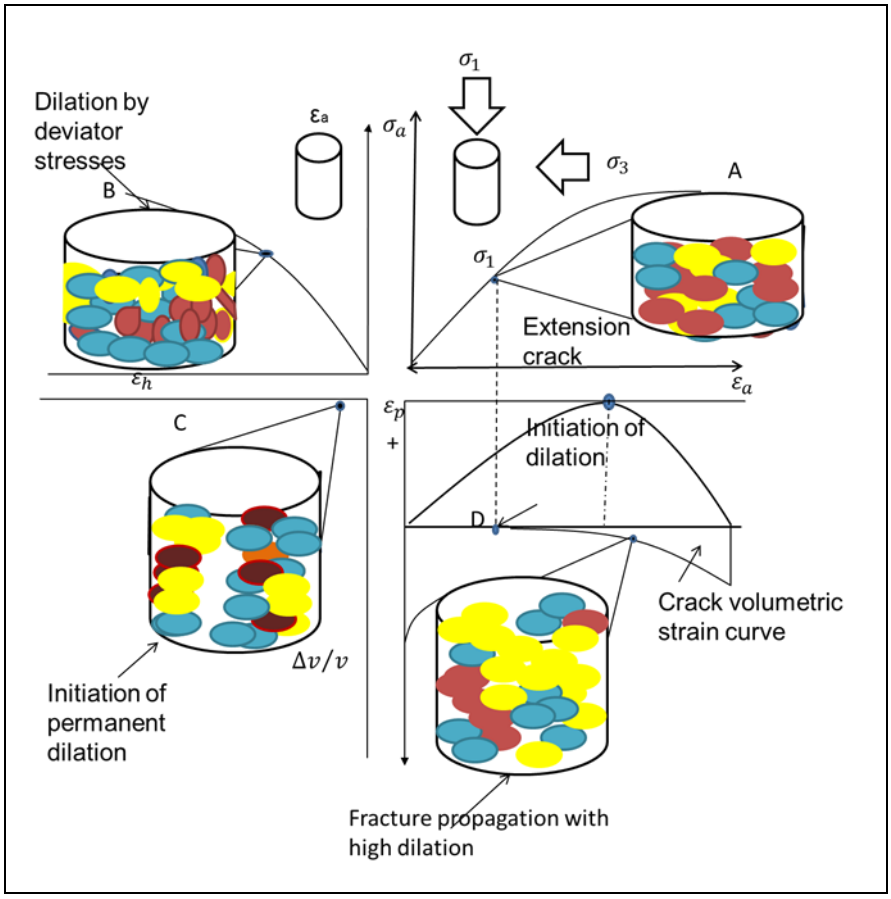

Figure 8.2 Illustration of dilation process from micro crack initiation and growth in brittle material subjected to compressive loading (Cho et al., 2007)

8.2 Influence of particle shape on crack initiations, crack damage and crack openings in dilation process

Micro-mechanical damage in the sandstone sample starts when the stress load reaches the crack initiation stresses and propagates to crack damage stresses (Figure 8.6 – 8.9). When the bond strength between the grains is stressed beyond crack closure boundary, the crack propagation is stable until when the stresses on the bond exceeds crack damage stress. Beyond the crack damage stress, dilation begins. The 3-particle clumped sample (model 3) is of more complex particle shape. This model can only support a high stress because of the high interlock in the structure but cracks were observed even at low force application. On the other hand, the appearance of crack in the highly spherical particle model is delayed because of the much inherent micro-cracks. Figure 8.6-8.9 presents the crack volumetric strains and the volumetric strains obtained for the 4 models. The Niger delta sandstone was reproduced with all parameters in the descriptive statistics but at different spherical

index of shapes. Further the crack damage point marked yellow asterisk starts at the reverse point of the volumetric strain. These values are due to the compression of particles in each sample. Next they move because the bonds are strained finally they begin to move gradually. The succeeding elastic expansion starts at the crack initiation stress. If the stress on the rock mass increases beyond the crack initiation stress threshold, then, the crack damage stress is reached and the particles fall away from their initial position where unstable crack begins to grow. During the simulations, the particles migrate from bonded positions. At the crack damage threshold, these particles lose their bond strength. This makes the cracks visible like lines (or dilation) within the particle assembly. Beyond this point of the peak strength of the rock mass, crack propagates and fractures sets in.

Diederichs et al. (2004) and Eberhardt et al. (1999) provided a description deformation of granite rock using Acoustic emission (AE), stating that point crack initiation stress is the first point where a new AE rises above background. AE point crack is the on-set of three successive crack damage stages where crack initiation stress is first determined. Also, the point where the stress volumetric strain deviates from the elastic trend is defined as the crack initiation stress. Another definition for crack initiation stress is the point where the crack volumetric strain deviates from the zero data (Martin, 1993). The crack volumetric strain is provided in the PFC text by Potyondy and Cundall (2004) in Equation 4.1 (Chapter 4).

By using the elastic properties due to the micro-mechanical damage, the micro-mechanical damage which has been explained above were similar to the findings of these authors. An additional parameter of interest that is obtainable in discrete modelling is the crack number produced. Cracks are formed when the bond connection between particles are broken due to crack damage stresses. These crack numbers are indicators of the crack damage stress. Here, the point of deviation of the crack number from zero which corresponds to the crack initiation stress will be identified. The crack number also curves inward corresponding to the crack damage stress, at this point, the crack number curves transmit into another direction and increases suddenly due to the increasing crack propagation that follows the crack initiation stage. The volumetric strain deviates from zero at the crack damage stress and the curve is seen reversing at the crack damage stress.

8.3 Damage threshold and grain shape

The shapes of mineral grains are crucial to simulate the damage thresholds of the bulk material. This is because particle shapes could affect the strength characters of geo-materials (Ting et.al., 1995; Ln, 1999). Thus the approach adopted to analyse the damage threshold of Niger delta sandstone involve representation of the grain content with different shapes of clumps. Matching spheres particles together makes a clump. The higher the spherical index of the clump, the rougher the surface of the rock (Ghazvinian and Diederichs, 2010). Here, the effect of grain shape is studied by clumping of particles in PFC. This morphological property can significantly influence the frictional property of rock (Guo and Morgan, 2004). Here, the stiffness parameters are constant while clumps are created to check possible shape effects of the grain of Niger delta sandstone. The test procedure is provided in Figure 8.3. Each clump created is used to build a model sample. The sample was subjected to tri-axial test and the micro-crack number was recorded following the procedure in the standard tri-axial test provided by PFC (Itasca, 2004). The plot of the crack number versus strain is used to show damage indicators. Table 8.1 shows the micro-parameters used to build each model sample. These parameters are peculiar to Niger delta sandstone as discussed in Chapters 5 and 6. In both DEM and experiments for the tri-axial test, confining pressure of 15MPa was applied in this study.

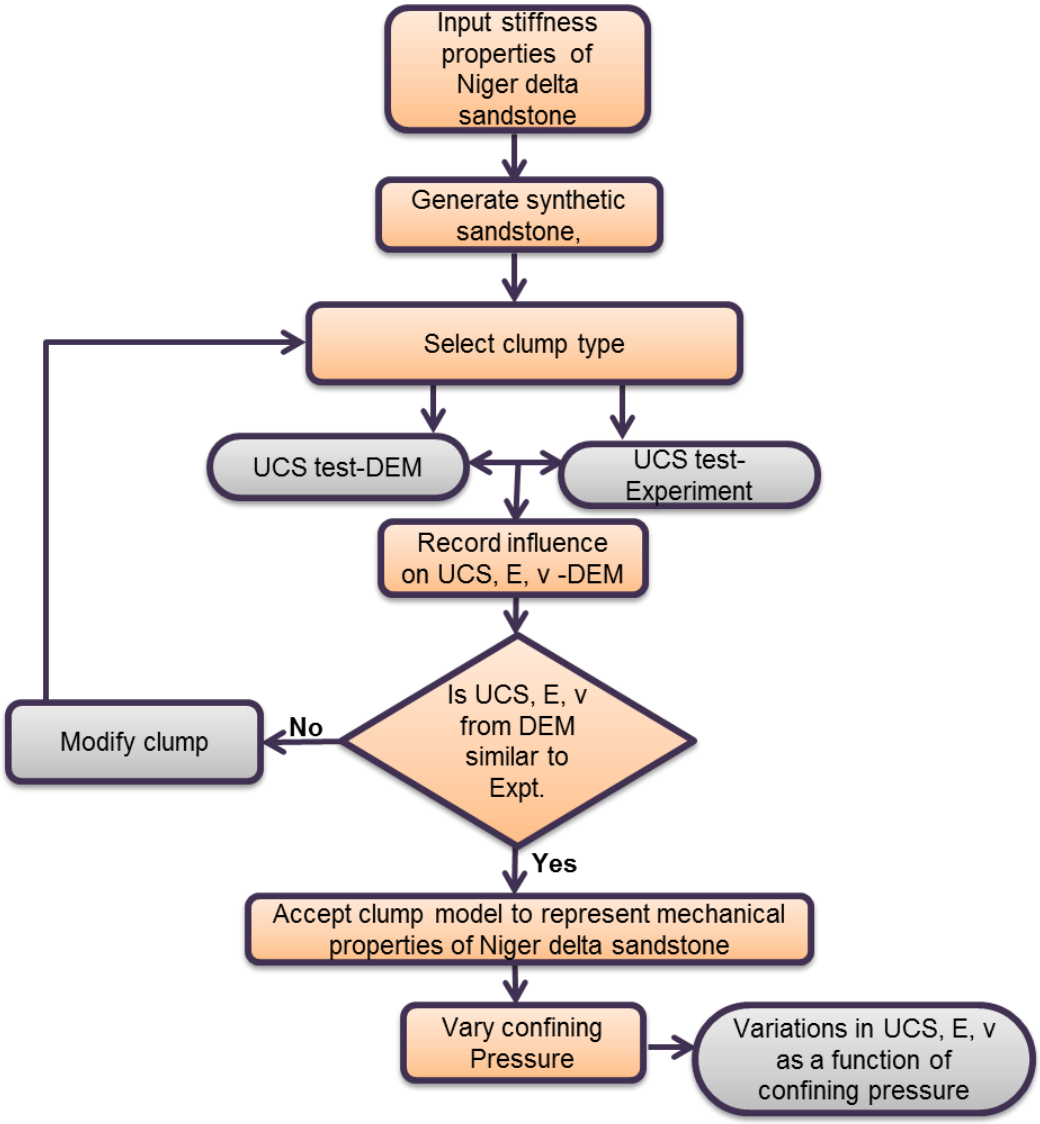

Figure 8.3 Block flow of the study: Influence of petrography on strength characteristics

Table 8.1 Descriptive statistics of grain contact parameter for the Niger delta sandstone

Parameter, unit	Quantity
Bond normal strength, mean (MPa)	**120**
Bond normal strength, std. dev (MPa)	20
Bond shear strength, mean (MPa)	120
Bond shear strength, std. dev (MPa)	20
Grain contact stiffness ratio, kn/ks	2.5
Grain contact Young's modulus (GPa)	18.6
Bulk density kg/m^3	2120
Grain density kg/m^3	2135
Grain radius ratio, Rmax/Rmin	1.66
Friction coefficient	0.6

8.3.1 Effect of grain shape on the micro-mechanical behaviour of Niger delta sandstone

In order to study the micro-mechanical behaviour of Niger delta sandstone, the influence of grain shape on the mechanical strength of simulated samples were examined. Four models of sandstone were generated with four different particle shapes. Model 1, model 2, Model 3 and model 4 were built with 2-clump particle shape, mixed shape and 3-clump particle shape respectively (Figure 8.4). Tri-axial test were performed numerically on each model and uniaxial confining strength, cohesion, and friction angle, φ were estimated for each model. These results were compared to the physical sandstone (Figure 8.5).

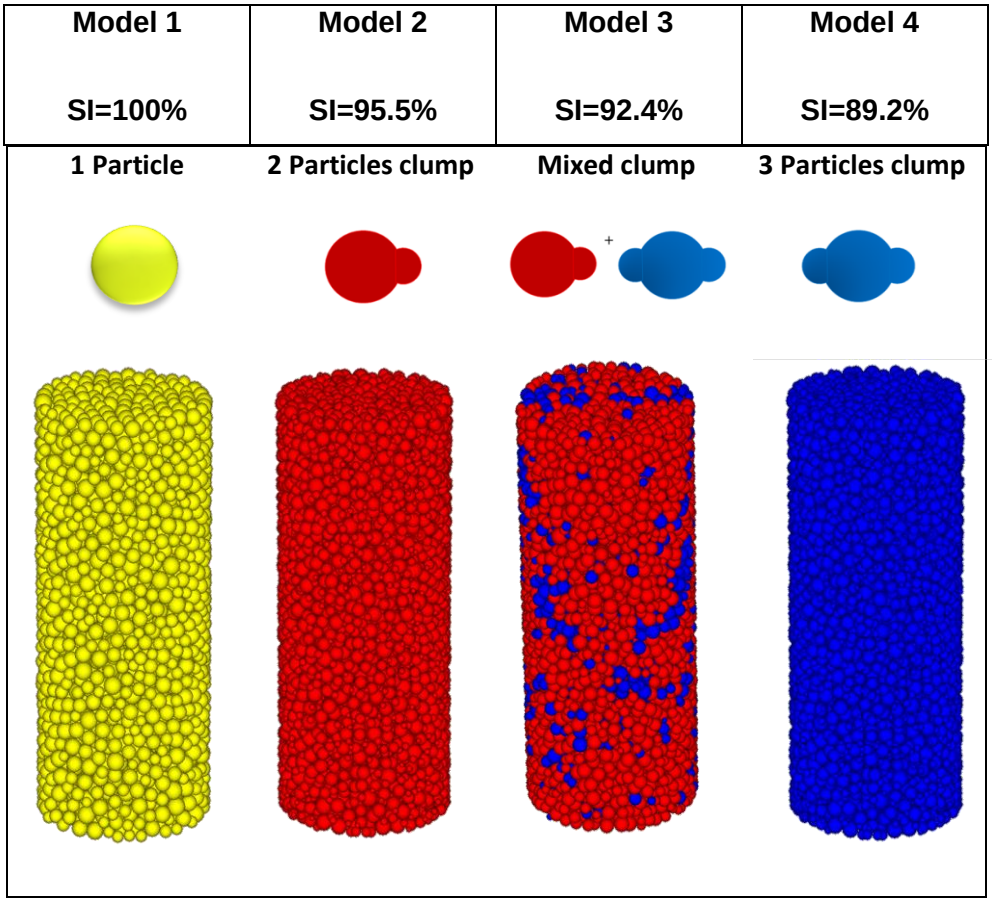

Figure 8.4 Physical sample and simulated sample models 1- 4 were built with 1 particle, 2 particles clump, mixed clump particles and 3-clump particles having spherical index (SI) of 100%, 95.9%,89.2%, and 92.4% respectively.

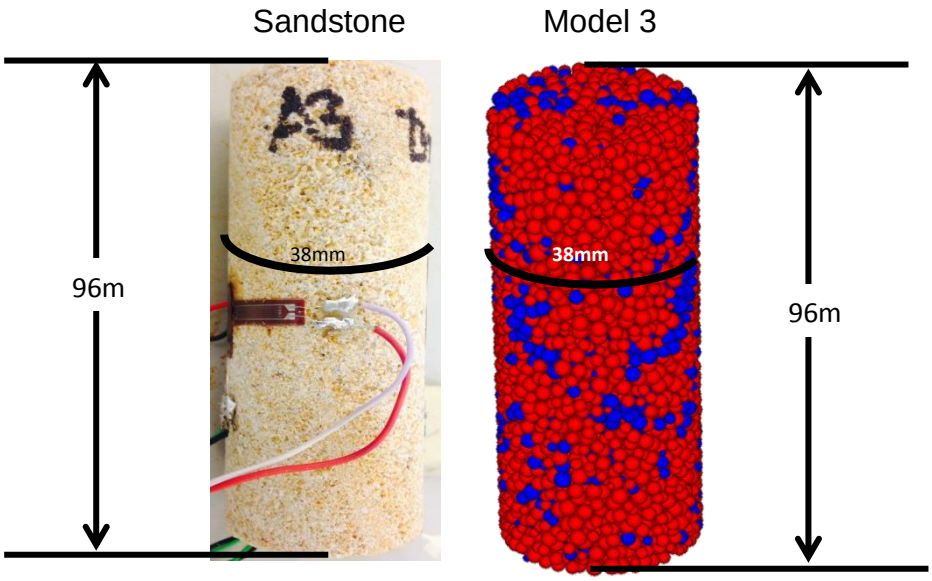

Figure 8.5 Natural sample and Model sample having same dimension

During the simulations, it was observed that under tri-axial compression, crack in orthogonal direction to compression closes under confined pressure. The micro-mechanical responses of the physical samples are provided in Figures 8.1-8.2. The crack number generated due to breakage in grain to grain contact was used to indicate the points of micro-mechanical damage which includes the crack closure stress (σcc), crack initiation stress (σci), the region of stable crack growth and crack damage stress (σcd).

This simulation was carried out at 15MPa confined pressure in DEM. The major features of micro-mechanical damage are provided in Figure 8.6-8.9. By model generated for the study is presented in 3, Figure 8.4 and Figure 8.5. The physical sample test also confirms the major points of micro-damage as presented in Chapter 4. By comparing these three models, with the characteristic data in Chapter 4, the mixed clump model represents well the natural sandstone (Figure 8.5). This could be due to the irregular grain characteristics of the quartzite mineral that provides the mineral support. It could also be due to the different grain size distributions in the mineral composition of the sandstone. However further parameters were analysed to verify the usefulness of the mixed clump model below.

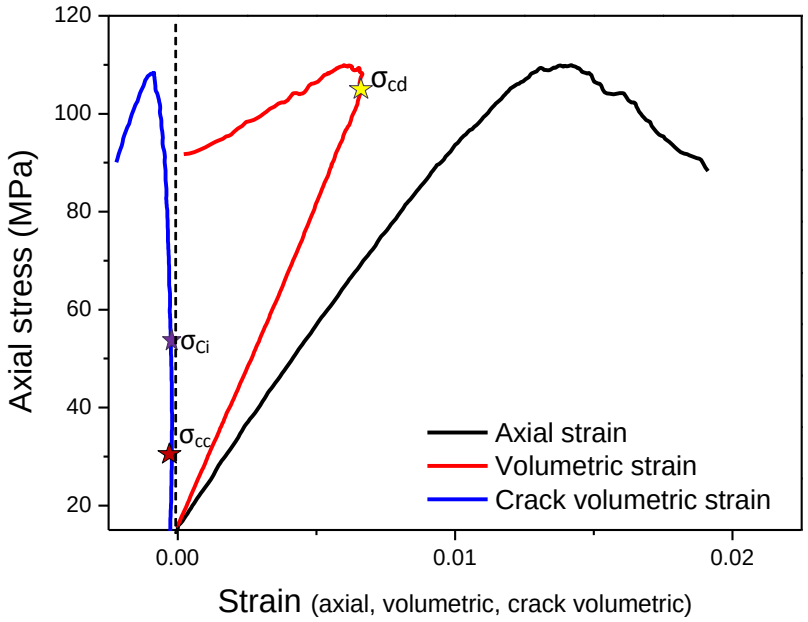

Figure 8.6 The crack initiation stress and crack damage stress of model 1 sample

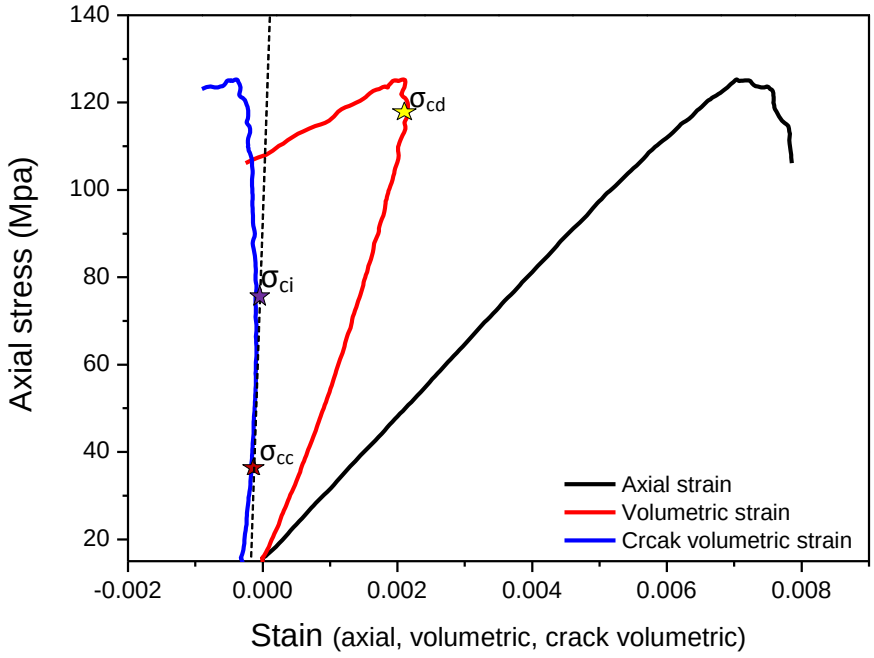

Figure 8.7 The crack initiation stress and crack damage stress of model 2 sample

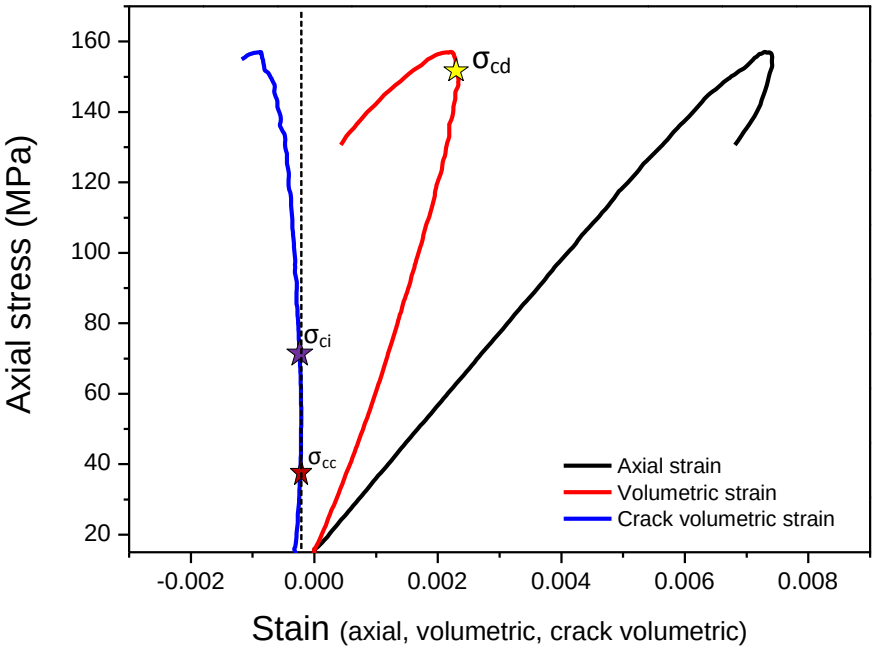

Figure 8.8 The crack initiation stress and crack damage stress of model 3 sample

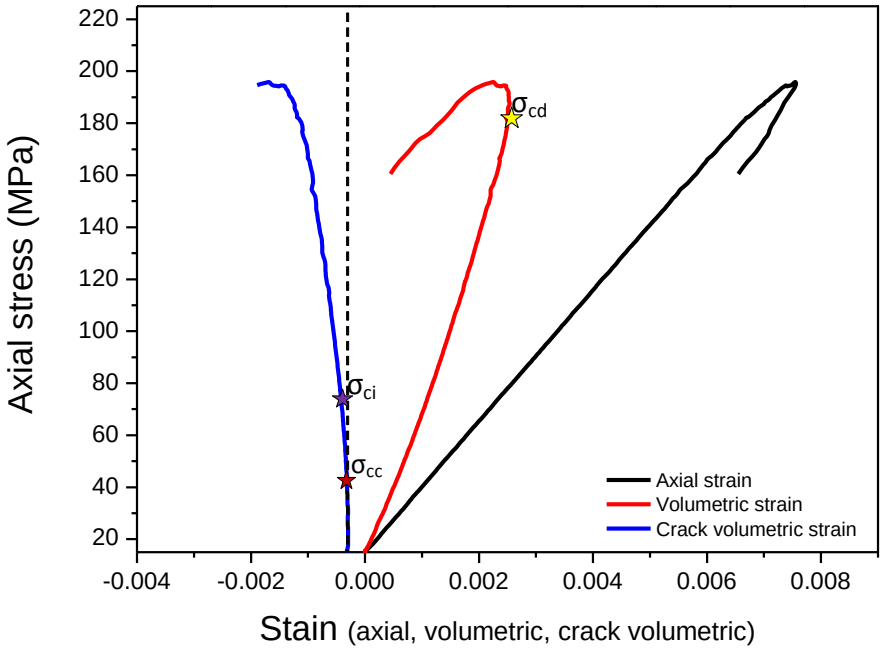

Figure 8.9 The crack initiation stress and crack damage stress of model 4 sample

8.3.2 Effect of grain shape on micro-mechanical characteristics of Niger delta sandstone

Figure 8.6 - 8.9, show that model built with high spherical index property exhibit low micro-mechanical strength the 100% spherical index properties indicated a crack initiation stress level of 50MPa with a corresponding damage stress level of 102MPa. these values are lower than the observed in the representative mixed model which have 68MPa and 158MPa as the initial and damage stress levels respectively. This means, the closer the shape is to a perfect sphere, the lower the bulk strength. The crack initiation stress is a microscopic response to stress which is at 60MPa for model 2 (Figure 8.7). The result show a similar trend to the simulation on quartz sandstone from Luojia Mountain (Rong et al., 2013). The size and shape of the particle are related in that the more spherical grain behave like large sized grain and strength decreases as grain size increases (Plumb et al., 1992). Hence grains with high spherical index value make the grain matrix to possess larger Griffith flaw at grain contacts which makes them weak under compression. The crack initiation of model - 4 with lower spherical index is at a stress level of 80MPa which is higher than the

observed 40MPa (in model 1) and 60MPa (in model 2). These models 1 and 2 are of higher spherical index compared to model 4.

The yield points for 2-particle clump model and 3-particle clump models are 119MPa and 193MPa respectively (Figure 8.7 and 8.9). The yield characteristics are even reflected in cohesion property held between the grains. This is because the reversal point of the volumetric strain for the 2-particle clumps drops sharply compared to the 3-particle clump. This indicates that the cohesive properties in the 3-particle clump are held stronger than the cohesive property of the 2-particle clump. Thus larger numbers of grain contact are found in rocks with complex shaped grain of low spherical index. The volumetric strain curve reflects brittle crack in the sharp drop of the curve identified with the yellow asterisk in Figures 8.6-8.9. This phenomenon was explained by Eberhardt et al. (1998).

8.4 Bulk porosity change on numerical models

Models 1 to 4 were built by specifying the same initial state of porosity for the numerical samples. This procedure was done by incorporating the bulk density (2120kg/m^3) and grain densities (2135kg/m^3) in the script. A significant difference in the porosity changes were observed in models 1 to 4 (Figure 8.6 to 8.9). The values of the crack damage stress are indicators of these observed differences. By utilizing the spherical index (SI) 1.0000, 0.9555, 0.9240 and 0.8920 for models 1 - 4 respectively, the observed C_{cd} stresses were 50MPa, 120MPa, 150MPa and 190MPa when each sample was subjected to tri-axial compression under 15MPa confined pressure. The significant differences in the damages stress data are caused by the different particle shapes which takes up some new coordination number during compression. The coordination number is porosity determinates. The porosity of every sample is not uniform at every point in the packed sample. Thus an obvious difficulty encountered during the simulated compression test is that the macroscopic response of each model are not the same when different particle shapes and same porosity are specified for generated rock model. The mixed model is in agreement with the damage stress (146MPa) for the experimental model. This observation can be supported by the theoretical analysis of the non-uniform porosity distribution in DEM model samples identified by Jing and Stephansson (2007). Therefore an initial

state of model porosity does not imply a uniform distribution of porosity throughout the generated model sample. In addition, the change in porosity is particularly defined by the particle shape of discrete member (Figure 8.6 to 8.9). This is because porosity changes are directly affected by the changes in coordination number. As the compression test progresses new contact are formed between contacting particles. The output data of the progressive compression is the porosity change characteristic responses which are stored as volumetric strain based on relative interaction of new particle contacts formed at every stage of compression. Thus in order to obtain the characteristics behaviour of natural rock, the right choice of particle shape is essential. A mixed clump was appropriate for Niger delta sandstone (Figure 7.8 and Figure 4.12a).

The cohesion and the internal frictional coefficient were calculated at some confined pressures of 5MPa to 20MPa (Figure 7.11). The mixed-clumped particle model was found to have exhibited a similar cohesive property and internal frictional characteristic behaviour similar to the natural sample. The reason for the adequate match in the natural and simulated rock sample can be attributed to the mixed clump particle packing technique which produced a bonded discrete assembly exhibiting porosity change characteristics similar to the natural sample. One single porosity value cannot provide the porosity of the sample model. This is because the porosity computation depends on the coordination number within the measurement sphere (Itasca, 2004). It turns out that, the addition of the experimental stiffness component to the contact model is a positive contribution to the model development.

8.4.1 Particle packing technique for mixed-clump model sample

In Chapter 3, the detail of the procedures adopted to generate the four model samples is provided. It is important to note that the contact stiffness (normal and shear) were obtained experimentally before the simulation was carried out. The value of the experimental stiffness was used to redefine the contact model. The PFC code, which uses the constructive method of particle insertion, was activated. During the development of the model, packing density was specified by scaling the clump sizes until the mixture reproducing the natural rock was obtained. Location of the measurement sphere were examined points where porosities were measured and stored. And one single porosity value cannot describe the sample porosity because

of the particle overlap and the limitation of the measurement sphere to a single location per calculation time in PFC (Itasca, 2000). The behaviour of the discrete assembly was simulated by associating the default linear contact with the value of the normal stiffness of 6MN/m and a shear stiffness of 2.4MN/n as a component which initiated a stiffness ratio of 2.5. This contact stiffness relates the contact force and relative displacement in the normal and shear directions using Equations 3.12 (Chapter 3) repeatedly.

The slip behaviour was defined by 0.66 frictional coefficient obtained experimentally. Contact model with each contact. The inclusion of a parallel bond and a dashpot to the contact model was implemented so that the entirety defines the contact force displacement behaviour of the natural rock. The input value a stiffness ratio of 2.5 was fixed because the parameter was validated experimentally using ultrasound measurements and the PSAT technique.

In the past the differences in the cohesion and frictional angle of the natural and simulated sample has been a challenge in DEM (Cho et al., 2007). The inclusion of the experimentally determined bulk and grain densities to the discrete assembly was a major step to combat the common discrepancies between cohesion and frictional angle of natural and simulated rock. Here, the application of this model script could resolve this problem because natural rock was simulated via clump modifications which enhance similar cohesion and frictional angle of simulated rock compared with the natural rock. In addition, a respective micro mechanical damage data are provided for supporting this approach.

8.5 Implementation of particle to particle cementation

All contacts were assigned the linear model which depended on the properties of all contacting entities. The experimental linear model were included to enabled the contact-bond to influence contact behaves as the natural sample. Parallel-bond behaviour was implemented by including a parallel-bond component to each contact. This component acts in parallel with the linear model at all contacts their properties modifies the contact behaviour due to specification of the contact stiffness. Thus corresponding stiffness properties modification was distributed throughout the

assembly for all components in the model. The wall command was used to set wall. The command changes and initialized. Clumped properties were set with the clump property command. The implementation of contact stiffness from experiments into the contact components between particle-particle contacts was enabled. Next the systematic particle packing technique has enhanced the simulation of the natural rock. Generally, micro-properties are defined in the development of DEM model (Boutt and McPherson, 2002). These properties are iterated until the model reproduces the natural. The problem encountered by this method is that the internal frictional coefficient exhibited by the numerical sample are usually too low compared to the natural sample (Thornton, 2000).

8.6 Young modulus and Poisson's ratio from micro-mechanical behaviour

Lower magnitude of elastic modulus (21.8GPa) was observed for the model developed with 2-particle clump compared to the elastic modulus data (25.6GPa) obtained for mixed-shape models (Figure 8.10).

Higher Poisson's ratio (0.33 and 0.29 was observed in models 1 and 2,) was observed for the particle with 100% spherical index and the 95%, (2-particle clump shape) compared to the Poisson's ratio (0.28) of the mixed-shape model and 0.27 of the 3-particle clump model. It was observed that these values were approximately equal to the nearest 0.1% in variations. Therefore, it is envisaged that the particle shape and bond held in cementations strength collapse towards the lateral direction which was not affected by the void space in the particle assembly. This may be due to the same confining pressures to which each samples are subjected too. That is the applied lateral stress is the same for all experiments.

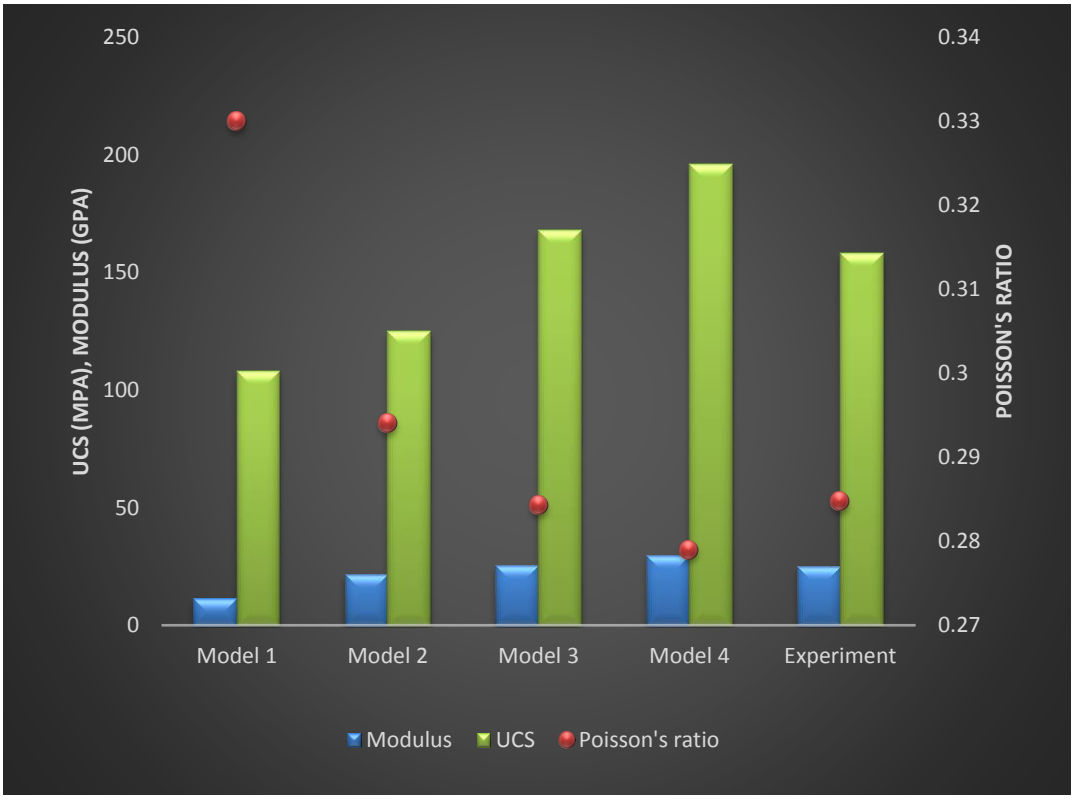

Figure 8.10 Elastic modulus and Poisson's ratio for Niger-delta sandstone and simulated models

8.7 Influence of internal frictional angle and cohesion on strength characteristics

By using the plots of peak stress versus confined pressure, the linear equations plotted in Figure 8.11 were obtained. The tri-axial test method has been adopted for micro-mechanical analysis by some authors e.g. (Singh and Rao, 2005) for the determination of internal frictional angle and cohesion. The results of the tri-axial test on three models were compared with the applied experimental data. Both relationships were related to the equation of the curve in Figure 8.11. The gradient was defined as "a" in Equation 8.1 which was used for the evaluation of frictional coefficient. In Equation 8.2 "b" is the intercept used for the evaluation of cohesion (Rong et al., 2013; Singh and Rao, 2005) in the vertical axis presented in Figure 8.11

$$\phi = arcsin\left(\frac{a-1}{a+1}\right) \tag{8.1}$$

$$c = \frac{b(1-sin\phi)}{2cos\phi} \quad (8.2)$$

Where “a” is the gradient of the curve and b is the intercept (Figure 8.11), ϕ is frictional coefficient and c is the cohesion.

Although a linear relationship exist between peak strength and confined pressure in all models, the mixed clumped particle model exhibit similar peak strength like the physical sample as shown in Figure 8.11. In Figure 8.12, this compliance of mixed shape model with the physical sandstone sample is reflected in the close value of the cohesion and internal frictional angle observed for both mixed shape model and the real sandstone sample in Figure 8.12 when the confining pressures were observed at 5MPa, 10MPa, 15MPa and 20MPa the sample behaviour was consistent for with the mixed particle model.

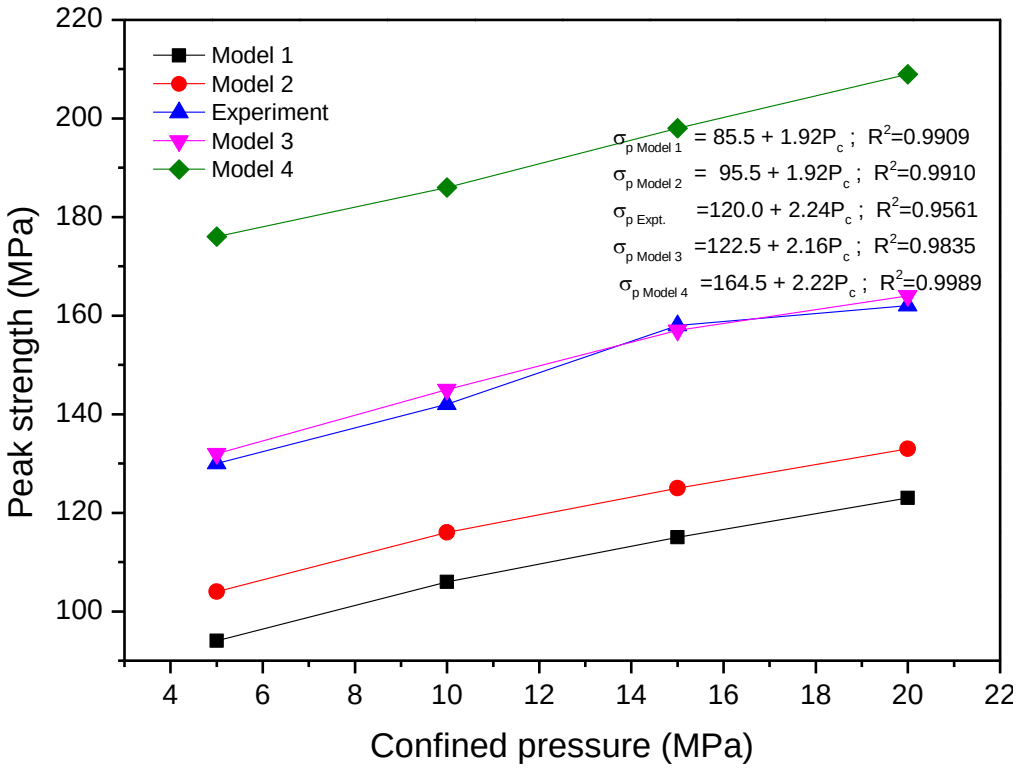

Figure 8.11 Confining pressures versus peak axial stresses at 5MPa, 10Mpa, 15MPa and 20MPa for experiments with Niger-delta sandstone and simulated models 1-4.

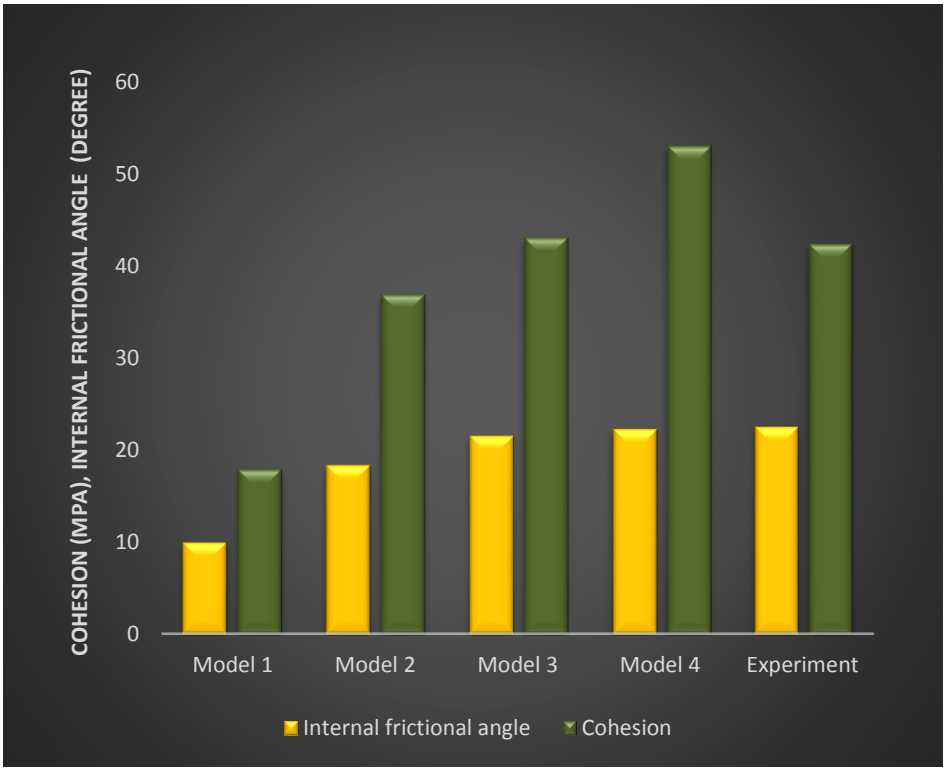

Figure 8.12 Internal frictional angle and cohesion for experiments with Niger-delta sandstone and simulated models 1-4.

From the tri-axial test carried out on 2 - particle clump model (sample 1) a low value of internal frictional angle and cohesion was observed. Also the results shows that the internal friction and cohesion was too high to reproduce the micro-mechanical behaviour of the Niger-delta sandstone. Therefore, the mixed shape model was appropriate to reproduce the frictional effect for the Niger-delta sandstone. A similar observation was found when sandstone was simulated by (Singh and Rao, 2005; Hajiabdolmajid, 2002). Rong et al. (2013) discovered variations in internal friction coefficient with shape for rock simulations using discrete models. The values of frictional coefficient provided in these work shows that there exist larger void space between the particles in models of high spherical index. Hence it reduces frictional opposition as compared to small void space in complex particle shape of low spherical index. The complex grained sandstone model are consolidated and well packed (Garcia et al., 2009) In Figure 4.12 Chapter 4, the crack volumetric strain is the point of deviation from zero which marks the stress initiation point at 68MPa for the Niger-delta sandstone. Figure 8.13 is a collection of the crack initiation and crack damages stress data for the three models and the real sandstone sample. The physical sandstone data are closer to the mixed shape model.

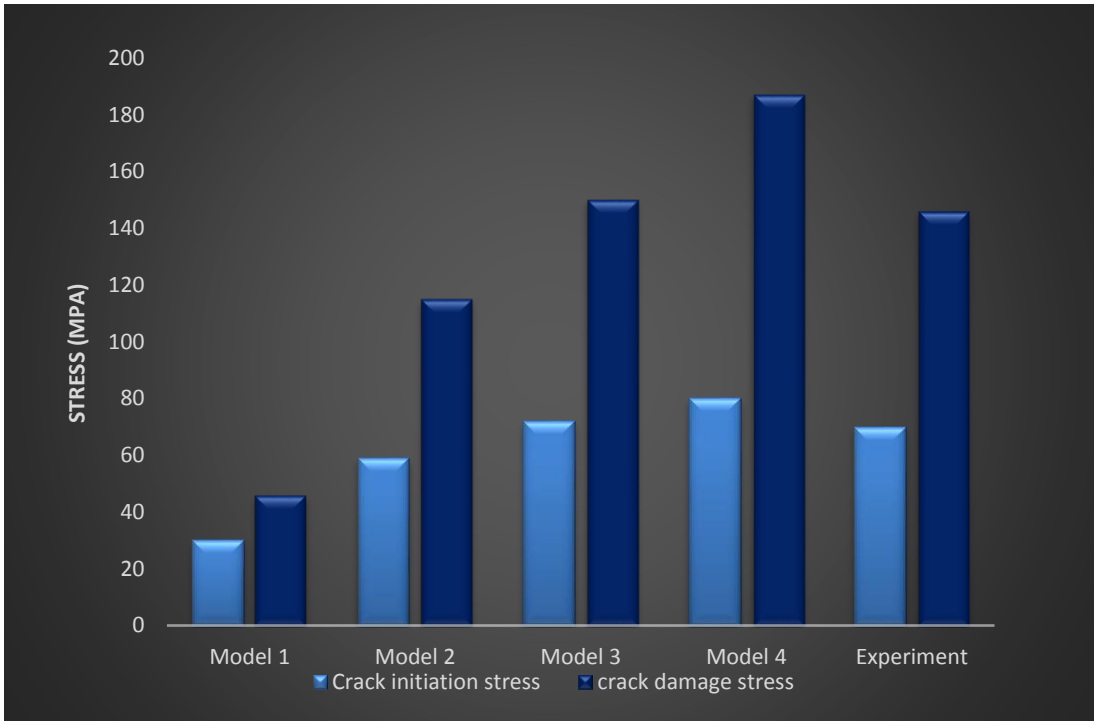

Figure 8.13 Crack initiation stress and crack damage stress for Niger-delta sandstone and simulated models

The 4 models show that the crack initiation and crack damage stresses are due to the particle compaction making up the sandstone. Apparently an inverse relationship holds for spherical index of constituent particle and stresses. Therefore the particle shapes are influential to rock deformation.

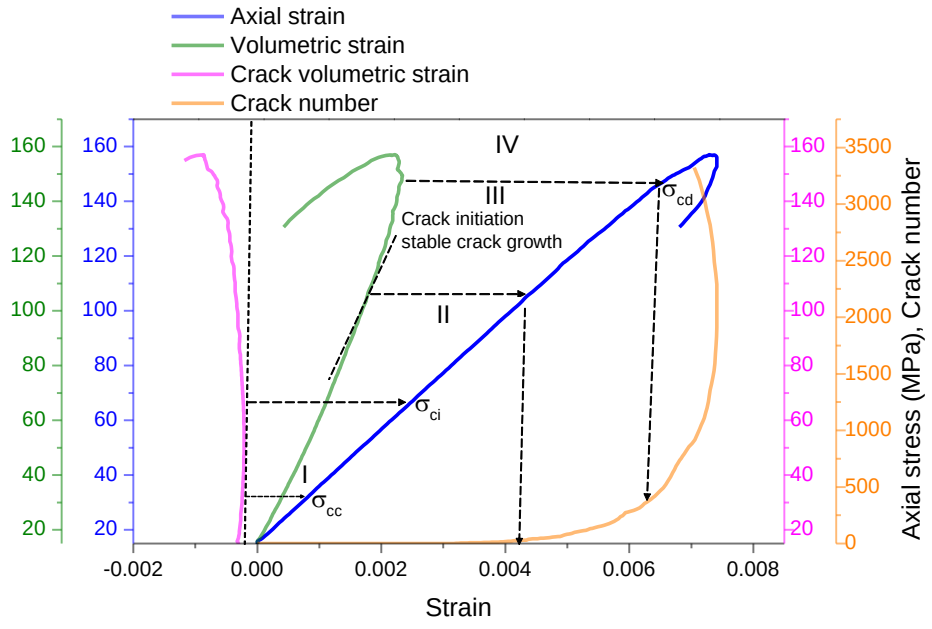

Figure 8.14 Simulated result for the stress-strain curves of Niger delta sandstone under tri-axial test at a confined pressure of 15MPa

Figure 8.14 shows the crack initiation stresses and crack damage stresses for the mixed clump particle using corresponding DEM simulations. This plots included the crack number characteristics curve showing the damage indicators. A schematic graph is provided in Figure 8.1. In Figure 8.14, the crack on sample surface is observed at 100PMa, 120MPa, 140MPa and 160MPa respectively. The corresponding images are presented in Figure 8.15 which presents the surface damaged images for 4 stages of axial stresses characterising the behaviour of the Niger delta sandstone.

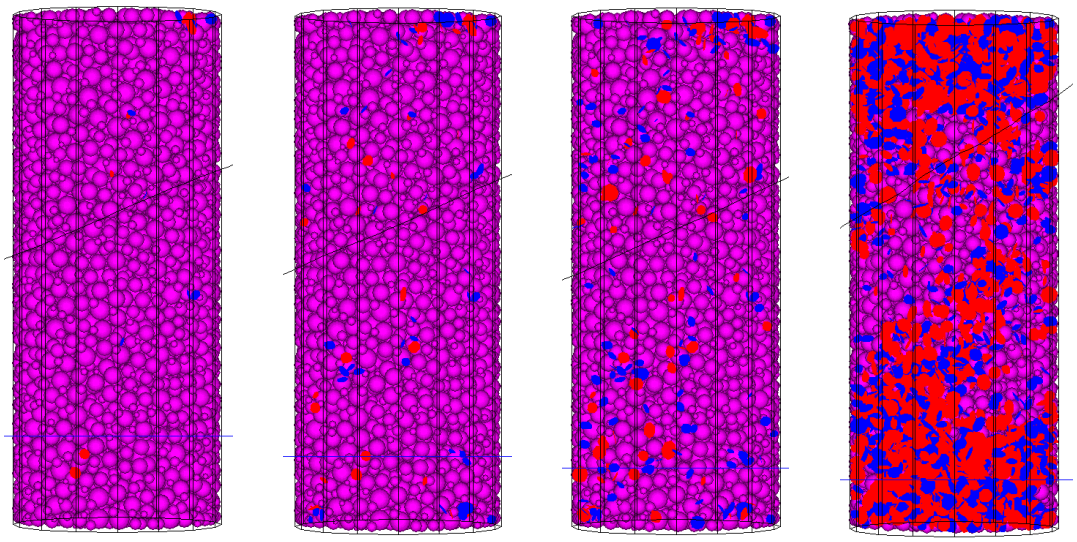

Figure 8.15 First crack and gradual crack accumulation at axial stresses at 100PMa, 120MPa, 140MPa and 160MPa done at 15MPa confined pressure. The damaged bond size is an average grain size indicated as red spots.

8.8 Corporative analysis and validation of bulk strength of Niger delta sandstone

Table 8.2 and 8.3 presents the crack initiation and the crack damage stresses of Niger delta sandstone and also compared with Berea sandstone results reported in existing literature and some evaluations from the present research. The micro-properties used in Chapters 5 and 6 are validated by these mechanical properties. In Table 8.3 further validation of micro-measurement data was done with the data of cohesion. The cohesive descriptions of the grains that constitute the rock are

compared with the standard measurement of Berea sandstone (Evans, 1012). From the above results, it can be observed that the elastic parameters are descriptive properties which show that Niger delta sandstone and Berea samples are composed of similar material Chapter 4 shows the mineralogical properties. This is not surprising because the two sandstones (Niger delta sandstone and Berea sandstone) are petroleum source rocks. The rock formations are thought to be of similar digenesis.

Table 8.2 Crack initiation and crack damaged of sandstone

Sample	E (GPa)	V	P (Kg/m^3)	Φ	σCI (MPa)	σCD (MPa)	Ref
Berea Sandstone	19.3 – 27.5	0.17-0.34	2100	0.19	41-58	71.3-74	Weinberger, et al., 1995
Berea Sandstone	20.2	0.27	2100	0.20	-	-	Busetti, and Reches, 2012
Berea Sandstone	18.5	0.4	2150	0.19	41	62-71.3	Eberhardt, 1998,
Berea Sandstone	20.6	0.32	2100	0.20	48	65	This research
Niger-Delta Sandstone	20.6	0.32	2125	0.22	50	70	This research

Table 8.3 Mechanical properties of sandstone

Macro properties	Niger delta sandstone (this research)	Berea sandstone (this research)	Berea sandstone (Evans, 2012)
Modulus (GPa)	20.7	20.6	27.58
Poisson's ratio	0.29	0.32	0.33
Cohesion (MPa)	18	14	13.04
Internal frictional angle (º)	28 º	42 º	38.14º

8.8.1 Experimental validations of micro-mechanical behaviour of Niger-delta sandstone using volumetric stiffness

The volumetric stiffness is rarely reported in the literature in this type of analysis, but it has been defined by Eberhardt (1998) as the ratio of volumetric strain data to the corresponding axial stress data. In other words, the slope of every two successive point in the curve presented in Figure 4.12a for Niger delta sandstone is obtained at different intervals which are their volumetric stiffness at the successive points and presented in Figure 8.16 under a confining pressure of 15MPa. Micro contact stiffness is generated when the grain overlap due to axial loading hence volumetric strain measures the porosity change in the grains and produce strain due to the pore collapse between grains in contact. In this, the material exhibit micro-cracks which are indicated by the sharp drop in the volumetric stiffness value. They reveal Figure 8.16 the micro-mechanical damage points. These values are plotted in Figure 8.16 which presents microscopic progression of micro-cracks, the crack multiplies and increases to show σ_{ci} (at 78MPa), σ_{cd} (at 86MPa) and σ_{ucs} (at 160MPa) stresses. These values correspond to the simulated data obtained in Figure 8.8 for the mixed clump model used to develop the Niger delta sandstone. Observe that the stress strain curve during the initial stages of force application reflects linear changes. These are the pore collapse or granular compaction state. Volumetric strain are derived from the axial and lateral strain therefore, the volumetric stiffness indicates that both axial and lateral stiffness are measured up to 48MPa this value is indicative of the crack number plotted in Figure 8.10. Therefore, the crack closure of Niger delta sandstone examined in this research is about 30% of the compressive strength. This implies that the increase in any velocity measurement during crack closure at the grain boundary starts at about 48MPa for the sandstone. Therefore, axial stress must be maintained at this value to prevent fracture. If on the other hand, the axial stress exceeds the 30% of the compressive stresses, lost circulation pills should be injected to prevent micro-crack formations. Under 15MPa confined pressure in a tri-axial test, the systematic crack growth peaks at a stress of 160MPa in Figure 8.13 while the damage was initiated at 98Mpa.

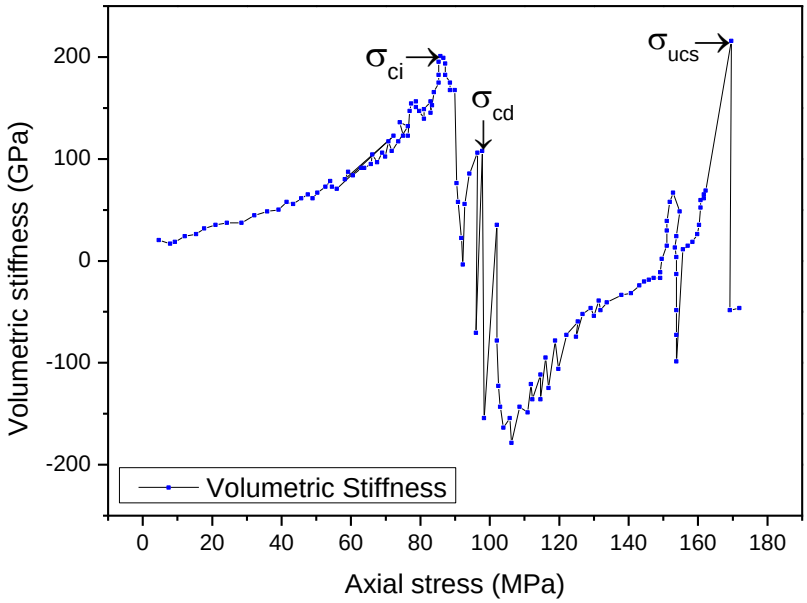

Figure 8.16 Volumetric stiffness vs axial stress

8.9 Conclusion

An extensive level of Dem simulations for the shape effects reveals its influence on the mechanical properties of sandstone. The mixed particle clumped model which is the model 3 type shape descriptor in agreement with experimental result is appropriate to model the micro-mechanical behaviour of the Niger delta sandstone.

The onset of micro fracturing is the crack initiation stress this was identified by deviation from linear strain response. Dilation begins at the crack damage stress, the rock volumes begin to increase was also pointed out by (Palchik and Hatzor, 2004). Next is the reversal point of total volumetric strain where the unstable crack begins its propagation. This point is still lower than the UCS. It was found that the crack damage stress of Niger delta sandstone is about 60% of the compressive strength under 15MPa confining pressure. Therefore, if it is difficult to distinguish the reversal point, the crack damage stress equals the compressive stress of the sandstone. (Hatzor and Palchik, 1997).

Chapter 9

Conclusion and Recommendation for Future Work

9 CONCLUSIONS AND RECOMMENDATION FOR FUTURE WORK

9.1 Conclusions

This work investigated the strength characteristics of Niger Delta sandstone using Photo Stress Tomography Technique (PSAT) for the first time, ultrasound measurement technique and Discrete Element Modelling (DEM). The urgency to determine the bulk strength characteristics of the source rock in relation to grain-scale properties has been the motivation of this research. This is because the friable nature of the rock constitutes a huge financial loss to the drilling industry. Current industrial approaches to fracture prevention in drilling source rock involve the use of "loss-circulation" pills which are used after the rock has fractured. It is an "after-loss" response which forms the motivation to carry out microscopic detection of the onset of fractures. Here, the statistical description of the grain contact stiffness and bond strength was utilized to simulate rock behaviour. Subsequently the micro-mechanical damage threshold were determined experimentally and numerically simulated to identify the onset of fractures in the rock. Furthermore, the direct relationships between petro-graphical properties and the micro-mechanical strength characteristics were established in this study. The findings are in line with the bulk strength dependence on grain aspect ratio (Yang et al., 2014; Hsieh et al., 2008; Azevedo and May, 2002). The key conclusions are summarised below:

(1) The Niger delta sandstone can be described as a sedimentary rock composed of mineral (quartz, feldspar, mica and clay) grains and particles (Table 4.1) bonded together by a combined contribution of inter-granular forces and cementation that creates locked-in stresses in the geo-material (Figure 4.12). Thus the composition of Niger delta sandstone is typical for a petroleum source rock when compared to the mineralogy of sandstone estimated by Guéguen and Palciauskas (1994). The strength characteristics of Niger delta sandstone are dependent on its inherent petrographic properties. Quartz content, mica and other stable mineral like feldspar provide the structural support. These minerals constitute the elemental forming content (plagioclase) and the extent of cementation. The shape of the mineral grains is responsible for the characteristic porosity which determines the characteristic strength and the microscopic-mechanical damage (Figure 4.12).

The anisotropy of the sandstone at grain-level is measured using PSAT methodology in terms of its stiffness ratio as 2.5. This agrees favorably with independent ultrasound-based measurements. The obtained average normal stiffness is 5.7MN/m and average shear stiffness is 2.3MN/m for the Niger-delta sandstone. However, the PSAT enables to evaluate these at point-scale (/grain scale) and such an outcome is entirely novel in this research. For statistical accuracy, the experiments were repeated for 54 Niger delta sandstone samples and the above outcomes were analyzed consistently. This implies that contact points exhibit anisotropy in the aggregates of quartz (Table 5.1). This observation is similar to the findings of Tilmann and Bennett (1973); Waterman and Teutonico (1957); Thill et al., (1969)

(3) Using the above stated experimental measures as input into DEM modelling as grain-scale material parameters, the bulk mechanical properties have been simulated using DEM modelling. The numerical simulation of the rock behaviour included the addition of the contact parameter between particles. The contact is based on a linear model carrying the corresponding experimental stiffness data of the Niger delta sandstone. Discrete model of Niger delta sandstone is based on the assumptions that finite size of cement binds the grains at their contact. The bulk strength characteristics evaluated from the DEM modelling agreed well with bulk experiments under uni-axial and tri-axial compression loading conditions. This supports the multi-scale approach employed in this research where grain-scale parameters link with the bulk strength characteristics using the combined experimental-numerical hybrid approach.

(4) DEM simulations were used to evaluate the influence of grain-scale properties on the fracture characteristics of the Niger sandstone. The damage threshold of the simulated model agrees with that of the natural sandstone characterised in Chapter 4. Thus the assumption in the DEM that the inter-grains with the bond strength of the cement approximates the geometry of the simulation sample is further confirmed because the elastic properties of the rock did not violate characteristic properties of similar reservoir sandstones viz., Berea and Doddington sandstones (Chapter 4) (Evan, 2012). Therefore, the realistic constitutive contact law driving the behaviour of grain within the

simulation assembly is significant and adequate to represent the Niger delta sandstone.

(5) The strength characteristics of the Niger delta sandstone has been presented by the damage indicators (Eberhardt et al., 1998) for micro-mechanical properties because these indicators predict the macroscopic damage. At about 30% of the compressive strength of Niger delta sandstone, crack closure stress reaches its critical state and micro-cracks began to form (this is the crack initiation stress).

9.2 Contributions to experimental survey (Chapter 2)

The capabilities of the study of strain in rock using photo elasticity has been available since 1966 (Pincus, 1966). But the technique has been underutilized in this regard and has not been adopted for point-based stress analysis. This current survey has established progressive principles for obtaining both normal and shear stress at a point location. Thus, while tracing the capability of the photo stress analysis (PSAT) with the principle of fracture initiation and stress concentrations at crack tips, an advanced experimental developmental methodology was idealized, which address the question of how micro-parameters can be estimated from rock/cemented granular materials. Although it is paramount that the surface of the material must be made to exhibit birefringence. The normal and shear data were supported by the extensive literature on ultrasound measurement techniques. Therefore calibration involves gradual application of load on the sandstone specimen. The incremental load is expressed as a sequence of light and dark fringes on the coated sandstone sample. At the maximum light appearance, dark colours appears as indicators of fringe orders. The first dark that appears is the first fringe order and the subsequent dark lines are the consecutive fringe order which provide consistency in calibration stages. Improvement of data quality depends on multi-fringe applications. The output results from this advanced technique is based on improved filtering of the colours for clear distinction in this particular research. Broader maroon colour can also be included to obtain an overall result range. The Red-Green-Blue (RGB) colour system can perform strain inspection in birefringence surface of bonded grains but the output can be affected by part of the more extreme values of stress in the sample.

9.3 Contributions to research method and assumptions made for DEM (Chapter 3)

The research method employed in this work is significant for identifying fracture propagation. The method is of central importance to discrete element modelling where the micro-mechanical behaviour of sandstone is needed, because it relies on the on-set of fracture. The experimentation and identification of the existence of grain contact at any arbitrary point in the sandstone was a tested concept, where bulk strength predictions were made from that hypothesis, and advanced experiments was included to check whether these predictions were correct. The predicted bulk strength were validated by well-known standard experimental test (ISRM), then the concept of micro-parameter determinations from rock was confirmed. Statistical analysis showed that 95% of all observations are reliable. Therefore, using micro-parameters as inputs to the simulations of rock offers a predictive power that shows quantitative and the qualitative bulk strength of the material. Overall this concept have a wide range of similar applications to other rock types, concrete and reinforced fibres which implies that, the method it is simple and coherent.

The assumptions that finite size of cement binds the grains at their contact were observed with the characterization results presented in Chapter 4. Hence these assumptions are valid for sandstone because they do not violate previous characterization result from similar reservoir sandstone materials. Therefore the methodology of specifying experimental micro-parameters as inputs for discrete modelling is a valid suggestion for simulations of sandstone.

9.4 Heterogeneity and anisotropy of rocks are significant to micro-structural measurements (Chapter 4 and 5)

Niger delta rock is anisotropy because of the stress properties at points in the medium are different with direction. The material is heterogeneous because the properties are different from point to point and discontinuous because there were spaces in the stress field in them. Sandstone exhibits this property intensely under stress. The anisotropy behaviour of this rock has been described to be continuous, linear and homogeneously elastic by the law that relates stress, strain and displacement in Hooke's law. This law has been used to estimate elastic properties of rock in standard

compression test. Here, it enhanced determination of contact models by the measurement of contact parameters from the rock. The contact parameters have been referred to as micro-parameters which have advanced the development of numerical rock models or behaviour. This is because experimental estimates were verified using the micro-parameters estimated from numerical experiments. The experiments are safer and faster compared to x-rays which are prune to affect human health.

9.5 Advanced experiments and experimental estimation of micro-parameters (Chapter 6 and 7)

The application of stress to a pack of cemented grains introduces strain into the residually stressed pack which relaxes the stresses surrounding any deformed location. Any force application perpendicular to any free surface (the deformed point, in this case) is considered a principal direction at which both shear and normal stresses were identified. Deformation at a point changes the stress within the immediate surrounding region, which leads to the corresponding changes in the local strains within the assembly of grains. These findings served as the foundation for the behaviour of stressed material which starts at a single point defect. Further, a chain of strain is a consequence for additional stress applications on this deformed point. Therefore the importance of obtaining a micro-scale measurements at a deformed point surrounded by residual stress was necessary. Since the point deformation progression did not contradict existing practical understanding of stressed materials on a large scale, the micro-parameters are valid inputs for simulating the behaviour of the bulk material. This concept solves the complexity of the blind-hole geometry, where, no closed-form solutions can be carried out with theory of elasticity for evaluations of stress except by use of some empirical coefficients. Principally because the point scale is considered blind due to the fact that the deformed point is relatively small compared to the bulk material.

Point stresses at a deformed locations with its immediate surroundings characterized by regular residual stress distributions is an established condition at which micro-parameters were evaluated. Additionally, the theoretical basis for the residual stress measurement method for bulk deformations of such materials is

hereby first developed and established for a known geometry, and was subsequently extended to different practical bulk scale. But the micro – parameter evaluation uses the ray of light which enters the strained point along the directions of principal stress before splitting into two waves. These waves traverse the strained point with different velocities, thus emerging with a phase relationship (or relative retardation). Since the material surface was made to exhibit birefringence property during stress applications on the point, single point stiffness was quantified. This invention is the first attempt made to measure strain at a micro scale, for the estimation of micro-parameter from rock.

9.6 Translation of crack nucleation to stiffness parameters

The deformation mechanism of brittle rock has been carried out by fixing microstructural natural parameter obtained from strain localized points in real sandstone. As the collective rock intrinsic features of fracture process growth are successfully translated into normal stiffness and shear stiffness parameter. This method of simulation contribute to solving the problem of complexity in microstructural representation of rock model numerically. The contact bond description using normal and shear stiffness data from experiment has enable the definition of fracture by bond breakage in tension and compression. Thus growth of fracture was captured experimentally solving the problem of fracture analysis in brittle material.

By combining the fracture mechanism of experimental finding with numerical solution, real data are estimated by the identification of crack nucleation and fracture propagation process which is significant in the photo stress images.

The porosity changes around crack nucleation zone and the response of the shear stress and shear displacement is a prolonged strength reduction which culminated into fracture. The behaviour of the simulated sample was controlled by the stiffness model of the natural sample. And this simplifies the simulations because the instruction script was imposed with specific model. The behaviour is displayed by the rearrangement of the grains which transmit micro-force with the stiffness data assigned to the simulated rock sample.

The development of constitutive contact law for grain assembly is very significant to the development of a numerical counterpart. Using a 3D discrete element model, the contact model has inculcated, the silent plastic deformability and non-linear elastic behaviour into the model by the use of experimental data as inputs. Hence using this as inputs to simulate tri-axial rock examination implies that, contact model retains the important features of the micro-mechanical behaviour of the natural rock. The material modulus increases with increased confined stress which is similar at in-situ conditions. Hence, the strength threshold can be identified for critical states in rock during mechanical handling.

9.7 The dependence of bulk strength on petrographic property (Chapter 8)

Sandstone was found to be the aggregate of mechanically cemented mineral grains. The pore space due to grain shape in the material, the mineral content and micro-flaws are inherent properties. Hence micro-fracturing are due to a single grain defected contact which is an initiated stress levels related to macroscopic yield state. This marks the elastic limit of the aggregate structure. Exhibition of the crack progression can be detected from micro-seismicity in its structure. Similar to the finding from the Photoelasticity and the report provided by Fjaer et al., (1992) stress fringes were produced when microscopic cracks were created. That is, stress is concentrated at the tip and rapidly ease propagation of new cracks. This cracks are directed with respect to direction of principal stresses as described by Griffith's theory. The strength of sandstone is dependent on its inherent petrographic properties. And as well as the quartz content, mica and other stable mineral like feldspar, the mineral forming content (plagioclase) and extent of cementation within these mineral content. Theses compositions are shape and porosity builders which determines the microscopic-mechanical damage process. Therefore, during simulation of rock, grain shape selection (for representation of discrete constituent mineral) is significant to the crack initiation stress, crack damage stress and the stress at rock failure.

9.8 Contributions to discrete modelling

Sandstone has been characterized as cemented-granular assembly and contact parameters are affected by the complex mineralogy (Chapter 4). The contact stiffness was estimated using velocity data from ultrasounds and photo stress analysis tomography (this methodology is adopted for the first time). The two experiments provided validations for each other. Thus grain contact stiffness ratio was adequate to develop the bulk material. The determination of the bond strength was enabled. Therefore it is possible to estimate micro-mechanical properties of natural rock. This is because the variation in the index of refraction is a function of the resulting strain. Thus, the light refracted and the fringe pattern is produced to give information on preferred grain orientation (due to residual or induced stress). Whereas the measurement of ultrasound wave velocity along various axis of symmetry in a specimen can provide information on preferred grain orientation (due to residual or induced stress).

Simulation of natural rock with experimental stiffness ratio (or micro-mechanical properties) has resolved the discrepancies between experimental elastic properties and the behaviour of natural rock under compressive strength. This is a common challenge in discrete models reported for rocks. The success of this approach has provided its applications to other anisotropic materials such as granite rock, fibre reinforced composites, concrete, etc.

9.9 Extension of work for further research

A further research can be built on this work based on the gap in knowledge which includes no existing experimental procedure to determine micro-parameters from natural rock. No micro-parameters are available for simulation of natural deformation process of rock. This implies that, there exist no experimental validations at micro scale and no adequate knowledge on certainty of material behaviour in the sub-surface. Macro-fracturing process is not yet fully understood due to complex minerology composition of rock. Therefore the prediction of rock fracture in drilling and allied areas is a stiff challenge.

Since the numerical representation of natural materials is still a stiff challenge, this work has used experimental-numerical hybrid approach towards the development of natural rock. The grains that make up the granular assembly have been represented with clumped. This script is coupled with other contact model parameters. By using these parameters, the bulk behaviour of the simulated rock matches that of the natural. Thus two areas of criticism is suggested to improve the work. (1.) Simulation of random grain shape for adequate representation of natural particle shape and interlock properties. (2.) Porosity implementation in Particle Flow Code (PFC) probably requires the simulated porosity values which is currently not be the exact geo-frame compared directly to that of natural rocks. This is because the rock is composed of random grains shape that are interlocked better than spheres. The natural rocks are typical of having a nature of finite sized cementation. Thus using a natural effect was not taken into account in the porosity estimation. However, the grain density and the bulk density was used. The numerical data provide a means of adopting general calculations of porosity changes and cementation.

The average coordination numbers for the natural sandstone (as revealed by the SEM-experiments) range from 7.5 to 9.0 whereas simulated porosity may be of greater average or lesser coordination number. The incorporation of the average coordination numbers of the natural rock were not considered and thus no identical frame was achieved for the natural porosity. The incorporation of a range may be consequential for porosity representation of the natural sample. For example, the greatest coordination number is 9 for the 22% porosity obtained whereas in the simulated model all the grains were identical in shape. The mode of coordination numbers is 9 (which is the value of a particle introduced into the model), except in the 22% porosity model- 3 (Chapter 8) with mixed particle clump. Thus, the average coordination numbers decrease slightly. Thus the range of coordination numbers can significantly influence porosity. It is likely that a relationship between porosity and mechanical properties exist if the simulation is followed by the reduction in the number of contacts which may ties to any increase in porosity to gives result influencing tortuosity of the force chains. This procedure may reproduce Young's modulus, Poisson's ratio and bulk strength of the natural rock.

9.10 Beneficiaries of this research

Oil Production Company (drilling engineers, production engineers): The Discrete Element Method (DEM) is yet to be perfected for simulation technique that allows practicable modelling of any mechanical interaction of granular materials. In the particular case of sandstones, clumped particles were used to represent quartz grains which are used to build the natural material by cementations of the inter-granular contacts. This condition is directly represented in building a natural petroleum oil reservoir by adequate definition of the grain density and bulk density of the natural sandstone. This yielded porosity and permeability properties which are major properties that enhance reservoir simulations by the oil producing industry. In this study, an extensive characterization of the natural sandstone has yielded micro-parameters necessary for an experimental-DEM-hybrid program which can be adopted to model the mechanical properties of the Niger Delta sandstone, an unconsolidated rock in the oil production producing state of Nigeria.

Predictors of earth quakes (or geologist): the intrusions of sandstone rock into granite rock is catastrophic causing earthquake or flood. When earthquake occurs, sediment may liquefy, as in the case of the 6.0-magnitude earthquake of the Christchurch, New Zealand, in 2011. This could have resulted due to an earthquake that forced the sedimentary rock into the granite rock in Colorado. With the knowledge that every grain remains discrete being attached to neighbouring particles to form the natural rock, the mechanism of the natural fractures can be identified by geologist.

9.11 Recommendation for future work

(1) Here it was difficult to distinguish the grain contact location from the bond location since the cementing clay at the contact are finite and occupy negligible space. This required assuming that the point-scale stiffness evaluated from PSAT is that of the inter-grains. Further studies are required to distinguish the variation of the stiffness within the cements bonding the individual grains of sandstone.

(2) As a follow up to this, it is recommended that the elasto-dynamic effects (stress wave propagation) are recorded and the Acoustic emission (AE) data are correlated to the crack number experimentally. This could be used further

to compare with similar outcomes using DEM simulations. The result can support the identification of the damage threshold (Chapter 4 and Chapter 8) and micro-crack can be further explained based on characteristic minerals at the localized area of micro-cracks.

(3) Quantitative assessment of rock deformations with the principles of fracture mechanics is important but it requires the knowledge of the Stress Intensity Factor (SIF). SIF solutions can differ with geometry and stress field (Ingraffea, 1987). The SIF for sandstone can be evaluated experimentally using PSAT, and its characteristics could provide further insights on the fracture properties of sandstone in future.

10 References

Adedapo, J., Ikpokonte, A., Schoeneich, K. and Kurowska, E. 2014. An Estimate of Oil Window in Nigeria Niger Delta Basin from Recent Studies. *gas.* **5**(11), pp.12-18.

Akram, M. and Sharrock, G. 2010. Physical and numerical investigation of a cemented granular assembly of steel spheres. *International Journal for Numerical and Analytical Methods in Geomechanics.* **34**(18), pp.1896-1934.

Akram, M.S., Sharrock, G. and Mitra, R. 2010. Physical and numerical investigation of conglomeratic rocks. *Univ New South Wales, Sydney, Australia.*

Allaby, M. and Park, C. 2013. *A dictionary of environment and conservation.* Oxford University Press.

Amadei, B. 1996. Importance of anisotropy when estimating and measuring in situ stresses in rock. In: *International journal of rock mechanics and mining sciences & geomechanics abstracts*: Elsevier, pp.293-325.

Amadei, B. 2012. *Rock anisotropy and the theory of stress measurements.* Springer Science & Business Media.

Amadei, B. and Stephansson, O. 1997. *Rock stress and its measurement.* Springer Science & Business Media.

Anderson, E. 2013. Economic Geology: Principles and Practice: Metals, Minerals, Coal and Hydrocarbons—Introduction to Formation and Sustainable Exploitation of Mineral Deposits. *Economic Geology.* **108**(6), pp.1517-1518.

Anthony, J.L. and Marone, C. 2005. Influence of particle characteristics on granular friction. *Journal of Geophysical Research: Solid Earth (1978–2012).* **110**(B8).

Antony, S.J. 2015. Imaging shear stress distribution and evaluating the stress concentration factor of the human eye. *Scientific reports.* **5**.

Appoloni, C., Fernandes, C.P. and Rodrigues, C.R.O. 2007. X-ray microtomography study of a sandstone reservoir rock. *Nuclear Instruments and Methods in Physics Research Section A: Accelerators, Spectrometers, Detectors and Associated Equipment.* **580**(1), pp.629-632.

Ashmawy, A.K., Hoang, V.V. and Sukumaran, B. 2003. Evaluating the influence of particle shape on liquefaction behavior using discrete element modeling. In: *The Thirteenth International Offshore and Polar Engineering Conference*: International Society of Offshore and Polar Engineers.

Aydin, A. 2014. Upgraded ISRM Suggested Method for Determining Sound Velocity by Ultrasonic Pulse Transmission Technique. *Rock mechanics and rock engineering.* **47**(1), pp.255-259.

Aydin, A., Borja, R.I. and Eichhubl, P. 2006. Geological and mathematical framework for failure modes in granular rock. *Journal of Structural Geology.* **28**(1), pp.83-98.

Azevedo, N. and May, I. 2002. Numerical simulations of plain concrete under shear loading conditions. In: *Numerical Modeling in Micromechanics via Particle Methods: International PFC Symposium, Gelsenkirchen, Germany, 6-8 November 2002*: CRC Press, p.79.

Baldi, G., Hight, D.W. and Thomas, G.E. 1988. A reevaluation of conventional triaxial test methods. *Advanced triaxial testing of soil and rock, ASTM STP.* **977**, pp.219-263.

Barla, G. 1974. *Rock anisotropy: theory and laboratory testing*. Springer-Verlag, New York. pp.131-169.

Bell, F. 1978. The physical and mechanical properties of the Fell Sandstones, Northumberland, England. *Engineering Geology.* **12**, pp.1-29.

Bell, F. and Lindsay, P. 1999. The petrographic and geomechanical properties of some sandstones from the Newspaper Member of the Natal Group near Durban, South Africa. *Engineering Geology.* **53**(1), pp.57-81.
Bell, F.G. 2013. *Engineering in rock masses.* Elsevier.
Benz, W. and Asphaug, E. 1995. Simulations of brittle solids using smooth particle hydrodynamics. *Computer physics communications.* **87**(1), pp.253-265.
Bernabé, Y., Fryer, D. and Hayes, J. 1992. The effect of cement on the strength of granular rocks. *Geophysical Research Letters.* **19**(14), pp.1511-1514.
Bevins, R.E. 1994. *A mineralogy of Wales.* National Museum Wales.
Bfer, G. 1985. An isoparametric joint/interface element for finite element analysis. *International journal for numerical methods in engineering.* **21**(4), pp.585-600.
Bieniawski, Z. 1967. MECHANISM OF BRITTLE FRACTURE OF ROCK. **PART III--FRACTURE, IN TENSION**.
Bjørlykke, K. 2015. Introduction to Sedimentology. *Petroleum Geoscience.* Springer, pp.31-90.
Blatt, H. 1979. Diagenetic processes in sandstones.
Blatt, H., Tracy, R. and Owens, B. 2006. *Petrology: igneous, sedimentary, and metamorphic.* Macmillan.
Bobet, A., Fakhimi, A., Johnson, S., Morris, J., Tonon, F. and Yeung, M.R. 2009. Numerical models in discontinuous media: review of advances for rock mechanics applications. *Journal of Geotechnical and Geoenvironmental Engineering.* **135**(11), pp.1547-1561.
Boutt, D.F. and McPherson, B.J. 2002. Simulation of sedimentary rock deformation: Lab‐scale model calibration and parameterization. *Geophysical research letters.* **29**(4).
Bowes, C. and Procter, R. 1997. Drillers Stuck Pipe Handbook. *Ballater, Scotland: Procter & Collins Ltd.*
Brace, W. and Byerlee, J.D. 1966. Recent experimental studies of brittle fracture of rocks. In: *The 8th US Symposium on Rock Mechanics (USRMS)*: American Rock Mechanics Association.
Brace, W., Paulding, B. and Scholz, C. 1966. Dilatancy in the fracture of crystalline rocks. *Journal of Geophysical Research.* **71**(16), pp.3939-3953.
Bradley, W.B. 1978. Bore hole failure near salt domes. In: *SPE Annual Fall Technical Conference and Exhibition*: Society of Petroleum Engineers.
Brewster, D. 1815. On the laws which regulate the polarisation of light by reflexion from transparent bodies. *Philosophical Transactions of the Royal Society of London.* **105**, pp.125-159.
Brown, N.J. 2013. Discrete element modelling of cementitious materials.
Bryant, F. 1958. Snell's Law of Refraction. *Physics Bulletin.* **9**(12), p317.
Bryant, S. and Blunt, M. 1992. Prediction of relative permeability in simple porous media. *Physical Review A.* **46**(4), p2004.
Burnley, P. 2013. The importance of stress percolation patterns in rocks and other polycrystalline materials. *Nature communications.* **4**.
Camborde, F., Mariotti, C. and Donzé, F. 2000. Numerical study of rock and concrete behaviour by discrete element modelling. *Computers and geotechnics.* **27**(4), pp.225-247.
Caputo, F. and Giudice, G. 1983. Photoelastic coating method approach to the study of stress distribution in composite materials. *Fibre Science and Technology.* **18**(4), pp.255-264.
Castagna, J.P., Batzle, M.L. and Eastwood, R.L. 1985. Relationships between compressional-wave and shear-wave velocities in clastic silicate rocks. *Geophysics.* **50**(4), pp.571-581.

Chang, C., Zoback, M.D. and Khaksar, A. 2006. Empirical relations between rock strength and physical properties in sedimentary rocks. *Journal of Petroleum Science and Engineering.* **51**(3), pp.223-237.

Chang, C.S., Sundaram, S.S. and Misra, A. 1989. Initial moduli of particulated mass with frictional contacts. *International Journal for Numerical and Analytical Methods in Geomechanics.* **13**(6), pp.629-644.

Cheung, L., O'Sullivan, C. and Coop, M. 2013. Discrete element method simulations of analogue reservoir sandstones. *International Journal of Rock Mechanics and Mining Sciences.* **63**, pp.93-103.

Cho, N., Martin, C. and Sego, D. 2008. Development of a shear zone in brittle rock subjected to direct shear. *International Journal of Rock Mechanics and Mining Sciences.* **45**(8), pp.1335-1346.

Cho, N.a., Martin, C. and Sego, D. 2007. A clumped particle model for rock. *International Journal of Rock Mechanics and Mining Sciences.* **44**(7), pp.997-1010.

Churcher, P., French, P., Shaw, J. and Schramm, L. 1991. Rock properties of Berea sandstone, Baker dolomite, and Indiana limestone. In: *SPE International Symposium on Oilfield Chemistry*: Society of Petroleum Engineers.

Cobbold, R.S. 2007. *Foundations of biomedical ultrasound.* Oxford University Press on Demand.

Colombo, I.S., Main, I. and Forde, M. 2003. Assessing damage of reinforced concrete beam using "b-value" analysis of acoustic emission signals. *Journal of materials in civil engineering.* **15**(3), pp.280-286.

Cook, N. 1976. Seismicity associated with mining. *Engineering Geology.* **10**(2), pp.99-122.

Corben, H.C. and Stehle, P. 1994. *Classical mechanics.* Courier Corporation.

Corbett, K., Friedman, M. and Spang, J. 1987. Fracture development and mechanical stratigraphy of Austin Chalk, Texas. *AAPG Bulletin.* **71**(1), pp.17-28.

Cramer, D. 1998. *Fundamental statistics for social research: step-by-step calculations and computer techniques using SPSS for Windows.* Psychology Press.

Cramer, D. and Howitt, D.L. 2004. *The Sage dictionary of statistics: a practical resource for students in the social sciences.* Sage.

Cross, W. 1902. The development of systematic petrography in the nineteenth century. *The Journal of Geology.* **10**(5), pp.451-499.

Cundall, P. 1974. A computer model for rock-mass behavior using interactive graphics for the input and output of geometrical data. *US Army corps of Engineers (Missouri River Division) Tech. Rep. MRD-2074.*

Cundall, P. and Fairhurst, C. 1986. Correlation of discontinuum models with physical observations–an approach to the estimation of rock mass behaviour. *Felsbau.* **4**(4), p1986.

Cundall, P.A. 1971. *The measurement and analysis of accelerations in rock slopes*. thesis, Imperial College London (University of London).

Cundall, P.A. 1980. *UDEC-A Generalised Distinct Element Program for Modelling Jointed Rock.* DTIC Document.

Cundall, P.A. and Hart, R.D. 1992. Numerical modelling of discontinua. *Engineering computations.* **9**(2), pp.101-113.

Cundall, P.A. and Strack, O. 1979a. The development of constitutive laws for soil using the distinct element method. *Numerical methods in geomechanics.* **1**, pp.289-317.

Cundall, P.A. and Strack, O.D. 1979b. A discrete numerical model for granular assemblies. *Geotechnique.* **29**(1), pp.47-65.

D-06, A. *Standard Test Method of Unconfined Compressive Strength of Cohesive Soil.* Astm Int'L.

Dally, J.W. and Riley, W.F. 1991. Experimental stress analysis, 1991. *McGraw and Hill, New York.*

Daniel, R. and Kaldi, J. 2012. *Atlas of Australian and New Zealand Hydrocarbon Seals: Worldwide Analogs for Cap Rocks and Intraformational Barriers in Clastic Depositional Settings, AAPG Studies in Geology 60.* AAPG.

Davies, T.R., McSaveney, M.J. and Deganutti, A.M. 2007. Dynamic rock fragmentation causes low rock-on-rock friction.

de Andrade Ramos, J.R. 2000. Stylolites: measurement of rock loss. *Brazilian Journal of Geology.* **30**(3), pp.432-435.

De Borst, R., Crisfield, M.A., Remmers, J.J. and Verhoosel, C.V. 2012. *Nonlinear finite element analysis of solids and structures.* John Wiley & Sons.

De Borst, R., Sluys, L., Muhlhaus, H.-B. and Pamin, J. 1993. Fundamental issues in finite element analyses of localization of deformation. *Engineering computations.* **10**(2), pp.99-121.

Deer, W.A., Howie, R.A. and Zussman, J. 1992. *An introduction to the rock-forming minerals.* Longman London.

den Brok, S.W., David, C. and Bernabé, Y. 1997. Preparation of synthetic sandstones with variable cementation for studying the physical properties of granular rocks. *Comptes Rendus de l'Académie des Sciences-Series IIA-Earth and Planetary Science.* **325**(7), pp.487-492.

Derski, W., Izbicki, R., Kisiel, I. and Mróz, Z. 2012. *Rock and soil mechanics.* Elsevier.

Diederichs, M., Kaiser, P. and Eberhardt, E. 2004. Damage initiation and propagation in hard rock during tunnelling and the influence of near-face stress rotation. *International Journal of Rock Mechanics and Mining Sciences.* **41**(5), pp.785-812.

Digby, P. 1981. The effective elastic moduli of porous granular rocks. *Journal of Applied Mechanics.* **48**(4), pp.803-808.

Doane, D.P. and Seward, L.E. 2011. Measuring skewness: a forgotten statistic. *Journal of Statistics Education.* **19**(2), pp.1-18.

Donzé, F.V., Richefeu, V. and Magnier, S.-A. 2009. Advances in discrete element method applied to soil, rock and concrete mechanics. *State of the art of geotechnical engineering. Electronic Journal of Geotechnical Engineering.* **44**, p31.

Dowla, N., Hayatdavoudi, A., Ghalambor, A., Okoye, C. and Alcocer, C. 1990. Laboratory investigation of saturation effect on mechanical properties of rocks. In: *SPWLA 31st Annual Logging Symposium*: Society of Petrophysicists and Well-Log Analysts.

Dvorkin, J., Nur, A. and Yin, H. 1994. Effective properties of cemented granular materials. *Mechanics of materials.* **18**(4), pp.351-366.

Dvorkin, J. and Yin, H. 1995. Contact laws for cemented grains: Implications for grain and cement failure. *International Journal of Solids and Structures.* **32**(17), pp.2497-2510.

Eberhardt, E., Stead, D. and Stimpson, B. 1999. Quantifying progressive pre-peak brittle fracture damage in rock during uniaxial compression. *International Journal of Rock Mechanics and Mining Sciences.* **36**(3), pp.361-380.

Eberhardt, E., Stead, D., Stimpson, B. and Read, R. 1998. Identifying crack initiation and propagation thresholds in brittle rock. *Canadian Geotechnical Journal.* **35**(2), pp.222-233.

Egger, P. and Pellet, F. 1990. Behaviour of reinforced jointed models under multiaxial loading. *Int 2nd Congr. Rock Joints.* pp.191-195.

Eslinger, E. and Pevear, D.R. 1988. *Clay minerals for petroleum geologists and engineers.* Society of Economic Paleontologists and Mineralogis ts.

Evamy, B., Haremboure, J., Kamerling, P., Knaap, W., Molloy, F. and Rowlands, P. 1978. Hydrocarbon habitat of Tertiary Niger delta. *AAPG bulletin.* **62**(1), pp.1-39.

Evans, B. 2012. Predicting CO2 injectivity properties for application at CCS sites. *A report to ANLEC, Project Number 3-1110.* **122**, p83pp.
Fairhurst, C. and Hudson, J. 1999a. Draft ISRM suggested method for the complete stress-strain curve for intact rock in uniaxial compression. *International Journal of Rock Mechanics and Mining Sciences.* **36**(3), pp.279-289.
Fairhurst, C. and Hudson, J. 1999b. International society for rock mechanics commission on testing methods: draft ISRM suggested method for the complete stress-strain curve for intact rock in uniaxial compression. *Int J Rock Mech Min Sci.* **36**, pp.279-289.
Fakhimi, A., Carvalho, F., Ishida, T. and Labuz, J. 2002. Simulation of failure around a circular opening in rock. *International Journal of Rock Mechanics and Mining Sciences.* **39**(4), pp.507-515.
Fakhimi, A. and Villegas, T. 2004. Calibration of a discrete element model for rock failure envelope and tensile strength. *Shimizu, Hart, et Cundall (Eds.), Numerical Modelling in Micromechanics via Particle Methods.* pp.383-390.
Fakhimi, A. and Villegas, T. 2007. Application of dimensional analysis in calibration of a discrete element model for rock deformation and fracture. *Rock Mechanics and Rock Engineering.* **40**(2), pp.193-211.
Feng, X.-T., Pan, P.-Z. and Zhou, H. 2006. Simulation of the rock microfracturing process under uniaxial compression using an elasto-plastic cellular automaton. *International Journal of Rock Mechanics and Mining Sciences.* **43**(7), pp.1091-1108.
Ferla, A., Lavrov, A. and Fjær, E. 2009. Finite-element analysis of thermal-induced stresses around a cased injection well. In: *Journal of Physics: Conference Series*: IOP Publishing, p.012051.
Ferrez, J.-A. 2001. Dynamic triangulations for efficient 3D simulation of granular materials.
Fertl, W.H., Chapman, R.E. and Hotz, R.F. 1994. *Studies in abnormal pressures.* Elsevier.
Fisher, Q., Knipe, R. and Worden, R. 2009. Microstructures of deformed and non-deformed sandstones from the North Sea: implications for the origins of quartz cement in sandstones. *Quartz Cementation in Sandstones: Special Publication 29 of the IAS.* **14**, pp.129-146.
Fu, Y. 2005. *Experimental quantification and DEM simulation of micro-macro behaviors of granular materials using x-ray tomography imaging*. thesis, Tongji University, China, 2001.
Garcia, X., Akanji, L.T., Blunt, M.J., Matthai, S.K. and Latham, J.P. 2009. Numerical study of the effects of particle shape and polydispersity on permeability. *Physical Review E.* **80**(2), p021304.
Ghazvinian, A., Azinfar, M. and Vaneghi, R.G. 2012. Importance of tensile strength on the shear behavior of discontinuities. *Rock mechanics and rock engineering.* **45**(3), pp.349-359.
Gill, W., Khalaf, F. and Massoud, M. 1977. Clay minerals as an index of the degree of metamorphism of the carbonate and terrigenous rocks in the South Wales coalfield. *Sedimentology.* **24**(5), pp.675-691.
Golubev, A. and Rabinovich, G. 1976. Resultaty primeneia appartury akusticeskogo karotasa dlja predeleina proconstych svoistv gornych porod na mestorosdeniaach tverdych isjopaemych. *Prikl. Geofiz. Moskva.* **73**, pp.109-116.
Goodman, R.E. 1989. Introduction to rock mechanics.
Goodman, R.E. and Shi, G.-H. 1988. The application of block theory to the design of rock bolt supports for tunnels. *Computers and Geotechnics.* **5**(1), p74.
Griffith, A.A. 1921. The phenomena of rupture and flow in solids. *Philosophical transactions of the royal society of london. Series A, containing papers of a mathematical or physical character.* pp.163-198.

Groeneveld, R.A. and Meeden, G. 1984. Measuring skewness and kurtosis. *The Statistician.* pp.391-399.
GROUP, I.C. 2008. *PFC2D (particle flow code in 2 dimensions) theory and background*. Minnesota, USA: Itasca Consulting Group Inc.
Guéguen, Y. and Palciauskas, V. 1994. *Introduction to the Physics of Rocks.* Princeton University Press.
Guo, Y. and Morgan, J.K. 2004. Influence of normal stress and grain shape on granular friction: Results of discrete element simulations. *Journal of Geophysical Research: Solid Earth.* **109**(B12).
Hafner, B. 2006. Energy Dispersive Spectroscopy on the SEM: A Primer. *Characterization Facility, University of Minnesota.* pp.1-26.
Hajiabdolmajid, V.R. 2002. *Mobilization of strength in brittle failure of rock.*
Hakala, M., Kuula, H. and Hudson, J. 2007. Estimating the transversely isotropic elastic intact rock properties for in situ stress measurement data reduction: a case study of the Olkiluoto mica gneiss, Finland. *International Journal of Rock Mechanics and Mining Sciences.* **44**(1), pp.14-46.
Halleck, P., Saucier, R., Behrmann, L. and Ahrens, T. 1988. Reduction of jet perforator penetration in rock under stress. In: *SPE Annual Technical Conference and Exhibition*: Society of Petroleum Engineers.
Halliday, R. 2001. Walker, Fundamentals of Physics. *derviation of magnetic moment of a circular loop of current.* pp.791-792.
Handy, M.R. 1990. The solid‐state flow of polymineralic rocks. *Journal of Geophysical Research: Solid Earth (1978–2012).* **95**(B6), pp.8647-8661.
Hardy, H.R. 1976. Handbook on mechanical properties of rocks: Vol. 1. VS Vutukuri, RD Lama, and SS Saluja. Trans Tech Publications, D-3392 Clausthal, Germany. *Cement and Concrete Research.* **6**(1), pp.165-166.
Hart, D.J. and Wang, H.F. 1995. Laboratory measurements of a complete set of poroelastic moduli for Berea sandstone and Indiana limestone. *Journal of Geophysical Research: Solid Earth (1978–2012).* **100**(B9), pp.17741-17751.
Hart, R., Cundall, P. and Lemos, J. 1988. Formulation of a three-dimensional distinct element model—Part II. Mechanical calculations for motion and interaction of a system composed of many polyhedral blocks. In: *International Journal of Rock Mechanics and Mining Sciences & Geomechanics Abstracts*: Elsevier, pp.117-125.
Hatzor, Y. and Palchik, V. 1997. The influence of grain size and porosity on crack initiation stress and critical flaw length in dolomites. *International Journal of Rock Mechanics and Mining Sciences.* **34**(5), pp.805-816.
Hauke, G. and Moreau, R. 2008. *An introduction to fluid mechanics and transport phenomena.* Springer.
Hawkes, I. and Mellor, M. 1970. Uniaxial testing in rock mechanics laboratories. *Engineering Geology.* **4**(3), pp.179-285.
Hazzard, J.F. 1998. *Numerical modelling of acoustic emissions and dynamic rock behaviour*. thesis, University of Keele.
Hazzard, J.F. and Mair, K. 2003. The importance of the third dimension in granular shear. *Geophysical Research Letters.* **30**(13).
Hazzard, J.F. and Young, R.P. 2002. Moment tensors and micromechanical models. *Tectonophysics.* **356**(1), pp.181-197.
Hazzard, J.F., Young, R.P. and Oates, S.J. 2002. Numerical modeling of seismicity induced by fluid injection in a fractured reservoir. In: *Mining and Tunnel Innovation and Opportunity, Proceedings of the 5th North American Rock Mechanics Symposium, Toronto, Canada*, pp.1023-1030.

Herrmann, H. 1991. Patterns and scaling in fracture. *Physica Scripta.* **1991**(T38), p13.
Heywood, R.B. 2013. *Photoelasticity for Designers: International Series of Monographs in Mechanical Engineering.* Elsevier.
Hillier, S. 2002. Quantitative analysis of clay and other minerals in sandstones by X-ray powder diffraction (XRPD). *Clay Mineral Cements in Sandstones: Special Publication.* **34**, pp.213-251.
Hiltl, M., Hagelberg, C., Swift, R., Carney, T. and Nellis, W. 1999. Dynamic response of Berea Sandstone shock-loaded under dry, wet and water-pressurized conditions. In: *International Association for the Advancement of High Pressure Science and Technology (AIRAPT) International Conference on High Pressure Science and Technology (AIRAPT-17)*.
Hoek, E., Carranza-Torres, C. and Corkum, B. 2002. Hoek-Brown failure criterion-2002 edition. *Proceedings of NARMS-Tac.* **1**, pp.267-273.
Hoek, E. and Diederichs, M.S. 2006. Empirical estimation of rock mass modulus. *International Journal of Rock Mechanics and Mining Sciences.* **43**(2), pp.203-215.
Hoek, E. and Franklin, J.A. 1967. *A simple triaxial cell for field or laboratory testing of rock.* Imperial College of Science and Technology, University of London.
Hoek, E. and Martin, C. 2014. Fracture initiation and propagation in intact rock–a review. *Journal of Rock Mechanics and Geotechnical Engineering.* **6**(4), pp.287-300.
Holcomb, D., Stone, C. and Costin, L. 1990. Combining acoustic emission locations and a microcrack damage model to study development of damage in brittle materials. In: *The 31th US Symposium on Rock Mechanics (USRMS)*: American Rock Mechanics Association.
Holt, R., Brignoli, M. and Kenter, C. 2000. Core quality: quantification of coring-induced rock alteration. *International Journal of Rock Mechanics and Mining Sciences.* **37**(6), pp.889-907.
Holt, R., Kjølaas, J., Larsen, I., Li, L., Pillitteri, A.G. and Sønstebø, E. 2005. Comparison between controlled laboratory experiments and discrete particle simulations of the mechanical behaviour of rock. *International Journal of Rock Mechanics and Mining Sciences.* **42**(7), pp.985-995.
Horii, H. and Nemat-Nasser, S. 1986. Brittle failure in compression: splitting, faulting and brittle-ductile transition. *Philosophical Transactions of the Royal Society of London A: Mathematical, Physical and Engineering Sciences.* **319**(1549), pp.337-374.
Howarth, D. and Rowlands, J. 1987. Quantitative assessment of rock texture and correlation with drillability and strength properties. *Rock Mechanics and Rock Engineering.* **20**(1), pp.57-85.
Hsieh, Y.-M., Li, H.-H., Huang, T.-H. and Jeng, F.-S. 2008. Interpretations on how the macroscopic mechanical behavior of sandstone affected by microscopic properties—revealed by bonded-particle model. *Engineering Geology.* **99**(1), pp.1-10.
Huang, W.T. 1962. *Petrology.* McGraw-Hill New York.
Hudson, J.A. and Harrison, J.P. 2000. *Engineering rock mechanics-an introduction to the principles.* Elsevier.
Huggett, J. 1986. An SEM study of phyllosilicate diagenesis in sandstones and mudstones in the Westphalian coal measures using back-scattered electron microscopy. *Clay Minerals.* **21**(4), pp.603-616.
Huggett, J.M. 1982. *The growth and origin of authigenic clay minerals in sandstones.*
Huggett, J.M. 1984. An SEM study of phyllosilicates in a Westphalian Coal Measures sandstone using back-scattered electron imaging and wavelength dispersive spectral analysis. *Sedimentary geology.* **40**(4), pp.233-247.

Hunt, S., Meyers, A. and Louchnikov, V. 2003. Modelling the Kaiser effect and deformation rate analysis in sandstone using the discrete element method. *Computers and Geotechnics.* **30**(7), pp.611-621.

Ingraffea, A.R. 1987. Theory of crack initiation and propagation in rock. *Fracture mechanics of rock.* pp.71-110.

Itasca, U. 2000. *Universal Distinct Element Code User's Guide*. USA.

Ivars, D.M., Pierce, M.E., Darcel, C., Reyes-Montes, J., Potyondy, D.O., Young, R.P. and Cundall, P.A. 2011. The synthetic rock mass approach for jointed rock mass modelling. *International Journal of Rock Mechanics and Mining Sciences.* **48**(2), pp.219-244.

Jiles, D.C. 2007. *Introduction to the principles of materials evaluation. Pg 140.* CRC Press.

Jing, L. 2003. A review of techniques, advances and outstanding issues in numerical modelling for rock mechanics and rock engineering. *International Journal of Rock Mechanics and Mining Sciences.* **40**(3), pp.283-353.

Jing, L. and Hudson, J. 2002. Numerical methods in rock mechanics. *International Journal of Rock Mechanics and Mining Sciences.* **39**(4), pp.409-427.

Jing, L. and Stephansson, O. 2007. *Fundamentals of Discrete Element Methods for Rock Engineering: Theory and Applications: Theory and Applications.* Elsevier.

Johnson, W.B. 2005. Design and testing of a laboratory ultrasonic data acquisition system for tomography.

Jong, I. and Rogers, B. 1990. *Engineering mechanics: dynamics.* Oxford University Press.

Kaiser, P. and Kim, B. 2008. Rock mechanics advances of underground construction and mining. *Korea rock mechanics, Seoul, Korea.* pp.1-16.

Karner, S.L., Chester, J.S., Chester, F.M., Kronenberg, A.K. and Hajash Jr, A. 2005. Laboratory deformation of granular quartz sand: Implications for the burial of clastic rocks. *AAPG bulletin.* **89**(5), pp.603-625.

Kazerani, T. and Zhao, J. 2010. Micromechanical parameters in bonded particle method for modelling of brittle material failure. *International journal for numerical and analytical methods in geomechanics.* **34**(18), pp.1877-1895.

Keller, W. 1961. *The common rocks and minerals of Missouri.* University of Missouri Press.

Kino, G.S. and Corle, T.R. 1996. *Confocal scanning optical microscopy and related imaging systems.* Academic Press.

Kobayashi, T. 1995. Mechanical properties and failure mechanism of gravelly soft rocks. *Rock Foundation.*

Konietzky, H. 2002. *Numerical Modeling in Micromechanics via Particle Methods: International PFC Symposium, Gelsenkirchen, Germany, 6-8 November 2002.* CRC Press.

Koyama, T. and Jing, L. 2007. Effects of model scale and particle size on micro-mechanical properties and failure processes of rocks—A particle mechanics approach. *Engineering analysis with boundary elements.* **31**(5), pp.458-472.

Kozicki, J. and Donzé, F. 2008. A new open-source software developed for numerical simulations using discrete modeling methods. *Computer Methods in Applied Mechanics and Engineering.* **197**(49), pp.4429-4443.

Kozicki, J. and Donzé, F. 2009. Yade-open dem: an open-source software using a discrete element method to simulate granular material. *Engineering Computations.* **26**(7), pp.786-805.

Krause, F.F. and Nelson, D. 1984. Stormevent Sedimentation: Lithofacies Association in the Cardium Formation, Pembina Area, West-Central Alberta, Canada.

Lai, P., Moulton, K. and Krevor, S. 2015. Pore-scale heterogeneity in the mineral distribution and reactive surface area of porous rocks. *Chemical Geology.* **411**, pp.260-273.

Lajtai, E.Z., Carter, B.J. and Duncan, E.S. 1991. Mapping the state of fracture around cavities. *Engineering Geology.* **31**(3), pp.277-289.
Lambert-Aikhionbare, D. and Shaw, H. 1982. Significance of clays in the petroleum geology of the Niger Delta. *Clay Minerals.* **17**(1), pp.91-103.
Lawn, B.R. 1993. *Fracture of brittle solids.* Cambridge university press.
Lesniak, J., Zickel, M., Bazile, D. and Boyce, B. 1999. Assessment Of Grey Field Photoelasticity. *SEM, Junio.* pp.7-9.
Lesniak, J.R. 2000. *Full field photoelastic stress analysis*. Google Patents.
Li, L. and Fjær, E. 2012. Modeling of stress‐dependent static and dynamic moduli of weak sandstones. *Journal of Geophysical Research: Solid Earth (1978–2012).* **117**(B5).
Lisjak, A. and Grasselli, G. 2014. A review of discrete modeling techniques for fracturing processes in discontinuous rock masses. *Journal of Rock Mechanics and Geotechnical Engineering.* **6**(4), pp.301-314.
Locknet, D. and Byerlee, J.D. 1995. Precursory AE patterns leading to rock fracture. *SERIES ON ROCK AND SOIL MECHANICS.* **19**, pp.45-58.
Luong, M. 2001. Nondestructive evaluation of rock material instability. *Frontiers of Rock Mechanics and Sustainable Development in the 21st Century.* pp.463-466.
Main, I.G., Meredith, P.G. and Jones, C. 1989. A reinterpretation of the precursory seismic b-value anomaly from fracture mechanics. *Geophysical Journal International.* **96**(1), pp.131-138.
Manual, P.D.U.s. 1995. Itasca Consulting Group. *Inc., Minneapolis, Minnesota, USA.*
Martin, C., Kaiser, P. and McCreath, D. 1999. Hoek-Brown parameters for predicting the depth of brittle failure around tunnels. *Canadian Geotechnical Journal.* **36**(1), pp.136-151.
Martin, C.D. 1993. *The strength of massive Lac du Bonnet granite around underground openings*. thesis, University of Manitoba Manitoba.
Martins, A., Santana, M., Gonçalves, C., Gaspari, E., Campos, W. and Perez, J. 1999. Evaluating the Transport of Solids Generated by Shale Instabilities in ERW Drilling-Part II: Case Studies. In: *SPE Annual Technical Conference and Exhibition*: Society of Petroleum Engineers.
Mas Ivars, D., Potyondy, D., Pierce, M. and Cundall, P. 2008. The smooth-joint contact model. *Proceedings of WCCM8-ECCOMAS.* **2008**, p8th.
Matsushima, T. 2004. 3-D image-based discrete element modeling for irregularly-shaped grains. In: *Proceedings of the 2nd International PFC Symposium on Numerical Modeling in Micromechanics via Particle Method-2004. AA Balkema, London*, pp.421-427.
Mavko, G., Mukerji, T. and Dvorkin, J. 2009. *The rock physics handbook: Tools for seismic analysis of porous media.* Cambridge university press.
McLellan, P. 1996. Assessing the risk of wellbore instability in horizontal and inclined wells. *Journal of Canadian Petroleum Technology.* **35**(05).
McLellan, P. and Wang, Y. 1994. Predicting the effects of pore pressure penetration on the extent of wellbore instability: Application of a versatile poro-elastoplastic model. In: *Rock Mechanics in Petroleum Engineering*: Society of Petroleum Engineers.
Mehta, N. 2008. *Textbook of engineering physics.* PHI Learning Pvt. Ltd.
Menéndez, B., Zhu, W. and Wong, T.-F. 1996. Micromechanics of brittle faulting and cataclastic flow in Berea sandstone. *Journal of structural geology.* **18**(1), pp.1-16.
Meng, Z. and Pan, J. 2007. Correlation between petrographic characteristics and failure duration in clastic rocks. *Engineering geology.* **89**(3), pp.258-265.
Meredith, P.G., Main, I.G. and Jones, C. 1990. Temporal variations in seismicity during quasi-static and dynamic rock failure. *Tectonophysics.* **175**(1), pp.249-268.

Micro-Measurements, V. 2005. *Introduction to Stress Analysis by the PhotoStress® Method.* Tech Note TN-702-2, Document.
Militzer, H. and Stoll, R. 1973. Einige Beitrageder geophysics zur primadatenerfassung im Bergbau, Neue Bergbautechnik. *Lipzig.* **3**, pp.21-25.
Mindlin, R. 2014. Compliance of elastic bodies in contact. *Journal of applied mechanics.* **16**.
Mindlin, R.D. and Deresiewica, H. 2014. Elastic spheres in contact under varying oblique forces. *Journal of applied mechanics.* **20**.
Mohiuddin, M., Awal, M., Abdulraheem, A. and Khan, K. 2001. A new diagnostic approach to identify the causes of borehole instability problems in an offshore Arabian field. In: *SPE Middle East Oil Show*: Society of Petroleum Engineers.
Momber, A. 2004. Wear of rocks by water flow. *International Journal of Rock Mechanics and Mining Sciences.* **41**(1), pp.51-68.
Moon, V.G. 1993. Geotechnical characteristics of ignimbrite: A soft pyroclastic rock type. *Engineering Geology.* **35**(1), pp.33-48.
Moos, D. and Barton, C. 2008. Modeling uncertainty in the permeability of stress-sensitive fractures. In: *The 42nd US Rock Mechanics Symposium (USRMS)*: American Rock Mechanics Association.
Mouchet, J.-P. and Mitchell, A. 1989. *Abnormal Pressures While Drilling: Origins, Prediction, Detection, Evaluation.* Editions Technip.
Munjiza, A., Owen, D. and Bicanic, N. 1995. A combined finite-discrete element method in transient dynamics of fracturing solids. *Engineering computations.* **12**(2), pp.145-174.
Nakata, Y., Bolton, M. and Cheng, Y. 2004. Macro-mechanical behavior for an assembly of grains modeled by bonding spheres. In: *Numerical Modeling in Micromechanics via Particle Methods-2004: Proceedings of the 2nd International PFC Symposium, Kyoto, Japan, 28-29 October 2004*: CRC Press, p.407.
Napier, J. and Peirce, A. 1995. Simulation of extensive fracture formation and interaction in brittle materials. *Proc. Mechanics of Jointed and Faulted Rock-MJFR.*
Narayanasamy, R. 2004. Numerical behavior of weak sand. In: *Proceedings of the Numerical Modeling in Micromechanics Via Particle Methods: Second International PFC Symposium, Kyoto. AA Balkema: Japan*.
Nemat-Nasser, S. and Hori, M. 2013. *Micromechanics: overall properties of heterogeneous materials.* Elsevier.
Nemcok, M., Schamel, S. and Gayer, R. 2009. *Thrustbelts: Structural architecture, thermal regimes and petroleum systems.* Cambridge University Press.
Nur, A. and Wang, Z. 1989. *Seismic and Acoustic Velocities in Reservoir Rocks: Recent Developments.* Soc of Exploration Geophysicists.
Nwozor, K. and Onuorah, L. 2014. GEOPRESSURE ANALYSIS AND RESERVOIR FLUID DISCRIMINATION IN A CENTRAL SWAMP FIELD, NIGER DELTA, NIGERIA. *Petroleum & Coal.* **56**(2), pp.124-140.
Nygaard, G. and Nævdal, G. 2006. Nonlinear model predictive control scheme for stabilizing annulus pressure during oil well drilling. *Journal of Process Control.* **16**(7), pp.719-732.
O'Sullivan, C., Cui, L. and Bray, J.D. 2004. Three-dimensional discrete element simulations of direct shear tests. *Numerical Modeling in Micromechanics via Particle Methods.* pp.373-382.
Oda, M., Nemat‐Nasser, S. and Mehrabadi, M.M. 1982. A statistical study of fabric in a random assembly of spherical granules. *International Journal for Numerical and analytical methods in Geomechanics.* **6**(1), pp.77-94.

Olsson, W.A. and Peng, S.S. 1976. Microcrack nucleation in marble. In: *International Journal of Rock Mechanics and Mining Sciences & Geomechanics Abstracts*: Pergamon, pp.53-59.

Oreskes, N., Shrader-Frechette, K. and Belitz, K. 1994. Verification, validation, and confirmation of numerical models in the earth sciences. *Science.* **263**(5147), pp.641-646.

Özbek, A. 2009. Variation of Schmidt hammer values with imbrication direction in clastic sedimentary rocks. *International Journal of Rock Mechanics and Mining Sciences.* **46**(3), pp.548-554.

Palchik, V. and Hatzor, Y. 2004. The influence of porosity on tensile and compressive strength of porous chalks. *Rock mechanics and rock engineering.* **37**(4), pp.331-341.

Pande, G., Beer, G. and Williams, J. 1990. Numerical methods in rock mechanics.

Papanastasiou, P. and Zervos, A. 2004. Wellbore stability analysis: from linear elasticity to postbifurcation modeling. *International Journal of Geomechanics.* **4**(1), pp.2-12.

Park, R.G. 2013. *Foundation of structural geology.* Routledge.

Petroski, H. 1996. *Invention by design: How engineers get from thought to thing.* Harvard University Press.

Pevear, D.R. 1999. Illite and hydrocarbon exploration. *Proceedings of the National Academy of Sciences.* **96**(7), pp.3440-3446.

Phillips, W.J. and Phillips, N. 1980. *An introduction to mineralogy for geologists.* John Wiley & Sons.

Picard, M.D. 1971. Classification of fine-grained sedimentary rocks. *Journal of Sedimentary Research.* **41**(1).

Pickett, G.R. 1963. Acoustic character logs and their applications in formation evaluation. *Journal of Petroleum technology.* **15**(06), pp.659-667.

Pidwirny, M. 2006. Introduction to the Oceans. *Fundamentals of Physical Geography.* **2**.

Pininska, J. 2000. ACOUSTIC EMISSION AS A RESULT OF TENSIL AND SHEARING PROCESSES IN STABLE AND UNSTABLE FRACTURING OF ROCKS. *Journal of Acoustic Emission.* **18**, p8.

Pinińska, J. 1997. Some problems of the stress distribution on structural contacts in natural rocks bodies. *I-sze Ukraińsko-Polskie Sympozjum Naukowe:" Mieszane zagadnienia mechaniki ośrodków niejednorodnych.*

Pinińska, J. 2008. Models of rock deformation under uniaxial compression conditions. *geologija.* **50**, pp.S108-S115.

Plumb, R., Herron, S. and Olsen, M. 1992. Composition and Texture on Compressive Strength Variations in the Travis Peak Formation. In: *SPE Annual Technical Conference and Exhibition*: Society of Petroleum Engineers.

Pollard, D.D. and Aydin, A. 1988. Progress in understanding jointing over the past century. *Geological Society of America Bulletin.* **100**(8), pp.1181-1204.

Pollard, D.D. and Fletcher, R.C. 2005. *Fundamentals of structural geology.* Cambridge University Press.

Potyondy, D. 2010. A grain-based model for rock: approaching the true microstructure. *Proceedings of Bergmekanikk i Norden.* pp.225-234.

Potyondy, D. 2013. *PFC3D flat joint contact model version 1. Itasca Consulting Group.* Minneapolis, Technical Memorandum ICG7234-L.

Potyondy, D. and Cundall, P. 2004. A bonded-particle model for rock. *International journal of rock mechanics and mining sciences.* **41**(8), pp.1329-1364.

Price, D.G. 2008. *Engineering geology: principles and practice.* Springer Science & Business Media.

Ramamurthy, T. 2004. A geo-engineering classification for rocks and rock masses. *International Journal of Rock Mechanics and Mining Sciences.* **41**(1), pp.89-101.
Ramesh, K. 2000. *Digital photoelasticity*. IOP Publishing.
Razali, N.M. and Wah, Y.B. 2011. Power comparisons of shapiro-wilk, kolmogorov-smirnov, lilliefors and anderson-darling tests. *Journal of statistical modeling and analytics.* **2**(1), pp.21-33.
Razumovsky, I.A. 2011. *Interference-optical Methods of Solid Mechanics.* Springer Science & Business Media.
Rendler, N. and Vigness, I. 1966. Hole-drilling strain-gage method of measuring residual stresses. *Experimental Mechanics.* **6**(12), pp.577-586.
Resende, R., Lamas, L., Lemos, J. and Calçada, R. 2010. Micromechanical modelling of stress waves in rock and rock fractures. *Rock mechanics and rock engineering.* **43**(6), pp.741-761.
Rong, G., Liu, G., Hou, D. and Zhou, C.-b. 2013. Effect of particle shape on mechanical behaviors of rocks: A numerical study using clumped particle model. *The Scientific World Journal.* **2013**.
Sabatakakis, N., Koukis, G., Tsiambaos, G. and Papanakli, S. 2008. Index properties and strength variation controlled by microstructure for sedimentary rocks. *Engineering Geology.* **97**(1), pp.80-90.
Sallam, A., Ashmawy, A. and Runkles, B. 2004. Experimental validation of modeling irregular particle shapes using DEM. In: *Numerical Modeling in Micromechanics via Particle Methods-2004: Proceedings of the 2nd International PFC Symposium, Kyoto, Japan, 28-29 October 2004*: CRC Press, p.363.
Sampson, R.C. 1970. A stress-optic law for photoelastic analysis of orthotropic composites. *Experimental Mechanics.* **10**(5), pp.210-215.
Santarelli, F., Dahen, D., Baroudi, H. and Sliman, K. 1992. Mechanisms of borehole instability in heavily fractured rock media. In: *International journal of rock mechanics and mining sciences & geomechanics abstracts*: Elsevier, pp.457-467.
Scholtès, L., Donzé, F.-V. and Khanal, M. 2011. Scale effects on strength of geomaterials, case study: coal. *Journal of the Mechanics and Physics of Solids.* **59**(5), pp.1131-1146.
Selley, R. 2000. Applied Sedimentology, x+ 523pp. *San Diego, San Francisco, New York, Boston, London, Sydney, Tokyo: Academic Press. Price US $82.50 (hard covers). ISBN 0.* **12**(636375), p7.
Shao, L., Stattegger, K. and Garbe-Schoenberg, C.-D. 2001. Sandstone petrology and geochemistry of the Turpan basin (NW China): implications for the tectonic evolution of a continental basin. *Journal of Sedimentary Research.* **71**(1), pp.37-49.
Shapiro, S.S. and Wilk, M.B. 1965. An analysis of variance test for normality (complete samples). *Biometrika.* **52**(3/4), pp.591-611.
Shi, G.-h. 1988. *Discontinuous deformation analysis: a new numerical model for the statics and dynamics of block systems.* University of California, Berkeley.
Shillington, D.J., Minshull, T.A., Peirce, C. and O'Sullivan, J.M. 2008. P‐and S‐wave velocities of consolidated sediments from a seafloor seismic survey in the North Celtic Sea Basin, offshore Ireland. *Geophysical Prospecting.* **56**(2), pp.197-211.
Shimizu, H., Murata, S. and Ishida, T. 2009. Distinct element analysis for rock failure considering AE events generated by the slip at crack surfaces. *Journal of Acoustic Emission.* **27**, pp.194-211.
Shimizu, Y., Hart, R. and Cundall, P. 2004. Numerical modeling in micromechanics via particle methods. In: *Proceedings of 2nd international PFC symposium*, pp.28-29.

Shukla, A., Zhu, C. and Sadd, M. 1988. Angular dependence of dynamic load due to explosive loading in two dimensional granular aggregate. *Journal of Strain Analysis.* **23**, pp.121-127.
Singh, M. and Rao, K.S. 2005. Bearing capacity of shallow foundations in anisotropic non-Hoek–Brown rock masses. *Journal of geotechnical and geoenvironmental engineering.* **131**(8), pp.1014-1023.
Sitharam, T. 2003. Micromechanical modelling of granular media: The power of discrete element modelling.
Šmilauer, V., Catalano, E., Chareyre, B., Dorofeenko, S., Duriez, J., Gladky, A., Kozicki, J., Modenese, C., Scholtès, L. and Sibille, L. 2010. Yade documentation. *The Yade Project.(http://yade-dem. org/doc/).*
Sokal, R.R. and Rohlf, F.J. 1969. *The principles and practice of statistics in biological research.* WH Freeman and company San Francisco:.
Solutions, D. 2010. EDEM v2. 3 User Guide, Edinburgh, UK. *DEM Solutions Ltd.*
Standard, A. 1993. Geotechnical Site Investigations. *AS1726-1993.*
Stoffler, D. and Hornemann, U. 1972. Quartz and feldspar glasses produced by natural and experimental shock. *Meteoritics.* **7**, p371.
Sziics, E. 1980. Similitude and modelling. *Fundamental Studies in Engineering.* **2**.
Tan, C., Yaakub, M.A., Chen, X., Willoughby, D., Choi, S. and Wu, B. 2004. Wellbore Stability of Extended Reach Wells in an Oil Field in Sarawak Basin, South China Sea. In: *SPE Asia Pacific Oil and Gas Conference and Exhibition*: Society of Petroleum Engineers.
Tarokh, A., Fakhimi, A. and Labuz, J. 2012. Size of process zone in fracture testing of rock. In: *46th US Rock Mechanics/Geomechanics Symposium*: American Rock Mechanics Association.
Terzaghi, K., Peck, R.B. and Mesri, G. 1996. *Soil mechanics in engineering practice.* John Wiley & Sons.
Theocaris, P.S. and Gdoutos, E.E. 2013. *Matrix theory of photoelasticity.* Springer.
Thill, R., Willard, R. and Bur, T. 1969. Correlation of longitudinal velocity variation with rock fabric. *Journal of Geophysical Research.* **74**(20), pp.4897-4909.
Thornton, C. 2000. Numerical simulations of deviatoric shear deformation of granular media. *Géotechnique.* **50**(1), pp.43-53.
Tilmann, S.E. and Bennett, H.F. 1973. Ultrasonic shear wave birefringence as a test of homogeneous elastic anisotropy. *Journal of Geophysical Research.* **78**(32), pp.7623-7629.
Timoshenkgo, S. and Goodier, J. 1970. *Theory of Elasticity. 1970*. McGraw-Hill, New York.
Tofel, P. and Trcka, T. 2013. Fracture Detection by Electro-Ultrasonic Spectroscopy. In: *ECF19*.
Trent, B. 1989. *Numerical simulation of wave propagation through cemented granular material.* Los Alamos National Lab., NM (USA).
Trent, B. and Margolin, L. 1992. A numerical laboratory for granular solids. *Engineering computations.* **9**(2), pp.191-197.
Tucker, M.E. 2003. *Sedimentary rocks in the field.* John Wiley & Sons.
Ulusay, R. and Hudson, J.A. 1974. The complete ISRM suggested methods for rock characterization. *Testing and monitoring.* **2006**, pp.121-132.
Ulusay, R. and Hudson, J.A. 2007. *The complete ISRM suggested methods for rock characterization, testing and monitoring: 1974-2006.* International Society for Rock Mechanics, Commission on Testing Methods.
Ulusay, R., Türeli, K. and Ider, M. 1994. Prediction of engineering properties of a selected litharenite sandstone from its petrographic characteristics using correlation and multivariate statistical techniques. *Engineering Geology.* **38**(1), pp.135-157.

Van Baars, S. 1996. *Discrete element analysis of granular materials.* TU Delft, Delft University of Technology.
Waldschmidt, W.A. 1941. Cementing materials in sandstones and their probable influence on migration and accumulation of oil and gas. *AAPG Bulletin.* **25**(10), pp.1839-1879.
Waltham, T. 2001. *Foundations of engineering geology.* CRC Press.
Waterman, P. and Teutonico, L. 1957. Ultrasonic double refraction in single crystals. *Journal of Applied Physics.* **28**(2), pp.266-270.
Welton, J.E. 1984. SEM petrology atlas, 237 pp. *Methods in Exploration Series.–Tulsa (AAPG).*
Wibberley, C.A. and Shimamoto, T. 2003. Internal structure and permeability of major strike-slip fault zones: the Median Tectonic Line in Mie Prefecture, Southwest Japan. *Journal of Structural Geology.* **25**(1), pp.59-78.
Wiles, T. 2006. Reliability of numerical modelling predictions. *International Journal of Rock Mechanics and Mining Sciences.* **43**(3), pp.454-472.
Willson, S., Last, N., Zoback, M. and Moos, D. 1999. Drilling in South America: a wellbore stability approach for complex geologic conditions. In: *Latin American and Caribbean petroleum engineering conference*: Society of Petroleum Engineers.
Winkler, K.W. 1983. Contact stiffness in granular porous materials: comparison between theory and experiment. *Geophysical Research Letters.* **10**(11), pp.1073-1076.
Wong, T.-f., Wong, R.H., Chau, K. and Tang, C. 2006. Microcrack statistics, Weibull distribution and micromechanical modeling of compressive failure in rock. *Mechanics of Materials.* **38**(7), pp.664-681.
Yang, S.-Q., Huang, Y.-H., Jing, H.-W. and Liu, X.-R. 2014. Discrete element modeling on fracture coalescence behavior of red sandstone containing two unparallel fissures under uniaxial compression. *Engineering Geology.* **178**, pp.28-48.
Yenulis, G. and Folsom, C. 1993. *Rotary blowout preventer adaptable for use with both kelly and overhead drive mechanisms*. Google Patents.
Yoon, J. 2007. Application of experimental design and optimization to PFC model calibration in uniaxial compression simulation. *International Journal of Rock Mechanics and Mining Sciences.* **44**(6), pp.871-889.
York, P.L., Prichard, D.M., Dodson, J.K., Dodson, T., Rosenberg, S.M., Gala, D. and Utama, B. 2009. Eliminating Non-Productive Time Associated with Drilling through Trouble Zones. In: *Offshore Technology Conference*: Offshore Technology Conference.
Zadler, B.J., Le Rousseau, J.H., Scales, J.A. and Smith, M.L. 2004. Resonant ultrasound spectroscopy: theory and application. *Geophysical Journal International.* **156**(1), pp.154-169.
Zang, A. and Stephansson, O. 2009. *Stress field of the Earth's crust.* Springer Science & Business Media.
Zhao, G. 2010. Development of micro-macro continuum-discontinuum coupled numerical method.
Zhao, J. and Cai, J. 2001. Transmission of elastic P-waves across single fractures with a nonlinear normal deformational behavior. *Rock Mechanics and Rock Engineering.* **34**(1), pp.3-22.
Zorlu, K., Gokceoglu, C., Ocakoglu, F., Nefeslioglu, H. and Acikalin, S. 2008. Prediction of uniaxial compressive strength of sandstones using petrography-based models. *Engineering Geology.* **96**(3), pp.141-158.

11 Appendix A - Statistics and z-test for normality (Chapter 5)

Table A 1 Descriptive statistics for stiffness data from ultrasound

	N	Minimum	Maximum	Mean	Std. Deviation	Variance
Normal stiffness _ Ultrasound (MN/m)	54	5.54	7.82	6.5373	0.55951	0.313
Shear stiffness _ Ultrasound (MN/m)	54	1.82	2.88	2.4564	0.26327	0.069
Stiffness ratio - Ultrasound	54	2.24	3.44	2.6839	.30485	0.093

Table A 2 Further descriptive statistics for stiffness data from ultrasound

	N	Mean	Skewness		Kurtosis	
	Statistic	Statistic	Statistic	Std. Error	Statistic	Std. Error
Normal stiffness _ Ultrasound (MN/m)	54	6.5373	0.552	0.325	0.035	0.639
Shear stiffness _ Ultrasound (MN/m)	54	2.4564	-.0226	0.325	-1.065	0.639
Stiffness ratio - Ultrasound	54	2.6839	0.536	0.325	-0.550	0.639

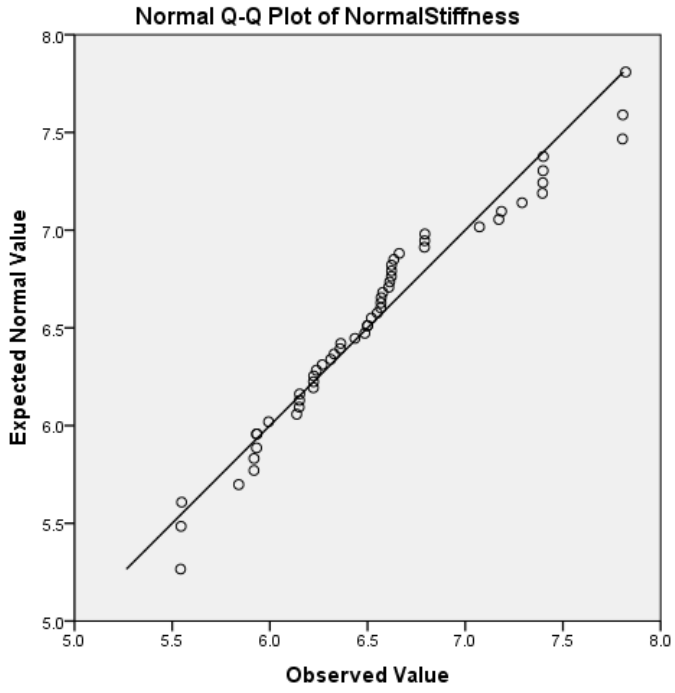

Figure A 1Q-Q Plot for normal stiffness the unit is provided in MN/m

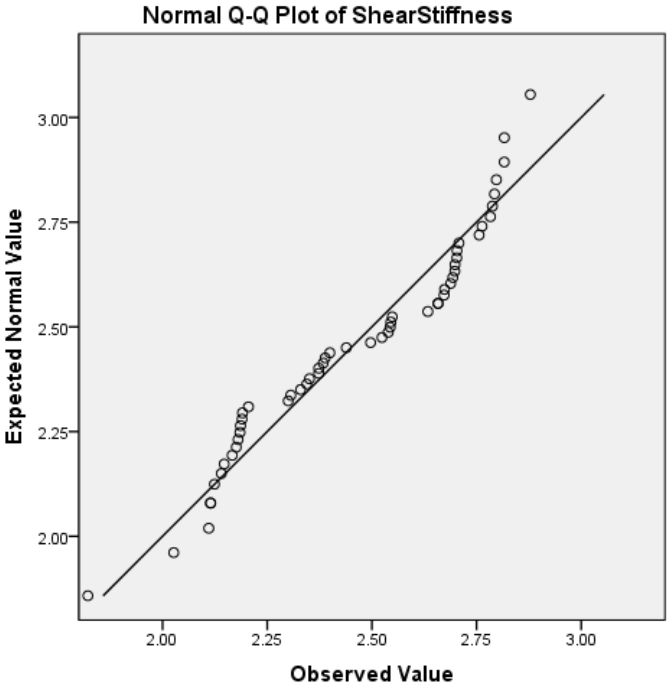

Figure A 2Q-Q Plot for shear stiffness the unit is provided in MN/m

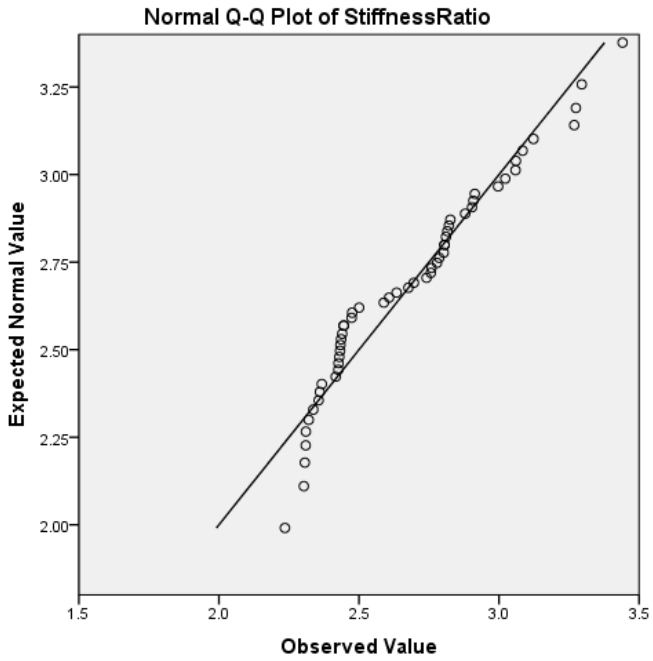

Figure A 3Q-Q plot for stiffness ratio

Table A 3 z-test for normality of data for normal stiffness and shear stiffness

z-test	z-value		z- value Calculated as ratio of statistics to standard error			
	Normal Stiffness_ Kn	Shear Stiffness _Ks	statistics		Standard error	
			Kn	Ks	Kn	Ks
Skewness	1.698	0.695	0.552	0.226	0.326	0.325
Kurtosis	0.055	1.667	0.325	1.065	0.639	0.639

Table A 4 Statistics for independent sample Z- test –Ultrasound

	Kn_NormalStiffness Ks_ShearStiffness			Statistic	Std. Error
KnKs	Kn	Mean		6.5373	.07614
		95% Confidence Interval for Mean	Lower Bound	6.3846	
			Upper Bound	6.6900	
		5% Trimmed Mean		6.5216	
		Median		6.5097	
		Variance		.313	
		Std. Deviation		.55951	
		Minimum		5.54	
		Maximum		7.82	
		Range		2.28	
		Interquartile Range		0.64	
		Skewness		0.552	0.325
		Kurtosis		0.035	0.639
	Ks	Mean		2.4564	0.03583
		95% Confidence Interval for Mean	Lower Bound	2.3845	
			Upper Bound	2.5282	
		5% Trimmed Mean		2.4620	
		Median		2.4679	
		Variance		0.069	
		Std. Deviation		0.26327	
		Minimum		1.82	
		Maximum		2.88	
		Range		1.06	
		Interquartile Range		0.51	
		Skewness		-.226	.325
		Kurtosis		-1.065	.639

Table A 5 Shapiro-Wilk value for statistical significance for normal and shear stiffness-ultrasound

Kn_NormalStiffness Ks_ShearStiffness	Kolmogorov-Smirnov[a]			Shapiro-Wilk		
	Statistic	df	Sig.	Statistic	df	sig
Kn	0.153	54	0.003	0.950	54	0.025
Ks	0.148	54	0.005	0.937	54	0.007

12 Apendix B – Statistics, ANOVA and z-test of normality (Chapter 6)

Table B 1 Descriptive statistics for stiffness data with valid N (listwise) from PSAT

	N	Minimum	Maximum	Mean	Std. Deviation	Variance
Normalstiffness_K1-PSAT	54	4.00	8.00	5.7001	0.93902	0.882
Shearstiffness_K2-PSAT	54	2.00	2.88	2.2735	0.21938	0.048
Stiffnessratio_K1/K2-PSAT	54	1.76	2.99	2.5059	0.30648	0.094

Table B 2 Further descriptive statistics for stiffness data with valid N (listwise) from PSAT

	N	Mean	Skewness		Kurtosis	
	Statistic	Statistic	Statistic	Std. Error	Statistic	Std. Error
Normalstiffness_K1-PSAT	54	5.7001	0.769	0.325	-0.181	0.639
Shearstiffness_K2-PSAT	54	2.2735	0.345	0.325	-0.525	0.639
Stiffnessratio_K1/K2-PSAT	54	2.5059	-0.260	0.325	-0.886	0.639

Table B 3 Further descriptive statistics for stiffness data with valid N (listwise) from PSAT

	N	Range	Mean		Skewness		Kurtosis	
	Stat.	Stat.	Stat.	Std. Error	Stat.	Std. Error	Stat.	Std. Error
Normal stiffness (K1) _ PSAT (MN/m)	54	1.84	4.9702	0.05404	-0.510	0.325	0.759	0.639
Shear stiffness (K2)_ PSAT (MN/m)	54	0.88	2.2735	0.02985	0.345	0.325	-0.525	0.639
Stiffness ratio _ PSAT	54	1.11	2.2038	0.03445	-0.388	0.325	-0.031	0.639

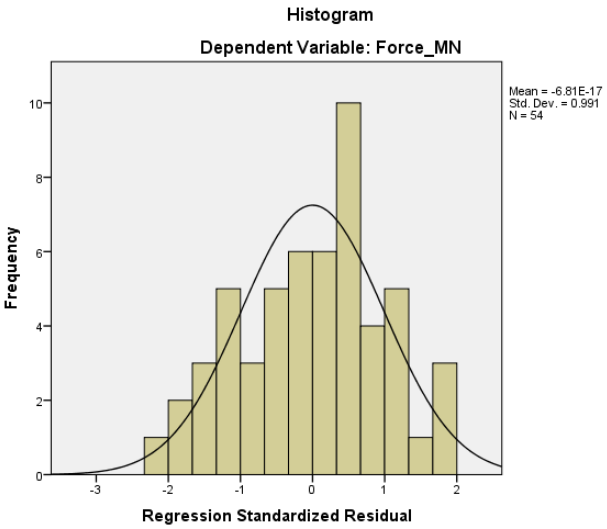

Figure B 1 Histogram of force distribution used for stiffness

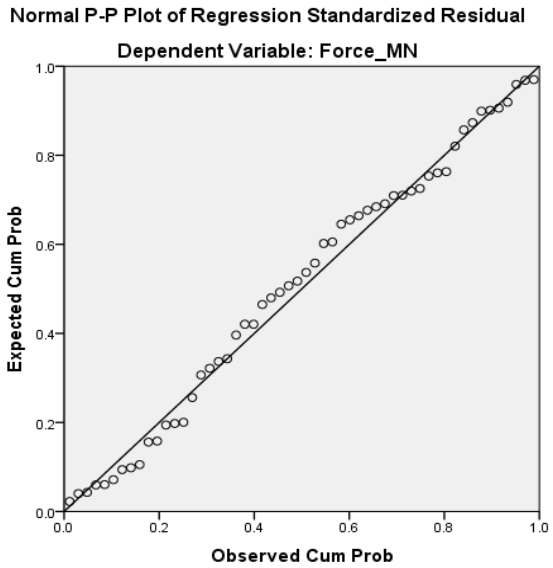

Figure B 2 P-P plot of regression standardized residuals

Table B 4 Descriptive statistics force and stiffness

	Mean	Std. Deviation	N
Force_MN	70.6977	15.63009	54
K1_MN_m	5.7001	0.93902	54
K2_MN_m	2.2735	0.21938	54

Table B 5 Z-test for normality of data for normal stiffness and shear stiffness-PSAT

z-test	z-value		z- value Calculated as ratio of statistics to standard error			
	Normal Stiffness_ Kn	Shear Stiffness _Ks	statistics		Standard error	
			Kn	Ks	Kn	Ks
Skewness	2.370	1.065	0.771	0.346	0.325	0.325
Kurtosis	0.285	0.796	-0.182	0.509	0.639	0.639

Coefficients[a]

Model		Unstandardized Coefficients		Standardized Coefficients
		B	Std. Error	Beta
1	(Constant)	67.261	22.481	
	K1_MN_m	-3.906	3.000	-0.235
	K2_MN_m	11.304	12.840	0.159

Table B 6 Coefficient value at 95%confidence interval for the B coefficient

Coefficients[a]

Model		95.0% Confidence Interval for B	
		Lower Bound	Upper Bound
1	(Constant)	22.128	112.394
	K1_MN_m	-9.928	2.117
	K2_MN_m	-14.473	37.080

Table B 7 Statistics for independent sample Z- test – PSAT

K1NormalStiffness_K2ShearStiffness				Statistic	Std. Error
K1K2	Kn	Mean		5.7002	0.12791
		95% Confidence Interval for Mean	Lower Bound	5.4436	
			Upper Bound	5.9567	
		5% Trimmed Mean		5.6587	
		Median		5.3100	
		Variance		0.883	
		Std. Deviation		0.93991	
		Minimum		4.00	
		Maximum		8.00	
		Range		4.00	
		Interquartile Range		1.57	
		Skewness		0.771	0.325
		Kurtosis		-0.182	0.639
	Ks	Mean		2.2733	0.02983
		95% Confidence Interval for Mean	Lower Bound	2.2135	
			Upper Bound	2.3332	
		5% Trimmed Mean		2.2621	
		Median		2.3150	
		Variance		0.048	
		Std. Deviation		.21922	
		Minimum		2.00	
		Maximum		2.88	
		Range		0.88	
		Interquartile Range		0.35	
		Skewness		0.346	0.325
		Kurtosis		-0.509	0.639

Table B 8 Shapiro-Wilk value for statistical significance for normal and shear stiffness-PSAT

K1_NormalStiffness K2_ShearStiffness	Kolmogorov-Smirnov[a]			Shapiro-Wilk		
	Statistic	df	Sig.	Statistic	df	Sig
Kn	0.205	54	0.000	0.895	54	0.000
Ks	0.137	54	0.013	0.914	54	0.001

13 Appendix C - Statistics and ANOVA (Chapter 7)

Statistical analyses of the mechanical parameters are provided below. Similar to the statistical analysis reported in the earlier chapters (section 4.11). Tables C1-C16 and Figures C1-C3 contain the statistical reliance of the micro-parameters used for the simulations of the bulk strength of Niger delta sandstone.

Table C 1 Analysis of variance

Output Created		19-SEP-2015 13:13:08
Input	Active Dataset	DataSet0
	N of Rows in Working Data File	54
	Definition of Missing	User-defined missing values are treated as missing.
	Cases Used	Statistics are based on all cases with valid data for all variables in the model.
Missing Value Handling		

Table C 2 Between subjects factors

		N
Ratio of standard deviation to mean of bond strength	0.14	18
	0.16	18
	0.25	18
Stiffness ratio	2.20	27
	2.60	27

Table C 3 Descriptive statistics

Dependent Variable: Peak stress _ reversal point of volumetric strain

Ratio of standard deviation to mean of bond strength	Stiffness ratio	Mean	Std. Deviation	N
0.14	2.20	75.9278	7.20113	9
	2.60	71.8789	10.53235	9
	Total	73.9033	8.99694	18
0.16	2.20	76.5589	8.41777	9
	2.60	74.8444	10.03369	9
	Total	75.7017	9.02773	18
0.25	2.20	68.9100	8.11772	9
	2.60	65.5856	11.85216	9
	Total	67.2478	10.00206	18
Total	2.20	73.7989	8.39725	27
	2.60	70.7696	11.12692	27
	Total	72.2843	9.88257	54

Table C 4 Levene's test of equality of error variances[a]

Dependent Variable: Peak stress _ reversal point of volumetric strain

F	df1	df2	Sig.
0.468	5	48	0.798

Tests the null hypothesis that the error variance of the dependent variable is equal across groups.[a]

a. Design: Intercept + ROSD + Kn_ks + ROSD * Kn_ks

Table C 5 Tests of between-subjects effects

Dependent Variable: Peak stress _ reversal point of volumetric strain

Source	Type III Sum of Squares	df	Mean Square	F	Sig.
Corrected Model	850.723[a]	5	170.145	1.888	0.114
Intercept	282150.763	1	282150.763	3130.999	0.000
ROSD	713.992	2	356.996	3.962	0.026
Kn_ks	123.882	1	123.882	1.375	0.247
ROSD * Kn_ks	12.850	2	6.425	0.071	0.931
Error	4325.533	48	90.115		
Total	287327.019	54			
Corrected Total	5176.256	53			

Table C 6 Tests of between-subjects effects and marginal mean estimated

Dependent Variable: Peak stress _ reversal point of volumetric strain

Source	Partial Eta Squared
Corrected Model	0.164
Intercept	0.985
ROSD	0.142
Kn_ks	0.028
ROSD * Kn_ks	0.003
Error	
Total	
Corrected Total	

a. R Squared = .164 (Adjusted R Squared = .077)

1. Grand Mean

Dependent Variable: Peak stress _ reversal point of volumetric strain

		95% Confidence Interval	
Mean	Std. Error	Lower Bound	Upper Bound
72.284	1.292	69.687	74.882

Table C 7 Ratio of standard deviation to mean of bond strength

Estimates

Dependent Variable: Peak stress _ reversal point of volumetric strain

Ratio of standard deviation to mean of bond strength	Mean	Std. Error	95% Confidence Interval	
			Lower Bound	Upper Bound
0.14	73.903	2.237	69.405	78.402
0.16	75.702	2.237	71.203	80.200
0.25	67.248	2.237	62.749	71.747

Table C 8 Pairwise comparisons I

Dependent Variable: Peak stress _ reversal point of volumetric strain

(I) Ratio of standard deviation to mean of bond strength	(J) Ratio of standard deviation to mean of bond strength	Mean Difference (I-J)	Std. Error	Sig.[b]
0.14	0.16	-1.798	3.164	1.000
	0.25	6.656	3.164	0.122
0.16	0.14	1.798	3.164	1.000
	0.25	8.454*	3.164	0.031
0.25	0.14	-6.656	3.164	0.122
	0.16	-8.454*	3.164	0.031

Table C 9 Pairwise comparison II

Dependent Variable: Peak stress _ reversal point of volumetric strain

(I) Ratio of standard deviation to mean of bond strength	(J) Ratio of standard deviation to mean of bond strength	95% Confidence Interval for Difference[b]	
		Lower Bound	Upper Bound
0.14	0.16	-9.648	6.052
	0.25	-1.194	14.506
0.16	0.14	-6.052	9.648
	0.25	0.604	16.304
0.25	0.14	-14.506	1.194
	0.16	-16.304	-0.604

Based on estimated marginal means

*. The mean difference is significant at the .05 level.

b. Adjustment for multiple comparisons: Bonferroni.

Table C 10 Univariate tests

Dependent Variable: Peak stress _ reversal point of volumetric strain

	Sum of Squares	df	Mean Square	F	Sig.	Partial Eta Squared
Contrast	713.992	2	356.996	3.962	0.026	0.142
Error	4325.533	48	90.115			

The F tests the effect of Ratio of standard deviation to mean of bond strength. This test is based on the linearly independent pairwise comparisons among the estimated marginal means.

Table C 11 Estimate (Stiffness ratio)

Dependent Variable: Peak stress _ reversal point of volumetric strain

Stiffness ratio	Mean	Std. Error	95% Confidence Interval	
			Lower Bound	Upper Bound
2.20	73.799	1.827	70.126	77.472
2.60	70.770	1.827	67.096	74.443

Table C 12 Pairwise comparisons for stiffness ratio I

Dependent Variable: Peak stress _ reversal point of volumetric strain

(I) Stiffness ratio	(J) Stiffness ratio	Mean Difference (I-J)	Std. Error	Sig.[a]	95% Confidence Interval for Difference[a]
					Lower Bound
2.20	2.60	3.029	2.584	0.247	-2.166
2.60	2.20	-3.029	2.584	0.247	-8.224

Table C 13 Pairwise comparison for stiffness ratio II

Dependent Variable: Peak stress _ reversal point of volumetric strain

(I) Stiffness ratio	(J) Stiffness ratio	95% Confidence Interval for Difference
		Upper Bound
2.20	2.60	8.224
2.60	2.20	2.166

Based on estimated marginal means

a. Adjustment for multiple comparisons: Bonferroni.

Table C 14 Univariate tests

Dependent Variable: Peak stress _ reversal point of volumetric strain

	Sum of Squares	df	Mean Square	F	Sig.	Partial Eta Squared
Contrast	123.882	1	123.882	1.375	0.247	0.028
Error	4325.533	48	90.115			

The F tests the effect of Stiffness ratio. This test is based on the linearly independent pairwise comparisons among the estimated marginal means.

Table C 15 Ratio of standard deviation to mean of bond strength*stiffness ratio

Dependent Variable: Peak stress _ reversal point of volumetric strain

Ratio of standard deviation to mean of bond strength	Stiffness ratio	Mean	Std. Error	95% Confidence Interval	
				Lower Bound	Upper Bound
0.14	2.20	75.928	3.164	69.566	82.290
	2.60	71.879	3.164	65.517	78.241
0.16	2.20	76.559	3.164	70.197	82.921
	2.60	74.844	3.164	68.482	81.207
0.25	2.20	68.910	3.164	62.548	75.272
	2.60	65.586	3.164	59.223	71.948

Table C 16 Post Hoc tests: ratio of standard deviation to mean of bond strength homogeneous subsets

Peak stress _ reversal point of volumetric strain

Ryan-Einot-Gabriel-Welsch Range[a]

Ratio of standard deviation to mean of bond strength	N	Subset	
		1	2
0.25	18	67.2478	
0.14	18		73.9033
0.16	18		75.7017
Sig.		1.000	0.572

Means for groups in homogeneous subsets are displayed.

Based on observed means.

The error term is Mean Square(Error) = 90.115.

a. Alpha = 0.05.

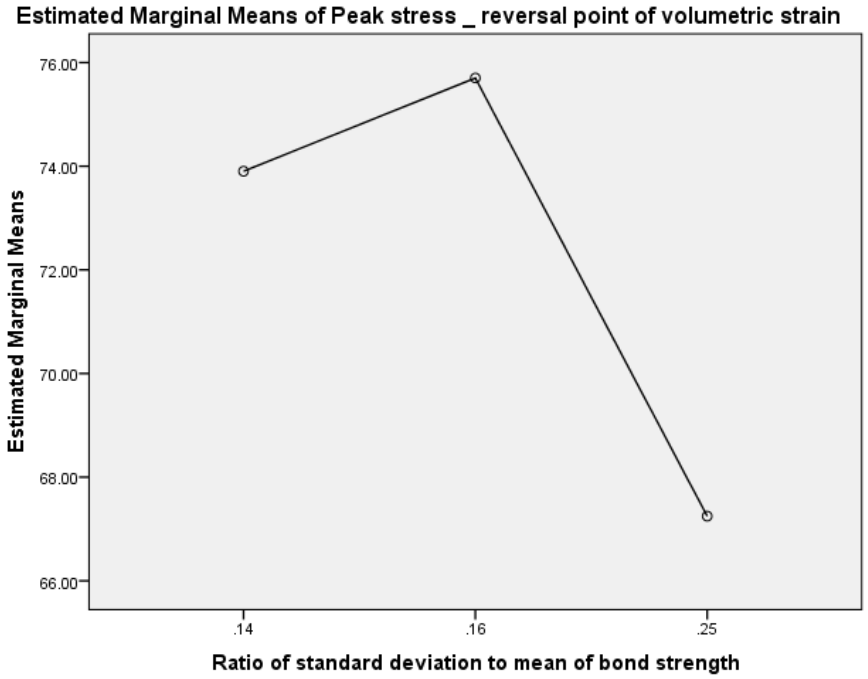

Figure C 1 Profile plot: Estimated marginal means of peak stress reversal point of volumetric strain for ratio of standard deviation to mean of bond strength

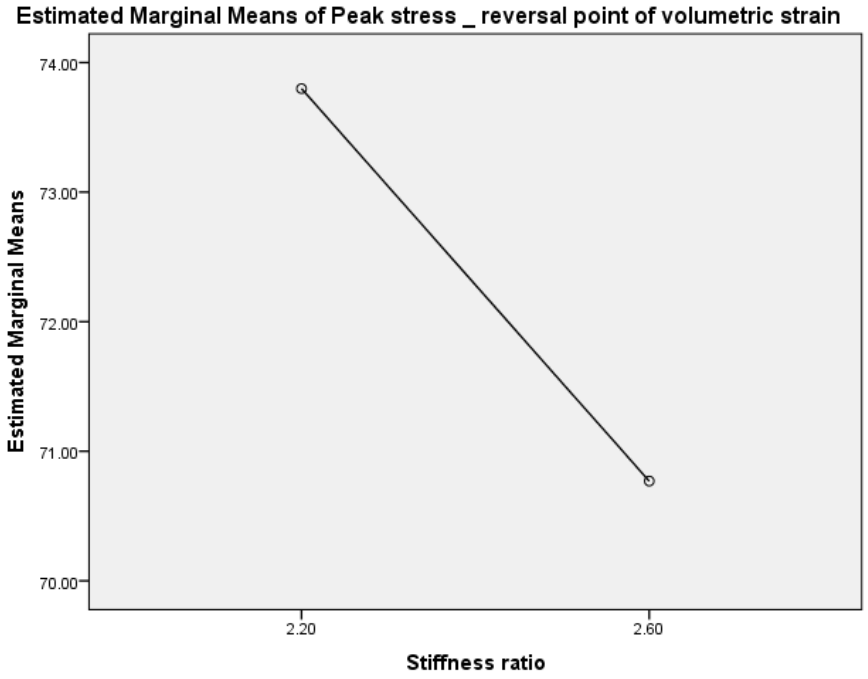

Figure C 2 Profile plot: Estimated marginal means of peak stress reversal point of volumetric strain for stiffness ratio

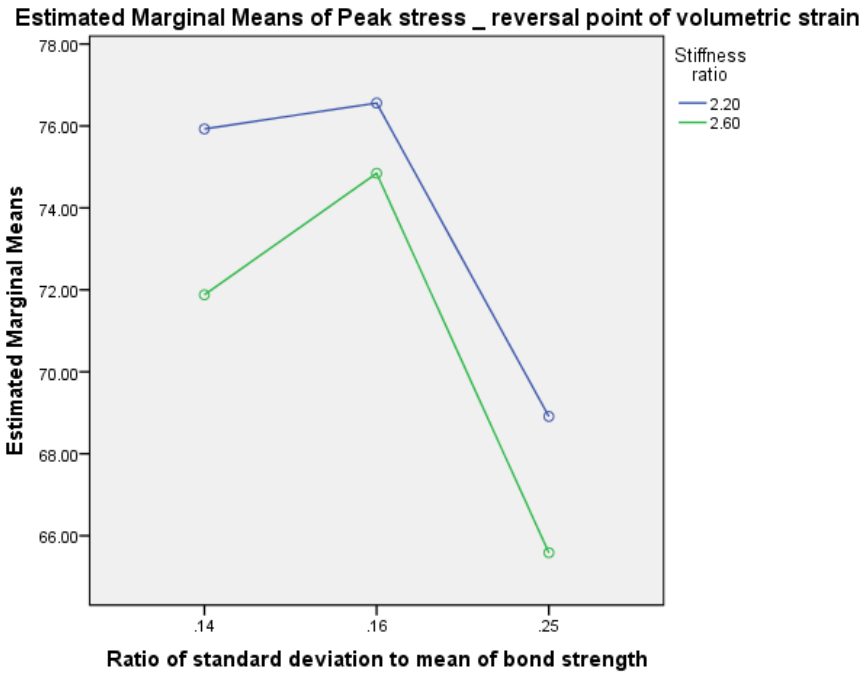

Figure C 3 Profile plot: Estimated marginal means of peak stress reversal point of volumetric strain for ratio of standard deviation to mean of bond strength